Accurate and efficient numerical solutions for the Saint Venant equations of open channel flow

by Amanda Jane Crossley, B.Sc. M.Sc.

Thesis submitted to the University of Nottingham
for the degree of Doctor of Philosophy, October 1999

Abstract

Within the field of hydraulics there is a growing trend towards the use of computer based models, which have proven to be an invaluable tool in engineering. A range of commercial packages is available which encompass different mathematical models and a variety of solution strategies.

A number of problems can be identified with the software currently available, and as a result, research continues into developing better numerical techniques for computational hydraulics. The issues most often addressed by researchers consider the application of faster and more accurate numerical methods, many of which were originally developed for gas dynamics problems. There has been a growing trend in favour of Riemann based methods constructed within the finite volume framework. Such methods are noted for their good conservation and shock capturing capabilities. However, the computational cost of employing theses algorithms can lead to excessively long run times, particularly when higher order mathematical models are used. This often is as a result of stability constraints placed upon explicit schemes, which require the smallest possible time step permitted throughout the grid, to be applied globally. One possibility for improving this situation is to use local time stepping, whereby individual cells are advanced by their own maximum allowable time steps. To incorporate this concept into a transient model requires the development of a suitable integration strategy, to ensure that the solution remains accurate in time. Two such strategies developed for the Euler equations are considered within this thesis for application to the Saint Venant equations of open channel flow. Both techniques have been demonstrated to reduce run times and improve the quality of solutions in the regions of discontinuities. The investigation considers the the first order scheme of Roe, together with a second order extension constructed using a flux limiter approach. The effects of using an upwind based source term treatment, specifically developed for Roe's scheme, are also considered, and the source term calculations are incorporated into the LTS framework. Results are presented for a series of steady state and transient test cases, which illustrate how local time stepping can lead to reduced run times and improved solution accuracy. The results also highlight the benefits of using an upwind source term treatment, particularly when variations in the channel geometry occur.

Notation

A	cross sectional area, Jacobian matrix of the flux vector
B	channel width at the free surface level
C^+	forward characteristic
C^-	backward characteristic
$\mathbf{F}$	flux vector
$\mathbf{F_{i+/12}}$	discrete approximation to the flux at the cell interfaces
F_r	Froude number
$\mathbf{G}$	flux vector
G	Jacobian matrix of the source term vector
H	total depth or surface elevation
I_1	hydrostatic pressure term
I_2	pressure term due to width variations
L	left state
P	wetted perimeter
Q	discharge
$\mathbf{R}$	source term vector
$\mathbf{R_i}$	discrete approximation to the sources for cell i
R	hydraulic radius
S_f	friction term due to the bed's roughness
S_0	friction term due to the bed's slope
$\mathbf{U}$	vector of conserved variables (for homogeneous conservation laws)
$\mathbf{U_i}$	discrete solution vector for cell i
a	speed of a scalar conservation law
b	bed width
c	wave celerity
$\mathbf{e}$	vector of eigenvalues of the Jacobian matrix
f	flux of a scalar conservation law
g	acceleration due to gravity
h	water depth
m	temporal index for LTS2 algorithm
n	Manning's n
r	argument for flux limiter function
t	time

u	velocity component in the x direction
v	velocity component in the y direction
x	coordinate direction, distance along the channel
y	coordinate direction, surface elevation or total depth
z	coordinate direction, bed level
α	wave strength from Roe's decomposition
Δt	time step
Δx	spatial step
δt	minimum permissible time step throughout the grid
η	depth integration variable
λ	mesh ratio, wave speed from Roe's decomposition
ν	Courant or CFL number
ρ	density
σ	channel width at a given depth
ϕ	elevation $\times$ acceleration due to gravity (gH), flux limiter

Acknowledgments

The author would like to thank the following people for their contributions and support to the work conducted as part of the thesis

Dr Nigel Wright for his supervision throughout the past few years.

Dr Chris Whitlow for suggesting an investigation into local time stepping.

Professor Pilar García-Navarro for information and helpful discussions on the upwind source term treatment.

The author is also grateful for the financial support received from the University of Nottingham which made the study possible.

Finally, a thank you to all of my friends, assortment of office-mates, colleagues and generally anyone else that has helped to keep me sane (!) during the thesis, especially those nice people who wrote LaTeX.

Chapter 1

Introduction

Computational Fluid Dynamics or CFD is a valuable tool for hydraulic engineers. Its use enables detailed predictions to be made about what the flow will be for a particular watercourse under certain conditions, without the need to take field measurements which can be time consuming and expensive. On a global scale, what happens within rivers and the sea has a fundamental impact on the environment and society, and anything which may affect the natural balance is of particular concern. Within the hydraulics community most applications of CFD focus on assessing the environmental impacts of specific projects. The applications of hydraulics are extremely diverse. Typical applications are studies involving dam break failures, flood alleviation schemes, morphological predictions, sediment transport and river rehabilitation.

The demand for efficient and accurate software that can deal with the problems faced by hydraulic engineers has lead to numerous commercial hydraulics packages appearing in the marketplace. In the past some of the more sophisticated software available required the use of powerful computers and long run times, as a result of the level of complexity involved. However this situation is improving with advances in computer hardware. In addition several other areas can be identified where numerical techniques encounter difficulties when applied to open channel flow problems. Firstly the highly irregular geometries of natural rivers can lead to problems in producing a computational grid to represent the structure. The occurrence of mixed regions of flow, for example at hydraulic jumps where a supercritical to subcritical transition takes place, leads to problems for some numerical methods resulting in either poor results or failure to produce a

solution. All numerical methods are subject to stability constraints which restrict the values allowed for the time step for a given grid. For explicit schemes, this can result in the need to use very small time steps which can be computationally expensive. Implicit schemes overcome this difficulty but at the expense of more complex algorithms. To improve this situation, better numerical techniques are needed for solving the equations which govern open channel flow.

Similar problems to those described above have been encountered in other areas where CFD is applied. Much of the knowledge that has been gained about the application of numerical techniques to open channel flow originated from the aeronautics industry, where many of the pioneering algorithms were developed. There are still some ideas left to be exploited from other fields that have not yet been considered for channel flow, which may resolve some of the present difficulties. In terms of improving the 'classical' methods which were originally applied to channel flows, the current trend is towards numerical schemes which base their solution on solving a series of Riemann problems. Such methods have a number of desirable properties, most noticeably the ability to predict discontinuities in the solution due to the presence of flow transitions, and so were chosen as a focal point for this thesis.

In any modelling situation, the basis for forming a more complex model is to begin with a simpler concept and to extend the ideas within it to include additional information. A number of mathematical models exist that are suitable for modelling open channel flows, ranging from the 1-d Saint Venant equations to the 3-d Navier-Stokes equations. All are based on the same underlying physics and the most suitable choice for a particular problem will depend on the actual problem being considered and the requirements of the solution, in particular what it is hoped to be achieved from the study. For the purpose of investigating ways to improve efficiency and reduce run times, the 1-d Saint Venant equations have been considered within the thesis, as a means to illustrate the ideas being presented. Although the Saint Venant equations are relatively simple compared to more sophisticated models such as the Navier-Stokes equations, they are nevertheless capable of predicting enough information to be of practical use and some of the popular commercial packages (such as ISIS which is the UK industry standard) are based on solving the 1-d system. In most instances the type of problems to which the Saint Venant equations may be applied do not result in exceptional computer costs and hence there may be limited enthusiasm for considering 'faster' methods for such flows. However it is hoped that the ideas presented herein could

be extended to more complex systems where reducing run times would be a practical benefit and serve to profit the end user. From a validation prospective, a number of standard test cases exist for the Saint Venant equations where analytical solutions are known for particular problems, and these act as a means of comparing one numerical method to another. Although such problems tend to be quite simple and not of practical interest to engineers, they are able to illustrate where particular methods will perform well or fail, and form an essential part of the development process.

In an attempt to address some of the existing problems within the computational hydraulics field, the main objective of this project is to develop ways of reducing computer run times whilst maintaining (or improving upon) the same level of accuracy as achievable by a particular scheme. An idea which has been successfully implemented elsewhere is that of local time stepping (LTS), whereby different cells throughout the domain are advanced to different points in time. This technique is especially suited to steady state problems where it is not necessary to maintain all of the cells at the same temporal level. However much less consideration has been given to the idea of time accurate local time stepping schemes for unsteady flows as the effort involved in ensuring that the cells are integrated in a suitable order can outweigh the potential benefits if not performed effectively. Within this thesis, two such algorithms developed for aeronautics will be presented and applied to a number of open channel flows problems, which will highlight the benefits of using such a technique. In addition, the benefits of employing an upwind based source term treatment over the conventional pointwise approach will also be investigated.

The thesis now goes on to introduce the 1-d Saint Venant equations and explain how they may be derived. Chapter 3 consists of an introduction to the solution methods of differential equations, followed by a more in depth look at the techniques available for conservation laws. Subsequently a review is made of the application of numerical methods to open channel flow problems, demonstrating what has been achieved so far. The next chapter then gives more detail on the Roe Riemann solver and discusses the implementation of boundary conditions and the construction of the upwind source term treatment. In Chapter 5, the concept of local time stepping is introduced, together with some extensions of the upwind source term treatment. This is followed by results for a series of test cases in Chapter 6. Finally Chapter 7 summarises the project and presents the conclusions of the study, in addition to giving some ideas on how this work might be extended.

Chapter 2

Mathematical Model

A number of mathematical models are available that have been developed to describe fluid flow, the most general of which are the Navier-Stokes equations used to predict the behaviour of a viscous compressible fluid in three dimensions. In practice when forming a mathematical model, many assumptions are made to simplify the problem under consideration, and the most basic equations that will capture the required phenomena are used. In open channel flow the most commonly used models fall under the classification of shallow water equations, in which it is assumed that the flow is shallow relative to the dimensions of the problem being considered. As with all fluid flow models, the basis for forming a shallow water model is to form a continuity equation, corresponding to conservation of mass, and to apply the laws governing classical physics which leads to an equation of motion. Depending on the construction, such equations can often be written as conservation laws representing the conservation of a particular quantity such as momentum or energy. Additional terms may be incorporated to include other effects such as friction, geometry variation, viscosity etc. and these are referred to as the source terms which generally correspond to some form of loss or gain from the system.

In the case of modelling predominantly one-dimensional flows, the Saint Venant equations are the most commonly used system for solving open channel flow problems, and these describe the gradually varied flow of an incompressible inviscid fluid. The equations consist of a continuity or mass equation, and an equation of motion which is formed by applying Newton's Second law of motion along the channel.

A number of fundamental assumptions are inherent within the model and these can be summarised as

- The flow is one-dimensional such that the velocity is constant over a cross section and the water level is horizontal
- the vertical component of the acceleration of the fluid is negligible so that the pressure variation with depth is hydrostatic (equivalent to saying that the streamline curvature is small)
- friction and turbulence can be represented using the same empirical laws that govern steady state flow (such as Manning's equation)
- the bed slope is small resulting in the cosine of the angle between the bed level and the horizontal being approximately unity.

A more complex system of equations known as the Boussinesq equations exist to describe the motion of rapidly varied flows, where the effects of the vertical acceleration are significant and are included by assuming that the magnitude of the vertical velocity increases linearly from zero at the bed to a maximum value at the free surface (see [1] for details). By setting the acceleration terms in this system to zero, the Saint Venant equations are reproduced.

2.1 Derivation of the Saint Venant equations

The Saint Venant equations appear in many forms in the literature and can either be written as a set of integral or differential equations. The following derivation is taken from a book written by Cunge *et al* [12] and applies to an arbitrarily shaped channel such as that shown in Figure 2.1.

Consider a control volume in the (x,t) plane between two cross sections x_1 and x_2 and between the times t_1 and t_2 as shown in Figure 2.2. Let A be the area of a wetted cross section and u be the uniform cross sectional velocity. Then the mass flow rate (density$\times$discharge) into the control volume is defined as $(\rho uA)_{x_1}$ and the rate leaving the region will be $(\rho uA)_{x_2}$, where ρ is the fluid density. To find the net mass inflow in to the control volume, the difference of the mass flow rates

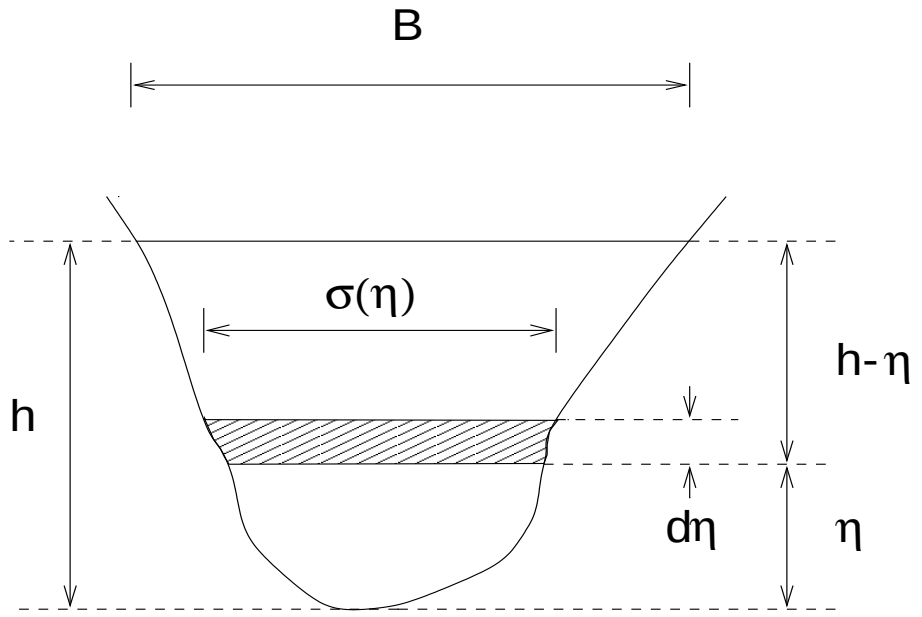

Figure 2.1: Typical cross section [12].

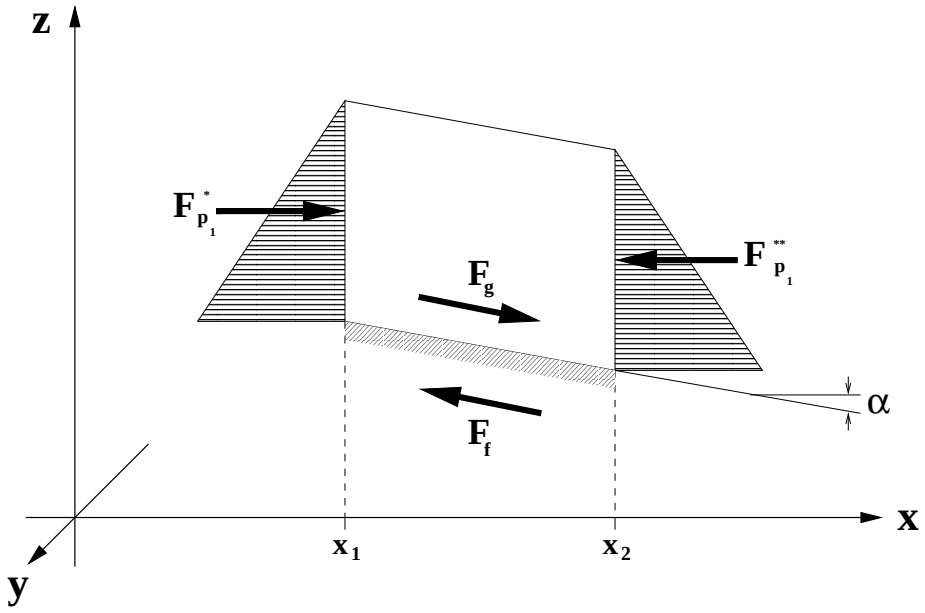

Figure 2.2: Control volume, section view [12].

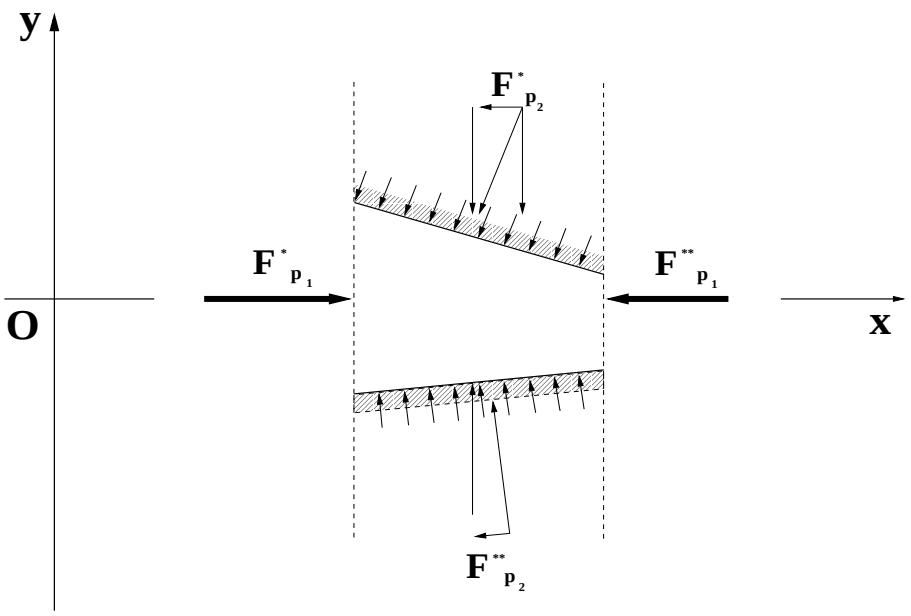

Figure 2.3: Pressure forces, plan view [12].

is integrated between the times t_1 and t_2, i.e.

$$\int_{t_1}^{t_2} [(\rho u A)_{x_1} - (\rho u A)_{x_2}] \, \mathrm{d}t. \tag{2.1}$$

From conservation of mass, the net inflow must be equal to the change in storage between x_1 and x_2 over the time interval which is given by

$$\int_{x_1}^{x_2} [(\rho A)_{t_2} - (\rho A)_{t_1}] \, \mathrm{d}x. \tag{2.2}$$

Substituting $Q = uA$ where Q is the discharge and assuming that the density is constant, equating (2.1) and (2.2) then gives

$$\int_{x_1}^{x_2} [(A)_{t_2} - (A)_{t_1}] \, \mathrm{d}x + \int_{t_1}^{t_2} [(Q)_{x_2} - (Q)_{x_1}] \, \mathrm{d}t = 0 \tag{2.3}$$

which is the integral form of the continuity equation for a channel of arbitrary cross section.

For the second equation, applying Newton's second law of motion implies that the change in momentum of the control volume over the time interval must be equal to the sum of the net inflow of momentum within the region and the integral with respect to time of the external forces acting upon it. As momentum is the product of mass and velocity, and momentum flux is given by the mass flow rate times the velocity, and is defined as

$$\text{momentum flux} = \rho u A \times u = \rho u^2 A.$$

The net momentum flux is the difference between flux entering and leaving the control volume and so the net inflow over the time interval becomes

$$M_f = \int_{t_1}^{t_2} [(\rho u^2 A)_{x_1} - (\rho u^2 A)_{x_2}] \, \mathrm{d}t. \tag{2.4}$$

At a particular time, the momentum within the control volume will be given by

$$\int_{x_1}^{x_2} \rho u A \, \mathrm{d}x$$

and so the net increase, ΔM, over the time interval is

$$\Delta M = \int_{x_1}^{x_2} [(\rho u A)_{t_2} - (\rho u A)_{t_1}] \, \mathrm{d}x. \tag{2.5}$$

From Figure 2.2 and Figure 2.3, consider the only important external forces acting upon the control volume in the x-direction to be as a result from pressure, gravity and frictional resistance. The resulting pressure force, F_{p_1} is given by the differences between the pressure forces $F_{p_1}^*$ and $F_{p_1}^{**}$ which act at the boundaries. By applying the hydrostatic pressure assumption, the pressure force $F_{p_1}^*$ can be defined by

$$F_{p_1}^* = g \int_0^{h(x)} \rho [h(x) - \eta] \sigma(x, \eta) \, \mathrm{d}\eta$$

where η is a depth integration variable, $h(x,t)$ is the water depth, and $\sigma(x,\eta)$ is the width of the cross section at a depth η such that $\sigma(x,h) = B(x)$ at the free surface. Hence the time integral of the net pressure force, F_{p_1} becomes

$$\int_{t_1}^{t_2} F_{p_1} \mathrm{d}t = \int_{t_1}^{t_2} (F_{p_1}^* - F_{p_1}^{**}) \, \mathrm{d}t = g \int_{t_1}^{t_2} [(\rho I_1)_{x_1} - (\rho I_1)_{x_2}] \, \mathrm{d}t \tag{2.6}$$

where for convenience I_1 is defined as

$$I_1 = \int_0^{h(x)} [h(x) - \eta] \sigma(x, \eta) \, \mathrm{d}\eta.$$

Consider an infinitesimal length of channel, $\mathrm{d}x$. The increase in pressure force due to a change in width is given by the corresponding increase in the wetted area, $\mathrm{d}\sigma \cdot \mathrm{d}\eta$ (for constant depth h_0), times the distance of the centroid from the free surface $h(x) - \eta$, i.e.

$$\rho g \left[\left(\frac{\partial \sigma}{\partial x} \right) \mathrm{d}x \cdot \mathrm{d}\eta \right]_{h=h_0} [h(x) - \eta].$$

To calculate the the total instantaneous force on the control volume, this force is integrated between $\eta = 0$ and $\eta = h(x)$ for a given cross section, and from x_1 to x_2, giving

$$F_{p_2} = \int_{x_1}^{x_2} \rho g \int_0^{h(x)} [h(x) - \eta] \left[\frac{\partial \sigma(x, \eta)}{\partial x} \right]_{h_0} \mathrm{d}\eta \, \mathrm{d}x.$$

To find the total force over the time interval, F_{p_2} is integrated between t_1 and t_2 and can be written as

$$\int_{t_1}^{t_2} F_{p_2}\,\mathrm{d}t = g\int_{t_1}^{t_2}\int_{x_1}^{x_2} \rho I_2\,\mathrm{d}x\,\mathrm{d}t \tag{2.7}$$

where

$$I_2 = \int_0^{h(x)} (h-\eta)\left[\frac{\partial\sigma}{\partial x}\right]_{h=h_0} \mathrm{d}\eta.$$

The gravity force, F_g can be found by assuming that the channel slope is small such that

$$S_0 = -\frac{\partial z}{\partial x} = \tan\alpha \approx \sin\alpha$$

where z is the bed level above some datum. Over the time interval, the total contribution from the gravity force will be

$$\int_{t_1}^{t_2} F_g\,\mathrm{d}t = \int_{t_1}^{t_2}\int_{x_1}^{x_2} \rho g A S_0\,\mathrm{d}x\,\mathrm{d}t. \tag{2.8}$$

The frictional resistance, F_f is as a result of shear along the channel bed and banks and can be expressed in terms of the friction slope, S_f (see [11] for details). The shear force per unit length of channel is then defined by $\rho g A S_f$ and the time integral of the friction force then becomes

$$\int_{t_1}^{t_2} F_f\,\mathrm{d}t = \int_{t_1}^{t_2}\int_{x_1}^{x_2} \rho g A S_f\,\mathrm{d}x\,\mathrm{d}t. \tag{2.9}$$

From conservation of momentum, the change in momentum, ΔM is equal to the the sum of the net gain of momentum, M_f and the external forces, thus

$$\Delta M = M_f + \int_{t_1}^{t_2} F_{p_1}\mathrm{d}t + \int_{t_1}^{t_2} F_{p_2}\mathrm{d}t + \int_{t_1}^{t_2} F_g\mathrm{d}t - \int_{t_1}^{t_2} F_f\,\mathrm{d}t$$

Hence from equations (2.4) to (2.9), and by assuming that the density is constant, this then leads to the standard from of the integral version of the momentum equation

$$\begin{aligned}\int_{x_1}^{x_2}[(uA)_{t_2} - (uA)_{t_1}]\,\mathrm{d}x \;=\; & \int_{t_1}^{t_2}[(u^2A)_{x_1} - (u^2A)_{x_2}]\,\mathrm{d}t + g\int_{t_1}^{t_2}[(I_1)_{x_1} - (I_1)_{x_2}]\,\mathrm{d}t \\ & -g\int_{t_1}^{t_2}\int_{x_1}^{x_2} I_2\,\mathrm{d}x\,\mathrm{d}t + g\int_{t_1}^{t_2}\int_{x_1}^{x_2} A(S_0 - S_f)\,\mathrm{d}x\,\mathrm{d}t.\end{aligned}$$

Alternatively, the terms containing A and Q may be rewritten using the relationship $Q = uA$ to give

$$\begin{aligned}\int_{x_1}^{x_2}\left[(Q)_{t_2} - (Q)_{t_1}\right]\,\mathrm{d}x \;=\; & \int_{t_1}^{t_2}\left[\left(\frac{Q^2}{A}\right)_{x_1} - \left(\frac{Q^2}{A}\right)_{x_2}\right]\mathrm{d}t + g\int_{t_1}^{t_2}\left[(I_1)_{x_1} - (I_1)_{x_2}\right]\,\mathrm{d}t \\ & -g\int_{t_1}^{t_2}\int_{x_1}^{x_2} I_2\,\mathrm{d}x\,\mathrm{d}t + g\int_{t_1}^{t_2}\int_{x_1}^{x_2} A\left(S_0 - S_f\right)\,\mathrm{d}x\,\mathrm{d}t.\end{aligned} \tag{2.10}$$

In most instances the differential form of the Saint Venant equations are quoted and these may be obtained from the integral from by assuming that the flow variables are continuous and differentiable and that the distance $x_2 - x_1$ becomes infinitely small. Then by applying Taylor series expansion, A and Q at t_2 can be written as

$$\begin{aligned}(A)_{t_2} &= (A)_{t_1} + \frac{\partial A}{\partial t}\Delta t + \frac{\partial^2 A}{\partial t^2}\frac{\Delta t^2}{2} + ... \\ (Q)_{t_2} &= (Q)_{t_1} + \frac{\partial Q}{\partial t}\Delta t + \frac{\partial^2 Q}{\partial t^2}\frac{\Delta t^2}{2} + ...\end{aligned} \tag{2.11}$$

Disregarding the second order and higher terms in (2.11), and taking the limit as Δt and Δx vanish to zero leads to the following

$$\lim_{t_2 \to t_1} \int_{x_1}^{x_2} [(A)_{t_2} - (A)_{t_1}] \mathrm{d}x = \int_{x_1}^{x_2} \int_{t_1}^{t_2} \frac{\partial A}{\partial t}\, \mathrm{d}t\, \mathrm{d}x$$

$$\lim_{t_2 \to t_1} \int_{x_1}^{x_2} [(Q)_{t_2} - (Q)_{t_1}] \mathrm{d}x = \int_{x_1}^{x_2} \int_{t_1}^{t_2} \frac{\partial Q}{\partial t}\, \mathrm{d}t\, \mathrm{d}x$$

and so the continuity equation may be rewritten as

$$\int_{x_1}^{x_2} \int_{t_1}^{t_2} \left[\frac{\partial A}{\partial t} + \frac{\partial Q}{\partial x}\right] \mathrm{d}t\, \mathrm{d}x = 0. \tag{2.12}$$

Applying Taylor series to the other terms in (2.10) gives

$$\begin{aligned}(Q^2/A)_{x_2} - (Q^2 A)_{x_1} &= \frac{\partial (Q^2/A)}{\partial x}\Delta x + \frac{\partial^2 (Q^2/A)}{\partial x^2}\frac{\Delta x^2}{2} + ... \\ (I_1)_{x_2} - (I_1)_{x_1} &= \frac{\partial I_1}{\partial x}\Delta x + \frac{\partial^2 I_1}{\partial x^2}\frac{\Delta x^2}{2} + ...\end{aligned} \tag{2.13}$$

By using only the first order terms in (2.13) and taking the limit as Δx and Δt tend to zero, equation (2.10) can then be written as

$$\int_{x_1}^{x_2} \int_{t_1}^{t_2} \left[\frac{\partial Q}{\partial t} + \frac{\partial (Q^2/A)}{\partial x}\right] \mathrm{d}t\, \mathrm{d}x = -g \int_{x_1}^{x_2} \int_{t_1}^{t_2} \left[\frac{\partial I_1}{\partial x} - I_2 - A(S_0 - S_f)\right] \mathrm{d}t\, \mathrm{d}x. \tag{2.14}$$

As (2.12) and (2.14) must hold for throughout the region, they can be replaced by the differential equations

$$\begin{aligned}\frac{\partial A}{\partial t} + \frac{\partial Q}{\partial x} &= 0 \\ \frac{\partial Q}{\partial t} + \frac{\partial}{\partial x}\left(\frac{Q^2}{A} + gI_1\right) &= gA(S_0 - S_f) + gI_2,\end{aligned} \tag{2.15}$$

which together form the differential version of the Saint Venant equations. Alternatively the momentum equation is sometimes written in the form

$$\frac{\partial Q}{\partial t} + \frac{\partial}{\partial x}(uQ) + gA\left(\frac{\partial h}{\partial x} - S_o\right) + gAS_f = 0$$

and this is referred to as the dynamic equation.

Although the above equations are written for an arbitrarily shape cross section, the range of conditions over which the equations remain valid is constrained by the Saint Venant hypothesis, and the assumptions made within the derivation must be borne in mind when a suitable model for a particular problem is being sought.

2.2 Alternative formulations

There are other ways of representing the Saint Venant equations which are based upon the same hypothesis but are expressed in terms of a different set of dependent variables. Equations (2.15) are known as the divergent form and represent a system of conservation laws. In general most texts only refer to the equations for a prismatic rectangular channel for which the I_1 term simplifies to $I_1 = A^2/2b$ and I_2 is zero. Some of the more commonly used alternatives [12] for general cross sections are presented as

1. Using Q and h

$$\frac{\partial h}{\partial t} + \frac{1}{B}\frac{\partial Q}{\partial x} = 0$$

$$\frac{\partial Q}{\partial t} + \frac{\partial}{\partial x}\left(\frac{Q^2}{A}\right) + gA\frac{\partial h}{\partial x} + gA(S_f - S_o) = 0$$

2. Using Q and y, where y is the surface elevation ($y = h + z$)

$$\frac{\partial y}{\partial t} + \frac{1}{B}\frac{\partial Q}{\partial x} = 0$$

$$\frac{\partial Q}{\partial t} + \frac{\partial}{\partial x}\left(\frac{Q^2}{A}\right) + gA\frac{\partial y}{\partial x} + gAS_f = 0$$

3. Using u and h

$$\begin{aligned} &\frac{\partial h}{\partial t} + \frac{A}{B}\frac{\partial u}{\partial x} + u\frac{\partial h}{\partial x} + \frac{u}{B}\left(\frac{\partial A}{\partial x}\right)_{h=\text{const}} = 0 \\ &\frac{\partial u}{\partial t} + u\frac{\partial u}{\partial x} + g\frac{\partial h}{\partial x} + g(S_f - S_o) = 0 \end{aligned} \tag{2.16}$$

4. Using u and y

$$\frac{\partial y}{\partial t} + \frac{A}{B}\frac{\partial u}{\partial x} + u\left(\frac{\partial y}{\partial x} + S_o\right) + \frac{u}{B}\left(\frac{\partial A}{\partial x}\right)_{y=\text{const}} = 0$$

$$\frac{\partial u}{\partial t} + u\frac{\partial u}{\partial x} + g\frac{\partial y}{\partial x} + gS_f = 0.$$

Depending on the particular problem being considered and the numerical technique being used, it may be more appropriate to deal with one particular form of the equations than another. If all the variables are at least once differentiable then all the sets of equations are equivalent. However, only the divergent form formulated in terms of A and Q may be expressed in conservation form for non-rectangular channels and consequently may be more conveniently written in vector form as

$$\mathbf{U}_t + \mathbf{F}_x = \mathbf{R} \tag{2.17}$$

where

$$\mathbf{U} = (A, Q)^T, \quad \mathbf{F} = (Q, \frac{Q^2}{A} + gI_1)^T$$

and

$$\mathbf{R} = (0, gI_2 + gA(S_o - S_f))^T.$$

Mathematically (2.17) represents a system of conservation laws with source terms which in this case result from the friction terms and irregularities in the channels geometry. The vector $\mathbf{U}$ is known as the vector of conserved variables, whilst $\mathbf{F}$ is the flux vector and $\mathbf{R}$ is the source term vector. To be able to apply a Riemann based method to any set of equations it is necessary to be able to express the system in conservation form and so for this reason the divergent form of the Saint Venant equations will be used throughout this thesis.

For more complex geometries where the flow conditions require a two dimensional treatment, a more general form of shallow water equations can be used. These

equations are based on the same hypotheses as the 1-d form with the exception that the transverse velocity and water level may vary within a cross section. Generally the 2-d forms are not quoted in text books, however various formulations are found in scientific and engineering journals. One of the more common forms of the equations encountered within the literature is written as

$$\mathbf{U}_t + \mathbf{F}_x + \mathbf{G}_y = \mathbf{R}$$

with the vectors defined by

$$\mathbf{U} = \begin{pmatrix} \phi \\ \phi u \\ \phi v \end{pmatrix}, \mathbf{F} = \begin{pmatrix} \phi u \\ \phi u^2 + \frac{1}{2}\phi^2 \\ \phi uv \end{pmatrix}, \mathbf{G} = \begin{pmatrix} \phi v \\ \phi uv \\ \phi v^2 + \frac{1}{2}\phi^2 \end{pmatrix}, \mathbf{R} = \begin{pmatrix} 0 \\ g\phi(S_{o_x} - S_{f_x}) \\ g\phi(S_{o_y} - S_{f_y}) \end{pmatrix}.$$

The term ϕ is defined by $\phi = gH$ where H is the total depth of the fluid or elevation (i.e. $H = y = h + z$) and the friction terms are now

$$S_{o_x} = -\frac{\partial z}{\partial x},\ S_{o_y} = -\frac{\partial z}{\partial y}$$

and

$$S_{f_x} = \frac{n^2 u\sqrt{u^2+v^2}}{(\phi/g)^{4/3}}, S_{f_y} = \frac{n^2 v\sqrt{u^2+v^2}}{(\phi/g)^{4/3}}.$$

Alternatively the system can be written using $\mathbf{U} = (h, hu, hv)^T$ whereby

$$\mathbf{F} = \begin{pmatrix} hu \\ hu^2 + \frac{1}{2}gh^2 \\ huv \end{pmatrix}, \mathbf{G} = \begin{pmatrix} hv \\ huv \\ hv^2 + \frac{1}{2}gh^2 \end{pmatrix}, \mathbf{R} = \begin{pmatrix} 0 \\ gh(S_{o_x} - S_{f_x}) \\ gh(S_{o_y} - S_{f_y}) \end{pmatrix}$$

where S_{f_x} and S_{f_y} are given by

$$S_{f_x} = \frac{n^2 u\sqrt{u^2+v^2}}{(h)^{4/3}}, S_{f_y} = \frac{n^2 v\sqrt{u^2+v^2}}{(h)^{4/3}},$$

or in terms of the primitive variables with $\mathbf{U} = (h, u, v)^T$ and

$$\mathbf{F} = \begin{pmatrix} hu \\ gh + \frac{1}{2}u^2 \\ uv \end{pmatrix}, \mathbf{G} = \begin{pmatrix} hv \\ uv \\ gh + \frac{1}{2}v^2 \end{pmatrix}, \mathbf{R} = \begin{pmatrix} 0 \\ g(S_{o_x} - S_{f_x}) \\ g(S_{o_y} - S_{f_y}) \end{pmatrix}$$

where the friction terms are the same as before.

Chapter 3

Literature Review

This chapter contains an overview of the background information and scientific literature relevant to the thesis. The review is broken down into two sections. The first section deals with solution methods for differential equations and introduces the method of characteristics and some of the fundamental concepts of numerical methods. A more detailed account of the numerical techniques available for solving problems based upon conservation laws is then given. In the second section, the application of numerical methods to open channel flow is considered, outlining what has been accomplished within the field of computational hydraulics. Particular emphasis is given to work based on using Riemann solvers and an improved source term treatment, in addition to identifying suitable test cases for the Saint Venant equations throughout the review.

3.1 Solution techniques for PDE's

In this section a review is made of some of the analytical and numerical methods available for solving PDE's. However it is important to note that PDE's fall into several categories and some methods may only be applied to certain types of equations. The three classifications are hyperbolic, elliptic and parabolic. As the Saint Venant equations fall into the classification of hyperbolic PDE's, the main focus will be on methods suitable for solving hyperbolic equations.

For a more detailed analysis of PDE theory and numerical solution methods see Ames [5]. A range of text books discuss the use of numerical methods to solve

general fluid flow problems (e.g. [19], [34] and [49]) and Cunge, Holly and Verwey [12] is a particularly useful text as it focuses on computational river hydraulics as does Abbott [1].

3.1.1 Analytical methods

Prior to the development of computers and their application to CFD, analytical techniques had to be used to solve PDE's. However their application to anything but the most simplest of problems could be quite cumbersome and require extensive hand computation. One particular method suited to solving problems based on conservation laws is known as the method of characteristics. This technique is still used today, most commonly as a semi-graphical method and also as a means to generate alternative differential equations. The underlying principles of the method of characteristics form the basis for many numerical schemes and so a description of the technique is included here. The following section is based on material taken from [41] and [61].

The method of characteristics

The method of characteristics can only be applied to hyperbolic PDE's and involves defining the characteristics along which disturbances propagate [12]. Characteristics can be thought of as lines in the space-time plane, along which (by definition) certain properties are constant. To illustrate the basis of the method, consider a first order PDE of the form

$$u_t + a(x,t)u_x = 0$$

with the initial data $u(x,0) = u_0(x)$. By the chain rule

$$\frac{du}{dt} = u_t + \frac{dx}{dt}u_x \tag{3.1}$$

and rearrangement gives

$$u_t = \frac{du}{dt} - \frac{dx}{dt}u_x.$$

Substituting the above expression for u_t into (3.1) then yields

$$\frac{du}{dt} + \left(a(x,t) - \frac{dx}{dt}\right)u_x = 0. \tag{3.2}$$

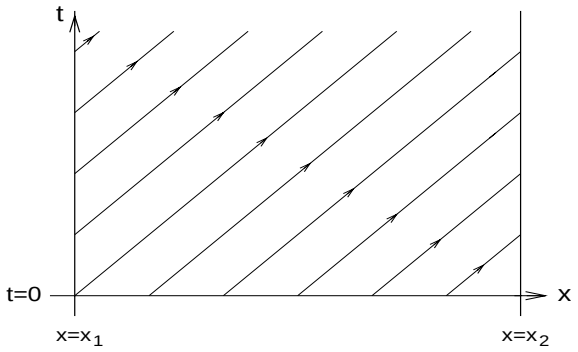

Figure 3.1: Characteristics over a finite domain.

From (3.2) it can be seen that $du/dt = 0$ along the lines defined by $dx/dt = a(x,t)$, which implies that the solution u is constant along these lines known as the characteristics. In principle if one can define a set of characteristic lines then it is possible to know the solution at all times (providing the lines do not intercept) just from the initial and boundary conditions of the problem. Mathematically this is equivalent to saying

$$u(x,t) = u(x - \int_0^t a(x,t)\ dt,\ 0).$$

If the method is applied over a finite region (see Figure 3.1), then it is necessary to specify the values along any boundary where the characteristics enter the region. For example in Figure 3.1 boundary data is needed along the line $x = x_1$, however data is not needed along $x = x_2$ as the characteristics leaving the region already have values specified on them.

The same principles can be applied to the case

$$u_t + a(u)u_x = 0$$

where if $f'(u) = a(u)$ then

$$u_t + f(u)_x = 0$$

which is a scalar conservation law. Now the characteristics are given by

$$\frac{dx}{dt} = a(u).$$

If u is constant along the characteristics so too is a and the characteristics are straight lines, with values determined by the initial conditions. From ODE theory it can be shown that for continuous u the characteristic lines do not cross. However hyperbolic PDE's admit discontinuous solutions, and for a general nonlinear conservation law with arbitrary initial conditions, the characteristics will

cross in finite time and a discontinuity or shock will form. In this instance it is no longer possible to trace back along the characteristic paths to find the solution. If a discontinuity does form, then if u has constant values either side of the shock then it is possible to calculate a speed s with which the shock moves by applying conservation principles over the region (see [41] and [61]). This leads to the Rankine-Hugoniot jump condition which relates the shock speed to the left and right values such that

$$s = \frac{f_R - f_L}{u_R - u_L}$$

where the subscripts L and R denote the values to the left and the right of the shock respectively. From the formula the shock position (x_s) can be deduced as $s = dx_s/dt$.

Similarly the theory of characteristics can be extended to linear systems of equations of the form

$$\mathbf{U}_t + A\mathbf{U}_x = 0$$

where $\mathbf{U}$ is a vector, A is a constant matrix and $\mathbf{F}(\mathbf{U}) = A\mathbf{U}$. The system can then be decoupled by diagonalising A to form a series of scalar equations, each of which will have its own equation to describe the characteristics. For a system of order n, the resulting decoupled equations can be rewritten as

$$(v_k)_t + \lambda_k (v_k)_x = 0 \qquad\qquad k = 1, 2, ..., n$$

where v is defined as $v = R^{-1}\mathbf{U}$ using R, the matrix of the right eigenvectors of A, and λ_k are the eigenvalues. The characteristics are then represented by

$$\frac{dx}{dt} = \lambda_k.$$

In terms of the Rankine-Hugoniot relationship, the jump condition becomes

$$A(\mathbf{U}_L - \mathbf{U}_R) = s(\mathbf{U}_L - \mathbf{U}_R)$$

where $\mathbf{U}_L - \mathbf{U}_R$ then corresponds to the eigenvectors of A and s relates to the eigenvalues. In the case where A is a non-constant matrix that depends upon $\mathbf{U}$, the system is non-linear and so it is not possible to decouple the equations as in the linear case. However it may still be possible to apply the technique to yield expressions for the characteristic lines for some simplified problems, though in general this will not be the case. The Rankine-Hugoniot relationships also hold for non-linear problems, but again in general it will not be possible to obtain a closed form for the solution.

The method of characteristics applied to the Saint Venant equations

So far the application of the method of characteristics to general conservation laws has been considered. This next section proceeds to derive expressions for the characteristics of the 1-d Saint Venant equations and also highlights how the concept of characteristics can be interpreted within the context of open channel flow. This section is predominantly taken from Cunge *et al* [12] (see also [32]).

To obtain an expression for the characteristics, the starting point is to decide which form of the Saint Venant equations to work with. Since all of these forms given in the previous chapter are equivalent, the choice is arbitrary. However given that the characteristics are usually written in terms of u, the wave speed, and c, the celerity, it is logical to select the form most closely based on these variables, i.e. the form written in terms of u and h (Equation (2.16) from Chapter 2)

$$\begin{aligned} \frac{\partial h}{\partial t} + \frac{A}{B}\frac{\partial u}{\partial x} + u\frac{\partial h}{\partial x} + \frac{u}{b}\left(\frac{\partial A}{\partial x}\right)_{h=\text{const}} &= 0 \\ \frac{\partial u}{\partial t} + u\frac{\partial u}{\partial x} + g\frac{\partial h}{\partial x} + g(S_f - S_o) &= 0. \end{aligned} \tag{3.3}$$

Consider the case of a prismatic channel of constant cross section and constant bottom slope S_o, then (3.3) becomes

$$\frac{\partial h}{\partial t} + \frac{A}{B}\frac{\partial u}{\partial x} + u\frac{\partial h}{\partial x} = 0 \tag{3.4}$$

and

$$\frac{\partial u}{\partial t} + u\frac{\partial u}{\partial x} + g\frac{\partial h}{\partial x} + g(S_f - S_o) = 0. \tag{3.5}$$

If the celerity is defined as

$$c = \left(g\frac{A}{B}\right)^{\frac{1}{2}}$$

where $A = A(h)$ then differentiating c^2 with respect to x and t gives

$$2c\frac{\partial c}{\partial x} = g\frac{\partial h}{\partial x} \quad \text{and} \quad 2c\frac{\partial c}{\partial t} = g\frac{\partial h}{\partial t}$$

where $\partial A/\partial h = B$. Using these expressions to eliminate h, equations (3.4) and (3.5) then become

$$2\frac{\partial c}{\partial t} + 2u\frac{\partial c}{\partial x} + c\frac{\partial u}{\partial x} = 0 \tag{3.6}$$

$$\frac{\partial u}{\partial t} + 2c\frac{\partial c}{\partial x} + u\frac{\partial u}{\partial x} + E = 0 \tag{3.7}$$

where $E = g(S_f - S_o)$. By adding and subtracting (3.6) and (3.7) the characteristic form of the equations are obtained

$$\left\{\frac{\partial}{\partial t} + (u+c)\frac{\partial}{\partial x}\right\}(u+2c) + E = 0$$

$$\left\{\frac{\partial}{\partial t} + (u-c)\frac{\partial}{\partial x}\right\}(u-2c) + E = 0$$

where the above differential operators are in fact total derivatives along the lines defined by $dx/dt = u \pm c$ (denoted as C^+ and C^-). Writing these as

$$\frac{D^+}{Dt} = \frac{\partial}{\partial t} + (u+c)\frac{\partial}{\partial x} \quad \text{and} \quad \frac{D^-}{Dt} = \frac{\partial}{\partial t} + (u-c)\frac{\partial}{\partial x}$$

then gives

$$\frac{D^+}{Dt}(u+2c) = -E \tag{3.8}$$

$$\frac{D^-}{Dt}(u-2c) = -E. \tag{3.9}$$

For a flat frictionless channel, i.e. one where $E = 0$ then

$$u + 2c = \text{constant} = J^+$$

along the C^+ characteristic and

$$u - 2c = \text{constant} = J^-$$

along the C^- characteristic, where the constants J^+ and J^- are known as the Riemann invariants. In cases where S_o and S_f are not zero it is possible to integrate equations (3.8) and (3.9) between two points 1 and 2 on the channel to give

$$[u+2c]_1^2 = g\int_{t_1}^{t_2}(S_o - S_f)dt$$

and

$$[u-2c]_1^2 = g\int_{t_1}^{t_2}(S_o - S_f)dt$$

where the left hand sides of the equations are now the Riemann quasi-invariants. For a general non-prismatic channel, it is not possible to derive an equivalent form of the Riemann invariants.

Returning now to the characteristics it is possible to introduce some useful concepts which will be of importance later on. Three types of fluid motion can be identified, depending on the direction of the two characteristics. In subcritical

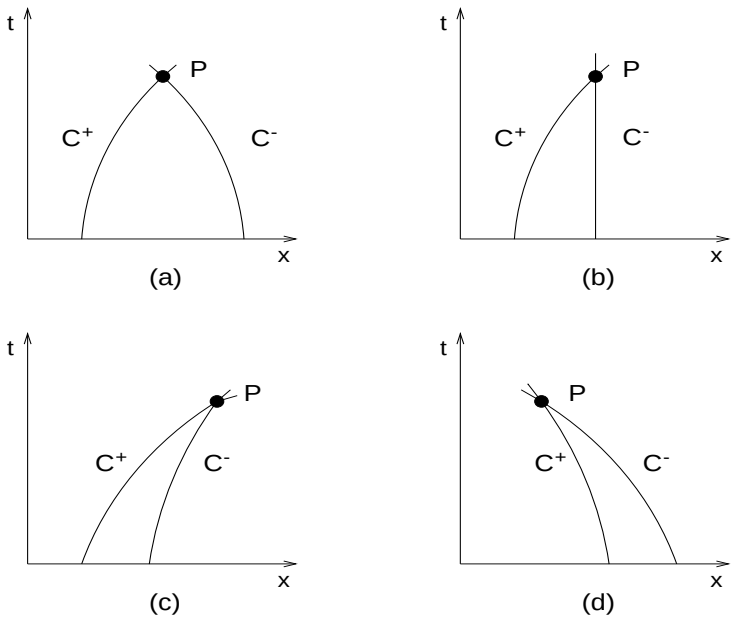

Figure 3.2: Characteristics and flow conditions. (a) Subcritical flow; (b) critical flow; (c) supercritical flow in a positive direction; (d) supercritical flow in a negative direction [12].

flow, the two characteristics have opposite signs and $c > |u|$ and any point within the flow (within the subcritical region) is affected from both the upstream and downstream directions. In critical flow, $|u| = c$ and one of the characteristic velocities is zero. For supercritical flow $|u| > c$ and the characteristics have the same sign. These possibilities are shown graphically in Figure 3.2. For both critical and supercritical flow, the conditions at any point are not influenced by the flow anywhere downstream of that point.

Through the characteristic lines it is possible to introduce the ideas of a range of influence and a domain of dependence. Consider a disturbance that occurs at some point Q at time $t = 0$. This disturbance may be transmitted both upstream and downstream (depending on the Froude number) and alter the flow conditions at a later time. The range of influence of Q is the region over which that disturbance propagates, and this is bounded by the characteristic lines emerging from Q, as seen in Figure 3.3(a). Conversely, taking a general point P it is possible to define a region which influences the flow at P and this is known as the domain of dependence. Any disturbance outside of this region will not alter the flow at P. Again this region is bounded by the characteristics that meet at P.

The ideas behind the method of characteristics can be used to form appropriate

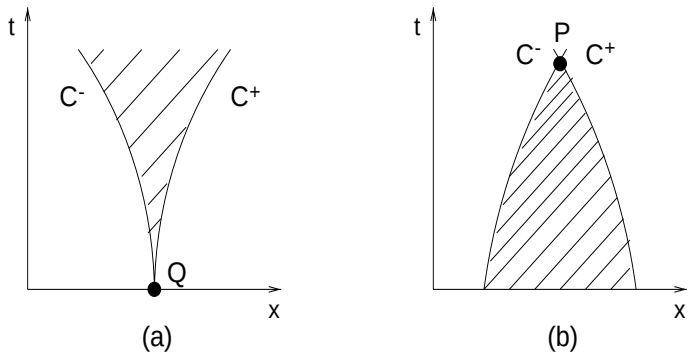

Figure 3.3: (a) Range of influence of Q; (b) domain of dependence of P [12].

boundary conditions and to account for the stability of numerical schemes, as is discussed later on.

3.1.2 An introduction to numerical methods

For most problems of practical interest it is not possible to find exact solutions by using analytical techniques such as the method of characteristics. As as result, this has lead to the development of numerical methods whereby the continuous problem, i.e. the governing equations, is transformed into a discrete form which then results in a series of algebraic equations which can be solved on a computer. The solution to the discrete problem represents an approximation to the solution of the continuous problem and various concepts have been developed in an attempt to quantify how well the calculated numerical solutions compare to the true solutions.

General classification of numerical methods

Many techniques are available for numerical simulation work, and a number of broad headings exist to describe how each particular method (or scheme) works. The four most popular types of method for general fluid flow problems are

1. Finite Difference methods (FDM)
2. Finite Element methods (FEM)
3. Spectral methods
4. Finite Volume methods (FVM).

There is a certain amount of overlap between these classifications and under certain circumstances a particular scheme may fall into more that one category so there is no strict definition as as to how to identify a method. The following general descriptions are taken from Hirsch [33] and Versteeg and Malalasekera [65].

Generally speaking a finite difference method represents the problem through a series of values at particular points or nodes. Expressions for the unknowns are derived via replacing the derivative terms in the model equations with truncated Taylor series expansions. The earliest numerical schemes are based upon finite difference construction and are conceptually and intuitively one of the easier methods to implement. However, fundamentally such techniques require a high degree of regularity within the mesh and so this limits their application to complex problems.

The basis of the finite element method is to divided the domain into elements such as triangles or quadrilaterals and to place within each element nodes at which the numerical solution is determined. The solution at any position is then represented by a series expansion of the nodal values within the local vicinity of that position. The nodal contributions are multiplied by basis functions (also known as shape, interpolation or trial functions) and the particular way in which the basis functions are defined determines the choice of variant of the finite element method. Spectral methods can be considered as a subset of the finite element method in which the basis functions are defined globally as opposed to the more common approach whereby the basis functions are local and so are zero outside the neighbourhood of the associated node. The original finite element method was developed within the field of stress analysis and this is reflected within the construction and nomenclature of the approach.

The finite volume method is based upon forming a discretisation from an integral form of the model equations, and entails subdividing the domain into a number of finite volumes. Within each volume, the integral relationships are applied locally and so exact conservation within each cell is achieved. The resulting expressions for the unknowns often appear similar to finite difference approximations and depending upon the particular method chosen, may be considered as a special case of either the finite difference or finite element techniques. With the emphasis of most fluid modelling problems being based upon conservation principles, the

finite volume method has become the more popular approach for general fluid flow problems.

Within the context of open channel flows, earlier worked focussed on the application of finite difference schemes and to some extent the finite element method. However more recently opinion has swung towards methods based on the finite volume construction.

Accuracy, consistency, stability, convergence and well posedness

In order to quantify how well a particular numerical technique performs in generating a solution to a problem, there are four fundamental criteria that can be applied to compare and contrast different methods. The four concepts are accuracy, consistency, stability and convergence. In theory these criteria apply to any form of numerical method though they are most easily formulated for finite difference schemes. The following is based upon descriptions from [7], [33], [57] and [65].

Accuracy is a measure of how well the discrete solution represents the exact solution of the problem. Two quantities exist to measure this – the local or truncation error, which measures how well the difference equations match the differential equations, and the global error which reflects the overall error in the solution and in reality is not possible to find unless the exact solution is known. An expression for the truncation error can be obtained by substituting the known exact solution of the problem into the discretisation, leaving a remainder which is then a measure of the error. Alternatively, the exact solution to the discretised problem could be substituted into the differential equation and the remainder obtained. For example for a PDE this would lead to an expression of the form $\tau = O(\Delta t^q, \Delta x^p)$ where τ is the truncation error and Δt and Δx and the time and spatial steps (assuming a regular grid). From this, the method is said to be qth order in time and pth order in space, and generally this is referred to as the level of accuracy of the scheme. It is natural to assume that by increasing the grid resolution then any errors will be reduced and this leads to the definition of consistency. Mathematically, for a method to be consistent then the truncation error must decrease as the step size is reduced, which is the case when $q, p \geq 1$, which is equivalent to saying that as $\Delta t, \Delta x$ tend to zero then the discretised equations should tend

towards the differential equation. For a scheme to be of practical use, it must be consistent.

Formally if a scheme is said to be stable then any errors in the solution will remain bounded. In practice if an unstable method is used then the solution will tends towards infinity. Most methods have stability limits which place restrictions on the size of the grid spacings (i.e. Δx, Δt) that can be used, usually in terms of a limit on the CFL (Courant-Friedrichs-Lewy) number. Physically a stable method can be interpreted to be one where the grid points used in the calculation enclose the characteristic lines or domain of dependence as discussed previously (see Figure 3.4). A number of methods are available for obtaining expressions for the stability conditions, and the appropriate choice depends on the actual problem.

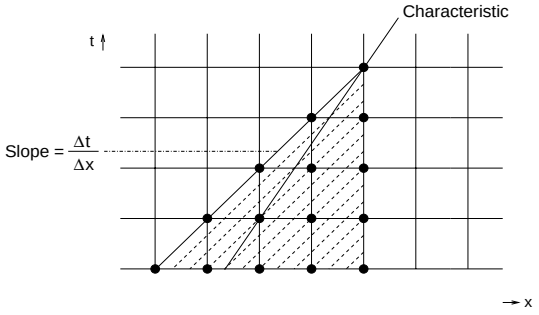

Figure 3.4: Stable upwind scheme.

Another requirement is that the numerical scheme should be convergent, which by definition means that the numerical solution should approach the exact solution as the grid spacing is reduced to zero. This is coupled with the global error. However it is usually not possible to prove the convergence of a particular scheme to a specific problem. Instead use is made of Lax's Equivalence theorem which states that *for a well posed initial value problem (IVP) and a consistent method, stability implies convergence*, in the case of a linear problem. For non-linear equations, stability and consistency are necessary but not sufficient conditions for convergence.

These criteria dictate whether a particular numerical scheme is suited to solving a particular problem. There is another condition, which has to be satisfied in order to produce a valid solution and this relates to the actual problem and is the issue of well posedness. In order to generate a numerical solution, the problem being considered must be well posed. For this to be the case then the following

conditions must hold

a) a solution must exist

b) the solution should be unique

c) the solution should depend linearly on the data in some way.

The last condition can be translated to mean that the solution should not be sensitive to small changes in the initial/boundary data of the problem. If a problem is not well posed, then a valid numerical solution can not be generated and any numerical treatment will either fail or produce poor results. One easy way to produce an ill posed problem is to apply inappropriate boundary conditions, for example by trying to enforce values of the quantities being modelled on the characteristics leaving the computational domain. If the initial data is not fully specified, then this also presents an ill posed problem as there will be no unique solution.

Grid generation and explicit/implicit formulations

An important factor in applying numerical techniques not yet mentioned here is the question of grid generation, which is an area of research in its own right. Early efforts focussed on using regular grids, whereby all the cells or elements were of the same size. Although this has advantages in terms of numbering the cells and forming the discrete equations, for problems requiring a fine resolution having small cells everywhere leads to unnecessary computation and is computationally expensive. In addition, for 2-d and 3-d problems, fitting a regular grid to complex geometries can often lead to problems. To overcome the difficulties created in implementing regular grids, attention has moved towards irregular grids where the cell sizes vary within the domain. Furthermore unstructured (as opposed to structured) gridding has been introduced, leading to the ability to map any region. However the resulting meshes generally have no apparent structure and so increase the level of complexity of generating suitable computer code. The predominant reason for using irregular gridding is the ability to concentrate the cells in areas where sharp gradients occur, and so a high level of accuracy can be maintained throughout the region without the need to use a fine grid everywhere. If such a grid is generated at the outset of a problem, it may be that as the simulation progresses, the initial choice is no longer the most suitable, and so this has led to

the idea of adaptivity whereby the grid evolves during the simulation, in a manner determined by the numerical solution.

Another distinction that can be drawn between different methods is whether they are explicit or implicit. For example, taking the linear advection equation

$$u_t + au_x = 0 \qquad a = \text{constant}$$

then if the solution is to be advanced to time level $n+1$, the spatial derivative may be approximated either in terms of the known values at time level n or the unknown quantities at level $n+1$. If an approximation for the spatial derivative is approximated at time level n then that corresponds to an explicit method, whereas using level $n+1$ represents an implicit formulation. Both explicit and implicit schemes have there relative merits. Explicit methods are generally simpler in terms of the resulting algebraic equations as implicit schemes usually require a matrix inversion which is more costly. However most implicit schemes are not restricted by the CFL stability constraints placed upon the explicit counterparts, and so allow the use of much larger time steps.

3.1.3 Numerical methods for conservation laws

This work is mainly concerned with modelling conservation laws which may be expressed either in differential or integral form, i.e. for a 1-d system in Cartesian coordinates

$$\mathbf{U}_t + \mathbf{F}_x = \mathbf{R} \tag{3.10}$$

or

$$\oint (\mathbf{U}dx - \mathbf{F}dt) = \int_\Omega \mathbf{R}d\Omega$$

where the integral form is more general than the differential form as it is valid for discontinuous solutions. In particular, the focus of the study is to investigate ways to improve (in terms of accuracy and reduced run times) the explicit schemes currently popular within the hydraulics community, which are predominantly formulated within the finite difference/finite volume framework and make use of Riemann based solutions. This section now goes on to identify some of the desirable/required properties of schemes suitable for solving conservation laws and discusses the concept of finite difference and finite volume schemes in more detail. Some of the 'classical' schemes are then introduced together with some subsequent advances made in their application. A description of the Godunov

method is made as this formed the starting point of the finite volume approach and Riemann based schemes.

Desirable properties of numerical methods for conservation laws

Aside from the requirements of ensuring that any chosen scheme be consistent, stable and convergent, a number of additional criteria can be defined for identifying methods that are suitable for modelling conservation laws. The fact that most conservation laws are non-linear introduces additional problems not apparent with linear equations and also complicates the mathematical analysis. In particular non-linear equations often give rise to discontinuous solutions, which in the case of the Saint Venant equations correspond to bores and hydraulic jumps. Some techniques experience difficulties in solving discontinuous flows and spurious oscillations can appear in the numerical solution. There is also the issue of generating the right solution, as discontinuous solutions correspond to weak solutions of the differential equations, meaning that there may be more than one correct (in terms of satisfying the differential equation) solution. Under such circumstances additional information is required to isolate the correct result.

There exists certain criteria for assessing if a particular scheme is suited to solving conservation law problems and these give rise to conservative methods (see [41]). If a method is conservative then when it is applied to a conservation law (expressed in conservation form), then the sum of contributions from the discrete representation of the flux terms should cancel everywhere except at the boundaries. Apart from ensuring that the discrete system is conservative, then if the solution is discontinuous, using a conservative method also means that the numerical solution will correspond to a weak solution of the equations, and this is the basis of a theorem by Lax and Wendroff. However this does not guarantee that the scheme will produce the physically correct weak solution for a given problem. In the case where more than one weak solution exists, the correct solution is determined via an entropy condition, so named after its origin in gas dynamics. Effectively this condition can be translated in terms of the characteristics mentioned previously, and says that the characteristics cannot emerge from a physically valid shock.

A strategy which can enable the use of some schemes which cannot resolve discontinuities correctly is to use a shock tracking approach. The idea then is to use the chosen scheme throughout most of the region and to isolate the position of

any discontinuities, which are then treated separately. Conversely shock capturing methods are ones in which no account is made of where any discontinuities occur and the same scheme is employed throughout the domain and any shocks formed occur at the correct location.

Another concern connected with discontinuous solutions is the generation of oscillations in regions containing strong gradients. Such oscillations are a problem as they can lead to non-physical quantities such as negative depths, and specific criteria have been developed to assess whether or not particular schemes will give rise to oscillations. Methods which satisfy these conditions are known as Total Variation Diminishing (TVD) schemes (see [41] for a mathematical analysis).

The manner in which the flux term is discretised can either be described as upwinded or centralised. The distinction between the two lies in which cells are used to approximate the flux at a particular point. Upwind methods take account of the flow direction, and so use values corresponding to the direction from which the characteristics originate. Central schemes use a symmetric discretisation and so make no allowances for the characteristic direction. For convective dominated flows, taking an upwind approach is generally considered to be the better option as the flow direction is considered.

Finite Difference methods

Finite difference methods were the first technique to be developed for approximating ordinary differential equations, and it is from such applications that the theories regarding their properties have been generated. This summary is taken from [33].

Finite difference methods are based on performing Taylor series expansions and substituting the truncated expressions into the differential equation. The idea is to approximate the differentials by differences in the solution at various points. By definition

$$u_x \equiv \left(\frac{\partial u}{\partial x}\right) = \lim_{\Delta x \to 0} \frac{u(x+\Delta x) - u(x)}{\Delta x}.$$

When Δx is small this formula can be used as an approximation for the derivative of u at x. From Taylor series

$$u(x+\Delta x) = u(x) + \Delta x u_x(x) + \frac{\Delta x^2}{2} u_{xx}(x) + ...$$

and so by rearrangement

$$\frac{u(x+\Delta x)-u(x)}{\Delta x} = u_x(x) + \frac{\Delta x}{2}u_{xx}(x) + ...$$

If Δx is small the successive terms in the expansion will decrease and so it is possible to write

$$u_x(x) = \frac{u(x+\Delta x)-u(x)}{\Delta x} + O(\Delta x). \tag{3.11}$$

From equation (3.11), the leading term of the error in approximating u_x by the right hand side is of order Δx and so this represents a first order approximation. It is possible to define other difference formula to approximate derivatives and these may have different orders of accuracy.

The above analysis deals with the continuous solution however the objective is to calculate u at a set of discrete points on the mesh, and this is the numerical solution. Let the mesh points be denoted by x_i where $i = 1, 2, ..., N$ and the region has been discretised into N equally sized elements of length Δx. Then the numerical solution, u_i can be thought of as point values where $u_i = u(i\Delta x)$. Following this notation, there are three common ways to approximate the first derivative of u with respect to x,

(i) Forward difference

$$(u_x)_i = \frac{u_{i+1}-u_i}{\Delta x} + O(\Delta x)$$

(ii) Backward difference

$$(u_x)_i = \frac{u_i-u_{i-1}}{\Delta x} + O(\Delta x)$$

(iii) Central difference

$$(u_x)_i = \frac{u_{i+1}-u_{i-1}}{2\Delta x} + O(\Delta x^2).$$

As can be seen, both the forward and backward differences are first order approximations whereas the central difference is second order, as can be shown by Taylor series analysis. These formula have different merits and the best choice depends on the problem being modelled. In the case of ODE's, many other difference formula can be derived and standard techniques are available for doing so. However for PDE's, most schemes are based upon using standard forward, backward and central difference formula.

Classical finite difference methods for conservation laws

The classical numerical methods used to solve partial differential equations are based upon finite difference construction and can be best illustrated through means of an example, in this case via the linear advection equation,

$$u_t + (au)_x = 0 \tag{3.12}$$

where $f = au$ and a is constant. This equation is often used as a test problem to validate methods for modelling transport dominated flows, as the analytical solution at a time t is given by the translation of the initial data by a distance at.

The general distinctions that can be made between different schemes refer to the way in which the terms in the differential equation are approximated, and this in turn corresponds to the temporal and spatial levels of the values within the difference equation. The way in which most schemes are described is to say whether they are explicit or implicit, upwind or centralised, TVD or not, and to specify the stability constraints and level of accuracy of the method. Some schemes are only applied to the spatial derivatives (or flux terms) and require a separate treatment of the temporal derivatives, whilst others combine both the time and space integrations. The following is mainly taken from [41] and [33] (see [1], [12] and [66] for the application to shallow water modelling).

One of the simplest schemes to implement for the linear advection equation is the first order upwind scheme. As the name suggest this method is first order in space (and time) and is based on using an upwind difference formula. For (3.12) this scheme can be written as

$$u_i^{n+1} = u_i^n - \nu \begin{cases} u_{i+1}^n - u_i^n & \text{if} \quad a < 0 \\ u_i^n - u_{i-1}^n & \text{if} \quad a > 0 \end{cases}$$

where $\nu = a\Delta t/\Delta x$ and is the Courant number or CFL value. Although this method has the advantages of being both upwinded and TVD, it is only first order accurate and so heavily smears discontinuous profiles.

To obtain a scheme with a higher formal order of accuracy, the central difference formula can be used. For example, the Leapfrog scheme uses central differencing for both the time and space derivatives to give

$$u_i^{n+1} = u_i^{n-1} - \nu(u_{i+1}^n - u_{i-1}^n).$$

One of the problems with this method is that the update involves three time levels which is both cumbersome in terms of memory storage and also in starting the simulation. In practice, methods involving more that two time levels in the update are not used to solve time dependent conservation laws problems. If the time derivative in the Leapfrog method is replaced with the one sided difference

$$u_t \approx \frac{u_i^{n+1} - u_i^n}{\Delta t} \tag{3.13}$$

then the resulting scheme is unstable. If u_i^n in (3.13) is replaced by the average $(u_{i+1}^n + u_{i-1}^n)/2$ then the Lax-Friedrichs scheme is obtained

$$u_i^{n+1} = \frac{1}{2}(u_{i+1}^n + u_{i-1}^n) - \frac{1}{2}\nu(u_{i+1}^n - u_{i-1}^n)$$

for which the solution is only first order in space and time. By returning to Taylor series and the expansion for u_i^{n+1}

$$u_i^{n+1} = u_i^n - a\Delta t u_t|_i^n + \frac{a^2\Delta t^2}{2}u_{tt}|_i^n + O(\Delta t^3), \tag{3.14}$$

and noting that from the original conservation law

$$u_t = -au_x \text{ and } u_{tt} = -a^2 u_{xx}$$

the Lax-Wendroff scheme can obtained by replacing the temporal derivatives in (3.14) with spatial derivatives, which are then substituted for central differences to give

$$u_i^{n+1} = u_i^n - \frac{1}{2}\nu(u_{i+1}^n - u_{i-1}^n) + \frac{1}{2}\nu^2(u_{i+1}^n - 2u_i^n + u_{i-1}^n).$$

The resulting scheme is second order in both space and time and is prone to oscillations in areas upstream of regions containing sharp gradients. Another scheme which is second order in space and time but based upon using a one-sided difference formula in (3.14) is the Warming and Beam (second order upwind) method. With this method oscillations due to discontinuities occur after the shocks and the resulting discretisation (for $a > 0$) is

$$u_i^{n+1} = u_i^n - \frac{1}{2}\nu(3u_i^n - 4u_{i-1}^n + u_{i-2}^n) + \frac{1}{2}\nu^2(u_i^n - 2u_{i-1}^n + u_{i-2}^n).$$

By averaging the Lax-Wendroff and Warming and Beam methods, the Fromm scheme is obtained which is also second order accurate. The resulting scheme still suffers from oscillations which occur both in front of and behind any shocks, but the magnitude of the oscillations is reduced (as compared with the Lax-Wendroff and Warming and Beam schemes).

All of the schemes listed so far are explicit. Corresponding implicit versions of these explicit difference methods can be obtained by evaluating the right hand sides of the update formulas at time level $n+1$. However in general a scheme produced in this way may have very different properties from its explicit counterpart. As explicit schemes are more practical to implement, most of the popular finite difference methods are constructed in this manner.

The simplest implicit scheme, known as the Backward Euler scheme can be written as

$$u_i^{n+1} = u_i^n - \frac{1}{2}\nu(u_{i+1}^{n+1} - u_{i-1}^{n+1})$$

for the linear advection equation, and is second order in space and first order in time. However this method leads to a tridiagonal matrix system, which may be easy to solve in the linear case (e.g. by using the Thomas algorithm) but will require the use of an iterative method for non-linear problems.

Another implicit method is the box scheme,

$$\left(\frac{u_{i+1}^{n+1} - u_{i+1}^n}{2\Delta t} + \frac{u_i^{n+1} - u_i^n}{2\Delta t}\right) + a\left(\frac{u_{i+1}^{n+1} - u_i^{n+1}}{2\Delta x} + \frac{u_{i+1}^n - u_i^n}{2\Delta x}\right) = 0$$

which is of particular importance to computational hydraulics as it forms the basis of the Preissmann scheme, which for a homogeneous conservation law is written as

$$\frac{U_{i+1}^{n+1} + U_i^{n+1}}{2\Delta t} - \frac{U_{i+1}^n + U_i^n}{2\Delta t} + \frac{\theta F_{i+1}^{n+1} + (1-\theta)F_{i+1}^n}{\Delta x} - \frac{\theta F_i^{n+1} + (1-\theta)F_i^n}{\Delta x} = 0$$

where $0.5 \leq \theta \leq 1$. The Preissmann scheme is the discretisation method used within the ISIS modelling package (one of the most popular river modelling packages in the UK). This method is known to experience difficulties in transcritical regions. However ISIS overcomes this problem by neglecting the non-linear flux term in the momentum equation whenever the flow is supercritical, resulting in the smearing of hydraulic jumps.

Extensions of classical methods – TVD schemes and systems of equations

All the methods introduced so far in this section have been constant coefficient schemes as were commonly used before the 1980's. One particular consequence of using constant coefficient schemes is Godunov's theorem, which states that it

is not possible to construct a constant coefficient scheme that is at least second order and will not give rise to spurious oscillations. As most conservation laws are non-linear and admit discontinuous solutions, an effort was made to overcome this difficulty by developing new higher order non-linear schemes which would satisfy the TVD conditions and so not generate oscillations around shocks. This led to the generation of high resolution TVD methods. TVD schemes can be subdivided into two classifications [60]

1. Post-processing schemes : These include Flux Corrected Transport (FCT) and flux limited schemes whereby the solution is obtained by a modified first order scheme.

2. Pre-processing schemes : The data is altered before application of the numerical method. Approaches of this kind include MUSCL, PPM and ENO schemes.

Within the context of this thesis and open channel flow, the flux limiter approach is to be considered and so this is now introduced in more detail (following the description in [60]). One way to view this approach is to consider a low order TVD method, such as the first order upwind scheme, and to add to this a limited amount of a higher order (non-TVD) scheme. This is done in such a way that the resulting method is TVD. For example, as seen before the first order upwind scheme for the linear advection equation can be written as

$$u_i^{n+1} = u_i^n - \nu \Delta u_{i-1/2}^n,$$

assuming that a is positive and using the notation $\Delta u_{i-1/2}^n = u_i - u_{i-1}$. The Lax-Wendroff scheme, can be rewritten as

$$u_i^{n+1} = u_i^n - \nu \Delta u_{i-1/2}^n - \frac{1}{2}\nu(1-\nu)\Delta_-(\Delta u_{i+1/2}^n) \tag{3.15}$$

where $\Delta_-(\Delta u_{i+1/2}^n) = \Delta u_{i+1/2}^n - \Delta u_{i-1/2}^n$, from which the right hand side of (3.15) can be seen to contain contributions from the first order scheme and an additional term which represents an anti-diffusive flux. The anti-diffusive flux term can then be limited with a flux limiter, ϕ_i, to give

$$u_i^{n+1} = u_i^n - \nu \Delta u_{i-1/2}^n - \frac{1}{2}\nu(1-\nu)\Delta_-(\phi_i \Delta u_{i+1/2}^n).$$

A number of limiters have been developed and each is based on a ratio of consecutive gradients of the solution, such that

$$\phi_i = \phi(r_i)$$

where

$$r_i = \frac{\Delta u^n_{i-1/2}}{\Delta u^n_{i+1/2}}.$$

Some of the more commonly used flux limiters (see [59] for further details) are

van Leer : $\phi(r) = \dfrac{r + |r|}{1 + |r|}$

Roe's Minmod : $\phi(r) = \max(0, \min(r, 1))$

Roe's Superbee $\phi(r) = \max(0, \min(2r, 1), \min(r, 2))$

and certain choices reproduce particular schemes, for example

$\phi(r) \equiv 0$ - First order upwind

$\phi(r) \equiv 1$ - Lax Wendroff

$\phi(r) \equiv r$ - Warming and Beam.

Although the schemes shown here have been presented within the context of the linear advection equation, they may be easily extended to linear systems of conservation laws. The application to non-linear systems is more complex and can involve the calculation of a Jacobian matrix. In addition, upwind schemes must take account of the wave speeds or characteristic directions and so become more complicated for non-linear problems, as illustrated in the next section.

Returning to symmetric discretisations (see [41] and [33]), the Lax-Friedrichs scheme for a non-linear system of the form

$$\mathbf{U}_t + \mathbf{F}(\mathbf{U})_x = 0$$

can be written as

$$\mathbf{U}^{n+1}_i = \frac{1}{2}(\mathbf{U}^n_{i-1} + \mathbf{U}^n_{i+1}) - \frac{\lambda}{2}(\mathbf{F}(\mathbf{U}^n_{i+1}) - \mathbf{F}(\mathbf{U}^n_{i-1}))$$

where $\lambda = \Delta t/\Delta x$. For the Lax-Wendroff scheme, defining the Jacobian matrix as $A(\mathbf{U}) = \mathbf{F}'(\mathbf{U})$, allows the scheme to be extended in the form

$$\mathbf{U}^{n+1}_i = \mathbf{U}^n_i - \frac{\lambda}{2}(\mathbf{F}(\mathbf{U}^n_{i+1}) - \mathbf{F}(\mathbf{U}^n_{i-1})) + \frac{\lambda^2}{2}[A_{i+1/2}(\mathbf{F}(\mathbf{U}^n_{i+1}) - \mathbf{F}(\mathbf{U}^n_i))$$

$$-A_{i-1/2}(\mathbf{F}(\mathbf{U}^n_i) - \mathbf{F}(\mathbf{U}^n_{i-1}))]$$

where $A_{i\pm1/2}$ is the Jacobian evaluated using the values $(\mathbf{U}_i^n + \mathbf{U}_{i\pm1}^n)/2$. However evaluating the Jacobian is costly and so an equivalent method has been developed based on a two step procedure, which can be represented by

$$\mathbf{U}_{i+1/2}^{n+1/2} = \frac{1}{2}(\mathbf{U}_i^n + \mathbf{U}_{i+1}^n) - \frac{\lambda}{2}(\mathbf{F}(\mathbf{U}_{i+1}^n) - \mathbf{F}(\mathbf{U}_i^n))$$

$$\mathbf{U}_i^{n+1} = \mathbf{U}_i^n - \lambda(\mathbf{F}(\mathbf{U}_{i+1/2}^{n+1/2}) - \mathbf{F}(\mathbf{U}_{i-1/2}^{n+1/2}))$$

and is known as Richtmyer's scheme. A similar method to this is McCormack's scheme, which first uses a forward difference followed by a backward difference

$$\mathbf{U}_i^* = \mathbf{U}_i^n - \lambda(\mathbf{F}(\mathbf{U}_{i+1}^n) - \mathbf{F}(\mathbf{U}_i^n))$$

$$\mathbf{U}_i^{n+1} = \frac{1}{2}(\mathbf{U}_i^n + \mathbf{U}_i^*) - \frac{\lambda}{2}(\mathbf{F}(\mathbf{U}_i^*) - \mathbf{F}(\mathbf{U}_{i-1}^*)).$$

Finite Volume methods

The fundamental difference between these methods and FDM's is that in FDM's the differential form of the equations are discretised, whereas for FVM's the discretisation is performed on an integral formulation of the equations. The resulting discretisation often resembles those obtained through the use of FDM's, and in addition the FVM may be thought of as a subdivision of the FEM [33]. The basis of the finite volume method is to construct an integral form of the governing equations which is valid for any arbitrary closed volume. On a Cartesian mesh, the conservation law can then be represented by

$$\oint(\mathbf{U}dx - \mathbf{F}dt) = \int_\Omega \mathbf{R}d\Omega.$$

The resulting expression is then applied locally within each cell or finite volume, ensuring that exact conservation of the conserved variables is maintained.

Within this framework, the discrete values of u are considered to be cell average values represented by

$$\mathbf{U}_i^n = \frac{1}{\Delta x}\int_{x_{i-1/2}}^{x_{i+1/2}} \mathbf{U}(x, t_n)dx, \tag{3.16}$$

where $x_{i\pm1/2}$ correspond to the cell boundaries. Generally the numerical solution is considered to be constant within each cell, however some methods assume other distributions for which the cell average is defined by (3.16). By treating the

numerical flux function as a time average value of the physical flux function, i.e. by defining the numerical flux as

$$\mathbf{F}_{i+1/2} = \frac{1}{\Delta t}\int_{t_n}^{t_{n+1}} \mathbf{F}[\mathbf{U}(x_{i+1/2}, t)]dt$$

the resulting discretisation of the integral formulation of the homogeneous form of the conservation law can be written as

$$\mathbf{U}_i^{n+1} = \mathbf{U}_i^n + \frac{\Delta t}{\Delta x}[\mathbf{F}_{i-1/2} - \mathbf{F}_{i+1/2}]. \tag{3.17}$$

which then resembles a finite difference scheme. As with finite difference methods, the way in which $\mathbf{F}_{i\pm1/2}$ is approximated correlates to a particular choice of numerical scheme. One way to generate the numerical flux is to solve a series of Riemann problems, and this will be discussed later.

Godunov type schemes and the finite volume framework

One of the first attempts to develop an upwind scheme suitable for solving systems of conservation laws was by Courant, Isaacson and Rees. The CIR method was based upon tracing the characteristics from one time level to the next and employed the characteristic form of the equations. Originally this technique was considered for the Euler equations, however as the construction was not based on the conservation form of the equations, the method was not well suited for solving problems containing discontinuities. Subsequently, in 1959 Godunov published a new technique which differed from previous schemes in that it assumed the numerical solution was constant within each cell, instead of considering nodal values. The basis of the method was to solve a series of Riemann problems between each of the cell interfaces and this led to an expression for the numerical flux. The method was explicit and required that the time step was limited in such a way that neighbouring Riemann problems would not interact. The method is introduced here because it was the starting point for the Riemann based schemes with which this project is concerned. This section is taken from [41] and [63].

The first stage of the Godunov method is to assign the discrete cell average values which are represented by the integral relationship

$$\mathbf{U}_i^n = \frac{1}{\Delta x}\int_{x-1/2}^{x_{i+1/2}} \mathbf{U}(x, t_n)dx$$

where $x_{i\pm1/2}$ are the cell boundaries and $\mathbf{U}(x, t_n)$ is the known solution at time t_n which is constant within each cell. This representation is illustrated in Figure 3.5.

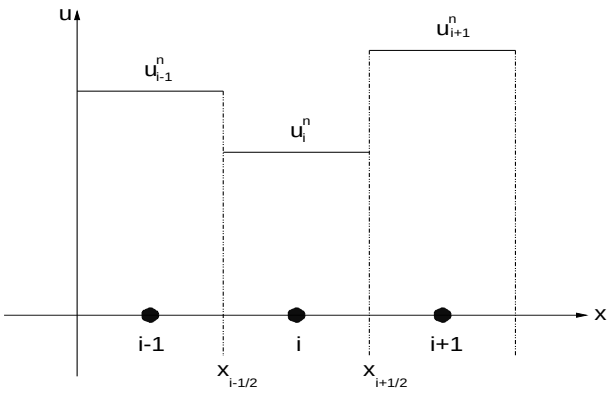

Figure 3.5: Piece-wise constant distribution at time level n [63].

The result is that at each interface, the discrete representation of the data corresponds to the initial data of a Riemann problem. Having calculated the exact solution of the Riemann problem over the time interval $[t_n, t_{n+1}]$, the solution at the next time level is then given by averaging the exact solution of the Riemann problem over each cell such that

$$\mathbf{U}_i^{n+1} = \frac{1}{\Delta x} \int_{x_{i-1/2}}^{x_{i+1/2}} \bar{\mathbf{U}}^n(x, t_{n+1}) dx \tag{3.18}$$

where $\bar{\mathbf{U}}^n(x, t_{n+1})$ is taken to be the exact solution of the Riemann problem at time t_{n+1}. As $\bar{\mathbf{U}}^n$ represents an exact solution to the conservation law, then applying the integral form of the conservation law within a particular cell gives

$$\int_{x_{i-1/2}}^{x_{i+1/2}} \bar{\mathbf{U}}^n(x, t_{n+1}) dx = \int_{x_{i-1/2}}^{x_{i+1/2}} \bar{\mathbf{U}}^n(x, t_n) dx + \int_{t_n}^{t_{n+1}} \mathbf{F}(\bar{\mathbf{U}}^n(x_{i-1/2}, t)) dt - \int_{t_n}^{t_{n+1}} \mathbf{F}(\bar{\mathbf{U}}^n(x_{i+1/2}, t)) dt.$$

From (3.18) and using $\bar{\mathbf{U}}^n(x, t_n) \equiv \mathbf{U}_i^n$ then the update for cell i becomes

$$\mathbf{U}_i^{n+1} = \mathbf{U}_i^n - \lambda[\mathbf{F}(\mathbf{U}_i^n, \mathbf{U}_{i+1}^n) - \mathbf{F}(\mathbf{U}_{i-1}^n, \mathbf{U}_i^n)]$$

when the numerical flux is defined as

$$\mathbf{F}(\mathbf{U}_i^n, \mathbf{U}_{i+1}^n) = \frac{1}{\Delta t} \int_{t_n}^{t_{n+1}} \mathbf{F}(\bar{\mathbf{U}}^n(x_{i+1/2}, t)) dt.$$

The problem then reduces to determining $\bar{\mathbf{U}}^n$ over the time interval $[t_n, t_{n+1}]$ at the point $x_{i+1/2}$, which by virtue of the Riemann problem is constant (assuming that the neighbouring Riemann problems do not interact). Denoting this value as $\mathbf{U}^*(\mathbf{U}_i^n, \mathbf{U}_{i+1}^n)$ then the flux becomes

$$\mathbf{F}(\mathbf{U}_i^n, \mathbf{U}_{i+1}^n) = \mathbf{F}(\mathbf{U}^*(\mathbf{U}_i^n, \mathbf{U}_{i+1}^n)) \tag{3.19}$$

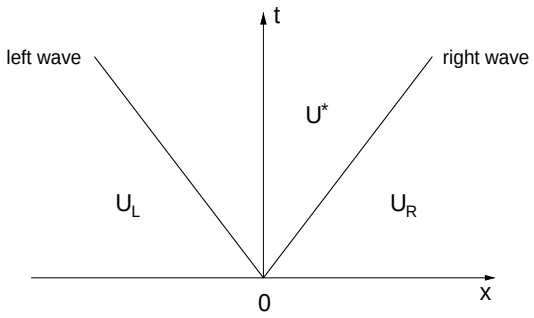

Figure 3.6: Solution of the Riemann problem [63].

and so the update can then be written as

$$\mathbf{U}_i^{n+1} = \mathbf{U}_i^n - \lambda[\mathbf{F}(\mathbf{U}^*(\mathbf{U}_i^n, \mathbf{U}_{i+1}^n)) - \mathbf{F}(\mathbf{U}^*(\mathbf{U}_{i-1}^n, \mathbf{U}_i^n))].$$

The Riemann problem and Riemann solvers

Having introduced Godunov's method and obtained the update formula which is based upon the solution of a Riemann problem, it is now necessary to explain what a Riemann problem is. The Riemann problem is defined as an initial value problem of the form

$$\mathbf{U}_t + \mathbf{F}_x = 0 \tag{3.20}$$

with the initial conditions

$$\mathbf{U}(x,0) = \begin{cases} \mathbf{U}_L & x < x' \\ \mathbf{U}_R & x > x' \end{cases}$$

where the initial values may be discontinuous across x', and (3.20) may correspond to a scalar conservation law or a system. The solution of the Riemann problem is problem dependent however the solutions to different Riemann problems (corresponding to different choices of $\mathbf{F}$) have certain properties in common. Away from the point x' the constant states $\mathbf{U}_L$ and $\mathbf{U}_R$ are maintained. These two regions are linked by 'waves', where the number of waves present in the solution is the same as the the number of equations in the conservation law, or the number of characteristics. In the case of the Saint Venant equation, two waves exist as illustrated in Figure 3.6. The region between the two waves is referred to as the star region, and within this section the variables are constant. The type of waves present depends upon the system being considered, and for the Saint Venant equations the waves are either bores or depressions. The possible configurations are shown in Figure 3.7. Except in the case where the left and right

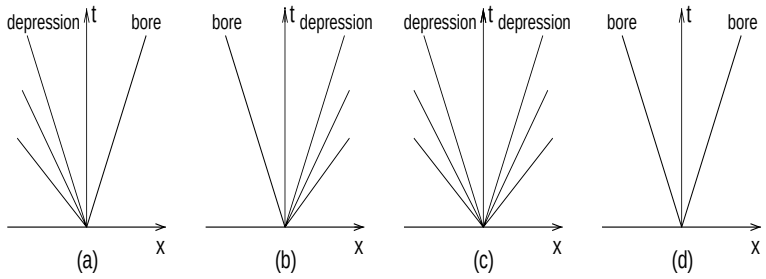

Figure 3.7: Possible wave configurations [63].

velocities are zero, i.e. the dam break problem, there is no direct way to solve the Riemann problem for the Saint Venant equations. However if the wave structure is known, then a solution can be found. It is possible to construct exact Riemann solvers which are based on an iterative procedure, however this process is costly. The original Godunov method involved finding the exact solution to the Riemann problem at each interface. As most of the information obtained from the solution is redundant within the final update, attention has been drawn towards devising approximate Riemann solvers, which can be used within the Godunov framework. One possibility for doing this, is to find an approximation for $\mathbf{U}^*$ within the Godunov flux (3.19). Another approach is to replace the function $\bar{\mathbf{U}}(x,t)$ used to define the cell average values of $\mathbf{U}_{i+1}^n$, with an approximate solution $\tilde{\mathbf{U}}^n(x,t)$ such that the discrete solution is evaluated using

$$\mathbf{U}_i^{n+1} = \frac{1}{\Delta x}\int_{x_{i-1/2}}^{x_{i+1/2}} \tilde{\mathbf{U}}^n(x, t_{n+1})dx.$$

Following the second philosophy, Roe [51] developed an approximate Riemann solver for the Euler equations, which has subsequently been used within open channel flow.

3.2 Application of numerical techniques to open channel flow

Having introduced the ideas and methodologies behind numerical techniques, this section now goes on to review the application of computational methods to open channel flow. The purpose of this section is to illustrate the progression of computational hydraulics in recent years and to highlight what has been achieved within the field. In addition, surveying the literature provides a means to identify suitable test cases for analysing the performance of numerical schemes.

The review is divided into two subsections. The first part covers one-dimensional studies and details of the various methods are included within the review. The second subsection is intended to give a global overview of how the original one-dimensional methods have been extended to higher dimensions, particularly within the finite volume framework. Most of the technical details are omitted for this subsection, as the study is predominantly concerned with improving the one-dimensional methods. However it is necessary to be aware how such techniques may be extended to problems of practical interest within the hydraulic community.

3.2.1 One-dimensional studies

Fennema and Chaudhry [15] presented a paper introducing three explicit schemes to the Saint Venant equations, and compared the results for problems containing shocks with solutions from the implicit Preissmann scheme. The three methods considered were the McCormack, Lambda and Gabutti schemes, all of which are formally second order accurate.

The McCormack scheme was applied to the (A, Q) formulation of the Saint Venant equations and was written as a predictor-corrector scheme in the form

Predictor step

$$\mathbf{U}^* = \mathbf{U}_i^n - \frac{\Delta t}{\Delta x}(\mathbf{F}_i^n - \mathbf{F}_{i-1}^n) + \Delta t \mathbf{R}_i^n$$

Corrector step

$$\hat{\mathbf{U}}_i - \frac{\Delta t}{\Delta x}(\mathbf{F}_{i+1}^* - \mathbf{F}_i^*) + \Delta t \mathbf{R}_i^*$$

from which the values at the new time level were given by

$$\mathbf{U}_i^{n+1} = \frac{1}{2}(\mathbf{U}_i^n - \hat{\mathbf{U}}_i).$$

The Lambda scheme considered the direction of the characteristics and was applied to a non-conservative form of the equations written as

$$\mathbf{V}_t + \mathbf{B}\mathbf{V}_x + \mathbf{Z} = 0, \tag{3.21}$$

where

$$\mathbf{V} = \begin{pmatrix} h \\ u \end{pmatrix}, \quad \mathbf{B} = \begin{pmatrix} u & d \\ g & u \end{pmatrix}, \quad \mathbf{Z} \begin{pmatrix} 0 \\ -g(S_o - S_f) \end{pmatrix}$$

and d is the hydraulic depth, defined as A/B. From (3.21), the following equations can be obtained,

$$h_t + \lambda^+ h_x + \frac{d}{c}(u_t + \lambda^+ u_x) - c(S_o - S_f) = 0 \tag{3.22}$$

$$h_t + \lambda^- h_x - \frac{d}{c}(u_t + \lambda^- u_x) + c(S_o - S_f) = 0 \tag{3.23}$$

with $\lambda^+ = u + c$ and $\lambda^- = u - c$. These equations are valid along the characteristics defined by $dx/dt = u \pm c$. Equation (3.21) can also be rewritten as

$$\mathbf{U}_t + \mathbf{B}^+ \mathbf{U}_x^+ + \mathbf{B}^- \mathbf{U}_x^- + \mathbf{Z} = 0$$

whereby the matrix $\mathbf{B}^+$ is associated with the positive characteristics and conversely $\mathbf{B}^-$ relates to the negative characteristics. The type of difference formula used to approximate the spatial derivatives depends upon the direction of the characteristics. Following addition and subtraction of (3.22) and (3.23), this strategy leads to

$$h_t + \frac{1}{2}(\lambda^- h_x^- + \lambda^+ h_x^+) + \frac{d}{2c}(\lambda^+ u_x^+ - \lambda^- u_x^-) = 0$$

$$u_t + \frac{c}{2d}(\lambda^+ h_x^+ - \lambda^- h_x^-) + \frac{1}{2}(\lambda^+ u_x^+ + \lambda^- u_x^-) - g(S_o - S_f) = 0.$$

Using a backward difference for the positive values, and a forward difference for the negative contributions, the update is calculated though a predictor-corrector sequence represented by

Predictor

$$\bar{\mathbf{V}}_x^+ = \frac{2\mathbf{V}_i - 3\mathbf{V}_{i-1} + \mathbf{V}_{i-2}}{\Delta x}$$

$$\bar{\mathbf{V}}_x^- = \frac{\mathbf{V}_{i+1} - \mathbf{V}_i}{\Delta x}$$

Corrector

$$\hat{\mathbf{V}}_x^+ = \frac{\bar{\mathbf{V}}_i - \bar{\mathbf{V}}_{i-1}}{\Delta x}$$

$$\hat{\mathbf{V}}_x^- = \frac{-2\bar{\mathbf{V}}_i + 3\bar{\mathbf{V}}_{i+1} - \bar{\mathbf{V}}_{i+2}}{\Delta x}.$$

Finally the values at the new level are obtained from

$$\mathbf{V}_i^{n+1} = \frac{1}{2}(\mathbf{V}_i^n + \hat{\mathbf{V}}_i).$$

The Gabutti scheme is an extension of the Lambda scheme and is based on the same formulation but uses a different predictor-corrector sequence,

1) Predictor step

$$\text{Part a} \quad \tilde{\mathbf{V}}_x^+ = \frac{\mathbf{V}_i - \mathbf{V}_{i-1}}{\Delta x}$$

$$\tilde{\mathbf{V}}_x^- = \frac{\mathbf{V}_{i+1} - \mathbf{V}_i}{\Delta x}$$

$$\text{Part b} \quad \bar{\mathbf{V}}_x^+ = \frac{2\mathbf{V}_i - 3\mathbf{V}_{i-1} + \mathbf{V}_{i-2}}{\Delta x}$$

$$\bar{\mathbf{V}}_x^- = \frac{-2\mathbf{V}_i + 3\mathbf{V}_{i+1} - \mathbf{V}_{i+2}}{\Delta x}$$

2) Corrector step

$$\hat{\mathbf{V}}_x^+ = \frac{\bar{\mathbf{V}}_i - \bar{\mathbf{V}}_{i-1}}{\Delta x}$$

$$\hat{\mathbf{V}}_x^- = \frac{\bar{\mathbf{V}}_{i+1} - \bar{\mathbf{V}}_i}{\Delta x}.$$

Following this procedure, the values at the next time level are given by

$$\mathbf{V}_i^{n+1} = \frac{1}{2}(\mathbf{V}_i^n + \bar{\mathbf{V}}_i + \hat{\mathbf{V}}_i - \tilde{\mathbf{V}}_i).$$

The paper showed a number of results for flows containing bores and illustrated how the explicit schemes gave rise to numerical oscillations around the discontinuity. By the addition of artificial viscosity, the oscillations were reduced and the profiles became similar to the results produced by the Preissmann scheme. The paper also showed that although the Preissmann scheme allowed the use of CFL numbers greater than one, doing so would smear any bores present in the solution and lead to reduced accuracy. Another point highlighted by the paper was the computational simplicity of explicit schemes as opposed to implicit methods, and it was stated that for the schemes tested and the problems considered, the Preissmann scheme required 4-8 times more CPU time on average for the simulations than the explicit schemes.

In a subsequent article, Fennema and Chaudhry [16] applied the Beam and Warming scheme and the Gabutti scheme to the Saint Venant equations, and compared the results obtained for the dam-break problem with solutions from the Preissmann method. The schemes considered incorporated a switching mechanism to alter between central and upwind differencing for subcritical and supercritical flows. The basis of this mechanism was to split the Jacobian into negative and

positive parts, such that the equations were written as

$$\mathbf{U}_t + \mathbf{A}^+\mathbf{U}_x^+ + \mathbf{A}^-\mathbf{U}_x^- - \mathbf{R} = 0$$

where $\mathbf{A}^+$ accounted for the positive eigenvalues and used a backward difference, and $\mathbf{A}^-$ included the negative eigenvalues and made use of forward differencing.

The general Beam and Warming scheme was presented in the form

$$\left[\mathbf{I} + \frac{\theta\Delta t}{1+\xi}\left(\frac{\partial \mathbf{A}^+}{\partial x} + \frac{\partial \mathbf{A}^+}{\partial x}\right)^n\right]\Delta_t\mathbf{U}^{n+1} = -\frac{\Delta t}{1+\xi}\left(\frac{\partial \mathbf{F}^+}{\partial x} + \frac{\partial \mathbf{F}^-}{\partial x}\right)^n + \frac{\xi}{1+\xi}\Delta_t\mathbf{U}^n \tag{3.24}$$

where $\mathbf{I}$ is the identity matrix and $\Delta_t\mathbf{U}^{n+1} = \mathbf{U}^{n+1} + \mathbf{U}^n$. Different choices of θ and ξ corresponded to specific schemes. In particular the values in Table 3.1 were considered in the study.

Scheme	θ	ξ
Euler implicit (backward Euler)	1	0
Three-point backward	1	$\frac{1}{2}$
Trapezoidal formula (Crank Nicolson)	$\frac{1}{2}$	0

Table 3.1: Beam and Warming scheme.

The differences in (3.24) were approximated using

$$\begin{aligned}\frac{\partial}{\partial x}\mathbf{A}^{+n}\Delta_t\mathbf{U}_i^{n+1} &= \frac{\mathbf{A}_i^{+n}\Delta_t\mathbf{U}_i^{n+1} - \mathbf{A}_{i-1}^{+n}\Delta_t\mathbf{U}_{i-1}^{n+1}}{\Delta x}\\ \frac{\partial}{\partial x}\mathbf{A}^{-n}\Delta_t\mathbf{U}_i^{n+1} &= \frac{\mathbf{A}_{i+1}^{-n}\Delta_t\mathbf{U}_{i+1}^{n+1} - \mathbf{A}_i^{-n}\Delta_t\mathbf{U}_i^{n+1}}{\Delta x}.\end{aligned} \tag{3.25}$$

or alternatively, by writing the coefficients of $\mathbf{A}$ in (3.25) at time level $n+1$, resulting in the need to use an iterative procedure. Non-conservative difference schemes were used to approximate the flux terms in (3.24), which took the form

$$\mathbf{F}_x^{-n} = \mathbf{A}_i^{-n}\frac{(\mathbf{U}_{i+1}^n - \mathbf{U}_i^n)}{\Delta x}$$

and

$$\mathbf{F}_x^{+n} = \mathbf{A}_i^{+n}\frac{(\mathbf{U}_i^n - \mathbf{U}_{i-1}^n)}{\Delta x}.$$

The Gabutti scheme was implemented in the same fashion as in the previous paper by the authors.

Results were presented for the Preissmann, Three point backward, Gabutti, Euler (non-iterative), Euler (iterative) and Trapezoidal schemes, for the dam-break problem with a reservoir to tailwater depth of 2:1. Artificial viscosity had to be added to the Gabutti scheme to remove the numerical oscillations near the bore. For this example, the Gabutti scheme gave results comparable to those obtained for the Preissmann scheme, whilst the implicit schemes were seen to be more diffusive. In this case the flow was subcritical throughout the region. To illustrate how the methods performed for transcritical flow, solutions for a reservoir to tailwater depth of 20:1 for the Euler (iterative and non-iterative) and Gabutti schemes were shown. This illustrated that the Gabutti scheme under predicted the speed of the bore in addition to over-estimating the depth in the constant region, whilst the two versions of the Euler scheme only slightly underestimated the shock speed. When the depth ratio was increased to 250:1, the Euler (non-iterative), Three point backward and Trapezoidal schemes all gave too slow a shock speed. Further analysis comparing the analytic and numerical solutions for a range of depth values showed the best results from the methods considered were obtained using the non-iterative Euler scheme ($\theta = 1$, $\xi = 0$) and that the Gabutti scheme failed to give a solution for a depth ratio of 50:1 was simulated.

Glaister published a series of articles based on applying the Roe Riemann solver (see Chapter 4 for details) to shallow water problems, and these represented the earliest consideration of Riemann solvers in open channel flow. In [27], the equations for a wide frictionless channel of rectangular cross section were written as

$$\mathbf{U}_t + \mathbf{F} = \mathbf{R}$$

using

$$\mathbf{U} = \begin{pmatrix} \phi \\ \phi u \end{pmatrix}, \quad \mathbf{F}(\mathbf{U}) = \begin{pmatrix} \phi u \\ \phi u^2 + \dfrac{\phi^2}{2} \end{pmatrix} \quad \text{and} \quad \mathbf{R}(\mathbf{U}) = \begin{pmatrix} 0 \\ g\phi h'(x) \end{pmatrix}$$

where ϕ represents the depth of the fluid above the datum level multiplied by g and h is the depth of the undisturbed water level, were used. In the case of a flat bed, the resulting first order scheme was written as

$$\frac{\mathbf{U}_P^{n+1} - \mathbf{U}_P^n}{\Delta t} + \frac{\sum_{i=1}^{2} \tilde{\lambda}_i \tilde{\alpha}_i \tilde{\mathbf{e}}_i}{\Delta x} = \mathbf{0}$$

where the point P corresponded to either the left or right (L or R) state of an interface, and the update procedure was presented in the form

$$\text{to add} \quad -\frac{\Delta t}{\Delta x} \tilde{\lambda}_i \tilde{\alpha}_i \tilde{\mathbf{e}}_i \quad \text{to} \quad \mathbf{U}_R \quad \text{when} \quad \tilde{\lambda}_i > 0$$

or

$$\text{to add} \quad -\frac{\Delta t}{\Delta x}\tilde{\lambda}_i\tilde{\alpha}_i\tilde{\mathbf{e}}_i \quad \text{to} \quad \mathbf{U}_L \quad \text{when} \quad \tilde{\lambda}_i < 0.$$

Glaister demonstrated a way to incorporate source terms arising from a smoothly varying bed within the Roe decomposition. Writing the approximate source term as

$$\tilde{\mathbf{R}} = \begin{pmatrix} 0 \\ g\tilde{\phi}\dfrac{\Delta h}{\Delta x} \end{pmatrix}$$

using $\tilde{\phi} = \sqrt{\phi_R\phi_L}$, then the source term can be projected onto the eigenvectors by

$$\tilde{\mathbf{R}} = \frac{1}{\Delta x}\sum_{i=1}^{2}\tilde{\lambda}_i\tilde{\beta}_i\tilde{\mathbf{e}}_i$$

and so by defining $\tilde{\gamma}_i = \tilde{\alpha}_i + \tilde{\beta}_i$ the scheme becomes

$$\text{to add} \quad -\frac{\Delta t}{\Delta x}\tilde{\lambda}_i\tilde{\gamma}_i\tilde{\mathbf{e}}_i \quad \text{to} \quad \mathbf{U}_R \quad \text{when} \quad \tilde{\lambda}_i > 0$$

or

$$\text{to add} \quad -\frac{\Delta t}{\Delta x}\tilde{\lambda}_i\tilde{\gamma}_i\tilde{\mathbf{e}}_i \quad \text{to} \quad \mathbf{U}_L \quad \text{when} \quad \tilde{\lambda}_i < 0.$$

Numerical results were shown for a series of dam-break scenarios, with reservoir to tailwater depth ratios of 2, 5, 10, 20 and 100. The Superbee flux limiter was used to generate second order accuracy. In all the cases presented, good agreement was obtained between the numerical and analytic solutions, though generally the number of mesh points had to be increased for the higher depth ratios to maintain the close agreement between the two solutions.

Alcrudo, García-Navarro and Savirón [2] extended the application of Roe's scheme to shallow water flows to include prismatic channels of arbitrary cross section. A series of solutions were presented and contrasted with those obtained from the McCormack and Lax-Friedrichs schemes. In particular the examples considered highlighted the shock capturing ability of Roe's scheme. Solutions for the dam-break problem with a depth ratio of 100:1 were shown. The McCormack scheme was used in conjunction with artificial viscosity and this enabled a solution to be produced, however the results were poor and included an unphysical stationary jump. The Lax-Friedrichs scheme generated a reasonable solution typical of a first order scheme. It was noted that the computation involved in finding the Roe solution was almost twice that of the other schemes. A solution for the same dam-break problem for a trapezoidal channel was shown, for which the Froude number behind the bore was 7.4. Although no analytical solution was available for this

problem, the solution appeared reasonable. The two other problems illustrated in the paper considered the case of one bore propagating over another, and a situation in which two bores travelling in opposing directions interacted. The Roe scheme performed well for both of these problems. However, oscillations were present in the McCormack solutions near the bores, and the Lax-Friedrichs solutions contained a substantial amount of numerical diffusion.

García-Navarro and Savirón [21] applied the McCormack scheme to a variety of discontinuous flow problems in rectangular channels. The authors presented the scheme in the form

$$\mathbf{U}_i^{(1)} = \mathbf{U}_i^n - \frac{\Delta t}{\Delta x}\left[(1-\varepsilon)\mathbf{F}_{i+1}^n - (1-2\varepsilon)\mathbf{F}_i^n - \varepsilon\mathbf{F}_{i-1}^n\right] + \Delta t\mathbf{R}_i^n$$

$$\mathbf{U}_i^{n+1} = \frac{1}{2}\left(\mathbf{U}_i^n + \mathbf{U}_i^{(1)}\right) - \frac{\Delta t}{2\Delta x}\left[\varepsilon\mathbf{F}_{i+1}^{(1)} + (1-2\varepsilon)\mathbf{F}_i^{(1)} + (\varepsilon-1)\mathbf{F}_{i-1}^{(1)}\right] + \frac{\Delta t}{2}\mathbf{R}_i^{(1)}.$$

By setting ε to be either 0 or 1, two different versions of the scheme are obtained, corresponding to different approximations for the spatial derivatives.

The paper included details of how to apply the method of characteristics to the boundaries in order to generate appropriate boundary data and also showed how to incorporate discontinuous flows at the upstream boundary via the shock relationships,

$$(A_R - A_L)V + Q_L - Q_R = 0$$

$$(Q_R - Q_L)V + \left(\frac{Q^2}{A} + \frac{gbh^2}{2}\right)_L - \left(\frac{Q^2}{A} + \frac{gbh^2}{2}\right)_R = 0$$

where V is the propagation speed of the shock. A description of how to implement internal weir boundary conditions was also given.

Results were presented for four test problems. The first was the uniform motion of a shock through a smooth rectangular channel. A comparison was made between the two versions of the scheme together with an adaptive version which alternated between the two values of ε. This example showed the first version of the scheme to be the most satisfactory, with the second producing an oscillatory solution and the combined scheme gave intermediate results. In all three cases the shock was resolved over a small number of cells.

The second problem involved the propagation and reflection of shock waves in a channel which was closed at the downstream boundary. Employing the adaptive version of the scheme eliminated the numerical oscillations and a reasonable solution was produced.

The third case considered was that of one shock propagating over another to form a larger shock. The conclusion made from this experiment was that comparisons made between this scheme and a third order explicit method showed that it was 'not worth going further for this kind of problems'.

The final example included the effects of source terms and consisted of flow over a ladder of cascades, which were enforced by use of the internal weir boundary condition. The steady state numerical solution was shown, which contained small oscillations due to the presence of the weirs.

García-Navarro, Alcrudo and Savirón [22] produced a subsequent paper in which a TVD variant of the McCormack scheme was introduced. The method was written in the form

$$\mathbf{U}_i^P = \mathbf{U}_i^n - \frac{\Delta t}{\Delta x}(\mathbf{F}_{i+1}^n - \mathbf{F}_i^n) + \Delta t \mathbf{R}_i^n$$

$$\mathbf{U}_i^C = \mathbf{U}_i^n - \frac{\Delta t}{\Delta x}(\mathbf{F}_i^P - \mathbf{F}_{i-1}^P) + \Delta t \mathbf{R}_i^P.$$

with the final update given by

$$\mathbf{U}_i^{n+1} = \frac{1}{2}(\mathbf{U}_i^P + \mathbf{U}_i^C).$$

For the new TVD version of the scheme, the third step was modified to

$$\mathbf{U}_i^{n+1} = \frac{1}{2}(\mathbf{U}_i^P + \mathbf{U}_i^C) + \frac{\Delta t}{\Delta x}(\mathbf{D}_{i+1/2}^n - \mathbf{D}_{i-1/2}^n),$$

where $\mathbf{D}_{i\pm 1/2}$ was defined as

$$\mathbf{D}_{i+1/2}^n = \frac{1}{2}\sum_{k=2}^{2} \tilde{\alpha}_{i+1/2}^k \psi(\tilde{\lambda}_{i+1/2}^k)\left(1 - \frac{\Delta t}{\Delta x}|\tilde{\lambda}_{i+1/2}^k|\right)\left[1 - \phi(r_{i+1/2}^k)\right]\tilde{\mathbf{e}}_{i+1/2}^k$$

following the standard notation of Roe (see Chapter 4). The term ψ represented an entropy correction for which

$$\psi(\lambda) = \begin{cases} |\lambda| & \text{if } |\lambda| \geq \delta \\ \delta & \text{if } |\lambda| < \delta \end{cases}$$

and δ was chosen to be a small positive number in the range 0.1 to 0.3. Results were shown for five different test cases. The first problem was the ladder of cascades problem in [21], but with different choices for S_o and n. Comparing the TVD and non-TVD versions of the scheme, small oscillations were present in the non-TVD version which were seen to be removed when the flux limiter was introduced.

The second problem considered a flood wave in a sloping trapezoidal channel, which contained three different sections of constant bed-slope. The initial conditions for the problem were taken to be the steady solutions generated by the respective schemes when a constant discharge was imposed. The TVD version of the scheme was deemed to perform much better than the non-TVD version.

The third example considered the steady flow over a bell shaped bump for which a hydraulic jump occurred. The numerical solution from the TVD scheme was shown to be in good agreement with the analytical solution, with the jump being well resolved without any oscillations.

The final two examples presented solutions for flow through a converging-diverging channel, created by a sinusoidal width variation. The first case was a steady state solution containing a hydraulic jump. As with the previous example, the analytic and TVD numerical solutions compared well. The second example consisted of a surge wave propagating downstream over still water. At the downstream end, a weir boundary condition was imposed, which initially resulted in the surge wave being partially reflected in the upstream direction. After the reflection, a steady state was reached in which a jump formed within the contraction. Again the TVD scheme performed well, however the non-TVD version was unable to predict the reflected wave.

Yang, Hsu and Chang [67] presented results from five different numerical methods for a number of problems. The schemes considered were based on two general formulations, giving rise to a set of finite different and finite element methods through various parameter values. The schemes selected corresponded to a second order TVD method, a second order ENO (essentially non oscillatory) and a third order ENO scheme through the finite difference formulation, and the equivalents of a second order TVD and a second order ENO methods via a finite element approach. For all five schemes results were shown for the dam-break problem, where the upstream to downstream depth was 100:1. All of the methods produced practically identical results in which the bore was well resolved and no oscillations were present. The second problem considered involved the head-on collision of two bore waves. Results from the three finite difference schemes were given and compared with a solution produced on a fine mesh. In each case the numerical solution closely matched the reference solution. The finite element results were stated to be very similar to those obtained from the finite difference schemes. The last example considered the sudden formation of a bore wave, resulting from

a piston motion at the upstream boundary. Numerical solutions generated from the second order finite difference ENO scheme were seen to compare well with the analytic solutions for two different scenarios.

Savic and Holly [54] presented a modified Godunov method for the calculation of dam-break flows. The scheme considered was formulated as

$$\mathbf{U}_i^{n+1} = \mathbf{U}_i^n - \frac{\Delta t}{\Delta x_i}(\mathbf{F}_{i+1/2}^{n+1/2} - \mathbf{F}_{i+1/2}^{n+1/2}) + \mathbf{R}_i^{n+1/2}$$

where $\mathbf{U}_i^n$ represented a spatial average and $\mathbf{F}_{i+1/2}^{n+1/2}$ was a time-average of the flux function over the cell. The basis of the method presented was to evaluate an appropriate value of $\mathbf{U}_{i+1/2}^{n+1/2}$ such that

$$\mathbf{F}_{i+1/2}^{n+1/2} = \mathbf{F}(\mathbf{U}_{i+1/2}^{n+1/2}).$$

The authors proposed an approach whereby shocks were isolated and treated separately to the rest of the flow via a Riemann problem. In the continuous regions of flow, two strategies were implemented within the method of characteristics for calculating $\mathbf{U}$. These were based on using using piecewise parabolic interpolation (PPM) and piecewise linear interpolation to extract approximations for the flow variables at the base of the characteristics.

The method was first applied to the dam-break problem for a depth ratio of 100:1. Both interpolation versions produced reasonable solutions, however the linear procedure gave rise to a more substantial amount of numerical diffusion. The PPM scheme was then used to simulate a dam-break like problem for rough sloping channel containing a sudden width expansion. The results obtained were compared with those produced by the Lax-Wendroff and Preissmann schemes and were found to be very similar. The experiment was repeated using a higher upstream to downstream ratio for which the Preissmann scheme could not generate a solution. A comparison was made with the Lax-Wendroff scheme, and from the discharge hydro-graph it could be seen that the Lax-Wendroff scheme suffered from oscillations, whereas the profile was smooth for the PPM approach. Finally a sudden width contraction was considered and results shown for both variants of the Godunov scheme. Again the linear solution was seen to suffer from more diffusion than the PPM scheme. The average amount of time required per time step by the different methods were compared, relative to the Godunov linear scheme. This showed that the PPM version was only slightly more expensive, whilst the Preissmann scheme required 1.82 times the computational effort of the linear scheme. The Lax-Wendroff scheme was quoted as requiring less than half

the expense but for the problems considered, solutions could only be obtained by using a time step ten times smaller than that used for the Godunov method.

García-Navarro, Priestley and Alcrudo [24] described an implicit TVD scheme for modelling water flow in channels and pipes. The method was based upon Roe's scheme (see Chapter 4) and the general discretisation was written as

$$\frac{\mathbf{U}_i^{n+1} - \mathbf{U}_i^n}{\Delta t} + \frac{1}{\Delta x}\left[\theta\delta^-(\mathbf{F}_{i+1/2}^{*n+1}) + (1-\theta)\delta^-(\mathbf{F}_{i+1/2}^{*n})\right] = \theta\mathbf{R}_i^{n+1} + (1-\theta)\mathbf{R}_i^n$$

where $\delta^-(\mathbf{F}_{i+1/2}^*) = \mathbf{F}_{i+1/2}^* - \mathbf{F}_{i-1/2}^*$. The numerical flux followed that in [2] but without the term associated with the combined space-time discretisation and was written as

$$\mathbf{F}_{i+1/2}^* = \frac{1}{2}(\mathbf{F}_{i+1} + \mathbf{F}_i) - \frac{1}{2}\sum_{k=1}^{2}\psi_{i+1/2}^k\left(1 - \phi(r_{i+1/2}^k)\right)\tilde{\alpha}_{i+1/2}^k\tilde{\mathbf{e}}_{i+1/2}$$

where $\psi_{i+1/2}^k$ was the entropy correction. Here r was taken to be

$$r_{i+1/2}^k = \frac{\tilde{\lambda}_{i+1/2-s}^k\alpha_{i+1/2-s}^k}{\tilde{\lambda}_{i+1/2}^k\alpha_{i+1/2}^k} \quad \text{with} \quad s = \text{sgn}(\tilde{\lambda}_{i+1/2}^k).$$

By expressing the Jacobian in its diagonal form, i.e.

$$\tilde{\mathbf{A}}_{i+1/2} = \tilde{\mathbf{P}}_{i+1/2}\text{diag}(\tilde{\lambda}_{i+1/2}^k)\tilde{\mathbf{P}}_{i+1/2}^{-1}$$

where $\tilde{P}$ represents the matrix of column eigenvectors of $\tilde{A}$, then the matrix B can be defined as

$$\mathbf{B}_{i+1/2} = \tilde{\mathbf{P}}_{i+1/2}\Lambda_{i+1/2}\tilde{\mathbf{P}}_{i+1/2}^{-1}$$

where $\Lambda_{i+1/2} = \text{diag}[\psi_{i+1/2}^k(1-\phi_{i+1/2}^k)]$ such that

$$\mathbf{B} = \frac{1}{\tilde{\lambda}^2 - \tilde{\lambda}^1}\begin{pmatrix} d^1\tilde{\lambda}^2 - d^2\tilde{\lambda}^1 & d^2 - d^1 \\ \tilde{\lambda}^2\tilde{\lambda}^1(d^1 - d^2) & d^2\tilde{\lambda}^2 - d^1\tilde{\lambda}^1 \end{pmatrix}$$

where $d^{1,2}$ are the diagonal elements of Λ. This enables the numerical flux to be represented as

$$\mathbf{F}_{i+1/2}^* = \frac{1}{2}\left(\mathbf{F}_{i+1} + \mathbf{F}_i - \mathbf{B}_{i+1}\delta\mathbf{U}_{i+1/2}\right).$$

where $\delta\mathbf{U}_{i+1/2} = \mathbf{U}_{i+1}^n - \mathbf{U}_i^n$. A number of linearisations were introduced into the implicit part of the scheme to render the resulting algebraic relationships linear in $\mathbf{U}$. Using a Taylor series expansion, the flux and source terms become

$$\mathbf{F}_i^{n+1} = \mathbf{F}_i^n + \mathbf{A}_i^n\Delta\mathbf{U}_i + O(\Delta t^2)$$

$$\mathbf{R}_i^{n+1} = \mathbf{R}_i^n + \mathbf{G}_i^n \Delta \mathbf{U}_i + O(\Delta t^2)$$

where the Jacobian of the source term is

$$\mathbf{G} = \begin{pmatrix} 0 & 0 \\ g\left[S_o + S_f\left(1 + \frac{4}{3}\frac{b}{b+2h}\right)\right] & -\frac{2gA}{Q}S_f \end{pmatrix}.$$

In addition $\mathbf{B}$ at the new time level was approximated by

$$\mathbf{B}_{i+1/2}^{n+1} = \mathbf{B}_{i+1/2}^n.$$

The resulting matrix system can then be written as

$$\mathbf{AA}_i \Delta \mathbf{U}_{i-1} + \mathbf{BB}_i \Delta \mathbf{U}_i + \mathbf{CC}_i \Delta \mathbf{U}_{i+1} = \mathbf{DD}_i$$

where the coefficients are 2×2 matrices defined as

$$\mathbf{AA}_i = -\frac{\theta \Delta t}{2\Delta x}\left(\mathbf{A}_{i-1} + \mathbf{B}_{i-1/2}\right)^n$$

$$\mathbf{BB}_i = \mathbf{I} - \theta \Delta t \mathbf{G}_i^n + \frac{\theta \Delta t}{2\Delta x}\left(\mathbf{B}_{i+1/2} + \mathbf{B}_{i-1/2}\right)^n$$

$$\mathbf{CC}_i = \frac{\theta \Delta t}{2\Delta x}\left(\mathbf{A}_{i+1} - \mathbf{B}_{i+1/2}\right)^n$$

$$\mathbf{DD}_i = -\frac{\Delta t}{\Delta x}\left(\mathbf{F}_{i+1/2}^* - \mathbf{F}_{i-1/2}^*\right)^n + \Delta t \mathbf{R}_i^n.$$

The resulting scheme was second order in space and first order in time.

A number of results were illustrated for different test problems using a variety of CFL numbers and $\theta = 1$, with the limiting function set to zero. Dam-break solutions were shown for a depth ratio of 20:1 for CFL values of 0.5, 1, 2 and 4. All the solutions were reasonable, but numerical diffusion could be observed. A number of other examples were given to illustrate how the method could be applied to flow networks via the implementation of suitable internal boundary conditions.

Jha, Akiyama and Ura [36] proposed a modification to the Beam and Warming scheme based on conservative splitting via an approximate Jacobian matrix, in an attempt to render the scheme conservative. The general form of the original method was

$$\mathbf{U}_i^{n+1} = \mathbf{U}_i^n + \Delta t\left[\alpha\left(\frac{\partial \mathbf{U}}{\partial t}\right)^{n+1} + (1-\alpha-\beta)\left(\frac{\partial \mathbf{U}}{\partial t}\right)^n + \beta\left(\frac{\partial \mathbf{U}}{\partial t}\right)^{n-1}\right]$$

where α and β were in the range $[0,1]$. Applying the scheme to the general form of a conservation law gave

$$\mathbf{U}_i^{n+1} = \mathbf{U}_i^n + \Delta t \left[\alpha \left\{ \left(\frac{\partial \mathbf{F}}{\partial x} + \mathbf{R} \right)^{n+1} + \left(\frac{\partial \mathbf{F}}{\partial x} + \mathbf{R} \right)^{n} \right\} + (1-\beta) \left(\frac{\partial \mathbf{F}}{\partial x} + \mathbf{R} \right)^{n} - \beta \left(\frac{\partial \mathbf{U}}{\partial t} \right)^{n-1} \right].$$

Applying Taylor series expansion to linearize the implicit terms and using the approximation

$$\left(\frac{\partial \mathbf{U}}{\partial t} \right)^{n} = \frac{\mathbf{U}^{n+1} - \mathbf{U}^{n}}{\Delta t}$$

then the scheme can be rewritten as

$$\mathbf{U}_i^{n+1} = \Delta t \left[\alpha \left(\frac{\partial (\mathbf{A}^n \mathbf{U}^{n+1})}{\partial x} + (\mathbf{G}^n \mathbf{U}^{n+1}) \right) \right] = \mathbf{U}^n + \Delta t \left[\alpha \left(\frac{\partial (\mathbf{A}^n \mathbf{U}^n)}{\partial x} + \mathbf{G}^n \mathbf{U}^n \right) - (1-\beta) \left(\frac{\partial \mathbf{F}}{\partial x} + \mathbf{R} \right)^{n} + \beta \left(\frac{\partial \mathbf{U}}{\partial t} \right)^{n-1} \right].$$

If the split form of the Jacobian matrix is introduced and the following difference formula used

$$\frac{\partial (\mathbf{A}^+ \mathbf{U})}{\partial x} = \frac{\mathbf{A}_i^+ \mathbf{U}_i - \mathbf{A}_{i-1}^+ \mathbf{U}_{i-1}}{\Delta x}$$

$$\frac{\partial (\mathbf{A}^- \mathbf{U})}{\partial x} = \frac{\mathbf{A}_{i+1}^- \mathbf{U}_{i+1} - \mathbf{A}_i^- \mathbf{U}_i}{\Delta x}$$

then the scheme becomes

$$\left[\mathbf{I} + \Delta t \alpha \left(\frac{\partial \mathbf{A}^+}{\partial x} + \frac{\partial \mathbf{A}^-}{\partial x} + \mathbf{G} \right)^{n} \right] \mathbf{U}^{n+1} = \left[\mathbf{I} + \Delta t \alpha \left(\frac{\partial \mathbf{A}^+}{\partial x} + \frac{\partial \mathbf{A}^-}{\partial x} + \mathbf{G} \right)^{n} \right] \mathbf{U}^{n} - \Delta t \left[(1-\beta) \left(\frac{\partial \mathbf{F}}{\partial x} + \mathbf{R} \right)^{n} - \beta \left(\frac{\partial \mathbf{U}}{\partial t} \right)^{n-1} \right]$$

where the terms contained within the square brackets before $\mathbf{U}$ represent operators.

The modification to the scheme involved redefining the approximation to the derivative of the flux term. Instead of the conventional approximation

$$\frac{\partial \mathbf{F}}{\partial x} = \mathbf{A} \frac{\partial \mathbf{U}}{\partial x} = \mathbf{A}^+ \frac{\partial \mathbf{U}}{\partial x} + \mathbf{A}^- \frac{\partial \mathbf{U}}{\partial x},$$

the derivative was replaced with

$$\frac{\partial \mathbf{F}}{\partial x} = \tilde{\mathbf{A}} \frac{\partial \mathbf{U}}{\partial x} = \tilde{\mathbf{A}}_{i-1/2}^+ \frac{\partial \mathbf{U}}{\partial x} + \tilde{\mathbf{A}}_{i+1/2}^- \frac{\partial \mathbf{U}}{\partial x}$$

where

$$\tilde{\mathbf{A}}_{i\pm1/2} = \tilde{\mathbf{A}}(\mathbf{U}_{i\pm1/2}) = \mathbf{A}(\mathbf{U}_i, \mathbf{U}_{i\pm1})$$

and use was made of the Roe averages.

Numerical solutions were presented for three problems — the sudden opening of a gate, the sudden closure of a gate and the dam-break problem, all of which contained bore waves. Comparisons were made between the original and modified Euler and Trapezoidal schemes ($\alpha = 1, \beta = 0$ and $\alpha, \beta = 0.5$). The experiments clearly demonstrated improvements in the results when supercritical regions were present in the flow. This was particularly apparent in the high ratio dam-break case, for which the modified schemes gave much better solutions and accurately predicted the fluid motion.

In a subsequent paper, Jha, Akiyama and Ura [37] applied the first order Roe scheme and various second order constructions to the dam-break problem. The three second order extensions were based upon a) the Lax-Wendroff numerical flux, b) the MUSCL (Monotone Upstream-centred Schemes for Conservation Laws) approach and c) the Modified flux technique. All three employed the use of flux/slope limiters to attain non-oscillatory solutions.

Using the convention

$$\mathbf{U}_i^{n+1} = \mathbf{U}_i^n - \gamma \left(\mathbf{F}_{i+1/2}^n - \mathbf{F}_{i+1/2}^n \right),$$

where $\gamma = \Delta t / \Delta x$, the Lax-Wendroff flux is written as

$$\mathbf{F}_{i+1/2} = \frac{1}{2}(\mathbf{F}_i + \mathbf{F}_{i+1}) - \gamma \mathbf{A}^2 (\mathbf{U}_{i+1} - \mathbf{U}_i). \tag{3.26}$$

To render the scheme TVD, a flux limiter is applied to (3.26) and together with the approximate Jacobian of Roe (see Chapter 4 for details), the resulting flux function is

$$\mathbf{F}_{i+1/2} = 0.5(\mathbf{F}_i + \mathbf{F}_{i+1}) - 0.5 \sum_{k=1}^{2} |\tilde{\lambda}_{i+/12}^k| \tilde{\alpha}_{i+1/2}^k \tilde{\mathbf{e}}_{i+1/2}^k$$

$$+0.5 \sum_{k=1}^{2} \phi |\tilde{\lambda}_{i+1/2}^k| [1 - (\gamma |\tilde{\lambda}_{i+1/2}^k|)^s] \tilde{\alpha}_{i+1/2}^k \tilde{\mathbf{e}}_{i+1/2}^k.$$

Setting $s = -1$ and $\phi = 1$ corresponds to Lax-Friedrichs scheme. Using $s = 1$ together with a flux limiter gives the limited Lax-Wendroff flux. The limiter chosen was one due to van Albada, which is defined by the function

$$\phi(r) = \frac{r + r^2}{1 + r^2}$$

where the argument is taken to be

$$r^k_{i+1/2} = \frac{\tilde{\alpha}_{i+1/2-\text{sign}(\tilde{\lambda}^k_{i+1/2})}}{\tilde{\alpha}^k_{i+1/2}}.$$

The MUSCL flux was defined as

$$\mathbf{F}_{i+1/2} = \mathbf{F}(\mathbf{U}^L_{i+1/2}, \mathbf{U}^R_{i+1/2})$$

where the left and right values of $\mathbf{U}$ were given by

$$\mathbf{U}^R_{i+1/2} = \mathbf{U}_{i+1} - 0.5(\overline{\overline{\Delta\mathbf{U}}})_{i+1/2}$$

$$\mathbf{U}^L_{i+1/2} = \mathbf{U}_i + 0.5(\overline{\Delta\mathbf{U}})_{i+1/2}$$

in conjunction with the Minmod slope limiter from which the 'bar' values were

$$(\overline{\Delta\mathbf{U}})_{i+1/2} = \text{minmod}[(\Delta\mathbf{U})_{i+1/2}, \theta(\Delta\mathbf{U})_{i-1/2}]$$

$$(\overline{\overline{\Delta\mathbf{U}}})_{i+1/2} = \text{minmod}[(\Delta\mathbf{U})_{i+1/2}, \theta(\Delta\mathbf{U})_{i+3/2}]$$

where

$$\text{minmod}(x, \theta y) = \left(\frac{x}{|x|}\right) \max\left\{0, \min\left(x, \left[\theta y \frac{x}{|x|}\right]\right)\right\}.$$

No details were given for θ.

The Modified flux approach redefined the numerical flux as

$$\mathbf{F}_{i\pm1/2} = 0.5(\mathbf{F}_i + \mathbf{F}_{i\pm1}) + 0.5\sum_{k=1}^{2}(E^k_i + E^k_{i\pm1})\tilde{\mathbf{e}}^k_{i+1/2}$$
$$-0.5\sum_{k=1}^{2}\psi(\tilde{\lambda}^k_{i\pm1/2} + \xi^k_{i\pm1/2})\tilde{\alpha}^k_{i\pm1/2}\mathbf{e}^k_{i\pm1/2}$$

where

$$E^k_i = \text{minmod}[\sigma(\tilde{\lambda}^k_{i+1/2})\tilde{\alpha}^k_{i+1/2}, \sigma(\lambda^k_{i-1/2})\alpha^k_{i-1/2}]$$

and

$$\xi^k_{i+1/2} = \begin{cases} \dfrac{(E^k_{i+1} - E^k_i)}{\tilde{\alpha}^k_{i+1/2}} & \tilde{\alpha}^k_{i+1/2} \neq 0 \\ 0 & \text{otherwise,} \end{cases}$$

with

$$\sigma(\tilde{\lambda}^k_{i+1/2}) = 0.5\left[\psi(\tilde{\lambda}^k_{i+1/2}) + \frac{\Delta t}{\Delta x}(\tilde{\lambda}^k_{i+1/2})^2\right].$$

The ψ term represents the entropy correction factor, defined here as

$$\psi(z) = \begin{cases} \dfrac{z^2 + \delta^2}{2\delta} & |z| < \delta \\ |z| & |z| \geq \delta. \end{cases}$$

The first experiment tested the first order Roe scheme against the analytical solution, using a fixed valued of δ, and a non-physical vertical drop was clearly visible in the numerical solution. Roe's scheme (variable δ) was then compared to the Lax-Friedrichs method and the Trapezoidal version of the Modified Beam and Warming [36] scheme, for which Roe's scheme was seen to produce the better solution. The second order schemes were then compared, where the van Albada flux limiter was used in the Lax-Wendroff extension. For a depth ratio of 20:1, the three methods gave almost identical solutions, however when this ratio was increased to 200:1, the Modified flux scheme under predicted the speed of the front. A comparison was then made between the first order approach and the Lax-Wendroff extension for the same depth ratio. The solutions appeared visually identical. Finally solutions from the first order scheme and the MUSCL approach for a depth ratio of 1000:1 were presented. The Lax-Wendroff and Modified flux versions were unable to produce a solution for this scenario. Visually there was no noticeable difference in the numerical solutions shown. In conclusion the paper argued that the first order Roe scheme gave much better results than the other first order schemes considered in the study, and that it gave comparable results to the second order extensions considered at a much lower computational cost.

Jha, Akiyama and Ura [38] carried out further tests on the Modified Beam and Warming scheme introduced in [36]. The modified versions of the Euler (explicit and implicit), Crank-Nicolson and Three point backward schemes were considered. The original and new versions were compared for the dam-break problem for the depth ratios 100:1 and 1000:1. In both cases the modified schemes gave much better results, with the explicit Euler method obtaining the best shock resolution whilst the Three point backward scheme produced the least favourable solution. The new scheme was also applied to the trapezoidal dam-break introduced in [2], giving similar behaviour to the rectangular case. Results were also shown for the shock problem in a frictional sloping trapezoidal channel in [16] and compared with the McCormack scheme. All of the versions of the modified approach gave better shock resolution than the McCormack scheme. Numerical solutions from the Crank-Nicolson variant were shown for two dam-break scenarios in a sloping rectangular frictional channel for which experimental data was available. In the first example a series of stage hydro-graphs were presented and it was observed that good agreement was obtained between the numerical and experimental data, except during the initial stages near the breach. The second case considered a dry bed dam-break for which the numerical method required a very small downstream depth to be introduced. Two hydro-graphs were given together with a water level

profile plot and a time evolution of the front location. Again the two solutions compared well. Further experiments were conducted on the standard dam-break problem to assess how the choice of Courant number affected the solution. Using the implicit Euler scheme and a depth ratio of 100:1, it was observed that for values in the range 1 to 2 the results were indistinguishable, however the accuracy deteriorated for values in excess of 2. The effect of friction was also considered by incorporating non-zero n into the dam-break problem, and what were considered to be reasonable solutions were obtained.

Jin and Fread [39] presented a paper which combined the Preissmann scheme with a characteristic based upwind explicit method. The article highlighted the benefits of using the upwind scheme in the case of the dam-break problem and in other situations where unsteady mixed flows occurred. However from a practical perspective, the paper took the viewpoint that it was preferred to use the Preissmann scheme where possible, and so provided evidence that the explicit and implicit schemes could be combined in such a way (via appropriate internal boundaries) that the benefits of both methods could be encompassed. Results were given for an actual dam break that had occurred, in which the explicit scheme was used upstream and the implicit scheme downstream. Reasonable agreement was obtained between the numerical and measured solutions.

Hicks, Steffler and Yasmin [35] presented a paper intended to illustrate the validity of applying 1–d techniques to non 1-d problems. The article considered the case of a dam-break scenario though a non-prismatic rectangular channel for which a series of experimental results had been obtained by Bellos *et al* [10]. The non-prismatic region of the channel consisted of a non-symmetric contracting/diverging length along one bank. The experimental data generated by Bellos *et al* included a series of depth measurements taken at five points along the channel at the mid-points of each cross section. Data was produced for a range of experiments which considered various bed-slopes and depth ratios, including dry downstream beds. In the paper [35], a comparison was made between solutions produced by a characteristic based finite element method and the Preissmann scheme, with the experimental data. A number of depth ratios over a horizontal bed were considered. In the first example, a depth ratio of 2:1 was used. The resulting flow was subcritical throughout the region and both schemes gave good agreement with the measured results. The most noticeable differences occurred at the breach location at the start of the simulation and towards the downstream boundary later on. The downstream discrepancy resulted from the fact that the

numerical treatment did not include the reflected wave that occurred in the experiment. Results were also included for the ratio 2.5:1. The finite element method gave similar results to before, however the Preissmann scheme experienced difficulties in this instance as a supercritical region developed within the channel contraction. Numerical experiments were also carried out using two non-uniform grids — one in which the grid spacing varied smoothly and one containing irregular changes in the distribution. It was noted that the similar results were obtained using the smoothly varying grid as with the uniform distribution of cells, but that the irregular grid gave rise to a more diffusive solution for the finite element scheme and a more oscillatory solution for the Preissmann scheme. Overall it was concluded that both methods had accurately predicted the flow for wholly subcritical simulations.

Meselhe, Sotiropoulos and Holly [43] presented the MESH scheme for open channel flows. The method formed a two-step predictor-corrector algorithm based on evaluating the derivatives at the $(i+1/2, n+1/2)$ level. The scheme was written as

Predictor

$$(\mu\mathbf{I} + \sigma|\mathbf{A}|^n_{i+1/2} - \phi\Delta t\mu\mathbf{G}^n_{i+1/2})\overline{\Delta\mathbf{U}}_{i+1/2} = -\sigma\delta\mathbf{F}^n_{i+1/2} + \Delta t\mu\mathbf{R}^n_{i+1/2}$$

$$\bar{\mathbf{U}} = \mathbf{U}^n + \overline{\Delta\mathbf{U}}$$

Corrector

$$(\mu\mathbf{I} - \sigma|\bar{\mathbf{A}}|^n_{i+1/2} + \phi\Delta t\mu\mathbf{G}^n_{i+1/2})\overline{\overline{\Delta\mathbf{U}}}_{i+1/2} = -\sigma\delta\bar{\mathbf{F}}^n_{i+1/2} + \Delta t\mu\bar{\mathbf{R}}^n_{i+1/2}$$

$$\mathbf{U}^{n+1} = \mathbf{U}^n + \frac{1}{2}(\overline{\Delta\mathbf{U}} + \overline{\overline{\Delta\mathbf{U}}})$$

where

$$\Delta\mathbf{U}^n = \mathbf{U}^{n+1} - \mathbf{U}^n$$

$$\mu[\ ]_{i+1/2} = \frac{1}{2}\{[\ ]_{i+1} + [\ ]_i\}$$

$$\delta[\ ]_{i+1/2} = [\ ]_{i+1} - [\ ]_i$$

and

$$\sigma = \frac{\Delta t}{\Delta x}.$$

The discretisation was second order accurate in both space and time and led to a bidiagonal matrix system. Non-oscillatory solutions could be obtained by adding artificial viscosity.

Results were shown for three steady state and two time-dependent problems. The first steady problem corresponded to flow over a bump [22] including a hydraulic jump. The jump appeared at the correct location but was slightly smeared. The second problem considered a sloping channel with three regions of constant S_o and included frictional effects. The slopes were such that a hydraulic jump formed in the central region. From comparison with the analytic solution, the MESH scheme gave better mass conservation for this problem than for the bump. This was due to the inclusion of friction which reduced the need for artificial viscosity. The final steady state problem looked at flow through a sloping non-prismatic frictional channel and compared the MESH scheme with results obtained using Glaister's implementation of the Roe scheme, using an irregular mesh. Both methods generated similar solutions, though some small oscillations appeared to be present in the solutions produced by Glaister's scheme.

The first time dependent problem considered a sloping rectangular channel which incorporated a sluice gate at the mid-point. The upstream and downstream boundary conditions were varied over the initial stages and then maintained at constant levels, resulting in a steady state flow. The resulting flow was subcritical and the numerical results of the MESH scheme were compared with those produced by the Preissmann method. Both techniques gave similar profiles. The second unsteady example consisted of transcritical flow over a weir. The weir was placed in the middle of the channel section and the boundary conditions were varied over the simulation resulting in a complex flow pattern, which the MESH scheme was able to predict.

MacDonald *et al* [42] presented a technique for generating analytic solutions for non-trivial problems for steady state open channel flows. The method was applicable to a range situations and could include non-prismatic cross sections, varying bed-slopes and transcritical flows. Four examples were given which considered prismatic rectangular and trapezoidal channels with non-uniform bed-slopes and a range of flow types.

Delis and Skeels [13] compared several TVD schemes and applied the methods to the dam-break problem and two of the test cases from MacDonald *et al* [42]. The schemes considered were formulated as

$$\mathbf{U}_i^{n+1} = \mathbf{U}_i^n - \frac{\Delta t}{\Delta x}\left[\tilde{\mathbf{F}}_{i+1/2}^n - \tilde{\mathbf{F}}_{i-1/2}^n\right] + \Delta t \tilde{\mathbf{R}}_i^n$$

using the flux function

$$\tilde{\mathbf{F}}_{i\pm1/2} = \frac{1}{2}\left[\mathbf{F}_i + \mathbf{F}_{i\pm1} + \mathbf{P}_{i\pm1/2}\mathbf{D}_{i\pm1/2}\right],$$

where $\mathbf{P}$ represented the matrix of right eigenvectors of the Jacobian and the choice of $\mathbf{D}$ corresponded to the different schemes. The source terms, $\mathbf{R}$, were included by taking the average of $\tilde{\mathbf{R}}_{i-1/2}$ and $\tilde{\mathbf{R}}_{i+1/2}$ where the approximate values were given by

$$\tilde{\mathbf{R}}^n_{i\pm1/2} = \begin{pmatrix} 0 \\ g\tilde{A}_{i\pm1/2}S_o - g\tilde{A}_{i\pm1/2}\tilde{u}^2_{i\pm1/2}n^2\left[\dfrac{\tilde{A}_{i\pm1/2}}{2\tilde{A}_{i\pm1/2}/\tilde{b}_{i\pm1/2} + \tilde{b}_{i\pm1/2}}\right]^{-4/3} \end{pmatrix}$$

together with

$$\tilde{A}_{i+1/2} = \sqrt{A_{i+1}A_i} \quad \text{and} \quad \tilde{b}_{i+1/2} = \frac{1}{2}\left(b_{i+1} + b_i\right).$$

The four methods considered were a second order symmetric TVD scheme, a second order upwind TVD scheme (corresponding to the Modified flux approach), the TVD McCormack scheme and a MUSCL scheme. All of the schemes were implemented by using the Roe Riemann solver. Denoting the elements of $\mathbf{D}_{i+1/2}$ as $d^k_{i+1/2}$, the various schemes were written as

(1) Symmetric TVD scheme

$$(d^k_{i+1/2})^s = -\frac{\Delta t}{\Delta x}(\tilde{\lambda}^k_{i+1/2})^2 L^k_{i+1/2} - \psi(\tilde{\lambda}^k_{i+1/2})[\tilde{\alpha}^k_{i+1/2} - L^k_{i+1/2}] \qquad k = 1, 2$$

where ψ was defined as

$$\psi(\lambda) = \begin{cases} |\lambda| & |\lambda| \geq \delta \\ \dfrac{\lambda^2 + \delta^2}{2\delta} & |\lambda| < \delta \end{cases}$$

using a varied value of δ, and L corresponded to a limiter function represented by

$$L^k_{i+1/2} = \text{minmod}(\tilde{\alpha}^k_{i-1/2}, \tilde{\alpha}^k_{i+1/2}) + \text{minmod}(\tilde{\alpha}^k_{i+1/2}, \tilde{\alpha}^k_{i+3/2}) - \tilde{\alpha}^k_{i+1/2}$$

and

$$\text{minmod}(x, y) = \text{sgn}(x)\max\{0, \min\left[|x|, y\,\text{sgn}(x)\right]\}.$$

(2) Upwind TVD scheme

$$(d^k_{i+1/2})^u = \sigma(\tilde{\lambda}^k_{i+1/2})(L^k_{i+1} + L^k_i) - \psi(\tilde{\lambda}^k_{i+1/2} + \gamma^k_{i+1/2})\tilde{\alpha}^k_{i+1/2}, \qquad k = 1, 2$$

with

$$\sigma(\alpha) = \frac{1}{2}\left(\psi(\alpha) - \frac{\Delta t}{\Delta x}\alpha^2\right)$$

and

$$\gamma^k_{i+1/2} = \begin{cases} \sigma(\tilde{\lambda}^k_{i+1/2})(L^k_{i+1} - L^k_i)/\tilde{\alpha}^k_{i+1/2} & \tilde{\alpha}^k_{i+1/2} \neq 0 \\ 0 & \tilde{\alpha}^k_{i+1/2} = 0. \end{cases}$$

For this scheme the limiter function was defined as

$$L^k_i = \text{minmod}(\tilde{\alpha}^k_{i+1/2}, \tilde{\alpha}^k_{i-1/2}).$$

(3) TVD McCormack scheme, written as

$$\mathbf{U}^{(1)}_i = \mathbf{U}^n_i - \frac{\Delta t}{\Delta x}(\mathbf{F}^n_{i+1} - \mathbf{F}^n_i) + (\Delta t)\mathbf{R}^n_i$$

$$\mathbf{U}^{(2)}_i = \mathbf{U}^n_i - \frac{\Delta t}{\Delta x}(\mathbf{F}^{(1)}_{i+1} - \mathbf{F}^{(1)}_i) + (\Delta t)\mathbf{R}^{(1)}_i$$

from which

$$\mathbf{U}^{n+1}_i = \frac{1}{2}\left(\mathbf{U}^{(1)}_i + \mathbf{U}^{(2)}_i\right) + \frac{1}{2}(\bar{\mathbf{P}}_{i+1/2}\bar{\mathbf{D}}_{i+1/2} - \bar{\mathbf{P}}_{i-1/2}\bar{\mathbf{D}}_{i-1/2})$$

where the elements of $\bar{\mathbf{D}}$ are given by

$$(d^k_{i+1/2})^{PC} = \psi(\tilde{\lambda}^k_{i+1/2})\left[1 - \frac{\Delta t}{\Delta x}|\tilde{\lambda}^k_{i+1/2}|\right](1 - L^k_{i+1/2})\tilde{\alpha}^k_{i+1/2}.$$

In this case the Minmod limiter becomes

$$L^k_{i+1/2} = \max(0, \min(1, r^k_{i+1/2})$$

where

$$r^k_{i+1/2} = \frac{\tilde{\alpha}^k_{i+1/2-s}}{\tilde{\alpha}^k_{i+1/2}} \quad \text{and} \quad s = \text{sgn}(\tilde{\lambda}^k_{i+1/2}).$$

The values $\bar{\mathbf{P}}$ and $\bar{\mathbf{D}}_{i+1/2}$ were evaluated using $\mathbf{U}^n$.

(4) MUSCL scheme

$$\mathbf{U}^L_{i+1/2} = \mathbf{U}_i + \frac{1}{4}\left[(1-m)\Delta^+_{i-1/2} + (1+m)\Delta^-_{i+1/2}\right]$$

$$\mathbf{U}^R_{i+1/2} = \mathbf{U}_{i+1} - \frac{1}{4}\left[(1-m)\Delta^-_{i+3/2} + (1+m)\Delta^-_{i+1/2}\right]$$

where

$$\Delta^-_{i+1/2} = \text{minmod}(\Delta_{i+1/2}\mathbf{U}, \beta\Delta_{i-1/2}\mathbf{U})$$

$$\Delta^{+}_{i+1/2} = \text{minmod}(\Delta_{i+1/2}\mathbf{U}, \beta\Delta_{i+3/2}\mathbf{U})$$

and β is a 'compression parameter' with a value in the range

$$1 \leq \beta \leq \frac{3-m}{1-m}$$

where m determined the spatial order of accuracy and was not set to one. In the work presented, m was chosen to be 1/3 leading to third order spatial accuracy. The flux function of the MUSCL scheme was written as

$$\tilde{\mathbf{F}}_{i+1/2} = \frac{1}{2}\left[\mathbf{F}(\mathbf{U}^{R}_{i+1/2}) + \mathbf{F}(\mathbf{U}^{L}_{i+1/2}) + \hat{\mathbf{P}}_{i+1/2}\hat{\mathbf{D}}_{i+1/2}\right],$$

together with

$$\hat{d}^{k}_{i+1/2} = -\psi(\tilde{\lambda}^{k}_{i+1/2})\hat{\alpha}^{k}_{i+1/2}.$$

The terms $\tilde{\lambda}^{k}_{i+1/2}$, $\hat{P}_{i+1/2}$ and $\hat{\alpha}^{k}_{i+1/2}$ are defined using the standard Roe formula by replacing $\mathbf{U}_{i+1}$ and $\mathbf{U}_{i}$ with $\mathbf{U}^{R}_{i+1/2}$ and $\mathbf{U}^{L}_{i+1/2}$.

The methods were first applied to the idealized dam-break problem. For a reservoir to tailwater depth ratio of 20:1, all the methods accurately predicted the flow. A comparison of the results obtained when the ratio was increased to 200:1 was then made and contrasted with the first order Roe scheme. The symmetric scheme gave the largest deviation from the analytical solution with the Roe, Modified Flux and MUSCL schemes giving similar solutions. The McCormack scheme appeared to give the best shock location. When the ratio was further increased to 1000:1, the McCormack scheme gave an oscillatory solution and again the symmetric scheme gave the least favorable position for the shock. The Roe, MUSCL and Modified flux approaches gave comparable solutions with the third order MUSCL scheme producing the best solution.

The application of the techniques to more complex problems was then considered through two examples taken from [42]. The first case considered had subcritical boundary conditions and contained a central supercritical region. The second case considered a situation where the flow was supercritical at both boundaries which were connected by a subcritical region. In both cases Roe's scheme was seen to clip the jump, whilst the symmetric scheme performed much better around the jumps but gave less favourable results in the smooth regions. McCormack's scheme overestimated the jump height for both problems. The MUSCL and Modified flux approaches gave similar solutions but had to be run at lower CFL numbers. In conclusion, each method had its relative merits depending on the problem being considered. It was stated that the treatment of the source terms used had given better results than the pointwise implementation.

3.2.2 Two-dimensional studies

Fennema and Chaudhry [17] applied the Beam and Warming scheme used in [16] to the two-dimensional shallow water equations. Using an approximate factorization, the 2-d problem was re-expressed as two 1-d problems, such that the two co-ordinate directions were considered in turn. The method was applied to the 2-d partial dam-break problem. The effects of friction and bed-slope were included in the study together with various boundary conditions, though the paper only presented results for a flat frictionless channel. The Euler implicit, Trapezoidal and Three-point backward versions of the scheme were applied to the depth ratio 2:1 and it was stated that the three schemes gave identical results. It was noted that for this problem, the McCormack scheme would fail for a depth ratio of 4:1 or more, and that Gabbutti's scheme would generate negative depths if this was increased to 5:1. For the Beam and Warming scheme, numerical solutions could be obtained for ratios up to 1000:1, and solutions were provided for the 500:1 case. Overall the results were seen not to contain any oscillations and it was observed that the bore was spread over more cells than would be the case with an explicit scheme.

In a subsequent paper, Fennema and Chaudhry [18] considered the McCormack and Gabutti explicit schemes for 2-d flows. The methods were applied to the same partial dam-break problem considered in [17] and results were shown for the depth ratio 2:1. Artificial dissipation had to be added to both schemes to remove the non-physical oscillations, and in comparison with the implicit results presented previously, the bore could be seen to be more sharply resolved. A visual comparison was made between the two schemes by comparing the transverse depth profiles along three x co-ordinate lines, together with the depth values at two points during the simulation. Overall the two schemes were deemed to give 'comparable' solutions. A comparison was also made with the Beam and Warming scheme via a longitudinal depth plot. Similarities could be observed between the solutions in addition to the smearing effect of the implicit scheme. The flow of a flood wave through a channel contraction was also considered, using a similar geometry to the dam-break scenario in which the width of the dam was increased. The time-evolving depth profiles at two points within the channel were shown along with transverse profiles along three y-values.

Glaister [28] applied the method introduced in [27] to the $(\phi, \phi u, \phi w)$ formulation of the two-dimensional shallow water equations. The 2-d equations were

re-expressed as two 1-d equations using the technique of operator splitting to which the approximate Riemann solver could be applied. Numerical solutions were presented for the two-dimensional radial dam-break problem which consists of a cylindrical bore followed by a depression. Results at a number of different times produced using the Minmod limiter were shown, and reasonable solutions were obtained.

Toro [62] presented several Riemann solvers within the context of shallow water flows, and considered their application through the Weighted Average Flux (WAF) method to a series of 1-d and 2-d problems. The paper illustrated how to determine the exact solution of the Riemann problem for the 1-d Saint Venant equations, which led to the development of Toro's Exact Riemann solver, the two-rarefaction (TR) approximate Riemann solver and the Two-shock approximate Riemann solver. The paper also considered the approximate Riemann solvers of Roe and Harten, Lax and van Leer (HLL). The WAF method was constructed by considering the solution of a Riemann problem at the cell interfaces (centered at $x = 0$) which on an irregular grid led to a numerical flux of the form

$$\mathbf{F}_{i+1/2} = \frac{1}{\frac{1}{2}\Delta x_i} \int_{-\frac{1}{2}\Delta x_i}^{0} \mathbf{F}(\mathbf{U}^*)dx + \frac{1}{\frac{1}{2}\Delta x_{i+1}} \int_{0}^{\frac{1}{2}\Delta x_{i+1}} \mathbf{F}(\mathbf{U}^*)dx \tag{3.27}$$

where $\mathbf{U}^*$ is the solution to the Riemann problem at time $t = \Delta t/2$. By assuming that waves in the solution of the Riemann problem are single rays, then equation (3.27) can be replaced by

$$\mathbf{F}_{i+1/2} = \sum_{k=1}^{N+1} W_k \mathbf{F}^k_{i+1/2}$$

where N is the number of waves present and the coefficients W^k are weights defined by

$$W^k = \frac{1}{2}\left(\nu_k - \nu_{k-1}\right) \quad \text{with} \quad \nu_0 = -1 \quad \text{and} \quad \nu_{N+1} = 1.$$

The weights are all positive and are such that the sum over k is equal to unity. Following these definitions, the flux can be re-expressed as

$$\mathbf{F}_{i+1/2} = \frac{1}{2}\left(\mathbf{F}_i + \mathbf{F}_{i+1}\right) - \frac{1}{2}\sum_{k=1}^{N} \nu_k \Delta \mathbf{F}^k_{i+1/2}$$

with

$$\Delta \mathbf{F}^k_{i+1/2} = \mathbf{F}^{k+1}_{i+1/2} - \mathbf{F}^k_{i+1/2}.$$

Alternatively an average state, $\bar{V}_{i+1/2}$ can be defined by

$$\bar{V}_{i+1/2} = \frac{1}{2}\left(V_i^n + V_{i+1}^n\right) - \frac{1}{2}\sum_{k=1}^{N} \nu_k \Delta V_{i+1/2}^k$$

from which the numerical flux becomes

$$\mathbf{F}_{i+1/2} = \mathbf{F}(\bar{V}_{i+1/2}).$$

The resulting scheme is second order and so can produce non-physical oscillations, but a corresponding TVD method can be constructed by applying a flux limiter. Using standard splitting techniques the method can be extended to higher dimensional systems of conservation laws.

The first problem considered was the idealized 1-d dam-break test case. Using the exact Riemann solver, solutions were presented using the TVD and non-TVD versions of the WAF method and the Godunov method. As expected the TVD WAF scheme gave the best solution, as oscillations occurred within the non-TVD version, and the Godunov method slightly smeared the shock in addition to including a non-entropy satisfying jump. Using the same limiter function, solutions were also presented using the approximate TS, TR and Roe Riemann solvers. These results were almost identical to those obtained using the exact Riemann solver. The second problem to be investigated was a 1-d flow over a non-uniform bed, which consisted of two flat sections at different heights connected by a region of uniform gradient. Plots at several different times were presented using the exact solver with a limiter. Though no exact solution was available for comparison, the numerical solution appeared well behaved and satisfactory. Finally the method was applied to the circular dam break problem in [28] using the TVD version together with TR solver, and again reasonable results were obtained.

Yang and Hsu [68] extended the second order ENO scheme considered in [67] to two-dimensional flows, using an operator splitting approach. The paper considered examples of flows containing bore diffraction. The first problem investigated the case of a bore wave impinging on a cylinder, and was analogous to an aeronautics test case. The solutions produced were in line with those seen in gas dynamics. The method was also applied to to the case of a bore travelling along a contracting/expanding channel and reasonable solutions were obtained.

Alcrudo and García-Navarro [3] considered a high-order Godunov-type scheme constructed within the finite volume framework. The method was based on the MUSCL approach and included the use of slope limiters. The scheme was first

introduced in one-dimension and then extended to two-dimensions. It was noted that within the finite volume approach, there was no need for the grid to be rectangular or to contain regular cells. Numerical results were presented for three test problems. The first was referred to as an oblique hydraulic jump for which an analytical solution was available. The channel geometry consisted of a converging wall, which in conjunction with certain initial conditions would induce a hydraulic jump at a particular angle. A grid containing rectangular cells was chosen and values close to the exact solution were generated. Next the 2-d dam-break was considered where the depth ratio was chosen to be 2:1. A reasonable solution was produced which did not contain any oscillations. Finally the method was applied to the circular dam-break in [28]. It was noted that this particular problem was radially symmetric and so solutions were obtained using grids generated from both polar and Cartesian co-ordinates. The two solutions contained noticeable differences — the rectangular grid produced a squaring effect in the velocity field plots, in addition to some peculiarities in the depth contours. This effect was also evident in the 3-d depth profile. In contrast the solution obtained from circular gird was perfectly symmetric.

Nujić [46] investigated two schemes for shallow water flow and considered the issue of non-uniform beds. Both methods were written as a predictor-corrector sequence with differing expressions for the numerical flux. The first scheme was based upon the Lax-Friedrichs approach, with the flux expressed as

$$\mathbf{F}_{i+1/2} = \mathbf{F}^{+}_{i+1/2} + \mathbf{F}^{-}_{i+1/2}$$

where

$$\mathbf{F}^{+}_{i+1/2} = \mathbf{F}^{+}_{i} + 0.5\delta\mathbf{F}^{+}_{i}$$

$$\mathbf{F}^{-}_{i+1/2} = \mathbf{F}^{-}_{i+1} - 0.5\delta\mathbf{F}^{-}_{i+1}$$

and

$$\mathbf{F}^{+}_{i} = 0.5(\mathbf{F}_i + \alpha\mathbf{U}_i), \qquad \mathbf{F}^{-}_{i} = 0.5(\mathbf{F}_i - \alpha\mathbf{U}_i).$$

The α term was a coefficient satisfying

$$\alpha \geq \max|\lambda_i|$$

over all of the cells. Alternatively, α could be defined locally over the cells in the computational stencil. The δ functions were defined as

$$\delta\mathbf{F}^{+}_{i} = \text{minmod}(\mathbf{F}^{+}_{i+1} - \mathbf{F}^{+}_{i}, \mathbf{F}^{+}_{i} - \mathbf{F}^{+}_{i-1})$$

$$\delta \mathbf{F}^-_{i-1} = \text{minmod}(\mathbf{F}^-_{i+1} - \mathbf{F}^-_i, \mathbf{F}^-_{i+2} - \mathbf{F}^-_{i+1})$$

using

$$\text{minmod}(a,b) = \begin{cases} a & \text{if} \quad |a| < |b| \quad \text{and} \quad ab > 0 \\ b & \text{if} \quad |b| < |a| \quad \text{and} \quad ab > 0 \\ 0 & \text{if} \quad ab \leq 0. \end{cases}$$

The second method took the flux

$$\mathbf{F}_{i+1/2} = 0.5[\mathbf{F}_R + \mathbf{F}_L - |A_{i+1/2}|(\mathbf{U}_R - \mathbf{U}_L)]$$

and re-wrote it as

$$\mathbf{F}_{i+1/2} = 0.5[\mathbf{F}_R + \mathbf{F}_L - \alpha(\mathbf{U}_R - \mathbf{U}_L)]$$

where

$$\mathbf{U}_L = \mathbf{U}_i + 0.5\delta\mathbf{U}_i$$

and

$$\mathbf{U}_R = \mathbf{U}_{i+1} - 0.5\delta\mathbf{U}_{i+1}$$

following the same definitions for α and the δ values as before.

The two methods were first applied to the 1-d dam-break problem for a depth ratio of 100:1. The results contained no oscillations and the jumps were correctly predicted. The first scheme was then applied to a 2-d dam-break problem and compared with some experimental data, and the MUSCL scheme in [3]. Both numerical methods captured the predominant flow features visible in the experimental data. An example was then given to illustrate the need to treat source terms in an appropriate manner, and it was suggested that the continuity equation should be written in terms of H ($H = h + z$). Also it was proposed that the I_1 term in the momentum equation should be removed from the flux function and discretised in the same way as the source terms, e.g. through central differencing. This new treatment was applied to the same steady state variable bed problem using the first scheme, and an improved solution was obtained.

Fraccarollo and Toro [20] compared numerical results generated by the WAF scheme with experimental data obtained from a dam-break like problem. The HLL Riemann solver was used together with a flux limiter to produce the numerical data. The comparison between the experimental and computational results highlighted certain differences, particularly near the dam location. However overall the numerical approach was seen to predict the predominant flow features.

Ambrosi [4] applied the Roe Riemann solver within the MUSCL and finite volume construction to a number of test problems. The first example considered the 1-d dam-break problem when the downstream bed was dry. In comparison with the exact solution, reasonable agreement was obtained with the most prominent differences occurring in the region of the wet/dry interface. The standard 1-d dam-break was also considered and reasonable results were generated. Finally the method was applied to the 2-d dam-break and produced typical results.

García-Navarro, Hubbard and Priestley [25] considered the application of a genuine multidimensional upwind technique to shallow water flows. The method was based on approximating the solution at the vertices of triangular cells and differed from the standard finite volume approach. The oblique hydraulic jump test problem was used to test the method on a variety of grids. The first was a structured triangular grid and the method was seen to generate a satisfactory solution. The solution from a finite volume TVD scheme on a quadrilateral grid (42×7) was then compared with the results obtained using the new method on an adaptive triangular grid with 96 cells. The new scheme was seen to give a better solution and required half the CPU time of the finite volume scheme. Numerical solutions were also generated for the dam-break experiments reported in [10] for a converging/diverging channel. A comparison was made between the multidimensional upwind method and the finite volume technique for the flat bed case and a sloping bed. Overall the two methods gave very similar solutions which correlated to the experimental data.

Zhao, Shen, Lai and Tabois III [72] compared three different approaches all based on using approximate Riemann solutions within the finite volume method. In particular the paper focussed on problems containing hydraulic jumps. The three methods tested were the flux vector splitting approach of Steger and Warming, the flux difference splitting method of Roe and the Osher scheme. The first problem to be considered was the 1-d dam-break. The solutions were obtained on a fixed grid using a fixed time step. By comparing the shock speed and height, and the velocity and water depth at the dam location, the Osher scheme gave the best results with the FVS producing the worst results, though the differences were only marginal. The second problem considered an advancing surge wave. The three methods gave very similar solutions, and the ratio of CPU run times for the FVS, FDS and Osher method were recorded as 1:1.18:1.04. Next the methods were applied to the two-dimensional dam-break problem and results comparable to those published elsewhere were obtained. Finally solutions were generated for

the oblique jump problem using a rectangular mesh. It was stated that there were no significant differences between the numerical solutions of the three methods, though the Roe scheme required a time step ten times smaller than the other two methods. A sensitivity analysis of how the different methods were affected by size of time steps, non-uniform grids and non-uniform beds was conducted. In summary, the paper concluded that all three methods produced very similar numerical solutions, though formally the Osher scheme was the most accurate and the FVS scheme the least accurate. In run time comparisons the FVS had required the least CPU time, whilst the FDS scheme had needed the most. From changes in Δt and Δx it was observed that the FVS scheme was the most stable and that the FDS scheme was the most sensitive to changes, though for changes in the bed-elevation the opposite was true.

Anastasiou and Chan [6] considered the application of a finite volume scheme based on unstructured triangular grids and the Roe flux. Both the inviscid and viscous form of the two-dimensional shallow water equations were considered. Results were shown for the standard 2-d dam break, the circular dam break and the oblique hydraulic jump problems. All of the solutions were as expected. Two examples including the effects of viscosity were also considered — flow over a backward step and jet flow through a circular reservoir. The solutions produced were stated to be in line with those given elsewhere. Finally an example from meteorology was considered, in which the convective nature of the scheme is tested, by imposing fixed velocities. Results were shown for the convection of a square profile and a cone, using both the Superbee and Minmod limiters. This example highlighted the different nature of the two limiters, as less diffusion was apparent in the solutions obtained using the Superbee limiter.

Sleigh, Berzins, Gaskell and Wright [56] applied an unstructured finite volume method based on the Roe Riemann solver to a number of shallow water test problems. The resulting SPRINT2D suite encompassed a variety of methods to perform the time integration and included procedures to control the temporal and spatial errors. Within the paper a number of issues were considered, including wetting/drying effects and the treatment of boundary conditions. Various results were presented to illustrate the potential of the package including the 2-d dam-break problem and results for the experiments conducted by Bellos *et al.* The solutions presented were in line with those seen elsewhere.

Molls and Molls [45] presented a new approach for solving 2-d flows, based on the integral form of the equations in which the space and time discretisations were combined. This new method did not require the addition of artificial viscosity or flux limiters, and no directional bias was contained within the discrete formulation. Results from the scheme were compared with the Lax-Wendroff and McCormack methods for the 1-d dam-break problem. The new scheme produced the best solution and gave comparable results to those from an upwind TVD scheme. The second example considered was that of a 1-d hydraulic jump and the numerical solutions from two different grids were compared with experimental results. Reasonable agreement between the results was observed. Using operator splitting, the 1-d approach was extended to the 2-d oblique hydraulic jump and a satisfactory solution was generated.

Mingham and Causon [44] used a finite volume method that incorporated the HLL Riemann solver and followed the MUSCL approach. Results were presented for a range of problems. The first was the 1-d dam-break problem and it was observed that varying the choice of slope limiter only produced a marginal difference. The circular 2-d dam-break was also considered on both a Cartesian and a polar mesh. The results highlighted the mesh dependency of the solution, as also seen in [3]. Variants of the oblique hydraulic jump scenario were also considered for a range of flow conditions, in addition to the 2-d dam break. All the solutions presented were reasonable and were in line with expectations.

Chapter 4

Roe Riemann solver

In this chapter, the approximate Riemann solver developed by Roe for the Euler equations is presented, together with details of the application of the method to open channel flow. Information is also given on the implementation of the boundary conditions, as well as an upwind source term treatment specifically constructed for use with Roe's scheme and the Saint Venant equations.

4.1 Roe construction

The information presented in this section is summarised from [34], [41] and [63].

The basis of Roe's method is to construct $\tilde{\mathbf{U}}(x,t)$ in the relationship

$$\mathbf{U}_i^{n+1} = \frac{1}{\Delta x}\int_{x_i-1/2}^{x_{i+1/2}} \tilde{\mathbf{U}}^n(x, t_{n+1})dx,$$

by employing a local linearisation and solving a constant coefficient system of linear conservation laws, with the corresponding flux $\tilde{\mathbf{F}}(\mathbf{U}) = \tilde{A}\mathbf{U}$. In terms of the Riemann problem, the matrix $\tilde{A}$ must depend upon $\mathbf{U}_L$ and $\mathbf{U}_R$ and the modified conservation law is represented by

$$\mathbf{U}_t + \tilde{A}(\mathbf{U}_L, \mathbf{U}_R)\mathbf{U}_x = 0. \tag{4.1}$$

Equation (4.1) is solved exactly, and this corresponds to replacing the original Riemann problem with an approximate Riemann problem. The solution obtained is then an approximate solution to the original conservation law. Using the local

linearisation allows the theory of constant coefficient linear systems to be extended to non-linear problems. The difficulty in extending the linear theory lies in determining an approximate Jacobian, $\tilde{A}$. Roe began by defining a series of properties which any suitable choice of $\tilde{A}(\mathbf{U}_L, \mathbf{U}_R)$ would need to satisfy. Collectively, these criteria were termed 'Property U' and and were interpreted by LeVeque [41] to say that the following conditions should apply

1. $\tilde{A}(\mathbf{U}_L, \mathbf{U}_R)(\mathbf{U}_R - \mathbf{U}_L) = \mathbf{F}(\mathbf{U}_R) - \mathbf{F}(\mathbf{U}_L)$
2. $\tilde{A}(\mathbf{U}_L, \mathbf{U}_R)$ is diagonalizable with real eigenvalues
3. $\tilde{A}(\mathbf{U}_L, \mathbf{U}_R) \rightarrow \mathbf{F}'(\mathbf{U})$ smoothly as $\mathbf{U}_L, \mathbf{U}_R \rightarrow \mathbf{U}$

The first condition ensures that if $\mathbf{U}_L$ and $\mathbf{U}_R$ are connected by a single shock, then the approximate Riemann solution reproduces the exact solution and the Rankine-Hugoniot relationship is satisfied. The second condition ensures that (4.1) is both hyperbolic and soluble. Finally the third requirement means that the solution will behave reasonably for smooth solutions. Although an obvious choice of some form of average such as $\tilde{A} = (A_L + A_R)/2$ or $\tilde{A} = A((\mathbf{U}_L + \mathbf{U}_R)/2)$ might satisfy the second and third conditions, in general such an average will not meet the first condition. Roe demonstrated how to construct a matrix for the Euler equations that would satisfy Property U. The linear theory is extended to non-linear systems by constructing a matrix $\tilde{A}$ for which

$$\tilde{A}\Delta\mathbf{U} = \Delta\mathbf{F}$$

where $\Delta(.) = (.)_R - (.)_L$, (i.e. condition 1.). This is equivalent to finding the approximate values (denoted by $\tilde{}$) that satisfy

$$\Delta\mathbf{U} = \sum \tilde{\alpha}_k \tilde{\mathbf{e}}_k \tag{4.2}$$

and

$$\Delta\mathbf{F} = \sum \tilde{\lambda}_k \tilde{\alpha}_k \tilde{\mathbf{e}}_k \tag{4.3}$$

where $\tilde{\alpha}_k$ corresponds to the strength of the kth wave in the Riemann solution travelling with speed $\tilde{\lambda}_k$, and $\tilde{\mathbf{e}}_k$ represent the right eigenvectors of the matrix $\tilde{A}$ with associated eigenvalues also defined by $\tilde{\lambda}_k$. Having generated the approximated quantities, the flux at the cell interface can be defined as

$$\mathbf{F}_{i+1/2}(\mathbf{U}_L, \mathbf{U}_R) = \frac{1}{2}(\mathbf{F}_L + \mathbf{F}_R) - \frac{1}{2}\sum \tilde{\alpha}_k |\tilde{\lambda}_k| \tilde{\mathbf{e}}_k. \tag{4.4}$$

4.2 Roe's scheme applied to the Saint Venant equations

Glaister [29] derived definitions for the approximate values for the 1-d Saint Venant equations. Following the Roe-Pike approach [52], and using the definitions

$$\mathbf{U} = \begin{pmatrix} A \\ Q \end{pmatrix} \quad \text{and} \quad \mathbf{F} = \begin{pmatrix} Q \\ Q^2/A + gI_1 \end{pmatrix},$$

the exact Jacobian, $\hat{A}$, for the homogeneous Saint Venant equations is defined as

$$\hat{A} = \frac{\partial \mathbf{F}}{\partial \mathbf{U}} = \begin{pmatrix} 0 & 1 \\ c^2 - u^2 & 2u \end{pmatrix}$$

with corresponding eigenvalues and eigenvectors

$$\lambda_1 = u + c \quad \text{and} \quad \lambda_2 = u - c$$

$$\mathbf{e}_1 = \begin{pmatrix} 1 \\ u + c \end{pmatrix} \quad \text{and} \quad \mathbf{e}_2 = \begin{pmatrix} 1 \\ u - c \end{pmatrix}.$$

From this, the approximate Jacobian, $\tilde{A}$ is deemed to have eigenvalues and eigenvalues of the form

$$\tilde{\lambda}_{1,2} = \tilde{u} \pm \tilde{c} \quad \text{and} \quad \tilde{\mathbf{e}}_{1,2} = \begin{pmatrix} 1 \\ \tilde{u} \pm \tilde{c} \end{pmatrix}.$$

The Roe construction is then based on determining the approximate quantities $\tilde{u}$ and $\tilde{c}$ which satisfy all of the constraints. In addition, expressions for $\tilde{\alpha}_{1,2}$ must be found. From (4.2) the following relationships are obtained

$$\Delta A = \tilde{\alpha}_1 + \tilde{\alpha}_2$$

$$\Delta Q = \tilde{\alpha}_1(\tilde{u} + \tilde{c}) + \tilde{\alpha}_2(\tilde{u} + \tilde{c}).$$

From which, $\tilde{\alpha}_1$ and $\tilde{\alpha}_2$ are given by

$$\tilde{\alpha}_1 = \frac{(\tilde{c} - \tilde{u})\Delta A + \Delta Q}{2\tilde{c}}$$

$$\tilde{\alpha}_2 = \frac{(\tilde{c} + \tilde{u})\Delta A - \Delta Q}{2\tilde{c}}.$$

To obtain expressions of $\tilde{u}$ and $\tilde{c}$, (4.3) is expanded to give

$$\Delta Q = (\tilde{u} + \tilde{c})\tilde{\alpha}_1 + (\tilde{u} - \tilde{c})\tilde{\alpha}_2$$

as before, and

$$\Delta(Q^2/A + gI_1) = (\tilde{u} + \tilde{c})^2\tilde{\alpha}_1 + (\tilde{u} - \tilde{c})^2\tilde{\alpha}_2.$$

Substituting for $\tilde{\alpha}_1$ and $\tilde{\alpha}_2$ and rearranging then gives

$$\Delta(Q^2/A) + \tilde{u}^2\Delta A = \tilde{c}^2\Delta A - \Delta g I_1. \tag{4.5}$$

To find $\tilde{u}$ and $\tilde{c}$, both sides of (4.5) are set to zero and expanded, resulting in the square root averages of Roe,

$$\tilde{u} = \frac{\sqrt{A_L}u_L + \sqrt{A_R}u_R}{\sqrt{A_L} + \sqrt{A_R}}$$

$$\tilde{c}^2 = \begin{cases} g\dfrac{I_{1_R} - I_{1_L}}{A_R - A_L} & \text{if} \quad A_R - A_L \neq 0 \\ (c_L + c_R)^2 & \text{if} \quad A_L = A_R \end{cases}.$$

Expressed in the form of (4.4), Roe's flux is conservative and TVD which are both desirable properties of schemes suited to solving conservation laws. However, this formulation is only first order in space and time. In addition, under certain circumstances, the scheme can lead to entropy violating solutions. Fortunately a number of 'entropy fixes' have been devised which rectify this problem, and these are based upon modifying the $|\tilde{\lambda}|$ term in (4.4). The two most popular approaches are based on re-evaluating $|\tilde{\lambda}|$ using the formula ([30] and [69])

$$|\tilde{\lambda}| = \begin{cases} |\tilde{\lambda}| & |\tilde{\lambda}| \geq \varepsilon \\ \varepsilon & |\tilde{\lambda}| < \varepsilon \end{cases}$$

or

$$|\tilde{\lambda}| = \begin{cases} |\tilde{\lambda}| & |\tilde{\lambda}| \geq \varepsilon \\ \dfrac{\tilde{\lambda}^2 + \varepsilon^2}{\varepsilon} & |\tilde{\lambda}| < \varepsilon \end{cases}$$

where ε is a small positive number and can be generated using

$$\varepsilon = \max(0, \tilde{\lambda}(U_L, U_R) - \lambda(U_L), \lambda(U_R) - \tilde{\lambda}(U_L, U_R)).$$

There are two ways to adapt Roe's scheme which result in a method that is formally second order in both space and time. One way is to use a MUSCL approach in which the data used within the Riemann solver (i.e. U_L and U_R) is modified and the update is performed in two stages using a predictor corrector type algorithm. The second approach can be considered as an extension to the Lax-Wendroff scheme and involves the use of flux limiters. The second approach is the one favoured here, and the following extract is taken from [2].

For a system of conservation laws, the Lax-Wendroff flux can be written as

$$\mathbf{F}^*_{i+1/2} = \frac{1}{2}(\mathbf{F}_i + \mathbf{F}_{i+1}) - \frac{1}{2}\hat{A}^2_{i+1/2}(\mathbf{U}_{i+1} - \mathbf{U}_i)$$

where the Jacobian matrix, $\hat{A}_{i+1/2}$ is based upon some average quantity such as

$$\hat{A}_{i+1/2} = \hat{A}\left(\frac{\mathbf{U}_{i+1} + \mathbf{U}_i}{2}\right).$$

An equivalent representation of the Lax-Wendroff flux written in terms of the Roe scheme is then

$$\mathbf{F}^*_{i+1/2} = \frac{1}{2}(\mathbf{F}_{i+1} + \mathbf{F}_i) - \frac{1}{2}\sum_{k=1}^{2}\tilde{\alpha}_k|\tilde{\lambda}_k|\tilde{\mathbf{e}}_k + \frac{1}{2}\sum_{k=1}^{2}\tilde{\alpha}_k|\tilde{\lambda}_k|\left(1 - \frac{\Delta t}{\Delta x}|\tilde{\lambda}_k|\right)\tilde{\mathbf{e}}_k. \quad (4.6)$$

In this form (4.6) is written as a first order scheme with a correction, resulting in a second order scheme. However to obtain a TVD version of the flux, the correction term must be limited and this can be done via a flux limiter, giving

$$\mathbf{F}^*_{i+1/2} = \frac{1}{2}(\mathbf{F}_{i+1} + \mathbf{F}_i) - \frac{1}{2}\sum_{k=1}^{2}\tilde{\alpha}_k|\tilde{\lambda}_k|\tilde{\mathbf{e}}_k + \frac{1}{2}\sum_{k=1}^{2}\phi(r_k)\tilde{\alpha}_k|\tilde{\lambda}_k|\left(1 - \frac{\Delta t}{\Delta x}|\tilde{\lambda}_k|\right)\tilde{\mathbf{e}}_k$$

or

$$\mathbf{F}^*_{i+1/2} = \frac{1}{2}(\mathbf{F}_{i+1} + \mathbf{F}_i) - \frac{1}{2}\sum_{k=1}^{2}\left(1 - \phi(r_k)\left(1 - \frac{\Delta t}{\Delta x}|\tilde{\lambda}_k|\right)\right)\tilde{\alpha}_k|\tilde{\lambda}_k|\tilde{\mathbf{e}}_k.$$

The argument of the limiter function is then

$$r_{i+1/2} = \frac{\tilde{\alpha}_{i+1/2-s}}{\tilde{\alpha}_{i+1/2}} \quad \text{where} \quad s = \text{sgn}(\tilde{\lambda}_{i+1/2}).$$

Several other Riemann solvers have been developed, the most popular of which are due to Osher ([14] and [47]) and Harten, Lax and van Leer [31]. However within the hydraulics community, the Riemann solver of Roe has been the most widely accepted and this has been applied to a variety of situations. Toro has developed several Riemann solvers for use specifically within the weighted average flux (WAF) scheme (see [63] for details of the WAF scheme and a number of Riemann solvers), detailed in the previous chapter.

4.3 Boundary conditions

In discussion so far only homogeneous conservation laws have been considered in isolation from any boundary or source term treatment. Both of these areas are an important consideration in any numerical technique and are now discussed in this section.

4.3.1 Application of the method of characteristics to the boundaries

The question of what to do at the computational boundaries of a problem brings the theory of characteristics back into focus. As mentioned previously, any characteristics which enter the domain should already have values prescribed upon them. As a result it is necessary to provide this information in some manner, or else the problem is not well posed. At the downstream boundary, any characteristics leaving the domain should contain information of the flow variables via the numerical solution. The result is that for any boundary, the number of pieces of information which must be specified relates to the number of characteristics entering/leaving that region.

Consider the upstream boundary. If the flow is subcritical, then the C^+ characteristic points into the computational domain, whereas the C^- characteristic leaves the region. The result is that one of the flow variables (typically Q) must be specified, from which a value of A can be generated from characteristic theory. If the flow is supercritical, then both characteristics enter the region at the upstream boundary, and so values for A and Q must be specified. For the downstream boundary, subcritical flow requires the specification of one variable (usually A) as in the upstream case. If the flow is supercritical then both characteristics should propagate information from the upstream direction downstream. Imposing any values in this case would over specify the problem and represent a contradiction in the mathematical theory. This situation is dealt with by considering a transmissive boundary in which dummy cells are created that mirror the values of the flow variables from the upstream direction. Conversely, a wall boundary maybe imposed whereby the flow cannot continue downstream and is reflected back in the upstream direction. Transmissive boundary conditions may also be applied at the upstream boundary. García-Navarro and Savirón [21] gave details how to apply the theory of characteristics to the boundary conditions of open channel flow problems for McCormack's method, as outline below.

The Saint Venant equations for a prismatic channel written in characteristic form are

$$\frac{\partial Q}{\partial t} + (u \pm c)\frac{\partial Q}{\partial x} + (-u \pm c)\left[\frac{\partial A}{\partial t} + (u \pm c)\frac{\partial A}{\partial x}\right] = gA(S_o - S_f). \qquad (4.7)$$

Consider the upstream boundary and the C^- characteristic as shown in Figure 4.1(a).

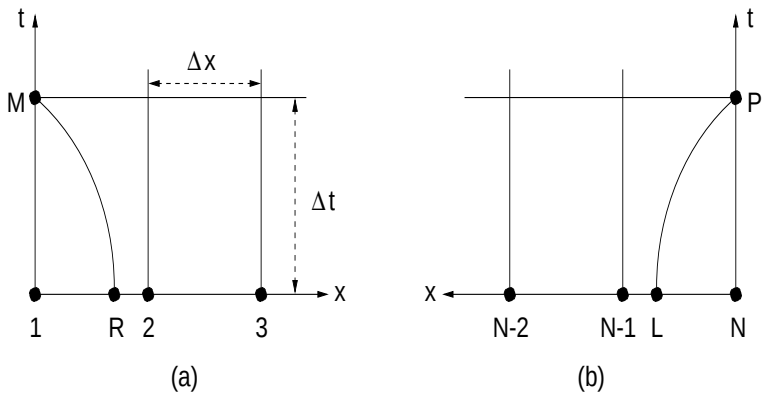

Figure 4.1: Boundary value calculation [21].

An estimate of the position x_R is obtained from

$$x_R = x_M - (u - c)_1^n \Delta t.$$

Assuming that $x_1 < x_R < x_2$ then values for Q and A at point R are found by using linear interpolation

$$Q_R = Q_2^n - (Q_2^n - Q_1^n)\frac{(x_2 - x_R)}{\Delta x}$$

$$A_R = A_2^n - (A_2^n - A_1^n)\frac{(x_2 - x_R)}{\Delta x}.$$

From (4.7), the points M and R are connected by

$$Q_M - Q_R + (-u - c)_R(A_M - A_R) = \Delta t[gA(S_o - S_f)]_R$$

from which, Q_M and A_M are

$$Q_M = Q_R + (u + c)_R(A_M - A_R) + \Delta t[(gA(S_o = S_f)]_R$$

$$A_M = \frac{Q_M - Q_R - \Delta t[(ga(S_o - S_f)]_R}{u + c} + A_R.$$

To obtain a more accurate estimate for either Q_M or A_M, this procedure can be used within an iteration. A new value for x_R can be obtained from

$$x_R = x_M - \frac{\Delta t}{2}[(u - c)_M + (u - c)_R].$$

New estimates for Q_R and A_R are then found using the same interpolations as before, and the resulting expression based upon the characteristic equation is then

$$Q_M - Q_R + \frac{(A_M - A_R)}{2}[(-u-c)_R + (-u-c)_M] = \frac{\Delta t}{2}[(gA(S_o - S_f))_R + (gA(S_o - S_f))_M]$$

from which

$$Q_M = Q_R + \frac{(A_M - A_R)}{2}[(u+c)_R + (u+c)_M] + \frac{\Delta t}{2}[(gA(S_o - S_f))_R + (gA(S_o - S_f))_M]$$

and

$$A_M = \frac{2Q_M - 2Q_R - \Delta t[(gA(S_o - S_f))_R + (gA(S_o - S_f))_M]}{[(u+c)_R + (u+c)_M]} + A_R.$$

The process can be repeated until convergence is obtained. Similarly, applying the same technique to the downstream boundary (see Figure 4.1(b))

$$x_L = x_P - (u+c)_N^n \Delta t$$

and so

$$Q_L = Q_N^n - (Q_N^n - Q_{N-1}^n)(x_N - x_L) \tag{4.8}$$

$$A_L = A_N^n - (A_N^n - A_{N-1}^n)(x_N - x_L). \tag{4.9}$$

The relationship obtained from the characteristic equation is

$$Q_P - Q_L + (-u+c)_L(A_P - A_L) = \Delta t[gA(S_o - S_f)]_L$$

giving

$$Q_P = Q_L + (u-c)_L(A_P - A_L) + \Delta t[gA(S_o - S_f)]_L$$

and

$$A_P = \frac{Q_P - Q_L - \Delta t[gA(S_o - S_f)]_L}{(u-c)_L} + A_L.$$

As before the process may be repeated using

$$x_L = x_P - \frac{\Delta t}{2}[(u+c)_L + (u+c)_P],$$

and using the interpolated values for A_L and Q_L then gives

$$Q_P - Q_L + \frac{A_P - A_L}{2}[(-u+c)_L + (-u+c)_P] = \frac{\Delta t}{2}[(gA(S_o - S_f)_L + (gA(S_o - S_f)_P].$$

Finally the new iterative values are

$$Q_P = Q_L - \frac{A_P - A_L}{2}[(u-c)_L + (u-c)_P] + \frac{\Delta t}{2}[(gA(S_o - S_f)_L + (gA(S_o - S_f)_P].$$

and

$$A_P = \frac{2Q_P - 2Q_L - \Delta t[(gA(S_o - S_f)_L + (gA(S_o - S_f)_P]}{[(u-c)_L + (u-c)_P]} + A_L.$$

Thus given either A or Q at a particular boundary where the flow is subcritical, then the other may be found by considering the characteristics.

4.3.2 Reflective and transmissive boundaries

Reflective boundary conditions [62] are intended to represented the flow impinging upon a fixed surface, such as a wall or where a channel has been closed at the downstream end. The conditions are implemented by creating dummy cells at the end of the reach, for which the the values A and Q are given by

$$A_{N+1} = A_N \qquad Q_{N+1} = -Q_N$$

and

$$A_{N+2} = A_{N-1} \qquad Q_{N+2} = -Q_{N-1}.$$

If the first order scheme is used, then only the first dummy cell, $N+1$ is needed.

A similar strategy is used to construct transmissive boundaries [62]. The idea of transmissive boundaries is in effect to consider the boundaries to be at infinity, such that they do not affect the local behaviour of the flow. If the flow is supercritical at the downstream boundary, then transmissive boundary conditions can also be employed to account for the characteristics leaving the domain. The values for the dummy cells at the downstream end are defined as

$$A_{N+1} = A_N \qquad Q_{N+1} = Q_N$$

and

$$A_{N+2} = A_{N-1} \qquad Q_{N+2} = Q_{N-1},$$

with a similar construction for the values at the upstream boundary.

4.3.3 Weir boundary condition

The weir boundary condition may be implemented at the downstream end of the reach to simulate the presence of a weir. The following treatment is for a sharp-crested weir [55].

The flow variables for a sharp-crested weir are connected through the relationship

$$u = \frac{2}{3} C_d \sqrt{(2gH)} \tag{4.10}$$

where C_d is a coefficient of discharge (taken to be 0.6) and H is the depth of the fluid above the level of the weir. Applying the method of characteristics to the weir, then for the C^+ characteristic which arrives at the weir, the relationship

$$u_0 + 2c_0 = u_1 + 2c_1 \tag{4.11}$$

can be applied, where '0' corresponds to a point just upstream of the weir, and '1' denotes the values at the weir. From (4.10) and (4.11) and using $gH = c^2 - gh_{wier}$, then

$$f(c_1) = u_0 + 2c_0 - \frac{2}{3}C_d\sqrt{2(c_1^2 - gh_{weir})} - 2c_1 \tag{4.12}$$

where h_{weir} corresponds to the height of the weir. From Equation (4.12), the Newton-Raphson technique can be used to find a value for c_1 and subsequently u_1. The values needed for the for the point where the characteristic emanates just upstream of the weir can estimated using the relationships (4.8) and (4.9).

4.4 Source terms

Within finite difference and finite volume schemes, the simplest way to incorporate source terms into a numerical method is to add on a pointwise approximation for each cell. The resulting scheme is then written as

$$\mathbf{U}_i^{n+1} = \mathbf{U}_i^n - \frac{\Delta t}{\Delta x}(\mathbf{F}^*_{i+1/2} - \mathbf{F}^*_{i-1/2}) + \Delta t \mathbf{R}_i^n.$$

where $\mathbf{R}_i^n = \mathbf{R}(\mathbf{U}_i^n)$. This implementation has proved satisfactory in many situations. However for flows in which the source terms play a significant role, this treatment can be inadequate and an upwind approach may be more suitable [53]. This situation was highlighted for the Saint Venant equations in a paper by Bermúdez and Vázquez [8], who then proposed a way to include the source terms via an upwinded discretisation. The paper considered non-uniform beds for which S_o was not constant, and showed how to construct a source term treatment that would not perturb an equilibrium solution. The analysis was performed on the equations written in terms of h and u for a prismatic rectangular channel, using the vectors

$$\mathbf{U} = \begin{pmatrix} h \\ hu \end{pmatrix}, \quad \mathbf{F}(\mathbf{U}) = \begin{pmatrix} q \\ \dfrac{q^2}{h} + \dfrac{1}{2}gh^2 \end{pmatrix} \quad \text{and} \quad \mathbf{G}(x, \mathbf{U}) = \begin{pmatrix} 0 \\ ghH'(x) \end{pmatrix}$$

where H represents the distance between the bed and a datum level and q is the discharge per unit width ($q = Q/b$). This form of the equations is directly obtainable from the (A, Q) divergent formulation.

The basis of the construction for the source term is as follows — the approximation to the source term, $\mathbf{R}_i^n$ is considered as a cell average value satisfying the

relationship

$$\mathbf{R}_i^n = \frac{1}{\Delta x}\int_{x_{i-1/2}}^{x_{i+1/2}} \mathbf{R}(x,\mathbf{U})dx.$$

Following the way in which numerical flux functions are defined, a numerical source function, $\mathcal{R}$, is generated which depends on the local variables such that

$$\mathbf{R}_i^n = \mathcal{R}(x_{i-1}, x_i, x_{i+1}, \mathbf{U}_{i-1}^n, \mathbf{U}_i^n, \mathbf{U}_{i+1}^n)$$

and can be written as the sum of left and right contributions to give

$$\mathcal{R}(x,y,z,X,Y,Z) = \mathcal{R}_L(x,y,X,Y) + \mathcal{R}_R(y,z,Y,Z).$$

The definitions of $\mathcal{R}_L$ and $\mathcal{R}_R$ depend on the numerical scheme being used and can generally be represented as

$$\mathcal{R}_L(x,y,X,Y) = \frac{1}{2}[I + |Q(X,Y)|Q^{-1}(X,Y)]\tilde{\mathbf{R}}(x,y,X,Y)$$

and

$$\mathcal{R}_R(y,z,Y,Z) = \frac{1}{2}[I + |Q(Y,Z)|Q^{-1}(Y,Z)]\tilde{\mathbf{R}}(y,z,Y,Z)$$

for schemes where the flux function is defined as

$$\mathbf{F}^*(X,Y) = \frac{\mathbf{F}(X)+\mathbf{F}(Y)}{2} - \frac{1}{2}|Q(X,Y)|(Y-X)$$

such as Roe's scheme where Q corresponds to the Jacobian, and $\tilde{\mathbf{R}}$ is some approximation to $\mathbf{R}$. Using the definitions of Glaister [27], i.e.

$$Q(\mathbf{U_L},\mathbf{U_R}) = A(\tilde{\mathbf{U}}) = \begin{pmatrix} 0 & 1 \\ \tilde{c^2} - \tilde{u}^2 & 2\tilde{u} \end{pmatrix}$$

where

$$\mathbf{U}_L = \begin{pmatrix} h_L \\ h_L u_L \end{pmatrix}, \quad \mathbf{U}_R = \begin{pmatrix} h_R \\ h_R u_R \end{pmatrix}, \quad \tilde{\mathbf{U}} = \begin{pmatrix} \tilde{h} \\ \tilde{h}\tilde{u} \end{pmatrix}$$

$$\tilde{c} = \sqrt{g\left(\frac{h_L+h_R}{2}\right)}$$

$$\tilde{h} = \sqrt{h_L h_R}$$

$$\tilde{u} = \frac{\sqrt{h_L}u_L + \sqrt{h_R}u_R}{\sqrt{h_L}+\sqrt{h_R}}$$

and

$$\tilde{\mathbf{R}}(x,y,\mathbf{U}_L\mathbf{U}_R) = \begin{pmatrix} 0 \\ \sqrt{h_L h_R}\left(\dfrac{H(y)-H(x)}{y-x}\right) \end{pmatrix}$$

Bermúdez and Vázquez introduced the concept of Property C, whereby a given scheme would satisfy Property C if in the case of stationary flow (zero discharge), there was an exact balance between the discrete components of the flux and the source terms. They showed that Roe's scheme would satisfy Property C approximately, within $O(\Delta x^2)$. It was also shown that by using a different definition of $\tilde{\mathbf{R}}$,

$$\tilde{\mathbf{R}}(x, y, \mathbf{U}_L \mathbf{U}_R) = \begin{pmatrix} 0 \\ g\left(\frac{h_L + h_R}{2}\right)\left(\frac{H(y) - H(x)}{y - x}\right) \end{pmatrix}$$

then Property C would be satisfied exactly, ensuring that an equilibrium solution would not be perturbed. From the analysis, the resulting expression for the source term when $Q = 0$ everywhere is

$$\mathbf{R}_i^n = \begin{pmatrix} -\frac{1}{2}\left\{\sqrt{g\left(\frac{h_i^n + h_{i+1}^n}{2}\right)}\frac{(H(x_{i+1}) - H(x_i))}{\Delta x} - \sqrt{g\left(\frac{h_{i-1}^n + h_i^n}{2}\right)}\frac{(H(x_i) - H(x_{i-1}))}{\Delta x}\right\} \\ \frac{1}{2}\left\{g\left(\frac{h_{i-1}^n + h_i^n}{2}\right)\frac{(H(x_i) - H(x_{i-1}))}{\Delta x} + g\left(\frac{h_i^n + h_{i+1}^n}{2}\right)\frac{(H(x_{i+1}) - H(x_i))}{\Delta x}\right\} \end{pmatrix}.$$

Following on from [8], García-Navarro and Vázquez-Cendón [26] described how to adapt this upwind approach to rectangular non-prismatic channels. The starting point was to verify the choice of definition for $\tilde{c}$. As I_1 and I_2 are defined by

$$I_1 = \int_0^{h(x,t)} (h - \eta)\sigma(x, \eta) d\eta$$

and

$$I_2 = \int_0^{h(x,t)} (h - \eta)\frac{\partial \sigma(x, \eta)}{\partial x} d\eta$$

where

$$\sigma(x, \eta) = \frac{\partial A(x, \eta)}{\partial \eta},$$

then following Leibnitz's rule

$$\frac{\partial I_1}{\partial x} = I_2 + A\frac{\partial h}{\partial x}. \tag{4.13}$$

From the Roe decomposition, the jumps in I_1 and A are connected by

$$g\Delta I_1 = \tilde{c}^2 \Delta A \tag{4.14}$$

which led to the definition

$$\tilde{c}_{i+1/2} = \begin{cases} \frac{1}{2}(c_i + c_{i+1}) & \text{if } A_i = A_{i+1} \\ \sqrt{g\frac{\Delta I_1}{\Delta A}} & \text{otherwise.} \end{cases}$$

From (4.13), the jump in I_1 can be represented by

$$\Delta I_1 = I_2 \Delta x + A \Delta h, \tag{4.15}$$

and as

$$\frac{\partial A}{\partial x} = \frac{\partial A}{\partial h}\frac{\partial h}{\partial x} + \frac{\partial A}{\partial b}\frac{\partial b}{\partial x} = b\frac{\partial h}{\partial x} + h\frac{\partial b}{\partial x}$$

for a rectangular channel, then

$$\Delta A = b\Delta h + h\Delta b$$

from which

$$\Delta h = \frac{\Delta A}{b} - h\frac{\Delta b}{b}$$

and so (4.15) becomes

$$\Delta I_1 = I_2 \Delta x + \frac{A}{b} h \Delta A. \tag{4.16}$$

From (4.16) it can be seen that from the expansion, ΔI_1 is connected to ΔA though only one term. Using this information in (4.14) by replacing ΔI_1 with $Ah\Delta A/b$ then gives

$$g\frac{A}{b}\Delta A = \tilde{c}^2$$

from which the new definition of $\tilde{c}$ is obtained

$$\tilde{c}_{i+1/2} = \sqrt{\frac{g}{2}\left[\left(\frac{A}{b}\right)_i + \left(\frac{A}{b}\right)_{i+1}\right]}.$$

The upwind source term discretisation introduced in [8] is re-expressed as

$$\mathbf{R}_i^n \Delta x = \frac{1}{\Delta x}\left(\frac{\Delta x}{2}(\psi_L)_{i-1/2} + \frac{\Delta x}{2}(\psi_R)_{i+1/2}\right)$$

for a uniform mesh, where

$$\psi_L = \tilde{\beta}\begin{pmatrix} s_1 - s_2 \\ \tilde{\lambda}_1(1+s_1) - \tilde{\lambda}_2(1+s_2) \end{pmatrix}$$

$$\psi_R = \tilde{\beta}\begin{pmatrix} s_2 - s_1 \\ \tilde{\lambda}_1(1-s_1) - \tilde{\lambda}_2(1-s_2) \end{pmatrix}$$

and $\tilde{\beta}$ is defined as

$$\tilde{\beta} = g\frac{\Delta x}{2\tilde{c}}\left(-\tilde{A}z_x - \tilde{A}\tilde{S}_f + \frac{\tilde{A}^2}{2\tilde{b}^2}b_x\right)$$

and s_1 and s_2 correspond to the signs of $\tilde{\lambda}_1$ and $\tilde{\lambda}_2$.

The paper considers the case of a non-prismatic rectangular channel such that

$$\frac{\partial b}{\partial x} = b_x \neq 0 \quad \text{and} \quad I_2 = \frac{gA^2}{2b^2} b_x.$$

In this case they show that from

$$\Delta \mathbf{U} = \begin{pmatrix} \Delta A \\ \Delta Q \end{pmatrix}$$

then

$$A\Delta \mathbf{U} = \begin{pmatrix} \Delta Q \\ \left(g\frac{A}{b} - \frac{Q^2}{A^2} \right) \Delta A + 2\frac{Q}{A}\Delta Q \end{pmatrix},$$

and

$$\Delta \mathbf{F} = \begin{pmatrix} \Delta Q \\ \Delta \left(\frac{Q^2}{A} \right) + \frac{g}{2} \Delta \left(\frac{A^2}{b} \right) \end{pmatrix} = \begin{pmatrix} \Delta Q \\ \left(g\frac{A}{b} - \frac{Q^2}{A^2} \right) \Delta A + 2\frac{Q}{A}\Delta Q - \frac{gA^2}{2b^2}\Delta b \end{pmatrix}$$

from which

$$\Delta \mathbf{F} \neq A\Delta \mathbf{U}.$$

Instead the relationship

$$\Delta \mathbf{F} = A\Delta \mathbf{U} + \mathbf{V}$$

holds, where

$$\mathbf{V} = \begin{pmatrix} 0 \\ -\frac{gA^2}{2b^2}\Delta b \end{pmatrix}.$$

The term $\mathbf{V}$ can be moved to the left hand side of the system and be treated as an additional source term giving

$$\hat{\mathbf{R}} = \mathbf{R} + \mathbf{V} = \begin{pmatrix} 0 \\ \frac{gA^2}{b^2} b_x + gA(S_o - S_f) \end{pmatrix}$$

leading to the new definition of $\tilde{\beta}$

$$\tilde{\beta} = g\frac{\Delta x}{2\tilde{c}} \left(-\tilde{A} z_x - \tilde{A}\tilde{S}_f + \frac{\tilde{A}^2}{\tilde{b}^2} b_x \right)$$

or

$$\tilde{\beta} = \frac{g}{2\tilde{c}} \left(-\tilde{A}\Delta z - \Delta x \tilde{A}\tilde{S}_f + \frac{\tilde{A}^2}{\tilde{b}^2}\Delta b \right) \tag{4.17}$$

The paper then considers the situation at equilibrium for which

$$\mathbf{U}_i^{n+1} = \mathbf{U}_i^n$$

and the discharge is zero everywhere. In order for the solution not to be perturbed from the equilibrium state then

$$\frac{\Delta t}{\Delta x}(\mathbf{F}^*_{i+1/2} - \mathbf{F}^*_{i-1/2}) = \frac{\Delta t}{\Delta x}\left(\frac{1}{2}(\psi_L)_{i-1/2} + \frac{1}{2}(\psi_R)_{i+1/2}\right) \tag{4.18}$$

must hold. The corresponding left and right sides of (4.18) in this situation are

$$LHS = \frac{\Delta t}{2\Delta x}\begin{pmatrix} -(\tilde{c}\Delta A)_{i+1/2} + (\tilde{c}\Delta A)_{i-1/2} \\ \left(\dfrac{gA^2}{2b}\right)_{i+1} - \left(\dfrac{gA^2}{2b}\right)_{i-1} \end{pmatrix}$$

and

$$RHS = \frac{\Delta t}{\Delta x}\begin{pmatrix} -\tilde{\beta}_{i+1/2} + \tilde{\beta}_{i-1/2} \\ (\tilde{c}\tilde{\beta})_{i+1/2} + (\tilde{c}\tilde{\beta})_{i-1/2} \end{pmatrix}.$$

Using the new definition of $\tilde{c}$ and the averages

$$\tilde{h} = \frac{1}{2}(h_{i+1} + h_i), \quad \tilde{b} = \frac{1}{2}(b_{i+1} + b_i) \quad \text{and} \quad \tilde{A} = \tilde{h}\tilde{b}$$

together with

$$\Delta z = z_{i+1} - z_i \quad \text{and} \quad \Delta b = b_{i+1} - b_i$$

and (4.17) for $\tilde{\beta}$, it can be shown that the top lines of the LHS and RHS balance and so equilibrium is achieved. Analysis of the bottom line gives

$$RHS = LHS + \frac{g}{4}(h_{i-1}h_i(b_i - b_{i-1}) + h_i h_{i+1}(b_{i+1} - b_i)).$$

Thus in order to maintain equilibrium, the numerical flux is modified to

$$\mathbf{F}^*_{i-1/2} = \frac{1}{2}(\mathbf{F}_{i-1} + \mathbf{F}_i + \mathbf{V}_{i-1/2}) - \frac{1}{2}\sum_k (|\tilde{\lambda}_k|\tilde{\alpha}_k\tilde{\mathbf{e}}_k)_{i-1/2}$$

$$\mathbf{F}^*_{i+1/2} = \frac{1}{2}(\mathbf{F}_i + \mathbf{F}_{i+1} - \mathbf{V}_{i+1/2}) - \frac{1}{2}\sum_k (|\tilde{\lambda}_k|\tilde{\alpha}_k\tilde{\mathbf{e}}_k)_{i+1/2}$$

where

$$\mathbf{V}_{i-1/2} = \begin{pmatrix} 0 \\ -\dfrac{h_{i-1}h_i}{2}(b_i - b_{i-1}) \end{pmatrix} \quad \text{and} \quad \mathbf{V}_{i+1/2} = \begin{pmatrix} 0 \\ -\dfrac{h_i h_{i+1}}{2}(b_{i+1} - b_i) \end{pmatrix}.$$

This approach has subsequently been extended to the 2-d shallow water equations and applied to coastal flows by Bermúdez *et al* [9].

Chapter 5

Local time stepping

By analysing the scientific literature a number of trends can be identified within the progress of computational hydraulics, and these have followed the advances in computer capability and developments within gas dynamics. Within the research community, attention has moved from the classical Lax-Wendroff and McCormack schemes towards their TVD variants, and techniques originally developed using the finite difference framework have been extended as finite volume methods. Despite this progress, there are still a number of areas which give rise to difficulties. In particular this thesis is concerned with finding ways to apply the reliable methods which have become available at a reduced computational cost, leading to shorter run times. Although in the case of one-dimensional problems, most simulations do not lead to prohibitively long run times, this problem is frequently experienced in two-dimensional situations. Implicit methods can reduce this effect, but the benefits produced by being able to use a larger time step are often counteracted by the increased complexity of the resulting algorithm. Another feature inherent with implicit schemes is the increased smearing effect visible in discontinuities. In some situations this may be of little consequence. Indeed this is an accepted feature of ISIS (though the origins are somewhat different), and is a necessity if the Preissmann scheme is to be applied to transcritical flows.

In investigating ways in which to improve the methods currently used in computational hydraulics, one option is to return to the field of aeronautics and see what possibilities are available. One technique which as yet does not appear to have been widely considered for unsteady channel flows, is local time stepping (LTS). The strategy behind local time stepping, is to advance individual cells in

time, using each cell's permitted time step rather than the global minimum value. The difficulty with this approach lies in ensuring that the correct integration procedure is followed, and if an efficient means of doing so cannot be devised, then the advantages of such a technique disappear. As this is not a consideration for steady flows, local time stepping is commonly used to accelerate the convergence of solutions in steady state problems.

The main benefit in employing a local time stepping approach, is the resulting reduction in computer run time of the simulation, in comparison to when global time stepping is used. In addition, using such a method may also result in an improved numerical solution, particularly when the flow conditions vary abruptly (as is the case with hydraulic jumps). In the context of open channel flow, one dimensional simulations do not generally require excessive run times, and rapid spatial transients can be modelled satisfactory using higher order TVD schemes. However, two dimensional simulations often do require excessive computing time, and the use of local time stepping may go some way to reduce this problem. With a view to investigating the potential benefits of applying local time stepping to higher dimensional problems, the application of local time stepping to one dimensional flows is now considered. The justification in assessing the impact of local time stepping to the one dimensional case is that generally new procedures are first evaluated for simpler/lower order problems, before being extended to more complex situations. In this way, it is generally easier to develop an understanding of the issues involved in employing a new technique. In addition, standard test cases are usually available for one-dimensional problems, in which a method's performance may be assessed against a standardised result. This is particularly true of open channel hydraulics, where most of the accepted test problems are for one-dimensional flows.

Two procedures for applying local time stepping to time dependent flows are outlined here. These strategies were originally demonstrated to be successful for the Euler equations and are subsequently developed here for the Saint Venant equations of open channel flow.

5.1 Local time stepping using a 'frozen flux' (LTS1)

Zhang, Trepánier, Reggio and Camarero ([70] and [71]) presented a technique for local time stepping which was based upon a frozen flux approach. This strategy

was implemented within the Roe Riemann solver and applied to 1-d and 2-d test cases for the Euler equations. From the examples presented, a number of features of the LTS procedure were identified

(1) Implementing the LTS strategy on a uniform grid gave little reduction in computer run times

(2) Implementing the LTS strategy on an irregular grid could give significant CPU savings

(3) The resolution of shocks was improved by using an LTS scheme.

The differences observed between uniform and non-uniform grids were as a result of the fact that the LTS procedure was only implemented for cells which had time steps greater than twice the global minimum value. As a consequence of this, if the flow was such that most cells were updated using global time stepping (GTS), then the efficiency of the approach was reduced. This effect was illustrated on a series of irregular grids which contained a region of uniform cells, connected to a non-uniform region. In order to examine the efficiency of the LTS method, a series of run time measurements were made and contrasted to those using the GTS approach. A variety of grids were considered, in which the ratio of the largest cell lengths to the uniform cell widths was varied. Results were generated for the shock tube problem, as shown in Table 5.1.

Scheme order	Grid points	Grid ratio	Total CPU GTS/LTS	SQRT CPU GTS/LTS
1	141	3.35	1.72	1.92
1	221	5.82	2.02	2.74
1	301	12.57	2.25	3.23
2	221	5.82	2.20	3.24

Table 5.1: Comparison of LTS and GTS run times [70].

The LTS procedure was also implemented within a second order scheme. From the table it can be seen that as the grid ratio was increased, then the efficiency gain of the LTS method to the GTS procedure increased accordingly. In addition, when a more complex flux function was used (corresponding to the second order scheme),

the LTS strategy was observed to give a greater run time saving than when the first order scheme was used. As the timings given in Table 5.1 include additional overheads which might prevent a true comparison of the GTS and LTS approaches, the CPU times required to perform the square root calculations were measured. As square roots were only evaluated as part of the flux calculation, this ratio should reflect the efficiency gain of the LTS technique without the cost of the additional computation necessary to implement the technique. It was also observed that the LTS results gave much sharper resolution of the moving shock, and closer agreement was obtained between the numerical and analytical solutions in the region of the rarefaction wave and contact discontinuity. This was a consequence of allowing individual cells to be advanced by their local CFL condition and hence resulted in a reduction of the local truncation error.

The method was extended to a two-dimensional problem on an unstructured triangular mesh. For this example, the LTS approach proved to be 2.2 times faster than using global time stepping and again better shock resolution was obtained.

A steady example was also considered for the viscous Navier-Stokes equations. In this case it was noted that a converged solution was produced 4.5 times faster using the LTS method. The increased performance of the procedure was attributed to the fact that the Navier-Stokes flux calculation was more complex than that of the Euler equations.

5.1.1 Implementation of the LTS1 strategy

The LTS procedure was outlined in the papers ([70], [71]) for a one-dimensional conservation law, for which the update from one time level to the next for a particular cell i was written as

$$\mathbf{U}_i^{n+1} = \mathbf{U}_i^n - \frac{\Delta t}{\Delta x_i}\left(\mathbf{F}_{i+1/2}^n - \mathbf{F}_{i-1/2}^n\right).$$

In terms of the stability criteria, instead of using the same value of Δt throughout the grid, each cell can be updated by a local time step Δt_i. Denoting δt as the global minimum time step, such that $\delta t = \min_i(\Delta t_i)$, then for each cell there will be some integer value of k which satisfies

$$k\delta t \leq \Delta t_i \leq (k+1)\delta t.$$

This allows the solution $\mathbf{U}_i^n$ to be advanced though a series of updates, using the flux values $\mathbf{F}_{i\pm1/2}^n$, which satisfy the stability requirements of the chosen method.

The update sequence is then given by

$$\mathbf{U}_i^{n+j} = \mathbf{U}_i^n - \frac{j\delta t}{\Delta x_i}\left(\mathbf{F}_{i+1/2}^n - \mathbf{F}_{i-1/2}^n\right)$$

or

$$\mathbf{U}_i^{n+j} = \mathbf{U}_i^n - \frac{\delta t}{\Delta x_i}\sum_{l=1}^{j}\left(\mathbf{F}_{i+1/2}^n - \mathbf{F}_{i-1/2}^n\right) \tag{5.1}$$

where $j = 1, 2, ..., k$. Note that the index j represents a series of local time steps. When j reaches the value of k, one global time step has been completed. Following this notation, the corresponding GTS procedure whereby the flux functions are re-evaluated at every local time step can be represented as

$$\mathbf{U}_i^{n+j} = \mathbf{U}_i^{n+j-1} - \frac{\delta t}{\Delta x_i}\left(\mathbf{F}_{i+1/2}^{n+j-1} - \mathbf{F}_{i-1/2}^{n+j-1}\right)$$

or

$$\mathbf{U}_i^{n+j} = \mathbf{U}_i^n - \frac{\delta t}{\Delta x_i}\sum_{l=1}^{j}\left(\mathbf{F}_{i+1/2}^{n+l} - \mathbf{F}_{i-1/2}^{n+l}\right). \tag{5.2}$$

In the case where $k = 1$, these two forms are equivalent. The update procedures (5.1) and (5.2) are similar apart from the fact that for the LTS version, the flux values are frozen at time level n. As calculating the flux generally corresponds to the most computationally expensive part of the time integration, using this approach should prove more efficient.

Following this strategy, individual cells are divided into two groups — those that require the use of global time stepping (G_1), and those to which the LTS procedure may be applied (G_2). The selection is based upon the values of Δt_i and is formulated as

$$\begin{aligned} G_1 \quad &\text{if} \quad \Delta t_i \leq 2\delta t, \\ G_2 \quad &\text{if} \quad \Delta t_i > 2\delta t. \end{aligned}$$

At the start of the simulation, all the values of $\mathbf{U}$ and $\mathbf{F}$ are known, and the values of Δt_i can be found, leading to a value of δt. All of the cells are then advanced by δt — the global minimum time step. To reach the next level, the flux values for all of the G_1 cells must be recalculated, whilst the G_2 cells can be updated using the previously calculated flux functions. The cell interface which connects regions of G_1 and G_2 cells, is included in the G_1 region. In addition, the local time step distribution needs to be re-evaluated so that fast propagating information from neighbouring cells reaches the appropriate cells at the correct moment in time. This is achieved by limiting the local time steps of any cells which would otherwise

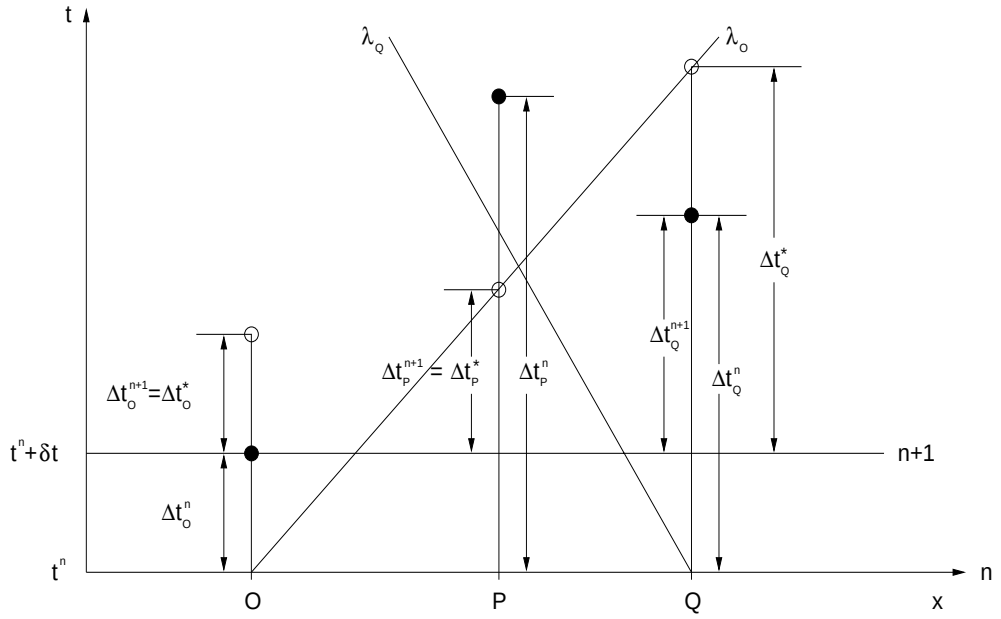

Figure 5.1: Local time step re-evaluation for LTS1 ([70], [71]).

not receive the correct information. This is achieved by setting the new local time step of the G_2 cells to be

$$\Delta t_i^{n+1} = \min\{(\Delta t_i^n - \delta t), \Delta t_i^*\}$$

where the $*$ value denotes the time at which any information from neighbouring cells will reach cell i. This is illustrated in Figure 5.1 for the cells O, P and Q (which are not necessarily adjacent). The fast propagating information from cell O (at time n) will reach P before the flux values of P are due to be re-calculated. Thus in order to ensure that the information reaches P at the correct time, the time step of P is re-evaluated on the basis of Δt_P^*. In the case of Q, the information from O will not reach Q until after the flux values are due to be updated, and so no limiting is necessary.

This procedure is repeated until the maximum allowable time step ($\max_i(\Delta t_i)$) is reached, and this represents the end of the local time stepping cycle. The process is then repeated from the beginning and continues until the end of the simulation.

Note that the formulas (5.1) and (5.2) (as presented in the original papers ([70] & [71])) serve as a means to illustrate the local time stepping concept, and consider the case where δt is constant throughout the global time step. In practise, δt must be evaluated for every local time step.

5.2 Local time stepping using full time integration (LTS2)

Kleb, Batina and Williams [40] presented a local time stepping technique for the Euler and Navier-Stokes equations on unstructured meshes. Unlike the previous method, this algorithm was based on updating the individual cells to a level near that allowed by the CFL limit. Linear interpolation was then used at the interface regions to extract information at the correct time level where necessary.

The method was demonstrated through two examples, the shock tube problem and the flow over an aerofoil. Results for the shock tube problem were presented on two grids containing a random distribution of cells. The first grid contained 100 cells, and the observed ratio of run times between the GTS and LTS approaches was 6.2. This ratio increased to 8.4 when the number of grid points was increased to 200. From the results shown, the LTS and GTS solutions appeared indistinguishable.

The Euler equations were also used to calculated the flow over an aerofoil. Several different grids were considered giving run time ratios between 3 and 9. Another aerofoil problem was also considered and solved using the Navier-Stokes equations. This example was a steady state problem, and the LTS approach proved to be between 6 and 7 times faster than global time stepping.

5.2.1 Implementation of the LTS2 strategy

To initiate the local time stepping procedure, the local time step values, Δt_i, are calculated and the corresponding minimum value, δt is found. Each cell is then assigned a value of m_i which corresponds to the local time step's power of 2 multiple of δt, calculated from

$$m_i = \text{int}\left[\frac{\log(\Delta t_i/\delta t)}{\log(2)}\right].$$

This relationship is such that

$$2^{m_i} \leq \frac{\Delta t_i}{\delta t} < 2^{m_i+1}.$$

Following this assignment, the local time steps are re-evaluated in terms of power of two multiples of the minimum time step. This is accomplished by defining the

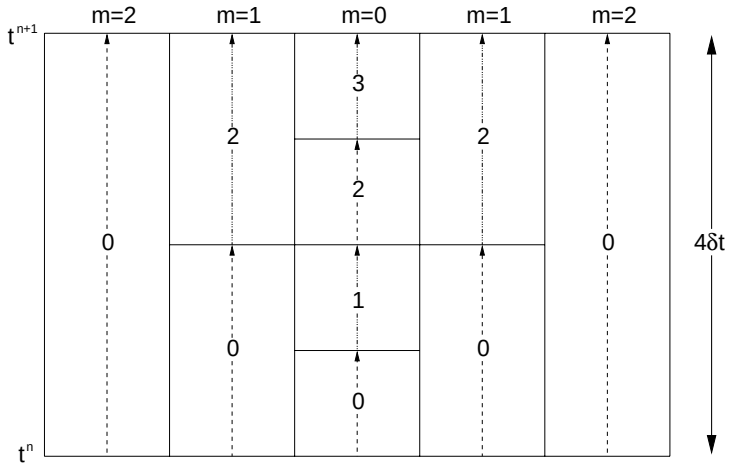

Figure 5.2: Integration sequence for LTS2.

new values as

$$\Delta t_i^{'} = \delta t \; 2^{m_i}.$$

The basis of the integration procedure is to form a series of 'passes' over the mesh and to update particular cells to their permitted point in time. On each pass, cells with a particular m-value will be integrated. On pass 0, all of the cells are updated by their respective time steps. On subsequent passes, those cells for which 2^m is an integer multiple of the pass number, are integrated. This is illustrated in Figure 5.2 for the values $m = 0, 1, 2$. The sequence is shown and the numbers for each update correspond to the pass number at which the update takes place.

As can be seen, cells for which $m = 0$ are always updated. If the cells which have a particular m value are to be integrated, then any cells having a lower value of m will also be updated.

The total number of passes which take place over a global time step, depends on the maximum value of m. Let $m_{max} = \max_i(m_i)$, then if P_{total} is the total number passes, then

$$P_{total} = 2^{m_{max}}$$

where the pass number takes the values $P_{number} = 0, 1, ..., 2^{m_{max}} - 1$. In Figure 5.2, m_{max} is 2, and a total of 4 passes are made.

Note that within this algorithm, the value of δt is the same throughout a single global time step.

The time step distribution presented was previously considered by Pervaiz and Baron [48] who applied local time stepping to chemically reactive flows. However,

Pervaiz and Baron followed a different integration procedure for updating the cells. In addition, the time step distribution was such that no cell had a time step that was greater than four times that of the neighbouring cells.

5.3 Additional considerations of using local time stepping

Both of the LTS strategies presented were applied to non-uniform grids and were implemented in conjunction with upwind techniques. The construction in both cases was such that the LTS strategy could be incorporated into other two time level methods. For the purpose of comparing the two approaches, it is necessary to base the formulations on the same numerical method. Given the popularity of Riemann based methods, the Roe scheme was chosen to analyse the relative merits of the two LTS algorithms. Another advantage of choosing Roe's scheme was that by using flux limiters, a comparison could also be made between the first order method and the second order extensions. In addition the upwind source term treatments proposed by Bermúdez and Vázquez [8] and extended by García-Navarro and Vázquez-Cendón [26], could also be considered within the LTS strategy. From the point of view of incorporating these ideas into solving problems governed by the Saint Venant equations, a number of issues must be addressed —

1) In the first LTS procedure, which G_2 cells require special treatment due to the interaction of neighbouring G_1 cells, and is this dependent on the choice of numerical scheme?

2) In the second LTS approach, is it necessary to limit the individual time steps to be at most four times that of the neighbouring cells (as suggested by Pervaiz and Baron [48]) Also, should the m values be subject to a upper limit?

3) Does using a second order scheme introduce any additional difficulties for either LTS procedure?

4) Can the source terms be incorporated into the LTS strategy?

It would seem natural to suppose that the time step limiting treatment needed for the first LTS method, would somehow depend upon the computational stencil

and perhaps on the local flow conditions. From the point of view of reducing computational costs, it would be beneficial to be able to include the source term effects within the LTS approach. In particular, for the frozen flux method, it would seem appropriate to have a frozen source term, which is only calculated when the flux is updated.

5.3.1 Application and development of the LTS1 procedure

In the description given by Zhang *et al* of the frozen flux local time stepping approach, it was suggested that at the location of the boundary between the G_1/G_2 regions, the flux at the interface should be treated as though it were contained within the G_1 region. It was also proposed that that the local time step distribution be re-assigned after each local time step, to account for information propagating from other cells, such that the flux values at the interfaces captured the appropriate information at the right point in time. The precise mechanism for addressing both of the issues raised requires further investigation, in order to establish an appropriate algorithm for implementing the strategy. An understanding of the procedure is particularly important if the LTS approach is to be incorporated into a higher order scheme.

The details presented by Zhang *et al* suggest that given a G_2 cell which is adjacent to a G_1 cell, it is sufficient to treat the interface to be contained within the G_1 region. In terms of implementing the LTS procedure, the G_1 cells can be identified, along with the fluxes bordering the G_1 cells, and these are then updated. If the mechanism for updating the flux values at the interfaces is implemented in this way, then the G_1/G_2 interface should not require any further special treatment (disregarding the issue of limiting the time steps). Another interpretation would be to treat any G_2 cells which border G_1 regions, as G_1 cells (with the exception of the treating the next interface along as a G_1/G_2 interface). The issue of how to treat the boundary must also be addressed in conjunction with the time step limiting idea. In practise, it would only be necessary to consider the effects of G_1 cells on any G_2 cells which are in the 'local vicinity' of the G_1 cells. Moreover, it would seem logical to deem the local vicinity of a cell to be viewed as neighbouring cells which may be influenced via the computational stencil of the chosen scheme. In terms of the first order Roe scheme, this would then translate to only limiting the time steps of G_2 cells which are directly adjacent to G_1 cells.

To evaluate the relative performances of different strategies for handling the G_1/G_2 boundaries, a test case is required. The dam break problem would appear to be a suitable test problem, particularly as an exact solution can be determined, and the presence of a travelling bore wave will test the shock capturing ability of the method. In addition, as there are no source terms, the LTS procedure can be evaluated independently of any source term treatment.

The dam break scenario considered for the comparison was generated from the initial conditions

$$h(x) = \begin{cases} h_l & x < 0 \\ h_r & x > 0 \end{cases}$$

where $h_l > h_r$ and the water was still everywhere. A 1km reach of channel which was centered at $x = 0$ was used, and the channel had a uniform rectangular cross section with a bottom width of 1m. The particular choice of channel length/width and values for h_l and h_r is arbitrary, as whatever values are considered, the same behaviour is produced but over different time scales. However to generate a supercritical region, then a certain ratio of h_l:h_r must be exceeded.

Using the values $h_l = 100m$ and $h_r = 1m$, the exact solution at time $t = 10$ seconds is shown in Figure 5.3. A comparison of the solutions obtained from the LTS1 and GTS procedures, gave identical results on a range of regular grids. This was as a result of the fact that on the regular grids tested, there were no G_2 cells. In addition, the overheads in implementing the LTS strategy meant that the LTS approach proved to be more computational expensive than using global time stepping. Subsequently, an irregular grid, was considered. The construction was such that a central region of uniform cells was connected to two outer regions of uniform cells, through two connecting regions, in which the cells lengths varied by a constant ratio. The grid was generated by specifying the total number of cells and a value n. The outermost cells were then n times the cell length of the innermost cells, and the resulting grid was symmetric about the centre point of the reach. For the initial investigation of the LTS strategy, 161 cells were used and n was set to 8. A mathematical description of how this grid was generated can be found in Appendix C (irregular grid A). A series of experiments were conducted to investigate the options of how to treat the G_1/G_2 interface, based on various interpretations of the ideas presented by Zhang *et al.* The best results were obtained when the G_2 cells on the interface were treated as G_1 cells, such that the flux on either boundary of the G_2 cell is updated. In addition, it was found beneficial to limit the new time step of the interface G_2 cell to the value

of the adjacent G_1 cell. The results in Figure 5.4 show a comparison of the LTS solution with the GTS scheme, together with the analytic solution.

In Figures 5.5 and 5.6, the bore and depression waves are shown in more detail. As can be seen there is a noticeable increase in accuracy of the solution, when the LTS approach is used. This reflects the fact that the solutions are generated using the local CFL numbers.

The solution presented in Figure 5.4 was obtained using the first order Roe scheme. The most noticeable improvement gained from using the LTS procedure, is the increased resolution of the bore. Typically, flux limiters would be used in conjunction with Roe's scheme to increase the accuracy of the solution. Figure 5.7 shows a comparison between the first order LTS and GTS results with those obtained using the GTS flux function with the Superbee limiter for the bore region.

As can be seen, the LTS approach gives a shock resolution comparable to that of the higher order scheme. A natural extension is to consider using the LTS strategy in a higher order scheme. Zhang *et al* concluded that the run time efficiencies of using the LTS procedure were greater when applied to a second order scheme, as the flux functions were more complex.

If the flux function defined as

$$\begin{aligned}\mathbf{F}_{i+1/2} = \quad & \frac{1}{2}\left(\mathbf{F}_i + \mathbf{F}_{i+1}\right) - \frac{1}{2}\sum_{k=1}^{2} \tilde{\alpha}^k_{i+1/2}|\tilde{\lambda}^k_{i+1/2}|\tilde{\mathbf{e}}^k_{i+1/2} + \\ & \frac{1}{2}\sum_{k=1}^{2} \phi(r^k_{i+1/2})\tilde{\alpha}^k_{i+1/2}|\tilde{\lambda}|\left(1 - \frac{\Delta t}{\Delta x}|\tilde{\lambda}^k_{i+1/2}|\right)\tilde{\mathbf{e}}^k_{i+1/2}\end{aligned}$$

is to be used in conjunction with the LTS algorithm, then the question arises what is the appropriate value of Δt to use in the flux function? Given that the flux $\mathbf{F}_{i+1/2}$ is used to update the cells i and $i+1$, one possibility would be to use a value based on the local time steps Δt_i and Δt_{i+1}. Various options could be considered, but the most logical would be to use the minimum value of the two local time steps, as this would correspond to the point up until which the flux function must be re-evaluated. The other question which arises is whether or not the time step limiting strategy used for the first order scheme, is sufficient for the second order scheme. Figure 5.8 shows the solutions obtained using the Superbee flux limiter in the LTS and GTS schemes.

As can be seen, the improvements visible with the first order scheme are less marked in the second order version. In addition, there is a slight oscillation in

the LTS results near the bore, suggesting that a more complex time step limiting procedure is necessary. Further investigation revealed that the oscillation could be removed by introducing an additional interface cell such that at the G_1/G_2 interface, the two G_2 cells nearest the boundary become G_1 cells. The time steps of the new G_1 cells are then limited by the minimum value of any original G_1 cells which are contained within the stencil of the modified cells. The results obtained following this procedure are shown in Figure 5.9. The first order scheme was also tested with the more complex time step limiting strategy, as shown in Figure 5.10.

There is little difference between the two time step limiting procedures when applied to the first order scheme. Closer inspection reveals that when only the direct neighbours are considered in the limiting procedure there is a marginal improvement in the solution near the bore. This is a consequence of the fact that widening the region which is used to restrict the time steps can result in a more severe condition being imposed on the G_2 cell.

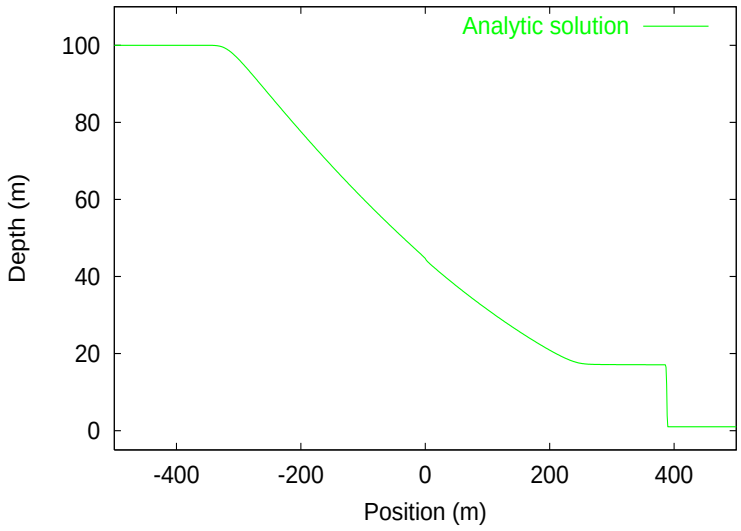

Figure 5.3: Analytic solution of the dam-break problem.

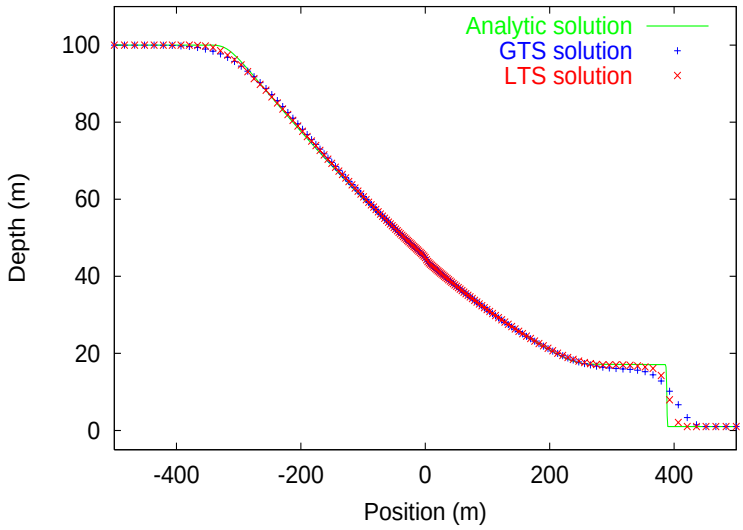

Figure 5.4: Comparison of LTS1 and GTS results.

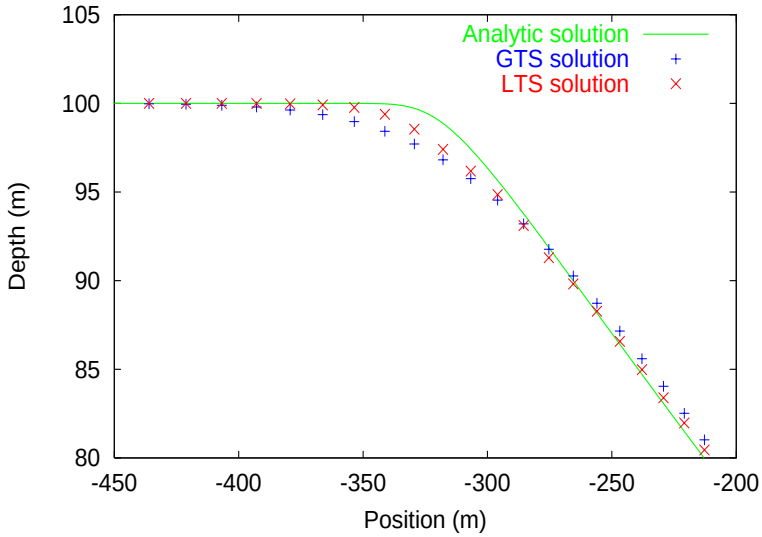

Figure 5.5: Comparison of LTS1 and GTS results — the depression.

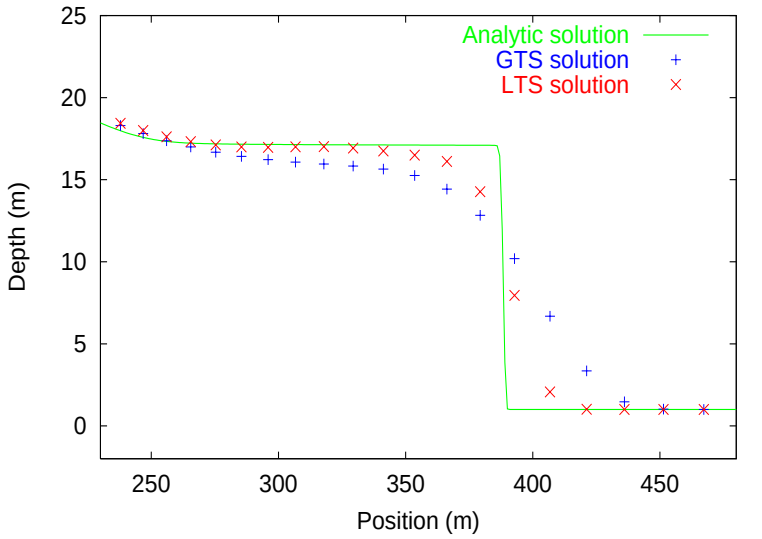

Figure 5.6: Comparison of LTS1 and GTS results — the bore.

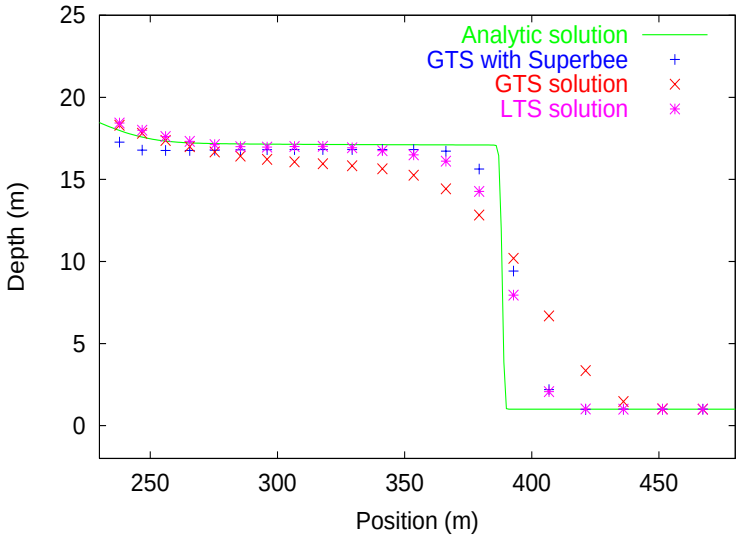

Figure 5.7: Comparison of LTS1 and GTS results with a second order GTS solution.

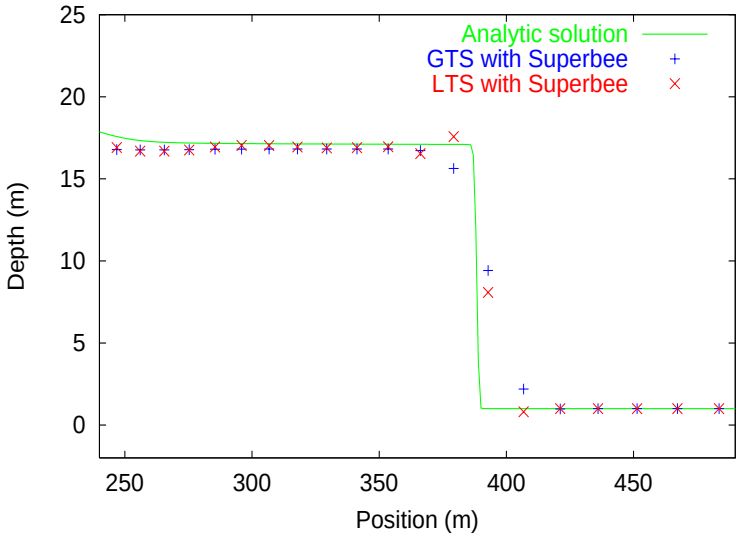

Figure 5.8: Comparison of LTS1 and GTS results with a second order GTS solution.

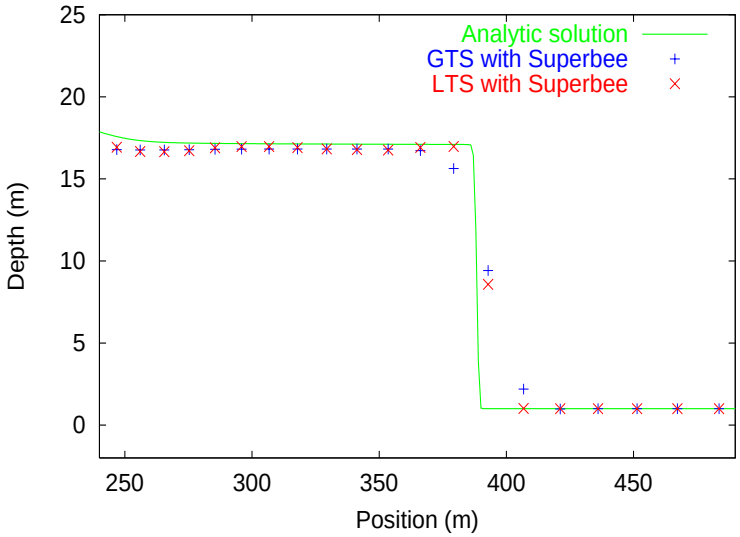

Figure 5.9: Comparison of LTS1 and GTS results with a second GTS solution.

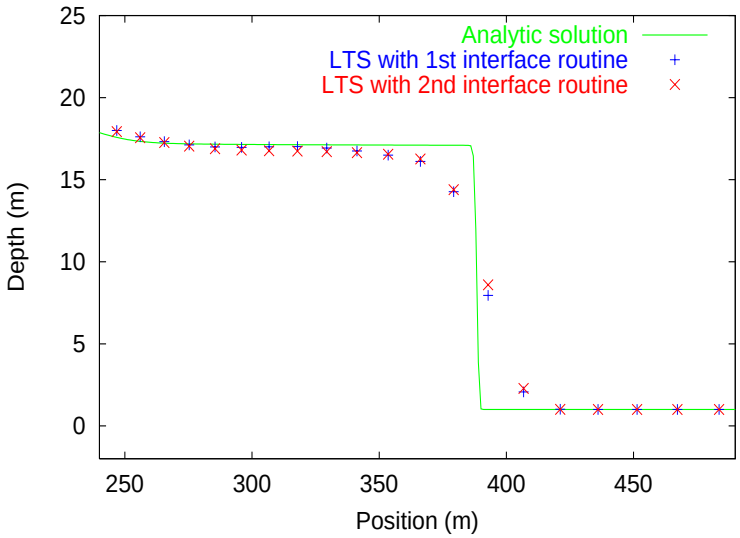

Figure 5.10: Comparison of LTS1 results using different interface strategies.

5.3.2 Application and development of the LTS2 procedure

In the procedure presented by Kleb *et al*, no mention was made of any additional restrictions which would need to be applied to the time step distribution, other than those based on the local stability conditions. However, in the description given by Pervaiz and Baron [48], it was suggested that an upper limit be set for the m values, and that no time step should be greater than four times that of its neighbours. The need to limit the maximum m value was described as necessary to ensure that flow features, such as jumps etc., would be correctly propagated, and the problem was referred to as 'temporal stiffness'. No suggestion was made as to how to select an appropriate limit, and in the examples given by Pervaiz and Baron, a fixed value was used throughout each simulation.

The suggestion made by Pervaiz and Baron that the time step of any individual cell should be no more than four times that of its neighbours, relates to the way in which regions of varying time steps should be connected. Given a region containing cells with a particular m value which bounds a region of cells with a differing value, some strategy must be developed to form an interface between the two regions, such that information is correctly propagated within the numerical simulation. The need for such an interface was demonstrated with the LTS1 procedure of Zhang *et al* in the previous section, whereby treating the boundary G_2 cells as G_1 cells and limiting the time step ensured that information from the G_1 cells was transmitted to the G_2 cells at the correct point in time. To investigate this issue further, the dam-break problem was again considered. Initially, a maximum m value of 1 was imposed and various options were considered for interfacing the 0/1 regions.

If no form of interface treatment was applied, then the solution in the vicinity of the bore (corresponding to the interface region), developed a spike in the depth profile which subsequently caused the program to crash. Following this, the effects of marking the bounding $m = 1$ cells at the interface as $m = 0$ cells was investigated. The number of cells to be marked was altered and the effects observed. Figure 5.12 shows a comparison of the results obtained, and Figure 5.13 shows the bore region in more detail.

As can be seen from the figures, if only one interface cell is used then the position of the is bore incorrectly predicted. In the case where two, three and four interface cells are used, the solution profiles are all very similar and accurately predict the

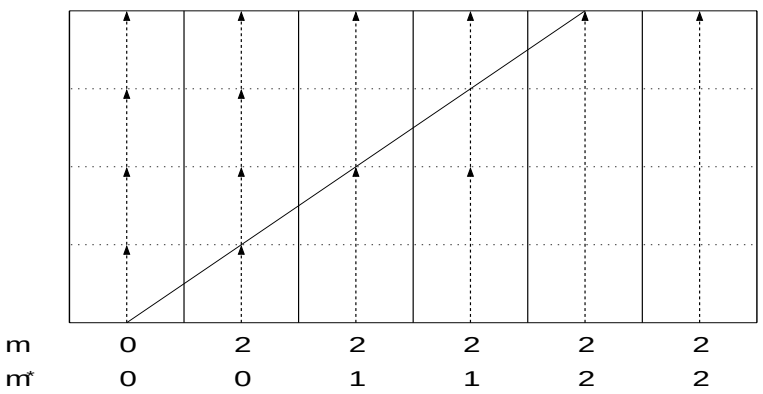

Figure 5.11: Construction of the interface region.

bore. However only slight improvement is obtained over the GTS solution.

Figure 5.14 shows the solutions obtained when the Superbee flux limiter was used in conjunction with the local time stepping. The same trends observed with the first order results are also present in the solutions obtained from the second order scheme.

For an insight into how the development of an interface strategy should progress, consider a regular grid consisting of a series of cells of length Δx. Consider the cell on this grid which gives rise to the global minimum time step, δt. Assuming a CFL number of 1, then in time δt, the information from that cell will propagate into the adjacent cell and can be considered to have travelled a distance Δx. In the subsequent time interval, the information from this cell will have then travelled a total distance of $2\Delta x$. Following this analogy, a path can be drawn to show how the information from this cell is transmitted to other cells. Mathematically this is described by

$$\text{total distance travelled} = \text{number of time steps} \times \Delta x.$$

In relation to the local time stepping procedure, given a cell which has a m value of 1 and borders a cell for which $m = 0$, it would appear necessary to then treat that cell as an $m = 0$ cell, to ensure that the information from the '0' region is correctly transmitted. This argument can be further extended to say a region of cells which have an m value of 2 and border $m = 0$ cells. The first '2' cell must be marked as a '0' cell, and the next two '2' cells are then marked as '1' cells, as illustrated in Figure 5.11, where m^* corresponds to the modified levels. Following this analysis, a general procedure for connecting the interface region can be outlined as follows

Given a region of cells with $m = m_1$ connected to a region of cells with $m = m_2$ (where $m_1 < m_2$), then if n is defined as the difference between m_1 and m_2 such that $n = m_2 - m_1$, then the number of cells which should be marked and deemed as the interface region is given by $2^n - 1$. In the case where $n = 1$, this corresponds to one cell, and is three cells when $n = 2$. Furthermore, the number of m_2 cells which should become m_1 cells is given by $2^0 = 1$, the number of m_2 cells which should become m_1+1 cells is given by $2^1 = 2$, the number of cells to become m_1+2 cells is $2^2 = 4$ and so on. Implementing this algorithm on a regular grid would then ensure that information propagating from one cell to another is transmitted at the correct time.

Although the above procedure is satisfactory for regular grids, it can only be used as a guide to suggest a means to construct the interface region when irregular grids are considered. A number of tests were conducted to illustrate how this algorithm would perform on the irregular grid considered previously for the LTS1 strategy. Using the first order Roe scheme, the results shown in Figure 5.15 were obtained, where the number of cells used to construct the 0/1 and 1/2 interfaces were varied. As can be seen, when one cell was used for the 0/1 region and two cells for the 1/2 area, the solution failed to predict the correct location of the bore. The remaining LTS solutions all compare favourably with the GTS results, and the corresponding improvement is more marked than when only one level of temporal embedding was permitted (Figure 5.13).

Figure 5.16 shows the solutions generated when the second order Roe scheme is used, and the same trends are evident in the solution profiles. For both the first and second order results, it can be seen that there is no appreciable difference between the 2/2 and 2/4 solutions and also for the 4/4 and 4/8 case. To investigate this further, some intermediate strategies for the interface regions were tested, and the first and second order results are shown in Figures 5.17 and 5.18 respectively. The most noticeable feature of the results shown is that solutions which have the same number of 0/1 interface cells (i.e. 3/2 and 3/4 or 4/2 and 4/4) appear identical, whereas the solutions generated using the same overall number of interface cells (2/4 and 4/2) are appreciably different. However, these differences are marginal in terms of comparing the LTS results with the analytic solution and in that sense all of the results are satisfactory.

The results listed so far were generated using up to two levels of temporal embedding (i.e. by using maximum m values of 2 or less). Further validation of the

second LTS procedure would require using higher maximum m values. However in the case of the dam-break problem, this is not possible due to the onset of numerical instability. In implementing this local time stepping approach, it is necessary that the flow conditions are such that the local time step of individual cells do not significantly decrease over a single global time step. This ensures that the stability conditions are satisfied throughout the global time step. However, should the case occur where the flow in a particular cell would correspond to a permitted time step which is less than the local time step value being used for the cell over the interval, then the local stability conditions will be violated and an unstable numerical solution will be generated. This effect shall subsequently be referred to as temporal stiffness (however its nature is different to the temporal stiffness reported by Pervaiz and Baron [48]). This situation is very evident in the dam-break problem, as during the initial stages the region near the breach ($x = 0$) is subject to rapid variations in flow conditions (which often leads to discussions of the validity of applying the Saint Venant equations to such flows) which results in significant variations in the local time distribution. A number of strategies were considered as ways to reduce this effect, based on limiting the occasions when local time stepping was used, increasing the interface region, and also only allowing cells which had permissible time steps that were increasing, to belong to non-zero temporal levels. In the tests performed, no strategy outperformed the results shown in terms of solution accuracy and reduced run times.

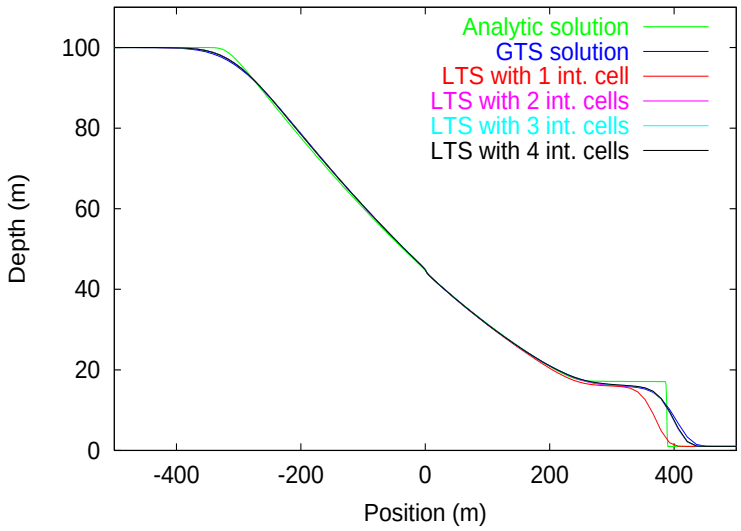

Figure 5.12: Comparison of GTS and LTS2 results with varying number of interface cells.

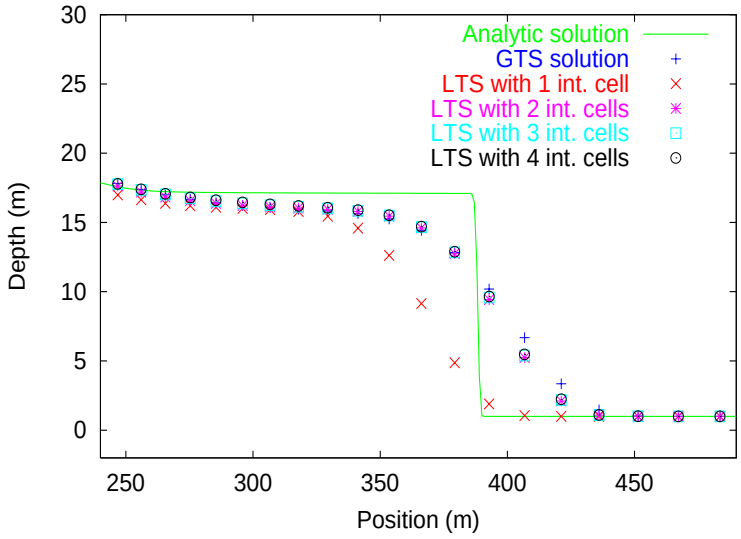

Figure 5.13: Comparison of GTS and LTS2 results with varying number of interface cells.

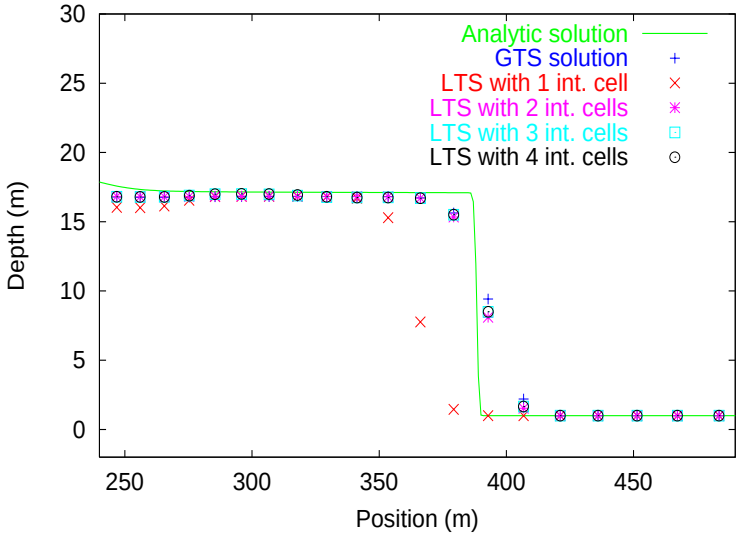

Figure 5.14: Comparison of GTS and LTS2 results with varying number of interface cells and using Superbee.

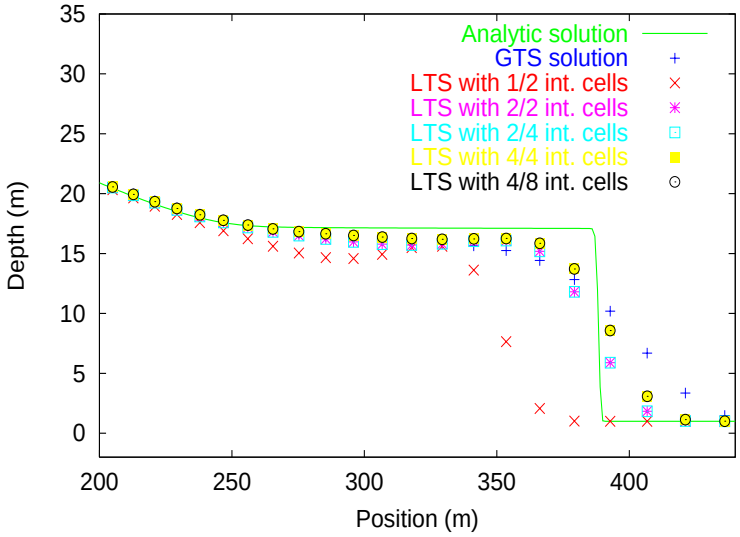

Figure 5.15: Comparison of GTS and LTS2 results with varying number of interface cells.

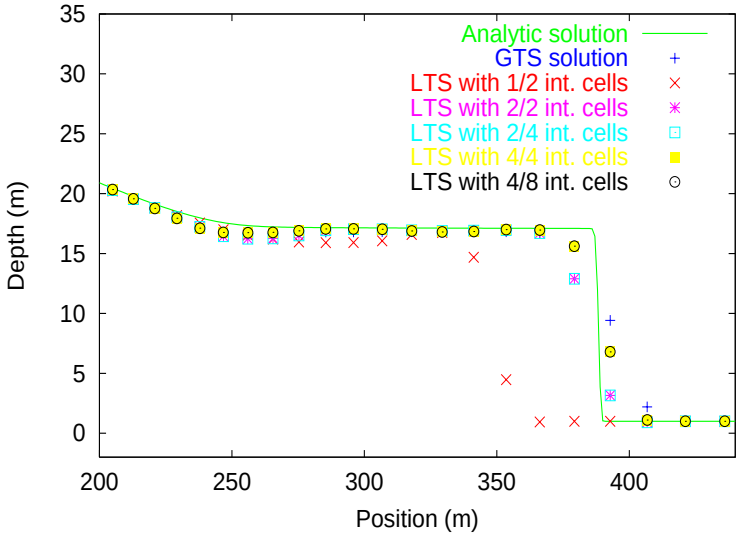

Figure 5.16: Comparison of GTS and LTS2 results with varying number of interface cells and Superbee.

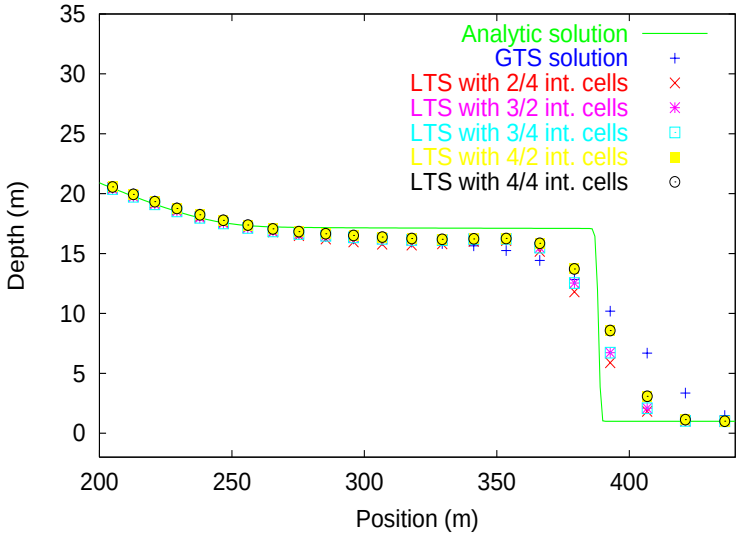

Figure 5.17: Comparison of GTS and LTS2 results with varying number of interface cells.

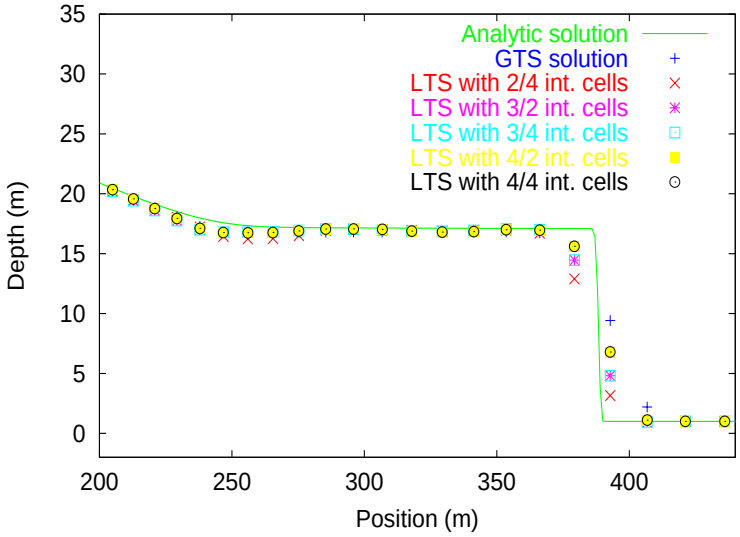

Figure 5.18: Comparison of GTS and LTS2 results with varying number of interface cells and Superbee.

5.3.3 Run Times

The main objective in implementing the LTS strategies was to reduce the computer run times of the corresponding global time stepping schemes. Using a profiling package, the run times for the results shown were measured. Table 5.2 shows the values for the global time stepping approach and the first LTS procedure, whilst Table 5.3 lists the results for the second LTS procedure. In addition, the number of flux evaluations made per run was also recorded (though in different runs to the run time measurements), to access the impact of using an LTS approach without the implementation costs.

Method		Run time	Eff. gain	No. of flux	Eff. gain
Time stepping	Order	(s)	(%)	calculations	(%)
GTS	1st	0.05601	—	36320	—
LTS1	1st	0.05456	2.6	20332	44.0
GTS	2nd	0.09190	—	37392	—
LTS1	2nd	0.08621	6.2	21917	41.4

Table 5.2: Comparison of run times for the GTS and LTS1 schemes.

From the first table, it can be seen that using the frozen flux local time stepping approach lead to a slight reduction in computer run times over the GTS versions of Roe's scheme, and that the improvement was more marked with the second order method. In terms of the number of flux calculations made, it can be seen that implementing the LTS procedure resulted in a significant reduction of flux calculations. The improvement is slightly higher for the first order scheme, which is as expected due to the additional interface cells employed within the second order scheme.

The run time measurements for the second LTS procedure showed that for the dam-break problem, the first order method was generally only more efficient when two levels of temporal embedding were used (with the exception being when only one interface cell was implemented). In addition, increasing the interface region reduced the efficiency of the approach, as would be expected. In comparing the flux evaluation measurements, the efficiency gains between corresponding variants of the first and second orders are very similar. In this instance the same interface strategy was used for both the first and second order scheme, unlike the case for the first LTS approach.

Level of embedding	Number of interface cells	Run time (s)	Eff. gain (%)	Number of flux calculations	Eff. gain (%)
1	1	0.05542	1.1	25345	30.2
	2	0.05610	-0.1	25784	29.0
	3	0.05644	-0.8	26007	28.4
	4	0.05687	-1.5	26223	27.8
2	1/2	0.04583	18.2	21713	40.2
	2/2	0.04679	16.5	22297	38.6
	2/4	0.04684	16.4	22331	38.5
	3/2	0.04752	15.2	22731	37.4
	3/4	0.04757	15.1	22769	37.3
	4/2	0.04830	13.8	23171	36.2
	4/4	0.04841	13.6	23209	36.1
	4/8	0.04858	13.3	23285	35.9

Table 5.3: Run times for the LTS2 procedure using the first order scheme.

Level of embedding	Number of interface cells	Run time (s)	Eff. gain (%)	Number of flux calculations	Eff. gain (%)
1	1	0.08513	7.4	26086	30.2
	2	0.08643	6.0	26531	29.0
	3	0.08709	5.2	26769	28.4
	4	0.08782	4.4	26996	27.8
2	1/2	0.07313	20.4	22128	40.8
	2/2	0.07534	18.0	22867	38.8
	2/4	0.07545	17.9	22896	38.8
	3/2	0.07619	17.1	23140	38.1
	3/4	0.07630	17.0	23170	38.0
	4/2	0.07801	15.1	23730	36.5
	4/4	0.07823	14.9	23777	36.4
	4/8	0.07850	14.6	23845	36.2

Table 5.4: Run times for the LTS2 procedure using the second order scheme.

In all the results it is apparent that the LTS methods lead to a greater efficiency gain when the flux limited version of the Roe scheme is used. This can be accounted for by the increased computational cost of the flux calculations for the second order scheme over the first order version. This results in the overheads in implementing the LTS strategies becoming less significant relative to the flux calculations. The implementation costs also account for the cases where the second LTS procedure required a longer run time than the GTS approach. The efficiency gains calculated by measuring the number of flux calculations performed highlight the benefits of using an LTS procedure. However the substantial differences between these values and those obtained from the run time measurements, show that the implementation costs have an appreciable significance in this example. It may also be noted that the efficiency gains reported in the original papers have not been achieved for this particular case, and the overall improvements observed have only been marginal. On this issue a number of points can be made - firstly the results presented have not included any source term calculations, and in subsequent examples, the source term treatment will be incorporated into the LTS strategy resulting in more significant efficiency gains; secondly, as this is a relatively simple problem which requires only a short run time, the CPU time required by the procedures in the program which do not form part of the time integration procedure (initialisation etc.) will account for a significant proportion of the measured run time. In addition, the time step distribution of the cells is dependent upon the particular grid used for the simulation. The observation that the second order results showed a marked difference in efficiency gains over the corresponding first order solutions also suggests the second point to be true. In summary, both LTS procedures must be applied to more complex problems in order for a more complete evaluation to take place.

Returning to the first three questions raised in section 5.3

1) In the first LTS procedure, which G_2 cells require special treatment due to the interaction of neighbouring G_1 cells, and is this dependent on the choice of numerical scheme?

2) In the second LTS approach, is it necessary to limit the individual time steps to be at most four times that of the neighbouring cells (as suggested by Pervaiz and Baron [48]) Also, should the m values be subject to a upper limit?

3) Does using a second order scheme introduce any additional difficulties for either LTS procedure?

The responses from the investigations conducted so far are

1) For the LTS1 scheme, those G_2 cells which are contained within the computational stencil of the G_1 cell on the G_1/G_2 interface, are treated as G_1 cells. In addition the time steps of those cells are limited to the values of any true G_1 cells contained within the modified cells stencil.

2) The proposed method for interfacing regions of varying m-values within the LTS2 scheme, is to be based on an analogy with the propagation of information on a regular grid. Following this approach, the time steps of individual cells will be no more that twice that of their neighbours. In addition, the necessity of imposing a maximum m-value was illustrated by the dam-break problem. From the preliminary results, the method to be adopted for developing the interface regions is to be based on re-assigning the m-values following a 4,2,4,8,16,... pattern. This strategy proved to be successful for the dam-break problem, though it requires validation for a larger range of problems.

3) The solutions produced by both LTS schemes were marginally improved when a flux limiter was used, and this introduced no additional problems providing that the interface region was treated appropriately.

The other question which needs to be addressed is the treatment of the boundary conditions within the LTS strategies. Given the possibilities as to how the boundaries maybe incorporated, such as the method of characteristics, the simplest option for the LTS1 method is to treat the boundary cells as G_1 cells. For the second LTS procedure, no special treatment of the boundary cells should be necessary. These strategies were satisfactory for the dam-break problem and will be more throughly tested by the problems considered in the next chapter.

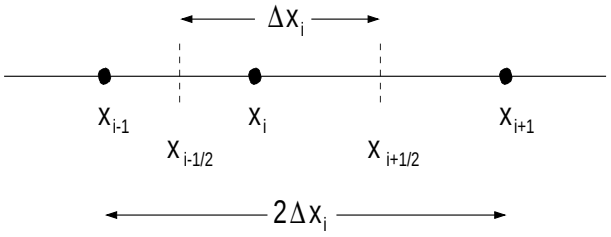

Figure 5.19: Irregular grid construction.

5.4 Inclusion of source terms in the LTS procedures

In applying the LTS procedures to the dam-break problem, the issue of how to treat the source terms was not a consideration. As noted in the previous chapter, the customary way of incorporating source terms into many numerical schemes, is to use a pointwise approach. However in some situations, this produces unsatisfactory results. More recently interest has grown in constructing upwind source term treatments for shallow water flows. The results presented in the previous chapter are now considered for use in conjunction with the local time stepping approach.

5.4.1 Upwind source term treatment on an irregular mesh

The upwind source term treatment originally proposed in [8] was constructed for a uniform grid, on the basis that exact conservation between the flux and source terms was obtained for the zero discharge case. Following this approach, the effect of implementing the upwind source term treatment on an irregular grid will now be considered.

Consider a one-dimensional irregular grid, such as the one in Figure 5.19. The discrete representation of the Saint Venant equations then becomes

$$\mathbf{U}_i^{n+1} = \mathbf{U}_i^n - \frac{\Delta t}{\Delta x_i}\left(\mathbf{F}_{i+1/2}^n - \mathbf{F}_{i-1/2}^n\right) + \Delta t \mathbf{R}_i^n$$

where, following the approach of Bermúdez and Vázquez, $\mathbf{R}_i^n$ is an approximation to

$$\frac{1}{\Delta x_i}\int_{c_i} \mathbf{R}(x, \mathbf{U}) dx$$

and the integration is performed over the cell, C_i, defined by the region $[x_{i-1/2}, x_{i+1/2}]$. In the original paper, the source term was defined as

$$\mathbf{R}_i^n = \mathcal{R}^L(x_{i-1}, x_i, \mathbf{U}_{i-1}, \mathbf{U}_i) + \mathcal{R}^R(x_i, x_{i+1}, \mathbf{U}_i, \mathbf{U}_{i+1})$$

where

$$\mathcal{R}^L = \frac{1}{2}\left(\mathbf{I} + |\tilde{\mathbf{A}}|\tilde{\mathbf{A}}^{-1}\right)\tilde{\mathbf{R}} \tag{5.3}$$

$$\mathcal{R}^R = \frac{1}{2}\left(\mathbf{I} - |\tilde{\mathbf{A}}|\tilde{\mathbf{A}}^{-1}\right)\tilde{\mathbf{R}} \tag{5.4}$$

and $\tilde{\mathbf{R}}$ was an approximation average to the source term, which for the Saint Venant equations in a smooth rectangular channel become

$$\tilde{\mathbf{R}}_i^n(x_L, x_R) = \begin{pmatrix} 0 \\ -g\left(\dfrac{(A_L + A_R)}{2}\right)\dfrac{z(x_L) - z(x_R)}{x_R - x_L} \end{pmatrix}.$$

In the steady state/zero discharge case where $\mathbf{U}_i^{n+1} = \mathbf{U}_i^n$ and $Q \equiv 0$, then for equilibrium to be obtained the flux and source terms must balance such that

$$\frac{\Delta t}{\Delta x_i}\left(\mathbf{F}_{i+1/2}^n - \mathbf{F}_{i-1/2}^n\right) = \Delta t \mathbf{R}_i^n \tag{5.5}$$

where substituting for the flux function gives

$$\frac{\Delta t}{2\Delta x_i}\begin{pmatrix} (\tilde{c}\Delta A)_{i-1/2} - (\tilde{c}\Delta A)_{i+1/2} \\ \left(\dfrac{gA^2}{2b}\right)_{i+1} - \left(\dfrac{gA^2}{2b}\right)_{i-1} \end{pmatrix} = \Delta t \mathbf{R}_i^n,$$

using

$$\tilde{c} = \sqrt{g\left(\frac{h_L + h_R}{2}\right)}$$

to define the average celerity. By imposing the equilibrium conditions then, the left and right source term contributions are found to be

$$\mathcal{R}^L = \frac{1}{2}\begin{pmatrix} 1 & 1/\tilde{c} \\ \tilde{c} & 1 \end{pmatrix}\tilde{\mathbf{R}}$$

$$\mathcal{R}^R = \frac{1}{2}\begin{pmatrix} 1 & -1/\tilde{c} \\ -\tilde{c} & 1 \end{pmatrix}\tilde{\mathbf{R}}$$

and if the source term is specified as before, then the resulting expression is

$$\mathbf{R}_i^n = \begin{pmatrix} -\dfrac{1}{2}b\left\{\sqrt{g\left(\dfrac{h_i^n + h_{i+1}^n}{2}\right)}\dfrac{(h(x_{i+1}) - h(x_i))}{x_{i+1} - x_i} - \sqrt{g\left(\dfrac{h_{i-1}^n + h_i^n}{2}\right)}\dfrac{(h(x_i) - h(x_{i-1}))}{x_i - x_{i-1}}\right\} \\ \\ \dfrac{1}{2}b\left\{g\left(\dfrac{h_{i-1}^n + h_i^n}{2}\right)\dfrac{(h(x_i) - h(x_{i-1}))}{x_i - x_{i-1}} + g\left(\dfrac{h_i^n + h_{i+1}^n}{2}\right)\dfrac{(h(x_{i+1}) - h(x_i))}{x_{i+1} - x_i}\right\} \end{pmatrix},$$

once the relationship $\Delta z + \Delta h = 0$ has been imposed. In the case of a regular grid, where Δx_i is a constant, then it can be shown that the given definitions of the flux and source functions balance, such that (5.5) is satisfied and equilibrium is maintained. However, if Δx_i is not constant, then in general the flux and source terms do not match and so the equilibrium is violated.

To enforce equilibrium, one possibility is to use the definitions of $\mathcal{R}^L$ and $\mathcal{R}^R$ provided by (5.3) and (5.4) together with weight functions, such that

$$\mathbf{R}_i^n = \left(W_{i-1/2}^L \mathcal{R}_{i-1/2}^L + W_{i+1/2}^R \mathcal{R}_{i+1/2}^R \right).$$

Enforcing (5.5) to be true, leads to the definitions

$$W_{i-1/2}^L = \frac{x_i - x_{i-1}}{\Delta x_i} \quad \text{and} \quad W_{i+1/2}^R = \frac{x_{i+1} - x_i}{\Delta x_i}.$$

This choice of weights will also maintain the equilibrium conditions if the extensions proposed by García-Navarro and Vázquez-Cendón [26] for non-prismatic rectangular channels are used. This formulation is based upon an intuitive approach of ensuring that Property C is maintained. A more mathematical treatment was recently published by Vázquez-Cendón [64] and corroborated this formulation. The article also considered the application of the upwind source term treatment to a variety of 1-d test cases, demonstrating further justification for using an upwind approach.

To illustrate the benefits of the upwind source term treatment, an extreme test case presented by García-Navarro and Vázquez-Cendón [26] is considered. The problem consists of stationary flow through a channel with variable bed slope and locally rectangular cross sections. The geometry of the channel is shown in Figures 5.20 and 5.21. If a fixed water level of $12m$ is imposed at the downstream boundary, then in the zero discharge case, the surface elevation should be $12m$ throughout the channel. By choosing the equilibrium solution to be the initial conditions for the simulation, then it is possible to assess the performance of a particular method by whether the initial solution is perturbed.

Using a pointwise source term treatment, the elevation and discharge profiles shown in Figures 5.22 and 5.23 are obtained. The solutions shown were produced after $200s$. For comparison, the solutions generated on a fine regular grid are also shown, and Figures 5.24 and 5.25 show an enlargement of the plots. As can be seen the solutions from the various schemes show significant deviations from the exact solution. Although refining the grid reduces this problem, the deviations

Time stepping scheme	Source term treatment	Run time (s)	Eff. gain (%)	No. of flux calculations	Eff. gain (%)
Global	Pointwise	0.2274	—	134400	—
LTS1		0.2096	7.8	79441	40.9
LTS2 (2 time levels)		0.2184	4.0	94636	30.0
LTS2 (4 time levels)		0.1867	17.9	83128	38.1
LTS2 (8 time levels)		0.1816	20.1	82521	38.6
Global	Upwind	0.2208	—	106400	—
LTS1		0.2015	8.7	69162	35.0
LTS2 (2 time levels)		0.2104	4.7	79176	25.6
LTS2 (4 time levels)		0.1867	15.4	71706	32.6
LTS2 (8 time levels)		0.1867	15.4	71706	32.6

Table 5.5: Run times comparison for the rectangular channel.

are still apparent. If the solution is allowed to evolve further, then a satisfactory converged solution cannot be obtained. In contrast the solutions produced by the upwind source term treatment are shown in Figures 5.26 and 5.27, from which it is apparent that the initial solution is not perturbed.

The run times for the results shown were measured and are given in Table 5.5. The percentage run time efficiency gains of the two LTS procedures over the GTS scheme are greater than those observed with the dam break problem. However, there is a reduction in the flux computation efficiency gains. The first point illustrates how the overheads in implementing the LTS strategies have become less significant in contrast to the overall calculations. The fact that there is a percentage increase in the number of flux calculations being performed suggests that the proportion of cells which are being advanced by the minimum time step has increased. This would be in keeping with the highly irregular geometry being considered. It may also be observed that the flow conditions and choice of grid permit only four time levels to be used, as observed by the fact that the run times measurements are the same when four and eight time levels are used for the upwind source term results.

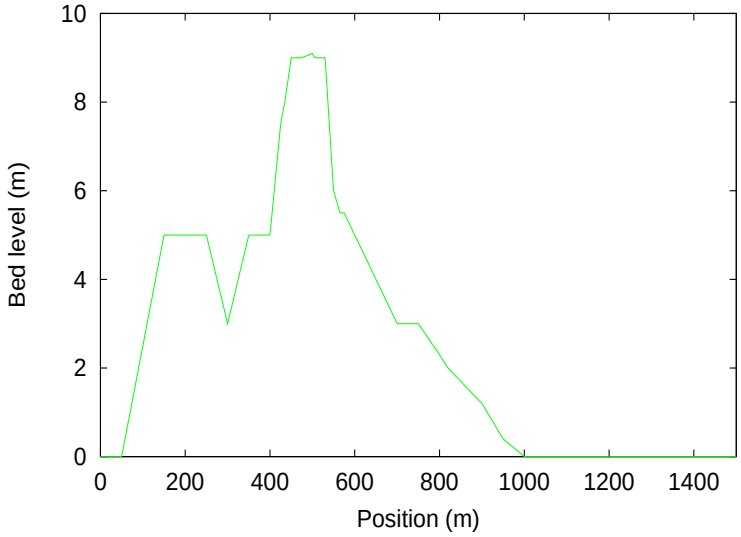

Figure 5.20: Bed level for irregular geometry test case [26].

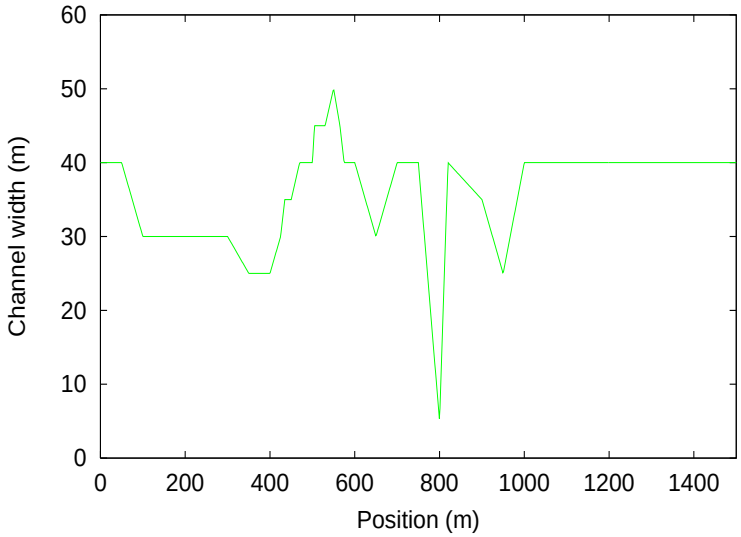

Figure 5.21: Width variation for irregular geometry test case [26].

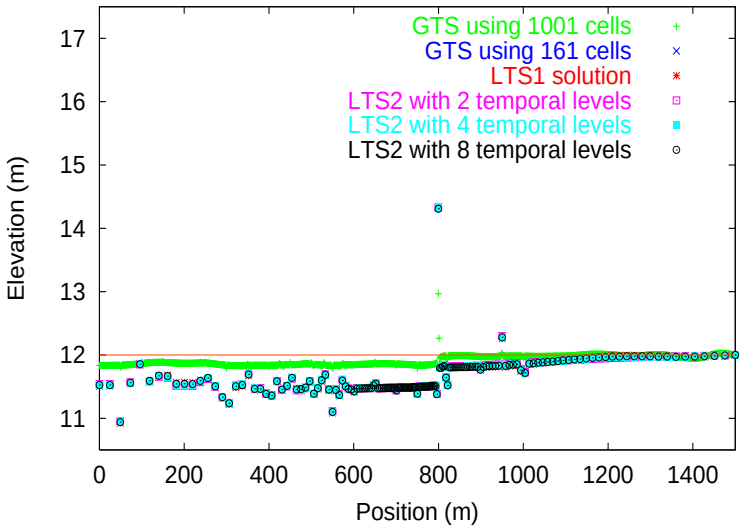

Figure 5.22: Elevation with pointwise source terms.

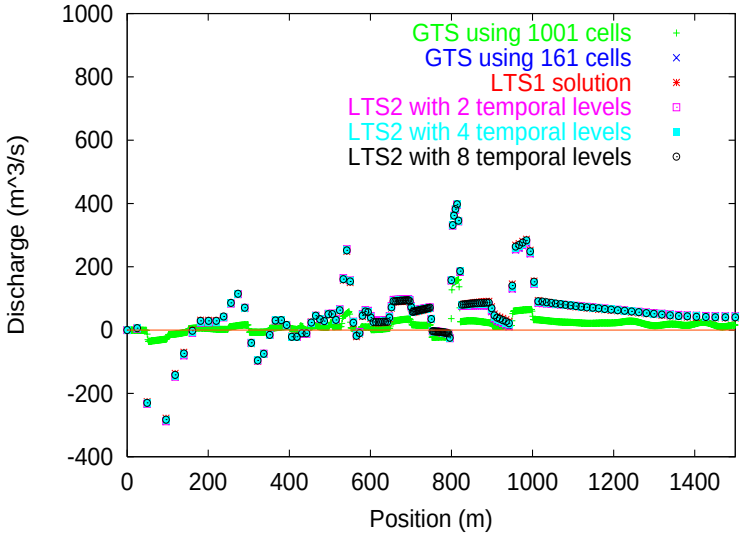

Figure 5.23: Discharge with pointwise source terms.

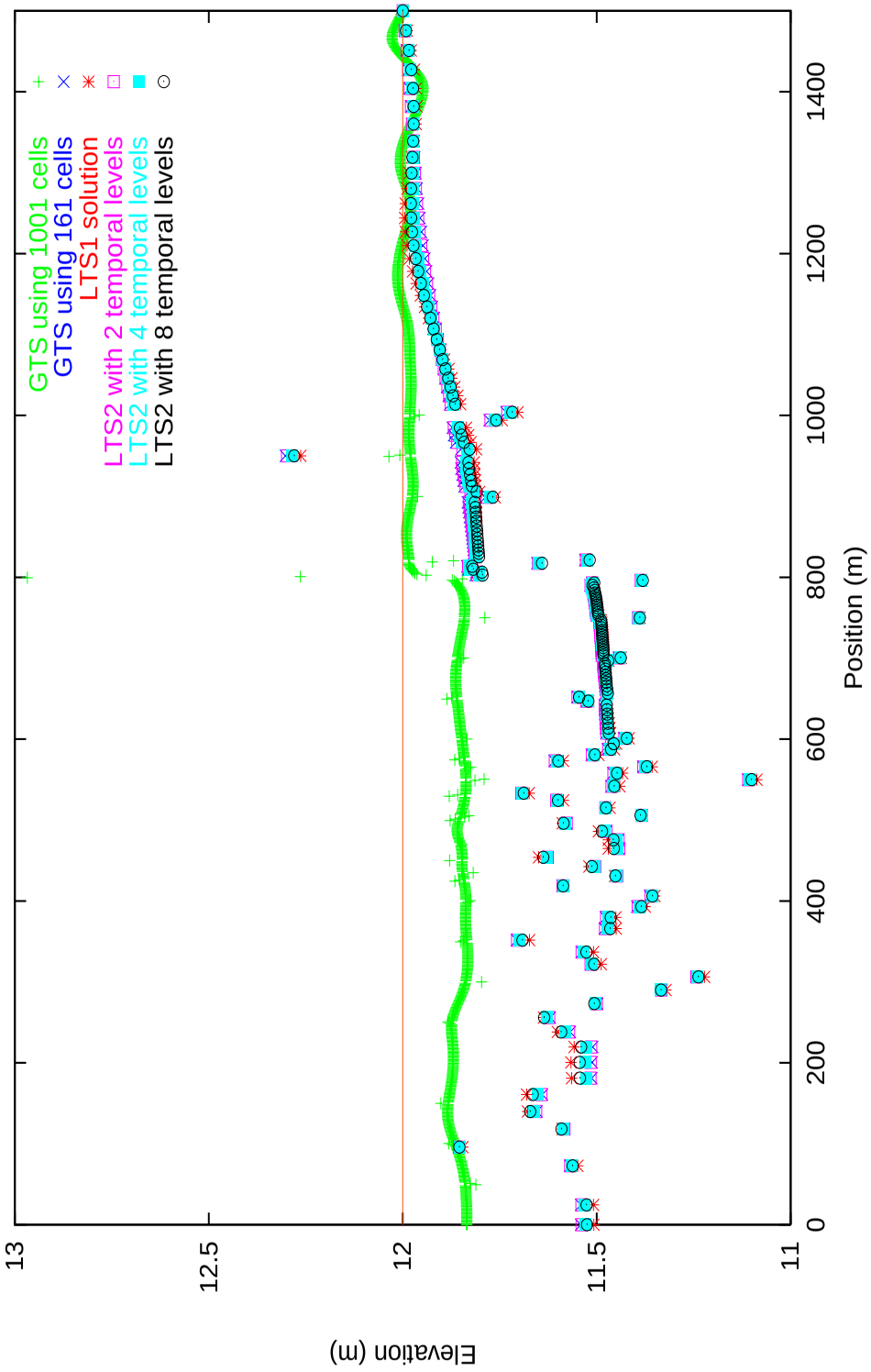

Figure 5.24: Elevation with pointwise source terms.

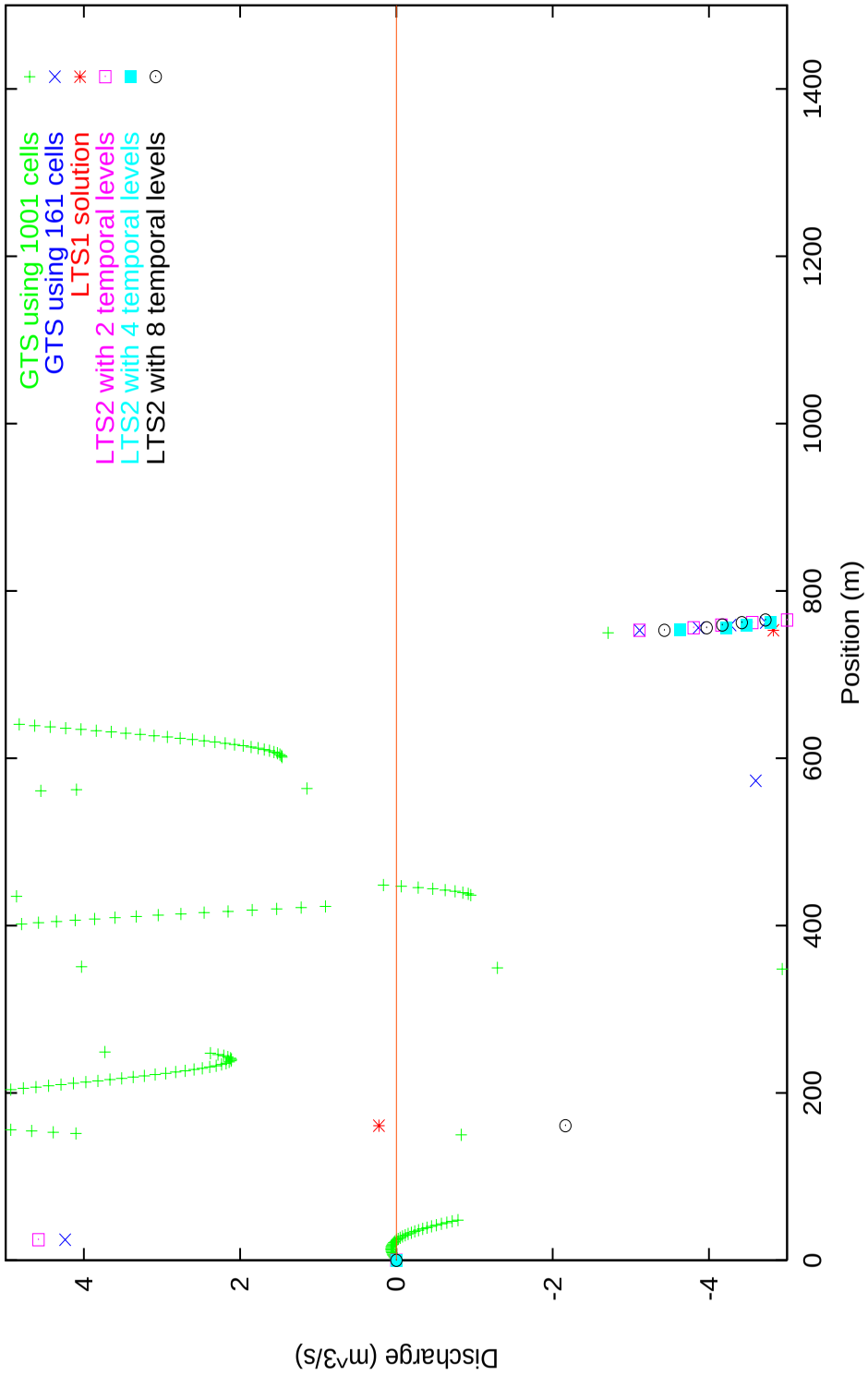

Figure 5.25: Discharge with pointwise source terms.

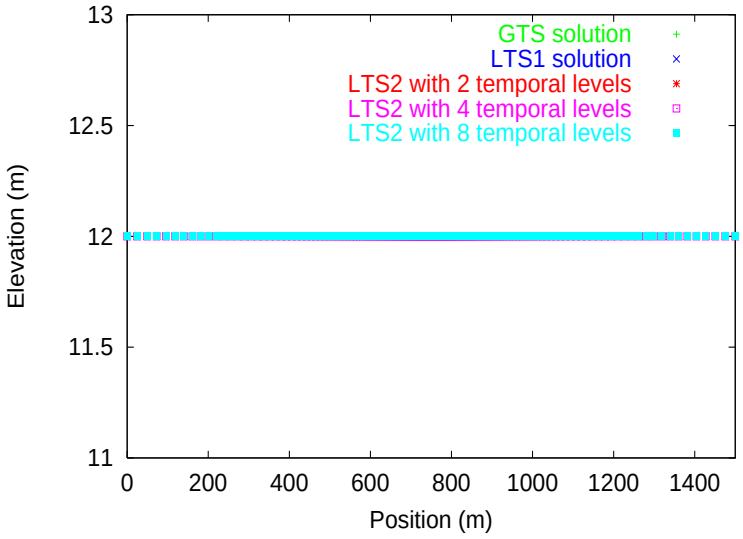

Figure 5.26: Elevation with upwind source terms.

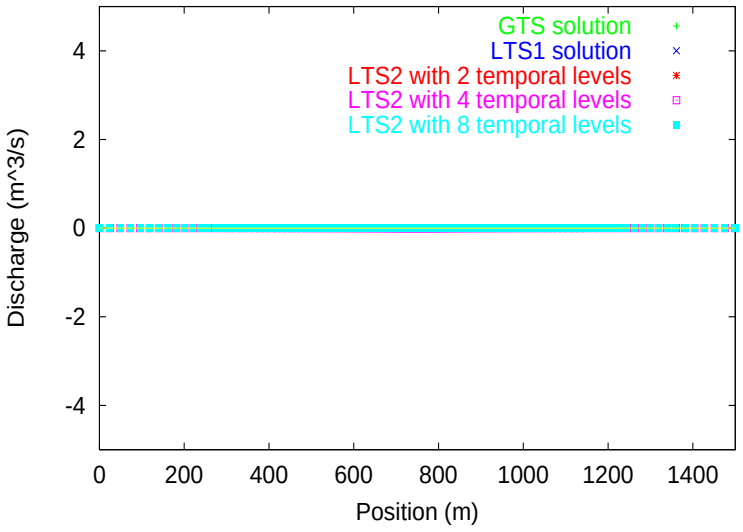

Figure 5.27: Discharge with upwind source terms.

5.4.2 Upwind source term treatment for prismatic trapezoidal channels

Both Bermúdez and Vázquez [8] and García-Navarro and Vázquez-Cendón [26] consider the application of the upwind source term treatment to rectangular channels. A natural extension would be to consider the application of the method to trapezoidal cross sections and to see if the same construction leads to a treatment that satisfies the conservation principle.

Consider the case of a smooth prismatic trapezoidal channel discretised by a regular grid. In the steady state/zero discharge situation, the flux function becomes

$$\frac{\Delta t}{2\Delta x}\begin{pmatrix} -(\tilde{c}\Delta A)_{i+1/2} + (\tilde{c}\Delta A)_{i-1/2} \\ (gI_1)_{i+1} - (gI_1)_{i-1} \end{pmatrix}$$

where

$$I_1 = \frac{bh^2}{2} + \frac{zh^3}{3}$$

for a trapezoidal channel, and the source term remains the same as for the rectangular case. Given that c and A differ for rectangular and trapezoidal cross sections, the question is then what are the appropriate choices for $\tilde{c}$ and $\tilde{A}$. Following the procedure of García-Navarro and Vázquez-Cendón [26] and starting from

$$\frac{\partial I_1}{\partial x} = I_2 + A\frac{\partial h}{\partial x}$$

and

$$g\Delta I_1 = \tilde{c}^2\Delta A \tag{5.6}$$

(from the Roe decomposition), then the change in I_1 can be represented by

$$\Delta I_1 = I_2\Delta x + A\Delta h. \tag{5.7}$$

As $A = h(b + zh)$ then

$$\frac{\partial A}{\partial x} = \frac{\partial A}{\partial h}\frac{\partial h}{\partial x} + \frac{\partial A}{\partial b}\frac{\partial b}{\partial x},$$

from which

$$\frac{\partial A}{\partial x} = (b + 2zh)\frac{\partial h}{\partial x} + h\frac{\partial b}{\partial x}$$

and

$$\Delta A = (b + 2zh)\Delta h + h\Delta b.$$

Thus substituting for Δh in (5.7) gives

$$\Delta I_1 = I_2\Delta x + A\left(\frac{\Delta A - h\Delta b}{b + 2zh}\right). \tag{5.8}$$

From (5.8) it can be seen that the jump in ΔI_1 is linked to the jump in A through one term. In the original paper, this factor was used as the basis to redefine the average celerity. In this instance, substituting for the jump value of I_1 in (5.6) leads to the relationship

$$g\frac{A}{b+2zh} = \tilde{c}^2.$$

For a rectangular channel, this resulted in the celerity being defined as

$$\tilde{c}_{i+1/2} = \sqrt{\frac{g}{2}\left(\left(\frac{A}{b}\right)_i + \left(\frac{A}{b}\right)_{i+1}\right)}$$

which given that $A = hb$ and that $\tilde{h}$ was defined as $(h_i + h_{i+1})/2$, could also be written as

$$\tilde{c}_{i+1/2} = \sqrt{\frac{g}{2}(h_i + h_{i+1})} = \sqrt{g\tilde{h}}.$$

By analogy, given that the celerity is usually defined in terms of A and B ($B = b + 2zh$), then the average value can be represented by

$$\tilde{c}_{i+1/2} = \sqrt{g\frac{\tilde{A}}{\tilde{B}}}. \tag{5.9}$$

The most obvious choices for $\tilde{A}$ and $\tilde{B}$ are

$$\tilde{A} = \tilde{h}(b + z\tilde{h}) \quad \text{and} \quad \tilde{B} = b + 2z\tilde{h}$$

using the same definition for $\tilde{h}$ as before. Following this process, the equilibrium condition then requires the following relationships to be satisfied

$$\frac{\Delta t}{2\Delta x}\left[(\tilde{c}\Delta A)_{i-1/2} - (\tilde{c}\Delta A)_{i+1/2}\right] = \frac{\Delta t}{2\Delta x}\left[\frac{g\tilde{A}}{\tilde{c}}(h_i - h_{i-1}) - \frac{g\tilde{A}}{\tilde{c}}(h_{i+1} - h_i)\right] \tag{5.10}$$

$$\frac{\Delta t}{2\Delta x}\left[(gI_1)_{i+1} - (gI_1)_{i-1}\right] = \frac{\Delta t}{2\Delta x}\left[g\tilde{A}(h_i - h_{i-1}) + g\tilde{A}(h_{i+1} - h_i)\right]. \tag{5.11}$$

From (5.10), if $\tilde{c}$ is defined using (5.9) then by considering the first term, equilibrium will be achieved if

$$\tilde{c}\Delta A = \frac{1}{\tilde{c}}g\tilde{A}(h_i - h_{i-1})$$

from which substituting for $\tilde{c}$ and ΔA gives

$$\sqrt{g\frac{\tilde{A}}{\tilde{B}}}(h_i - h_{i-1})\left[b + z(h_i + h_{i-1})\right] = \sqrt{\frac{\tilde{B}}{g\tilde{A}}}\tilde{A}(h_i - h_{i-1}).$$

resulting in the definition of $\tilde{B}$

$$\tilde{B} = b + z(h_i + h_{i-1}) = b + 2z\tilde{h}.$$

Note that this choice is independent of the definition of $\tilde{A}$.

Having established the criteria for (5.10) to be satisfied, it is necessary to see if the specified averages will also lead to satisfy Property C in (5.11). However, following through the analysis, it is found that the left and right hand sides of (5.11) do not match, as

$$LHS = \frac{\Delta t}{2\Delta x}\left\{g\left[\frac{b}{2}\left(h_{i+1}^2 - h_{i-1}^2\right) + \frac{z}{3}\left(h_{i+1}^3 - h_{i-1}^3\right)\right]\right\}$$

and

$$RHS = \frac{\Delta t}{2\Delta x}\left\{g\left[\frac{b}{2}\left(h_{i+1}^2 - h_{i-1}^2\right) + \frac{z}{4}\left(h_{i+1}^3 - h_{i-1}^3 + h_i h_{i+1}^2 - h_i^2 h_{i+1} + h_{i-1}h_i^2 - h_{i-1}^2 h_i\right)\right]\right\},$$

from which the difference between the two sides is

$$LHS - RHS = \frac{\Delta t}{2\Delta x}\left\{g\left[\frac{1}{12}z\left(h_{i+1}^3 - h_{i-1}^3 - 3h_i h_{i+1}^2 + 3h_i^2 h_{i+1} - 3h_{i-1}h_i^2 + 3h_{i-1}^2 h_i\right)\right]\right\}$$

which maybe more concisely written as

$$LHS - RHS = \frac{\Delta t}{2\Delta x}\frac{gz}{12}\left[\left(h_{i+1} - h_i\right)^3 + \left(h_i - h_{i-1}\right)^3\right]. \tag{5.12}$$

Thus to satisfy the equilibrium requirements, a correction term can be added based on (5.12), which will ensure that Property C is established. If an irregular grid is used, the same corrections can be applied and will satisfy the equilibrium criteria.

To validate this approach, the bed-level used in the test problem described by García-Navarro and Vázquez-Cendón [26] was used within a prismatic trapezoidal channel with a wall-slope of unity. The results produced by using a pointwise source term treatment are shown in Figures 5.28 and 5.29, and enlarged in Figures 5.30 and 5.31. As with the non-prismatic rectangular case, the equilibrium solution is perturbed. The deviation from the expected water level is less marked than for the rectangular case, due to the constant channel width. The solutions obtained using the upwind source terms are shown in Figures 5.32 and 5.33, where it can be seen that the equilibrium solution is maintained.

The run time measurements for the problem are given in Table 5.6. For both the pointwise and upwind source term treatments, the efficiency gains obtained are slightly less than for the previous example. As before, the second LTS procedure was found to be less efficient than global time stepping when only two time levels were used. In this instance the pointwise source term treatment led to a shorter

Time stepping scheme	Source term treatment	Run time (s)	Eff. gain (%)	No. of flux calculations	Eff. gain (%)
Global	Pointwise	0.1756	—	97920	—
LTS1		0.1686	4.0	64346	34.3
LTS2 (2 time levels)		0.1753	0.2	72897	25.6
LTS2 (4 time levels)		0.1549	11.8	66063	32.5
LTS2 (8 time levels)		0.1549	11.8	66063	32.5
Global	Upwind	0.2114	—	97280	—
LTS1		0.1947	7.9	63862	34.4
LTS2 (2 time levels)		0.2023	4.3	72434	25.5
LTS2 (4 time levels)		0.1796	15.0	65488	32.7
LTS2 (8 time levels)		0.1796	15.0	65488	32.7

Table 5.6: Run times comparison for the trapezoidal channel.

run time for all of the time stepping procedures, over the upwind approach. This is to be expected due to the increase level of computation necessary to compute the upwinded values. This factor also contributes to the slightly better efficiency gains observed when the LTS procedures are combined with the upwind source term treatment. It may be noted that for this problem the flow conditions only permitted four time levels to be used within the LTS2 method.

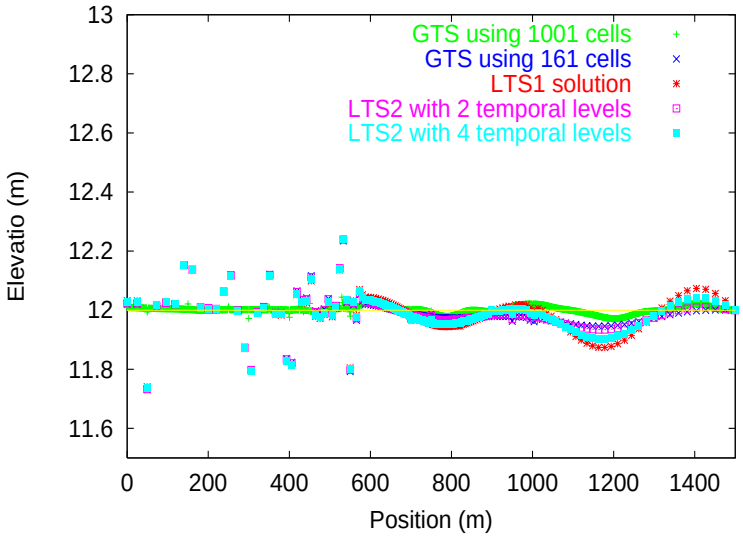

Figure 5.28: Elevation with pointwise source terms.

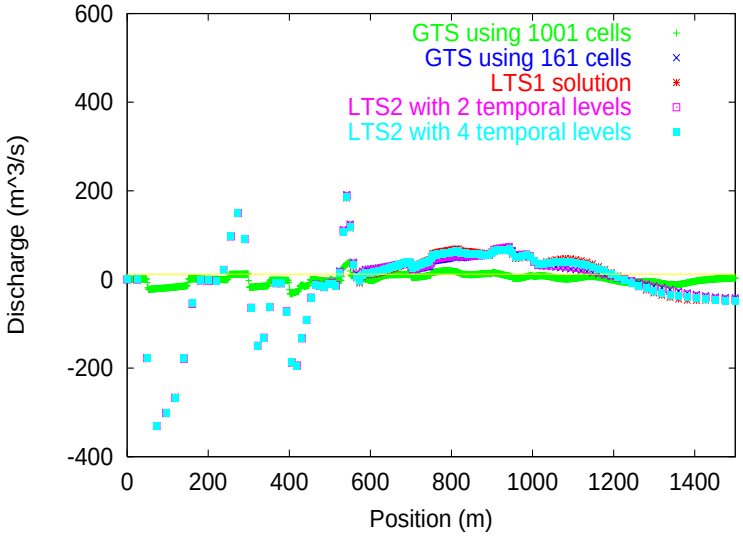

Figure 5.29: Discharge with pointwise source terms.

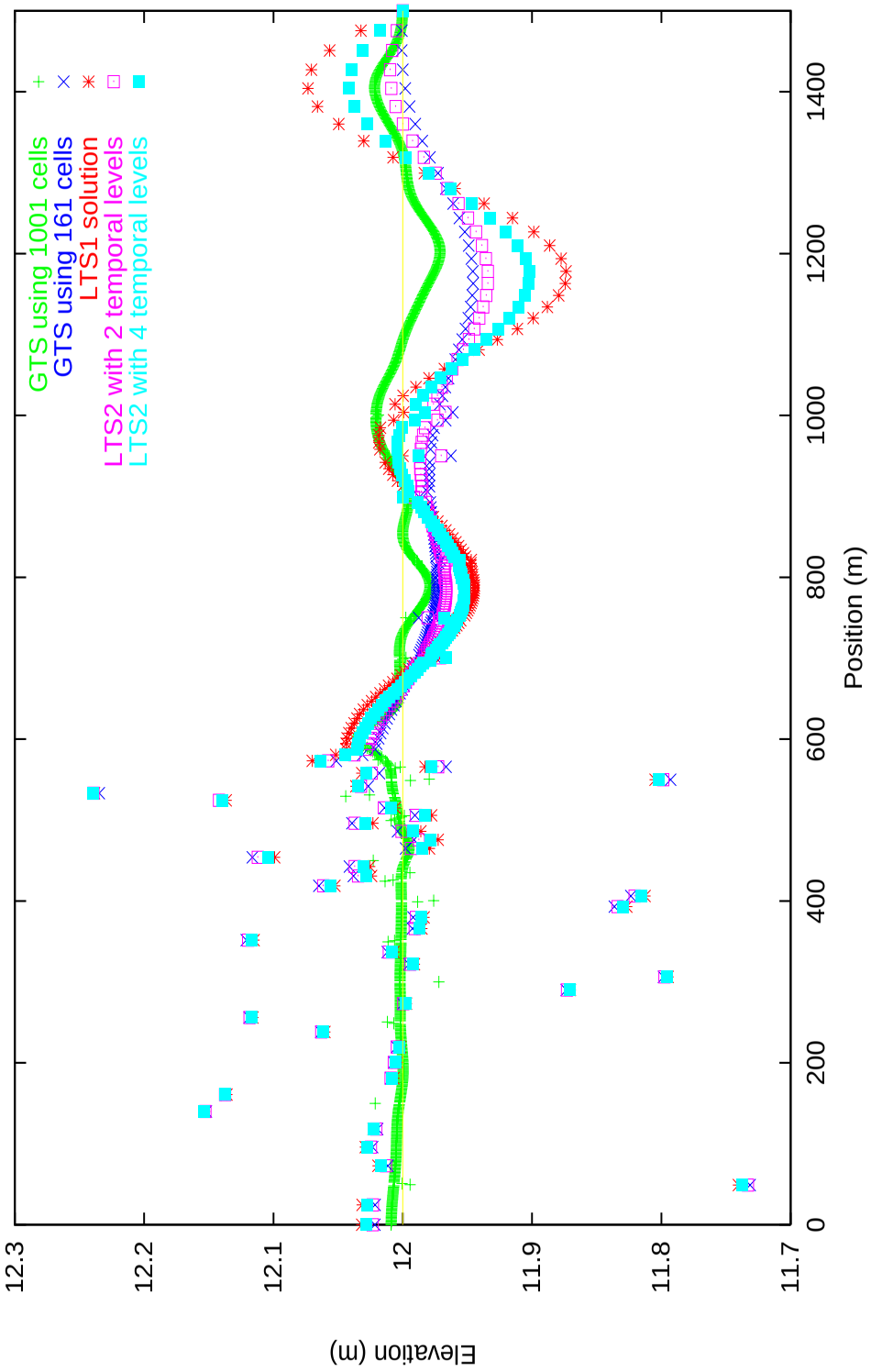

Figure 5.30: Elevation with pointwise source terms.

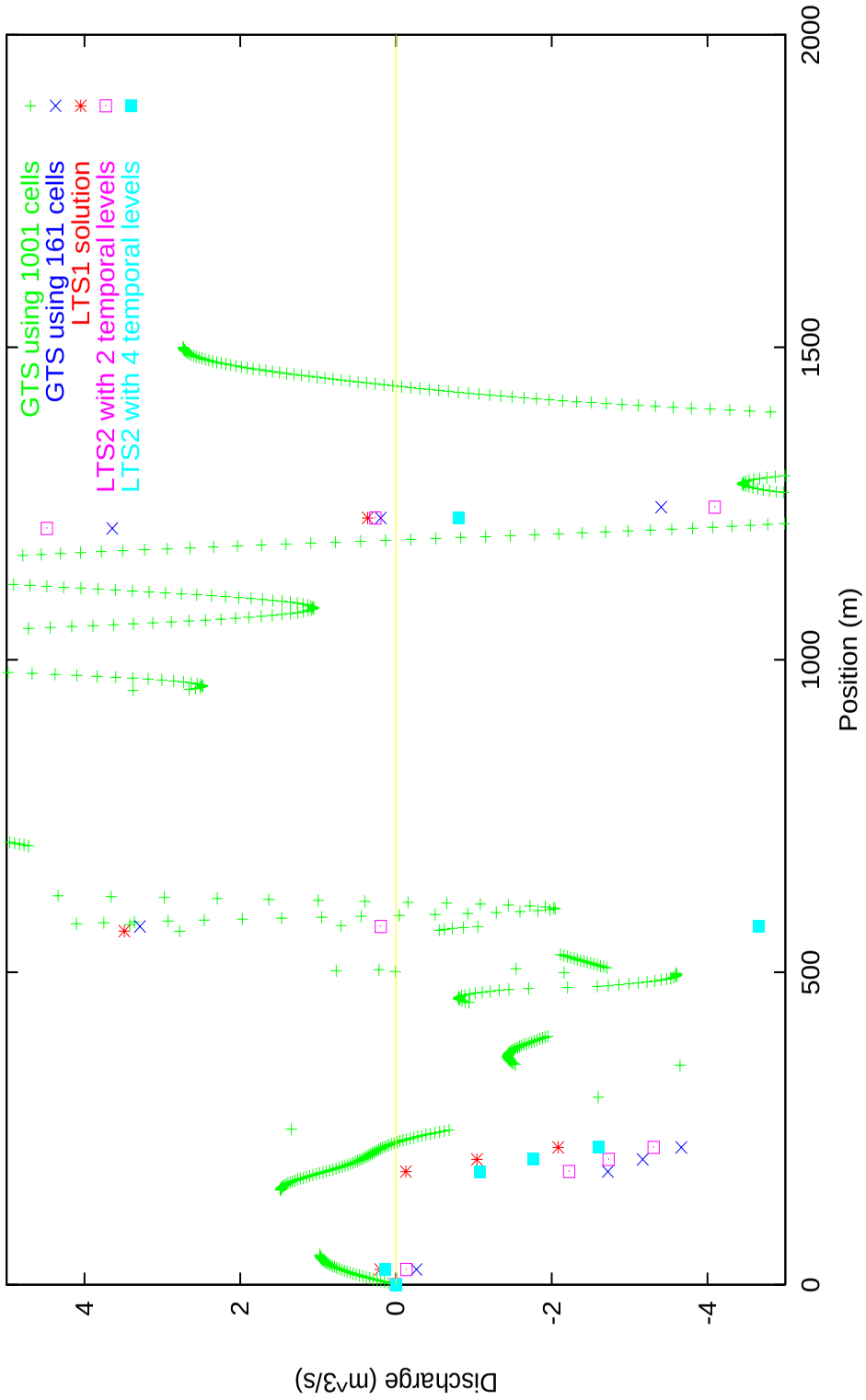

Figure 5.31: Discharge with pointwise source terms.

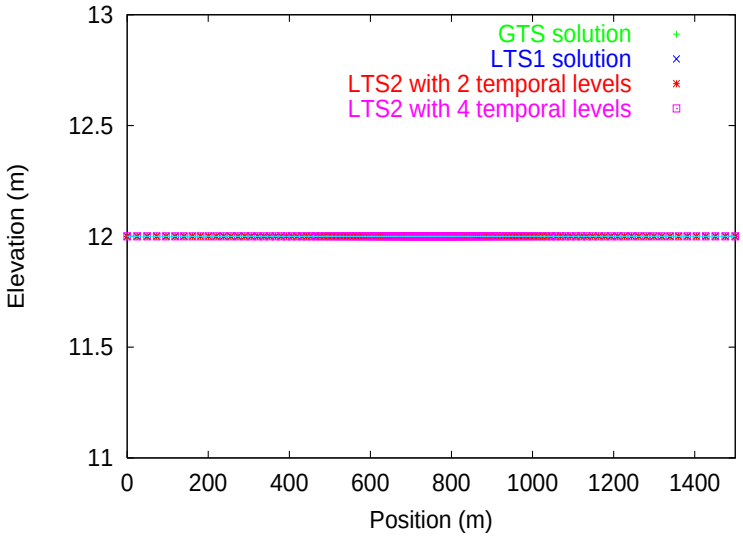

Figure 5.32: Elevation with upwind source terms.

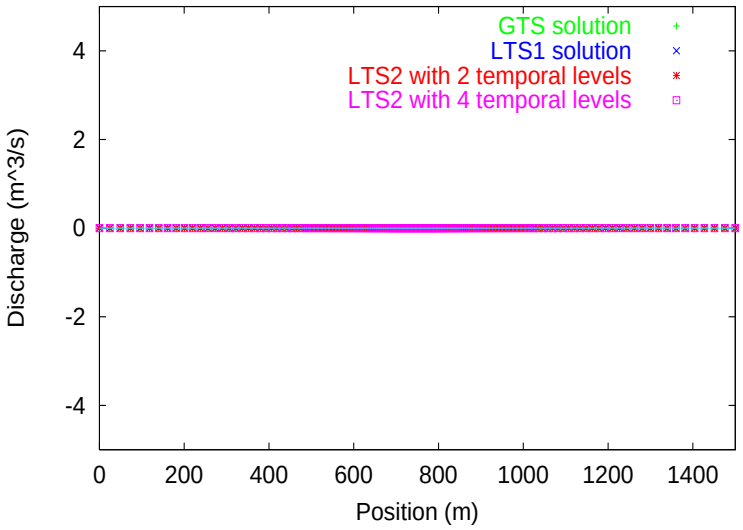

Figure 5.33: Discharge with upwind source terms.

5.5 Summary of development

The development of the two LTS approaches within this chapter has highlighted a number of points that will be investigated in more detail in the next chapter

- Using an LTS procedure has the potential to reduce computer run times
- LTS methods can lead to increased local accuracy, noticeably in the region of bores
- Source term calculation may also be included within the LTS strategy (though this has only been illustrated for a steady state problem).

From the two cases considered, the second LTS procedure was seen to lead to faster run times than the first procedure, only when four or more time levels were used. However the number of flux calculations performed was higher, due to the much larger interface region employed. For both approaches the efficiency gains were higher when the complexity of the calculations was increased, as illustrated with the second order results and also by the presence of source terms.

In the examples considered in this chapter, the upwind source term treatment (together with the proposed extensions for irregular grids and trapezoidal cross sections), was seen not to perturb the given equilibrium solutions, and produced more satisfactory results than when the pointwise treatment was used.

Chapter 6

Test cases and results

From the available literature, a number of test cases have been identified and are now considered for comparing the global and local time stepping strategies for a range of problems. Though most test cases are in general too simple to be of practical interest, they nevertheless provide an invaluable means to compare and contrast the performance of different numerical methods with benchmark solutions. The range of problems for which analytic solutions are available is somewhat limited and is generally restricted to only 1-d steady state problems. Though the LTS approaches being considered here are intended for transient calculations, they may equally be applied to steady state situations.

6.1 Steady state test cases

García-Navarro, Alcrudo and Savirón [22], considered the case of the flow over a bump for a prismatic rectangular channel (**S1**). The channel is $1m$ wide and has a bed which forms a bell-shaped curve. At the upstream boundary a constant head of $10m$ is imposed, whilst at the downstream end, a depth of $6m$ is maintained. This causes the upstream subcritical flow to reach critical conditions over the bump and subsequently become supercritical. A hydraulic jump then forms to connect the flow with the subcritical downstream region.

By solving a cubic equation for the depth profile (resulting from the application of Bernoulli's/constant head equation) either side of the jump, and by applying the jump relations to connect the two regions, an analytic solution to this problem

can be found (see Appendix A for details).

In the same paper the steady flow through a converging/diverging channel is also considered (**S2**). The channel consists of a series of rectangular cross sections which contain a sinusoidal width contraction/expansion together with a flat bed. The width of the channel decreases from $5m$ down to the critical width ($3.587m$ in the example given) which induces a critical flow, leading to the formation of a supercritical region and a hydraulic jump. The initial conditions given in the paper are a depth profile of $2m$, together with a fixed upstream discharge of $20m^3s^{-1}$. A weir boundary condition is imposed at the downstream end of the reach. Applying a similar strategy to before, an analytic solution can also be generated for this example.

This problem can be adapted to create a wholly subcritical flow by increasing the width of the channel at the contraction (**S3**). In this example, the channel width reduces to $4.5m$ at the narrowest point. The initial and boundary conditions are set to the values given in the original example.

MacDonald *et al* [42] proposed a means to generate problems with analytic solutions for a range of conditions and geometries. Specifically, four test cases were presented for both rectangular and trapezoidal rough prismatic channels with non-uniform beds.

The first problem (**S4**) is for a $1km$ long rectangular channel of width $10m$ and steady discharge of $20m^3s^{-1}$. The Manning roughness coefficient for the channel is 0.03 and a downstream depth of $0.748409m$ is imposed. The bed slope for the problem is represented by

$$S_o(x) = \left[1 - \frac{4}{g\hat{h}(x)^3}\right]\hat{h}'(x) + 0.36\frac{[2\hat{h}(x)+10]^{4/3}}{[10\hat{h}(x)]^{10/3}}$$

where $\hat{h}(x)$ represents the analytic depth profile and is given by

$$\hat{h}(x) = \left(\frac{4}{g}\right)^{1/3}\left\{1 + \frac{1}{2}\exp\left[-16\left(\frac{x}{1000} - \frac{1}{2}\right)^2\right]\right\}$$

and

$$\hat{h}'(x) = -\left(\frac{4}{g}\right)^{1/3}\frac{2}{125}\left(\frac{x}{1000} - \frac{1}{2}\right)\exp\left[-16\left(\frac{x}{1000} - \frac{1}{2}\right)^2\right].$$

The second problem (**S5**) is also for a $1km$ long rectangular channel of width $10m$ and discharge of $20m^3s^{-1}$. The conditions are such that the flow is subcritical at

inflow and supercritical at outflow with critical conditions being attained at the midpoint of the reach. A value of 0.02 is set for the Manning coefficient and the bed slope is defined by

$$S_o(x) = \left[1 - \frac{4}{g\hat{h}(x)^3}\right]\hat{h}'(x) + 0.16\frac{[2\hat{h}(x)+10]^{4/3}}{[10\hat{h}(x)]^{10/3}}$$

together with the depth function

$$\hat{h}(x) = \begin{cases} \left(\frac{4}{g}\right)^{1/3}\left\{1 - \frac{1}{3}\tanh\left[3\left(\frac{x}{1000} - \frac{1}{2}\right)\right]\right\} & 0 \le x \le 500 \\ \left(\frac{4}{g}\right)^{1/6}\left\{1 - \frac{1}{3}\tanh\left[6\left(\frac{x}{1000} - \frac{1}{2}\right)\right]\right\} & 500 \le x \le 1000, \end{cases}$$

and the gradient

$$\hat{h}'(x) = \begin{cases} -\left(\frac{4}{g}\right)^{1/3}\frac{1}{1000}\mathrm{sech}^2\left[3\left(\frac{x}{1000} - \frac{1}{2}\right)\right] & 0 \le x \le 500 \\ -\left(\frac{4}{g}\right)^{1/3}\frac{1}{1000}\mathrm{sech}^2\left[6\left(\frac{x}{1000} - \frac{1}{2}\right)\right] & 500 \le x \le 1000. \end{cases}$$

The third problem (**S6**) presented is for a $5km$ trapezoidal channel for which the surface level width, B, is defined by $B = 10 + 4h$, and the wetted perimeter, P, by $P = 10 + 2h\sqrt{5}$ (corresponding to a wall slope of $z = 2$). Again the discharge is set at $20m^3s^{-1}$ and the flow is subcritical throughout the channel. The downstream depth is specified as $1.125m$ and the Manning coefficient is 0.03. The bed slope function is defined by

$$S_o(x) = \left\{1 - \frac{400[10 + 4\hat{h}(x)]}{g[10 + 2\hat{h}(x)]^3}\right\}\hat{h}'(x) + 0.36\frac{[10 + 2\hat{h}(x)\sqrt{5}]^{4/3}}{[10 + 2\hat{h}(x)]^{10/3}\hat{h}(x)^{10/3}}$$

together with

$$\hat{h}(x) = \frac{9}{8} + \frac{1}{4}\sin\left(\frac{\pi x}{500}\right)$$

and

$$\hat{h}'(x) = \frac{\pi}{2000}\cos\left(\frac{\pi x}{500}\right).$$

The final example (**S7**) considered in the paper is for a $1km$ trapezoidal channel ($B = 10 + 2h$ and $P = 10 + 2h\sqrt{2}$ (implying $z = 1$)) with a discharge of $20m^3s^{-1}$ and a downstream depth of $1.349963m$. The conditions are such that the upstream

subcritical flow becomes supercritical, leading to the formation of a hydraulic jump at a point two thirds along the distance of the channel. In this case, Manning's n is set to 0.02, and the bed slope is given by

$$S_o(x) = \left\{1 - \frac{400[10 + 2\hat{h}(x)]}{g[10 + \hat{h}(x)]^3\hat{h}(x)^3}\right\}\hat{h}'(x) + 0.16\frac{[10 + 2\hat{h}(x)\sqrt{2}]^{4/3}}{[10 + \hat{h}(x)]^{10/3}\hat{h}(x)^{10/3}}.$$

and

$$\hat{h}(x) = \begin{cases} 0.723449\left[1 - \tanh\left(\dfrac{x}{1000} - \dfrac{3}{10}\right)\right] & 0 \le x \le 300 \\ 0.723449\left\{1 - \dfrac{1}{6}\tanh\left[6\left(\dfrac{x}{1000} - \dfrac{3}{10}\right)\right]\right\} & 300 < x \le 600 \\ \dfrac{3}{4} + \displaystyle\sum_{k=1}^{3} a_k \exp\left[-20k\left(\dfrac{x}{1000} - \dfrac{3}{5}\right)\right] + \dfrac{3}{5}\exp\left(\dfrac{x}{1000} - 1\right) & 600 < x \le 1000 \end{cases}$$

with

$$\hat{h}'(x) = \begin{cases} -0.723449 \times 10^{-3}\mathrm{sech}^2\left(\dfrac{x}{1000} - \dfrac{3}{10}\right) & 0 \le x \le 300 \\ -0.723449 \times 10^{-3}\mathrm{sech}^2\left[6\left(\dfrac{x}{1000} - \dfrac{3}{10}\right)\right] & 300 < x \le 600 \\ -\dfrac{1}{50}\displaystyle\sum_{k=1}^{3} a_k \exp\left[-20k\left(\dfrac{x}{1000} - \dfrac{3}{5}\right)\right] + \dfrac{3}{5000}\exp\left(\dfrac{x}{1000} - 1\right) & 600 < x \le 1000 \end{cases}$$

where $a_1 = -0.111051$, $a_2 = 0.026876$ and $a_3 = -0.217567$.

6.2 Transient/Unsteady test cases

As discussed in the previous chapter, the dam-break problem (**U1**) is one of the most popular unsteady test cases for 1-d open channel flows. The exact solution for the given depths h_l and h_r was originally determined by Stoker [58], and can be found using the procedure given by Glaister [29] as outlined in the Appendix B. In this section a depth ratio of 100:1 for the water upstream and downstream of the dam is again considered.

Yang *et al* [67] considered the case of the unsteady head-on collision of two bore waves generated by two dam-break scenarios (**U2**). The initial conditions are given as

$$u(x, 0) = 0$$

and

$$h(x,0) = \begin{cases} 100 & 0 \leq x < 0.4 \\ 1 & 0.4 \leq x < 0.6 \\ 10 & 0.6 \leq x < 1. \end{cases}$$

The channel has a rectangular cross section which is taken to be of width $1m$. Transmissive boundary conditions are imposed at both ends of the channel.

Alcrudo, García-Navarro, and Savirón [2] considered the head-on collision and interaction of two bores in a trapezoidal channel (**U3**). The channel is of length $1km$ and $1m$ wide at the base with a wall slope of unity. The initial conditions given are

$$Q(x,0) = \begin{cases} 100 & -500 \leq x < -400 \\ 10 & -400 \leq x < 0 \\ 0 & 0 \leq x < 500 \end{cases}$$

$$h(x,0) = \begin{cases} 3.6 & -500 \leq x < -400 \\ 2.0 & -400 \leq x < 0 \\ 2.6 & 0 \leq x < 500. \end{cases}$$

A reflective boundary condition is imposed downstream which causes the surge wave to be reflected back upstream once it has reached the boundary.

Toro [62] presented a test case for flow over an elevated bed in a rectangular channel of length $30m$ (**U4**). The bed level is set by

$$z(x) = \begin{cases} 0 & 0 \leq x < 10 \\ 0.1x - 1 & 10 \leq x < 20 \\ 1 & 20 \leq x \leq 30. \end{cases}$$

and the initial elevation (fluid depth + bed level) by

$$H(x,0) = \begin{cases} 4 & 0 \leq 0 < 5 \\ 2 & 5 \leq x \leq 30. \end{cases}$$

Transmissive boundary conditions are employed for this problem.

Savic and Holly [54] looked at a series of dam-break like problems, the most complex of which involved sloping channels and non-prismatic cross-sections. The first of these problems to be considered here (**U5**) is for a $100km$ long rectangular channel of slope 0.1% and Manning roughness coefficient 0.04. The channel width increases from $50m$ to $250m$ over a single cell located at $55km$. For both problems, the method of characteristics is used to determine the flow at the boundaries,

with a discharge of $0m^3s^{-1}$ specified at the upstream end, and a fixed depth of $1m$ imposed downstream.

The second problem (**U6**) is similar to the previous case, except that the channel width decreases from $50m$ to $10m$ at the same point as before. In both instances the initial conditions are still water with an elevation of $100m$ for the first $50km$, and a depth of $1m$ downstream of the dam.

6.3 Results

To evaluate and contrast the global and local time stepping strategies, solutions to each of the problems presented in the previous section have been generated. To illustrate how the performance of the various approaches varies with the grid on which the solution is obtained, a range of grids have been considered. The basis of construction for the grids used is outlined in Appendix C (irregular grid B), and follows the notion of a central region of fine equally sized cells of length d, which are connected to the outermost cells of length nd at the channel boundaries. The intermediate regions consist of cells whose length varies by a uniform ratio. In the examples shown, the central region contains three cells of equal size, and the value of n is varied between 1 (regular grid) and 128. In the discussion to follow, references made to the n grid correspond to this ratio.

The effects of choosing either a pointwise or upwind source term treatment are also considered. For the examples in which source terms are involved, solutions are presented using both the upwind and the pointwise treatments. Solutions are also shown for when the pointwise approach is applied together with the Superbee flux limiter [59]. In the cases where no source terms are present, solutions are generated using the first and second order (flux limited) versions of Roe's scheme.

In the following sections, a representative range of profiles are shown, which focus on the particular regions of interest in each case, using the different numerical approaches. A representative sample of the run time and flux count data measurements is also given, and the complete set of tables can be found in Appendix D. In all of the steady state simulations, the initial discharge was set to zero in every cell except at the upstream boundary, with the exception of **S1**, where a value of zero was used everywhere. The initial elevations (depth + bed level) were set using the prescribed downstream boundary condition, or analytical value where

available. For **S2** and **S3** where a weir boundary condition is imposed, the depth was set to $2m$ throughout the channel. For the problems **U1**, **U2** and **U3** which do not include any source terms, the run time measurements given were obtained with the source term calculations removed.

6.3.1 Steady state results

For the first steady state test case, **S1**, there is little appreciable difference between the elevation plots produced by the various time stepping procedures and source term treatments. In all cases, there is good agreement between the numerical and analytical solutions, and the hydraulic jump is well captured. Figure 6.1 shows the solution obtained on the 4 grid using the upwind source term treatment. The elevation of the point which lies on the jump line varies slightly between the differing grids and source terms. However in all cases, the results from the two local time stepping approaches coincide with the global time stepping solutions.

As this problem is steady state, the discharge should be constant throughout the channel. Figures 6.2 and 6.3 are more interesting than the elevation plots, as they highlight the noticeable variations in the discharge values that occur. The solutions produced using the first order scheme with the pointwise source term treatment show the greatest variation from the constant value, particularly in the region just before the contraction. Using a flux limiter reduces the deviation, and the upwind results maintain an almost constant value except at the jump point. Differences between the GTS results and those produced using the two LTS schemes with the pointwise source terms and Superbee flux limiter, are particularly apparent. In this instance the values obtained using the global time stepping are comparable to those using the various time stepping strategies together with the upwind source term treatment. Note that all of the results show a spike at the location of the hydraulic jump.

The results from the run time and flux count measurements show several trends as illustrated by Table 6.1. In general, for the same grid and time stepping procedure, the run times measured using the upwind source term treatments are slower than using the pointwise calculations, but are faster than using the pointwise approach together with a flux limiter. The efficiency gains calculated using the run time values for LTS1 lie in the range of -14.17 to 32.87 percent. For LTS2, the range is -21.20 to 49.49 percent. The negative values corresponding to lower values of

n and the efficiency gain increases with n. In addition, as n increases then so too does the level of temporal embedding that can be used with the LTS2 strategy, corresponding to higher values of m. The changes in efficiency gains between successive grids in which the maximum m level has changed, is generally more appreciable than when m remains the same. In the case of the pointwise and pointwise plus Superbee results, the limit between the 64 and 128 grids actually decreases (due to numerical instability, resulting in the need to enforce a maximum m value to overcome temporal stiffness), as can be observed by the efficiency gains. Another observation is that for the LTS1 algorithm, the efficiency gains given from the run time measurements for the pointwise results, are generally less than the upwind and pointwise plus Superbee values, which are more comparable.

In comparing the two LTS methodologies, the LTS1 approach is generally faster when only one temporal level is permitted by the LTS2 method, but the LTS2 approach leads to noticeably higher efficiency gains when a maximum value of $m = 3$ (the highest of all the results) can be used. One point to note is that the loss in efficiency of the LTS1 algorithm on the regular grid is less than in the case of the 2 grid. This is because the algorithm incorporates a check to see if whether the maximum local time step is at least twice the minimum value. If not then it does not proceed any further with the local time stepping update. Similar checks are included in the LTS2 procedures for when the maximum value of m is zero.

The flux count measurements show very similar trends to those evident from the run time values. The efficiency gains recorded are higher, as the implementation costs of the algorithms are not taken into account. One noticeable feature is that generally the flux count efficiencies of the two LTS approaches are more similar on the same grid than the run time efficiencies are. In addition, the differences between the run time and flux count efficiencies for the LTS2 algorithm are typically less than for the LTS1 method. This suggests that the implementation costs within the LTS1 procedures are more significant than for the LTS2 routines. Another effect that can be observed is that for the LTS1 results, the flux count on the regular grid for the upwind results, and the 1 and 2 grids for the pointwise source term treatments, are slightly higher than when global time stepping is used.

For the second steady state case, **S2**, in which the channel contracts and then expands, the depth profiles obtained are very similar in character to those in the previous example. Figure 6.4 shows the solutions on the 128 grid when the pointwise source terms are used together with Superbee. One point of interest in

this particular plot is that the value located on the jump line produced by the GTS method, differs from the value obtained from the LTS schemes. The discharge profiles for the two grids are shown in Figures 6.5 and 6.6. The deviations from the expected value show the same traits as for **S1**, although the magnitude is generally less. The run time and flux count data is again similar. However slightly higher efficiency gains using the LTS2 approach can be noted in the upwind and pointwise source term treatment values, as a maximum m value of 5 could be used on the higher ratio grids.

Figure 6.7 shows the solution obtained for the **S3** problem when the pointwise source terms are used on the 4 grid. On this scale no differences can be observed between the solutions produced using the different time stepping procedures and source terms. Figures 6.8 to 6.13 show the depth values obtained using the various treatments in the vicinity of the channel contraction. As can be seen in Figures 6.8 and 6.9, the solutions obtained on the 4 and 128 grids using the upwind source terms show close agreement with the analytical depth values. In the case of the pointwise treatment, Figures 6.10 and 6.11 show a deviation between the analytic and predicted values, which is more significant on the 128 grid. Applying a flux limiter eliminates this problem, as can be observed in Figures 6.12 and 6.13 where Superbee has been used. In these plots it is apparent that the LTS results again match the GTS solutions.

The discharge comparisons are shown in Figures 6.14 and 6.15. As with the previous two examples, the solutions produced using the upwind source term treatments reproduce the steady state value. The pointwise solutions show the greatest deviation, which is reduced by the introduction of the Superbee flux limiter. With the upwind and pointwise results, it can be seen that the GTS and LTS solutions all coincide. In Figure 6.14, differences between the different time stepping procedures used in conjunction with the pointwise source term treatment are clearly visible, with the GTS results falling closer to the expected value.

The efficiencies gains measured for the LTS1 results range from -13.11 to 29.76 percent for the run time values, and between -0.62 to 67.63 percent for the flux count measurements. For the LTS2 method, the measured efficiency gains range from -22.84 to 54.20 percent, and from 0 to 65.30 percent for the run time and flux count measurements respectively. Comparison of the LTS1 and LTS2 efficiency gains again shows that there is closer agreement between the flux count efficiencies than there is between the run time values.

The complete solution obtained for **S4** on the 128 grid with the upwind source terms is shown in Figure 6.16. The elevation plots over the entire channel length show no variation between the different treatments. Figures 6.17 to 6.19 show the depth profiles over the range [400:600] for the 128 grid. As before, the upwind results match the analytic solution, whilst there is a discrepancy with the pointwise results, which is reduced by using a flux limiter. In this instance it can be seen that the GTS and LTS results are identical, except in the pointwise and Superbee results. In this example, the two LTS approaches produce slightly different solutions to those obtained using global time stepping.

The discharge plots for this example are shown in Figures 6.20 and 6.21 and appear quite similar in character to the discharge profiles of example **S3**. The trends visible in the recorded run time and flux count data are also the same as seen in the previous examples.

The solution produced to problem **S5** using the pointwise source term treatment with Superbee on the 4 grid is shown in Figure 6.22. An inspection of all of the depth profiles showed no appreciable differences in the quality of the solutions produced. The discharge values are shown in Figures 6.23 and 6.24. Again it can be observed that only the upwind results exactly match the prescribed discharge value, with the pointwise source term (no limiter) results showing the largest error, though reaching a constant value towards the downstream end of the channel. The differences between the GTS and LTS results for the pointwise plus Superbee solutions are clearly visible, and on the 128 grid, the GTS solution is constant throughout almost all of the channel. Inspection of the run time and flux count data shows the same trends as evident in the examples considered so far.

Example **S6** considers the flow over a rippled channel bed, as can be seen in Figure 6.25, which shows the solution using the pointwise source terms on the 128 grid. The depth profile over the complete range of the channel are shown in Figures 6.26 to 6.31. This particular example shows the most significant deviations from the analytical solution out of the examples considered, due to the nature of the bed level variation. As with the other cases considered, the upwind results are best, though the 128 grid results do show some discrepancies. The pointwise and pointwise plus Superbee solutions show the magnitudes of both the crests and troughs to be under predicted, with the Superbee results appearing slightly better than the first order solutions. Note that the solutions presented were those obtained once convergence had been achieved. The discharge plots

for this example are shown in Figures 6.32 and 6.33. The typical behaviour seen previously is again observed. In this instance the upwind results on the 128 grid show a slight drop in the discharge values at the non-boundary cells. The efficiency gains recorded take on similar values as before, with the same trends recurring.

An example of the elevation results obtained for the final steady state problem, **S7**, is given in Figure 6.34 which shows the upwind solutions on the 4 grid. The elevation plots are again all quite similar. For this test case, the largest deviation between the analytical and predicted depths occurs just before the hydraulic jump, as is illustrated in Figures 6.35 to 6.37. Here the upwind results exactly match the analytical solution, whilst the pointwise approach over predicts the values. Using Superbee with the pointwise source terms reduces the error. Figures 6.38 and 6.39 show the discharge predictions. As with the **S1** and **S2** results, a spike appears at the location of the hydraulic jump in all of the results. However in this problem, only the upwind solutions show the discharge returning to the correct value. The tabulated results again follow the same trends as the previous examples.

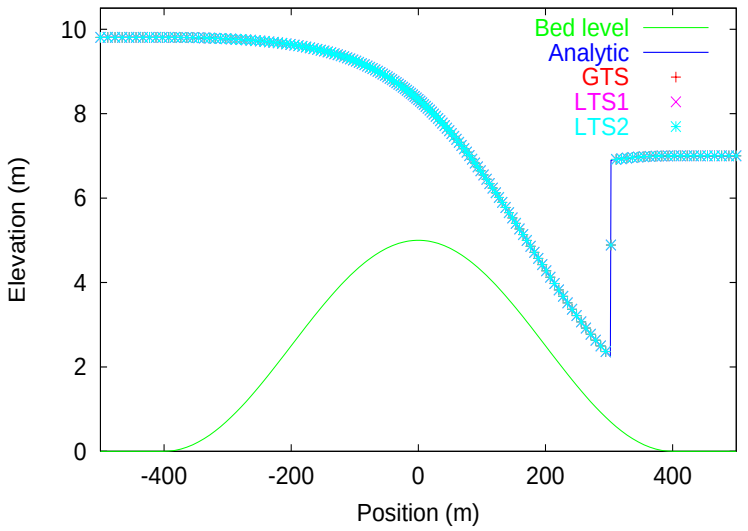

Figure 6.1: Elevation profile for S1 on 4 grid with upwind source terms.

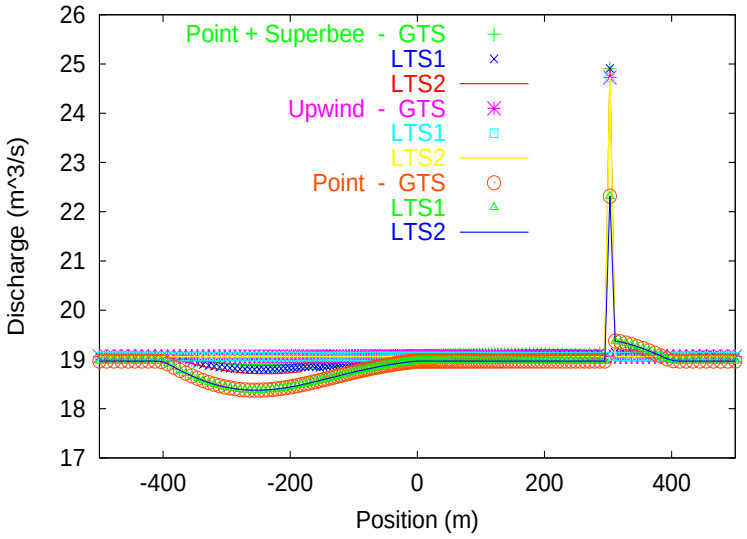

Figure 6.2: Discharge profiles for S1 on 4 grid.

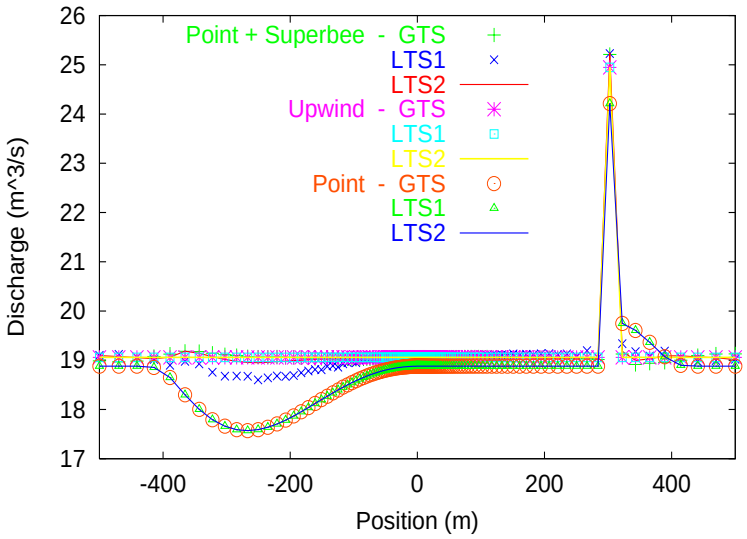

Figure 6.3: Discharge profiles for S1 on 128 grid.

Problem	Source term	Grid	GTS		LTS1				LTS2				
			Time (s)	Count	Time (s)	Gain	Count	Gain	Level	Time (s)	Gain	Count	Gain
S1	Upwind	1	1.424	679360	1.442	-1.26	685123	-0.85	1	1.671	-17.35	677152	0.33
		2	1.477	704320	1.603	-8.53	702427	0.27	1	1.723	-16.66	700214	0.58
		4	2.190	1046240	2.171	0.87	857548	18.04	2	2.225	-1.60	864175	17.40
		8	3.391	1622560	3.084	9.05	1006994	37.94	3	2.765	18.46	1055743	34.93
		16	5.443	2607840	4.518	16.99	1309886	49.77	3	3.677	32.45	1399209	46.35
		32	9.005	4319680	7.009	22.17	1860207	56.94	3	5.347	40.62	1994032	53.84
		64	15.28	7337120	11.33	25.85	2769639	62.25	3	8.760	42.67	3037868	58.60
		128	26.47	12724480	18.78	29.05	4234467	66.72	3	13.37	49.49	4840618	61.96
	Point	1	1.165	678720	1.184	-1.63	684511	-0.85	1	1.412	-21.20	676570	0.32
		2	1.209	704320	1.345	-11.25	705639	-0.19	1	1.449	-19.85	700315	0.57
		4	1.792	1045600	1.822	-1.67	842636	19.41	2	1.881	-4.97	860935	17.66
		8	2.772	1620800	2.631	5.09	1030873	36.40	2	2.340	15.58	1052790	35.05
		16	4.446	2603840	3.910	12.06	1333548	48.79	3	3.108	30.09	1395140	46.42
		32	7.350	4310880	6.120	16.73	1874322	56.52	3	4.535	38.30	1986883	53.91
		64	12.46	7318720	9.953	20.12	2826385	61.38	4	6.647	46.65	2910229	60.24
		128	21.58	12686400	16.61	23.03	4180629	67.05	3	11.41	47.13	4826376	61.96
	Point + Superbee	1	1.833	697820	1.854	-1.15	691158	0.95	1	2.123	-15.82	695626	0.31
		2	1.898	722256	2.167	-14.17	711701	1.46	1	2.274	-19.81	714059	1.13
		4	2.817	1072724	2.861	-1.56	888688	17.16	1	2.908	-3.23	884429	17.55
		8	4.364	1663452	4.034	7.56	1045753	37.13	2	3.673	15.83	1076922	35.26
		16	7.012	2673200	5.862	16.40	1437722	46.22	3	4.945	29.48	1424475	46.71
		32	11.61	4427344	9.001	22.47	2081536	52.98	3	7.131	38.58	2029572	54.16
		64	19.68	7518252	14.19	27.90	3086498	58.95	3	10.99	44.16	3103275	58.72
		128	34.20	13035048	22.96	32.87	4712482	63.85	2	20.47	40.15	5787442	55.60

Table 6.1: Results table for S1.

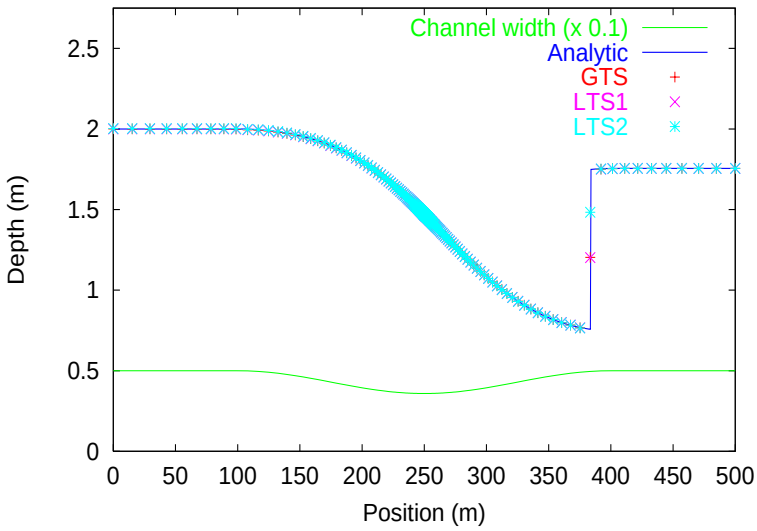

Figure 6.4: Depth profile for S2 on 128 grid with pointwise source terms and Superbee.

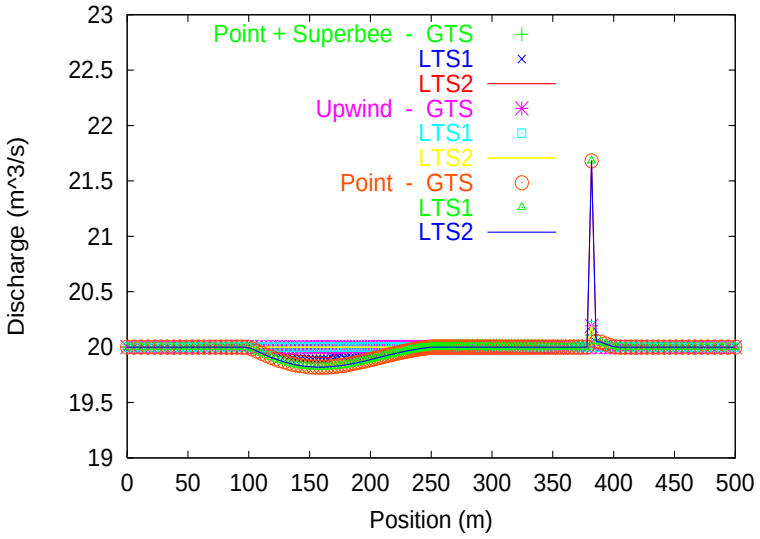

Figure 6.5: Discharge profiles for S2 on 4 grid.

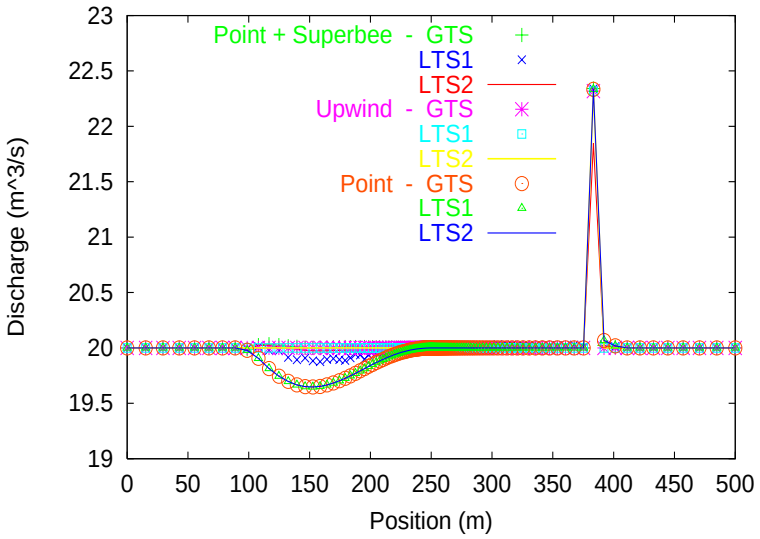

Figure 6.6: Discharge profiles for S2 on 128 grid.

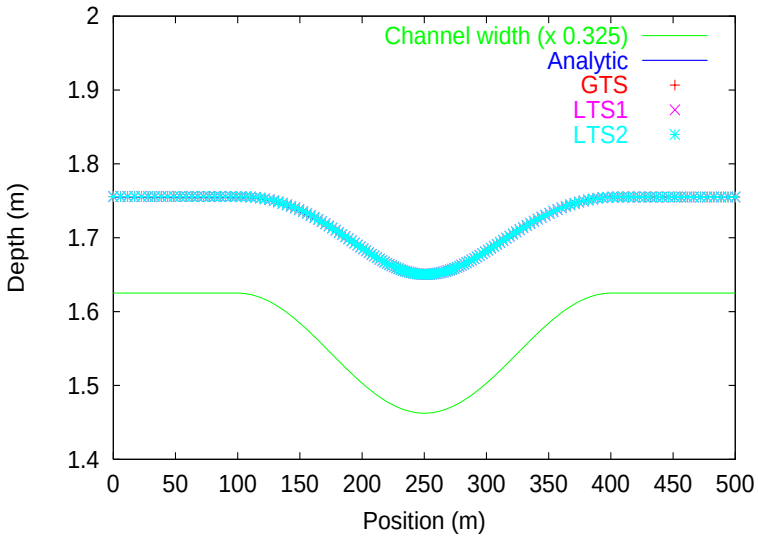

Figure 6.7: Depth profile for S3 on 4 grid with pointwise source terms.

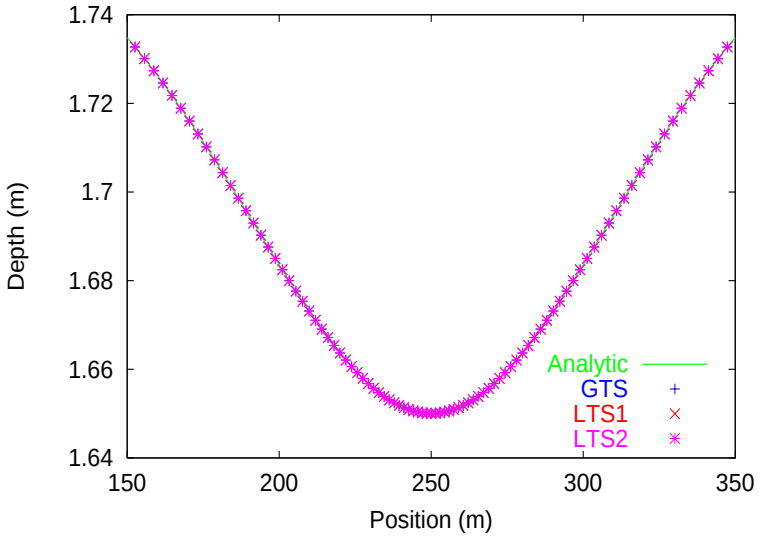

Figure 6.8: Depth profile for S3 on 4 grid with upwind source terms.

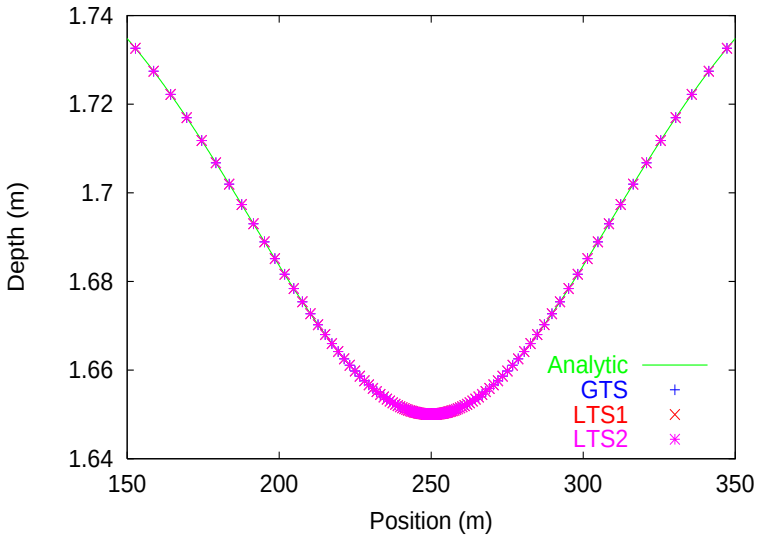

Figure 6.9: Depth profile for S3 on 128 grid with upwind source terms.

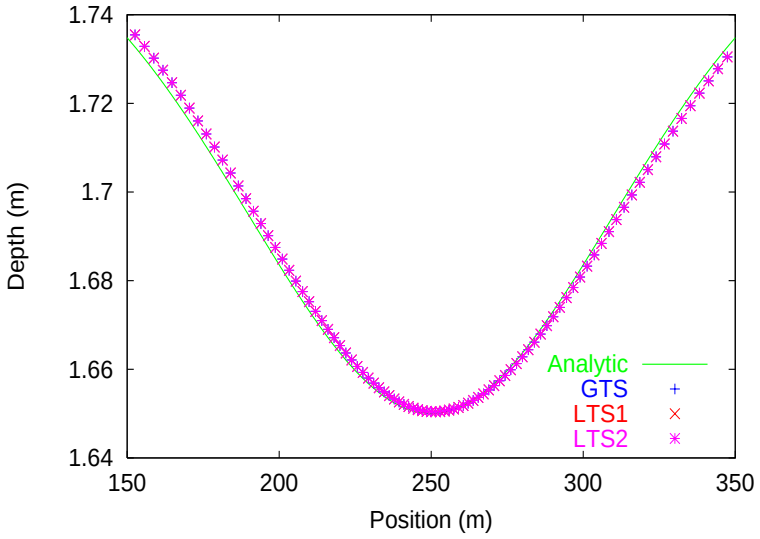

Figure 6.10: Depth profile for S3 on 4 grid with pointwise source terms.

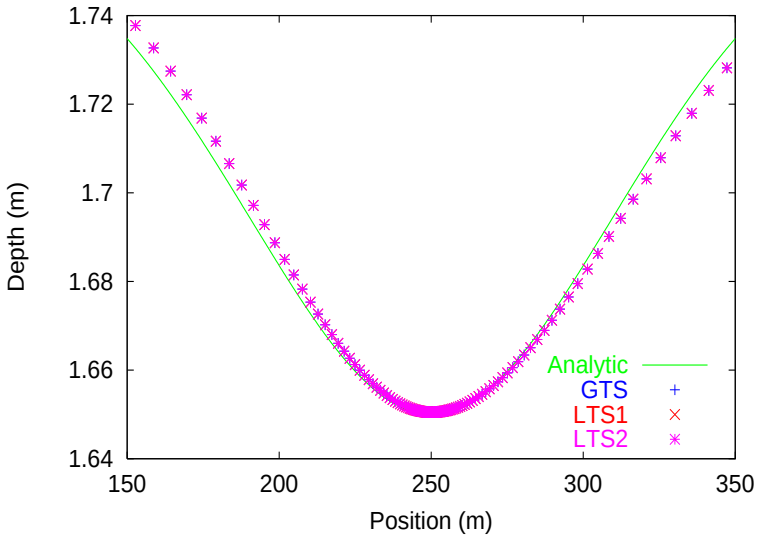

Figure 6.11: Depth profile for S3 on 128 grid with pointwise source terms.

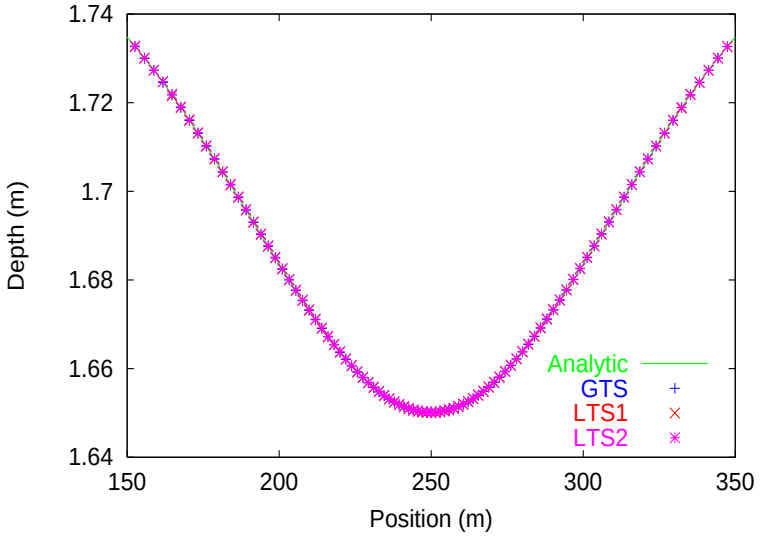

Figure 6.12: Depth profile for S3 on 4 grid with pointwise source terms and Superbee.

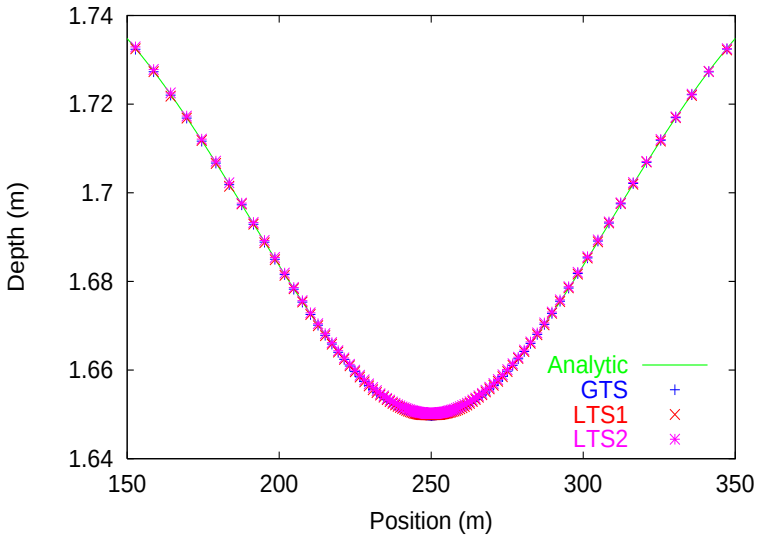

Figure 6.13: Depth profile for S3 on 128 grid with pointwise source terms and Superbee.

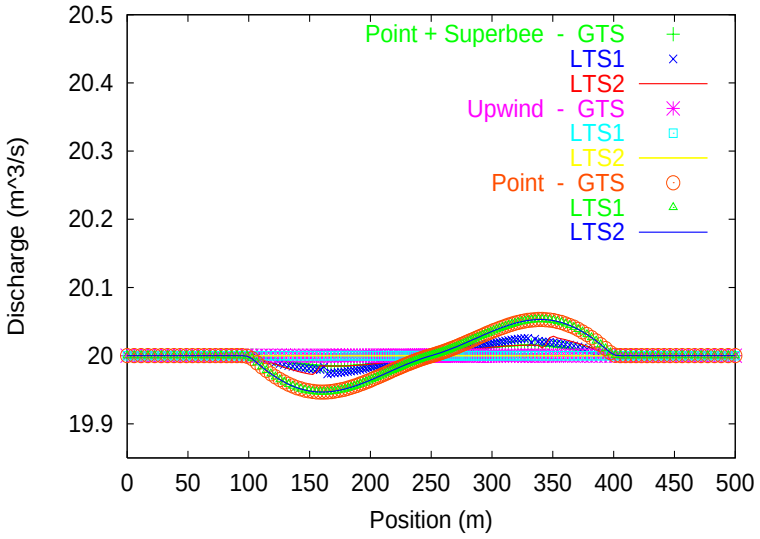

Figure 6.14: Discharge profiles for S3 on 4 grid.

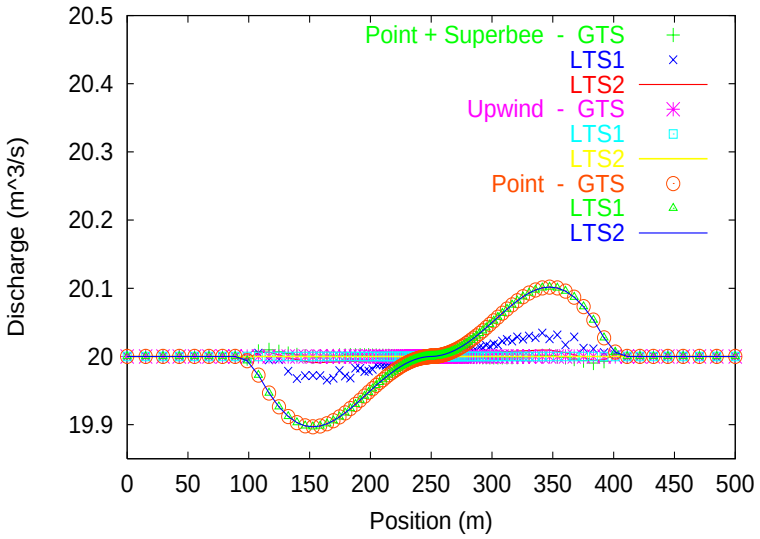

Figure 6.15: Discharge profiles for S3 on 128 grid.

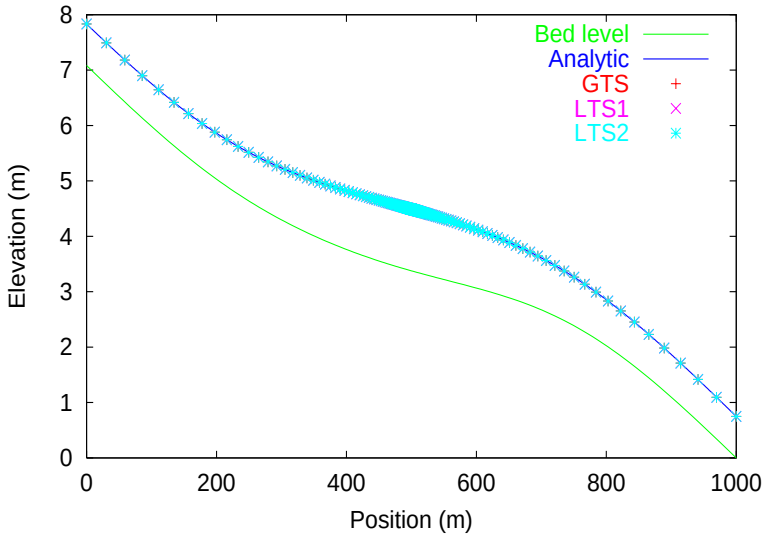

Figure 6.16: Elevation profile for S4 on 128 grid with upwind source terms.

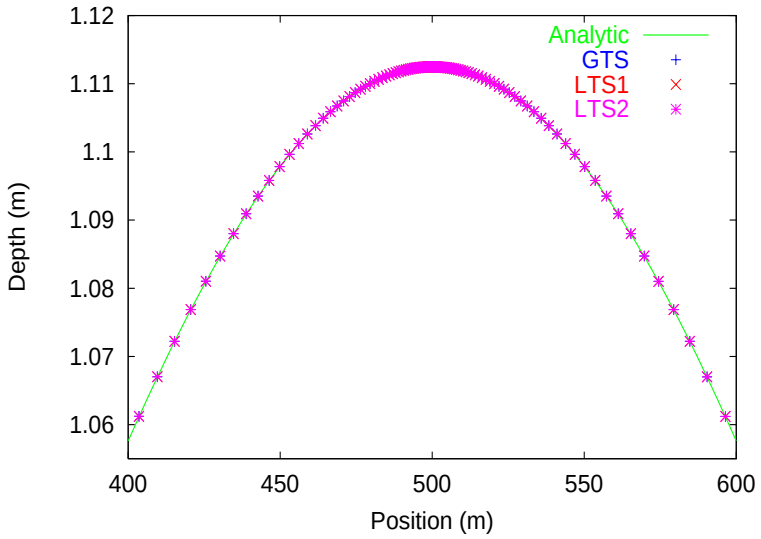

Figure 6.17: Depth profile for S4 on 128 grid with upwind source terms.

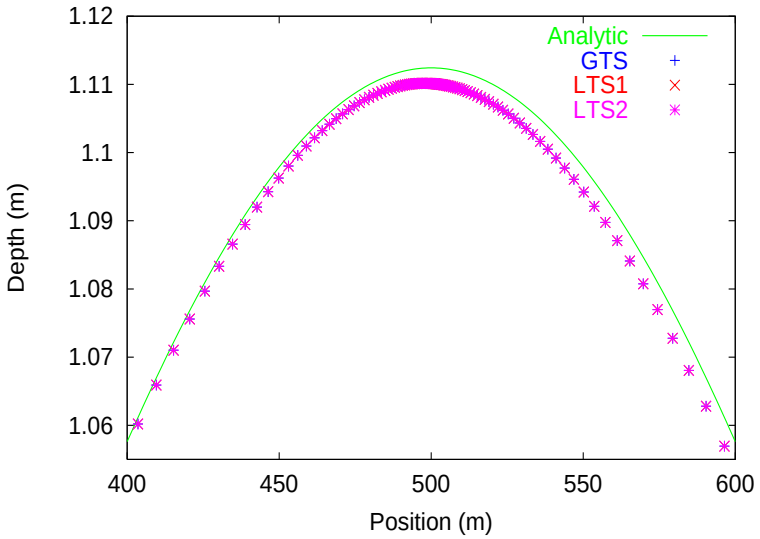

Figure 6.18: Depth profile for S4 on 128 grid with pointwise source terms.

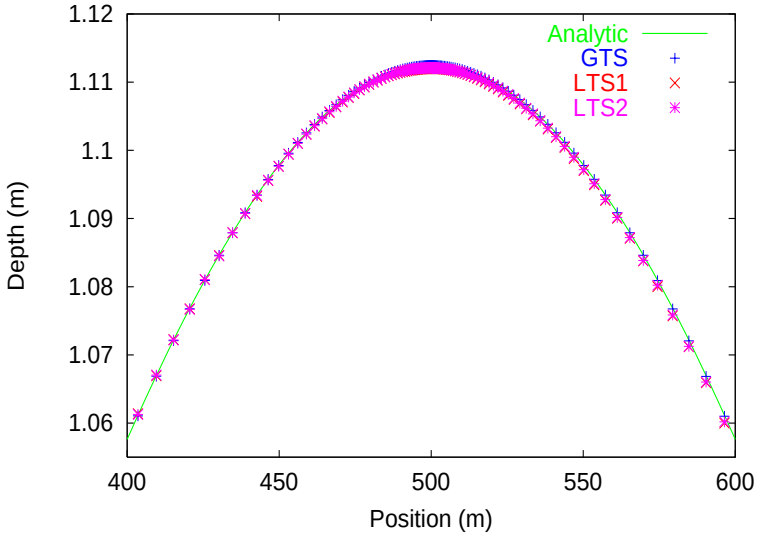

Figure 6.19: Depth profile for S4 on 128 grid with pointwise source terms and Superbee.

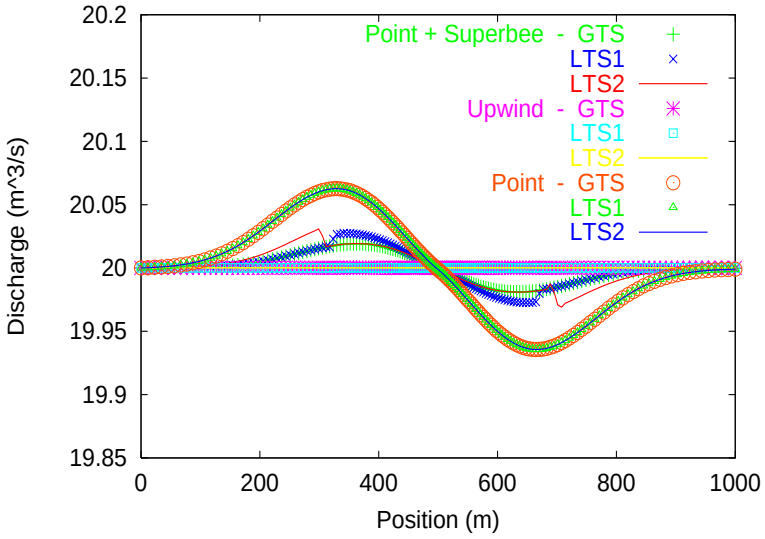

Figure 6.20: Discharge profiles for S4 on 4 grid.

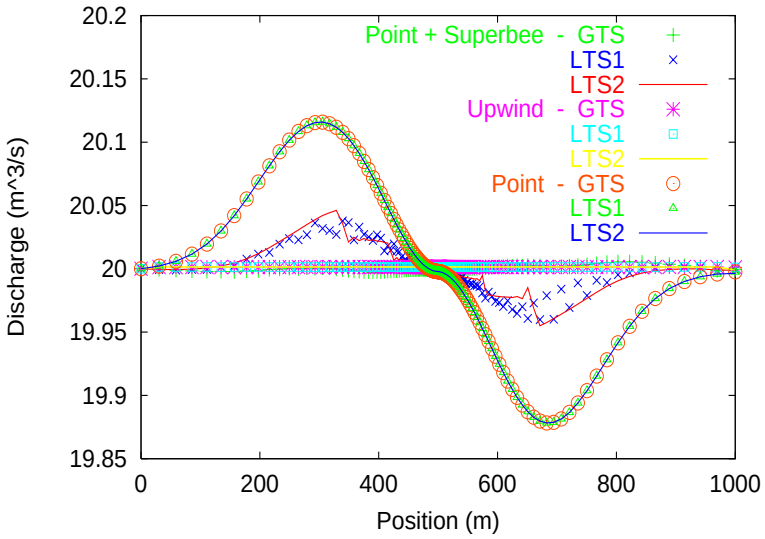

Figure 6.21: Discharge profiles for S4 on 128 grid.

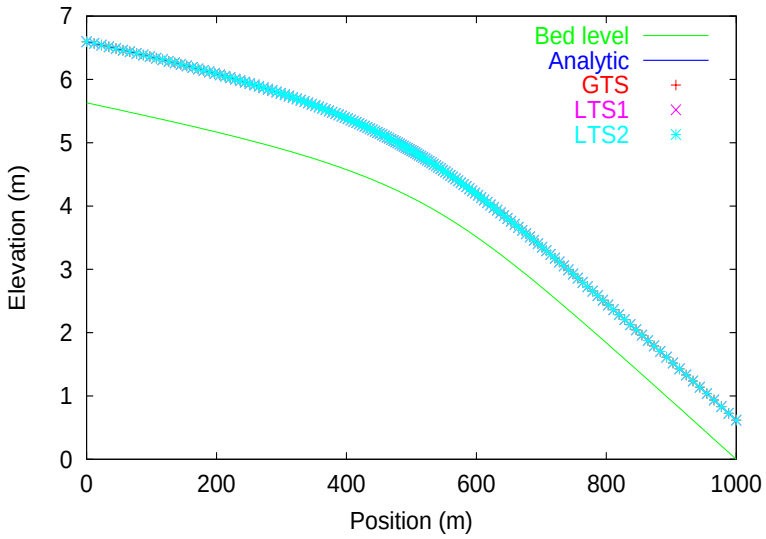

Figure 6.22: Elevation profile for S5 on 128 grid with pointwise source terms and Superbee.

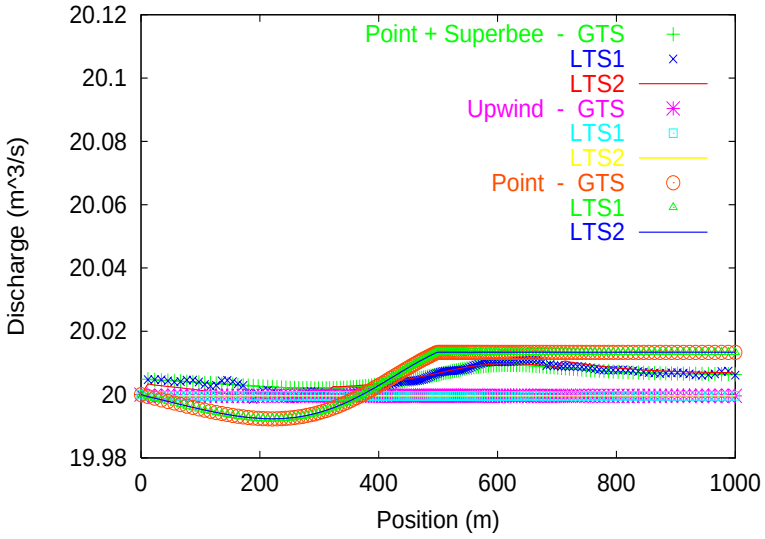

Figure 6.23: Discharge profiles for S5 on 4 grid.

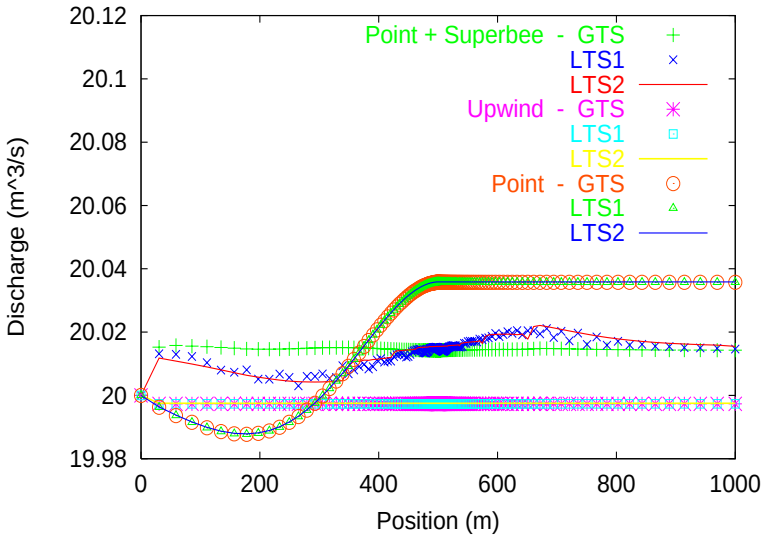

Figure 6.24: Discharge profiles for S5 on 128 grid.

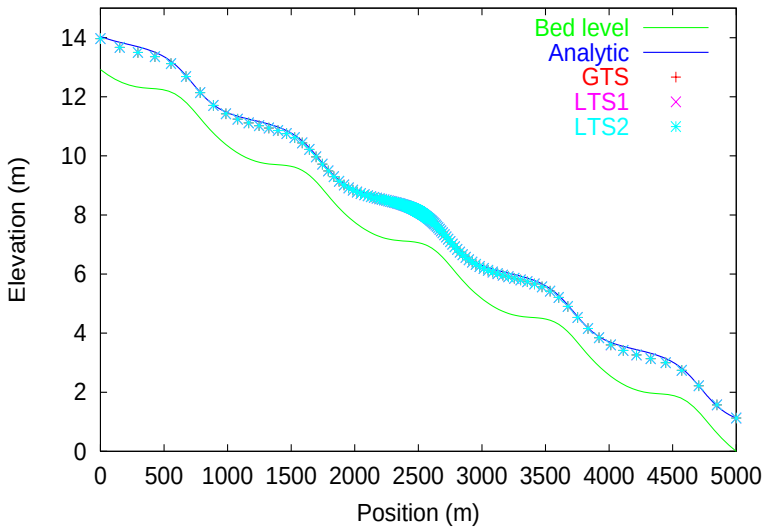

Figure 6.25: Elevation profile for S6 on 128 grid with pointwise source terms.

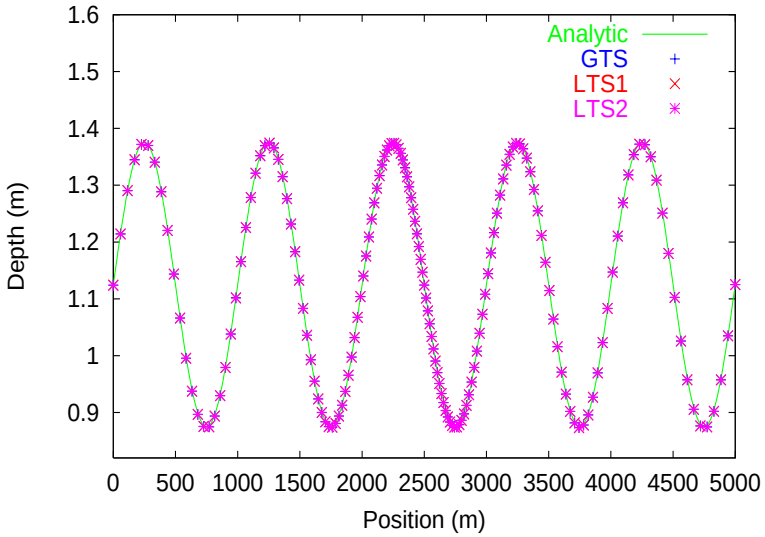

Figure 6.26: Depth profile for S6 on 4 grid with upwind source terms.

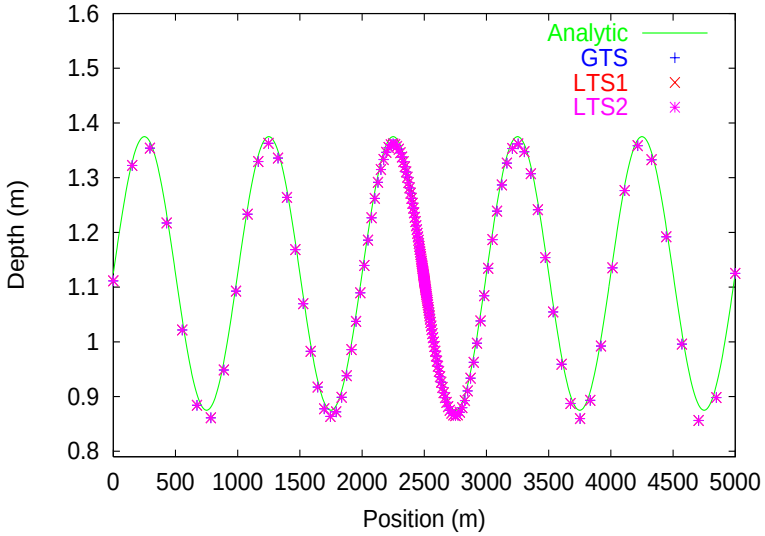

Figure 6.27: Depth profile for S6 on 128 grid with upwind source terms.

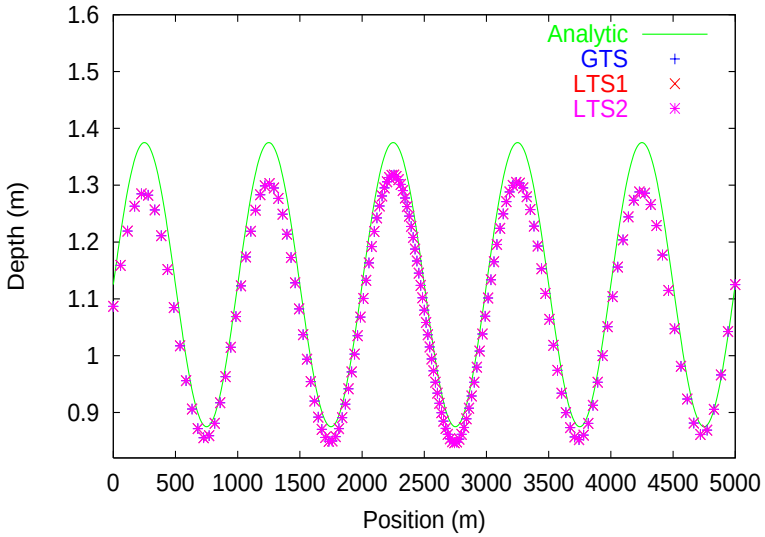

Figure 6.28: Depth profile for S6 on 4 grid with pointwise source terms.

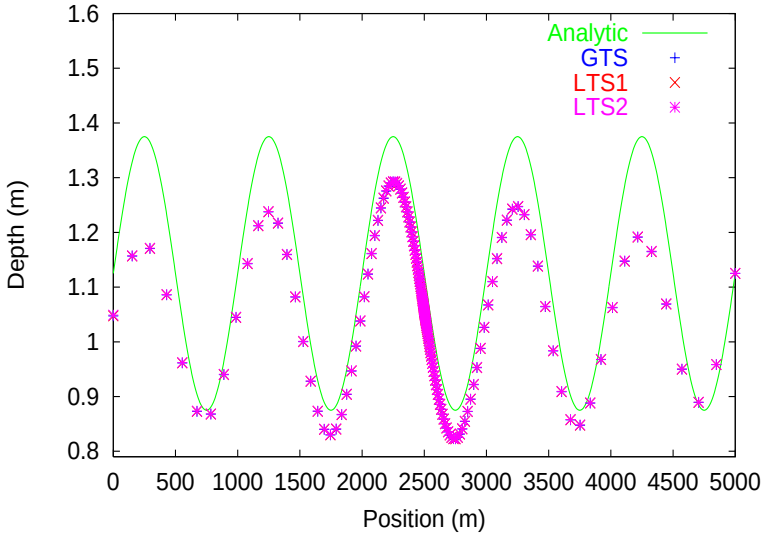

Figure 6.29: Depth profile for S6 on 128 grid with pointwise source terms.

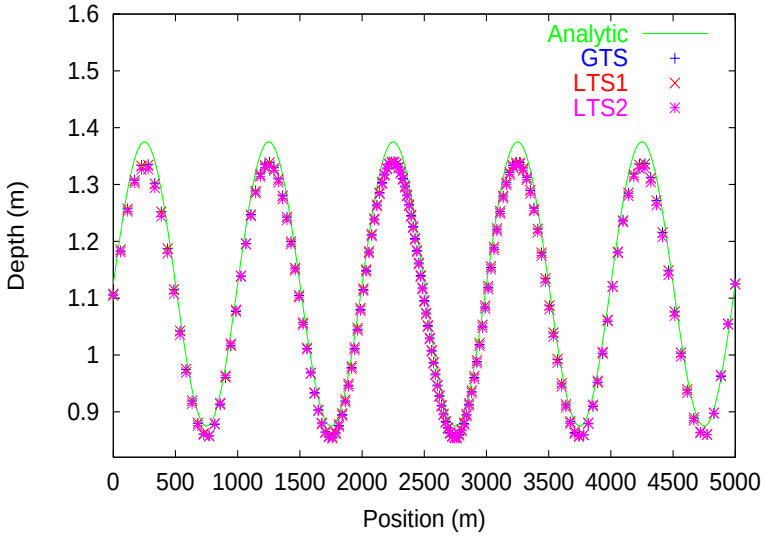

Figure 6.30: Depth profile for S6 on 4 grid with pointwise source terms and Superbee.

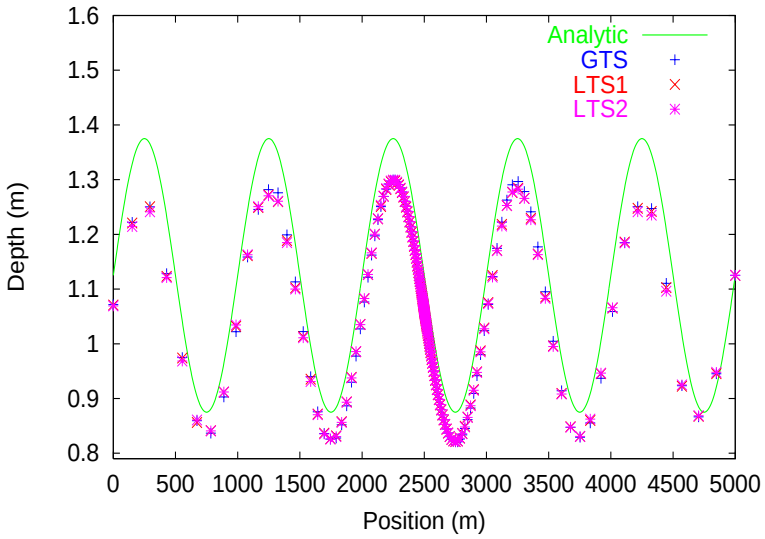

Figure 6.31: Depth profile for S6 on 128 grid with pointwise source terms and Superbee.

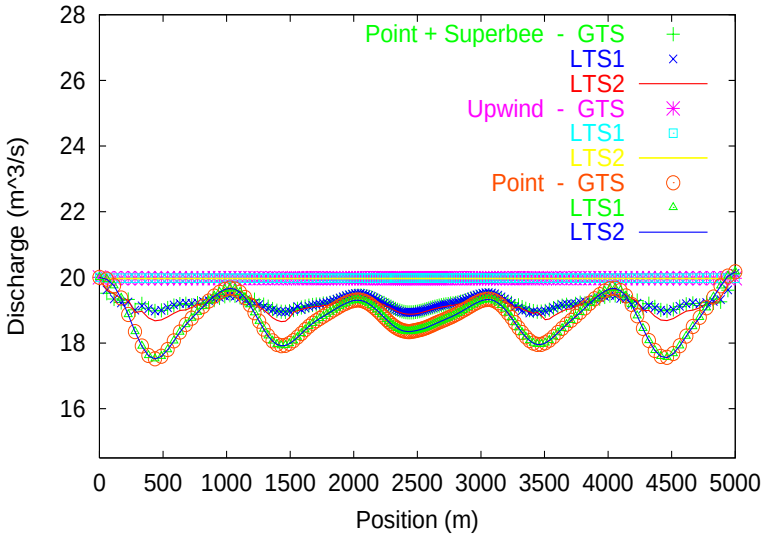

Figure 6.32: Discharge profiles for S6 on 4 grid.

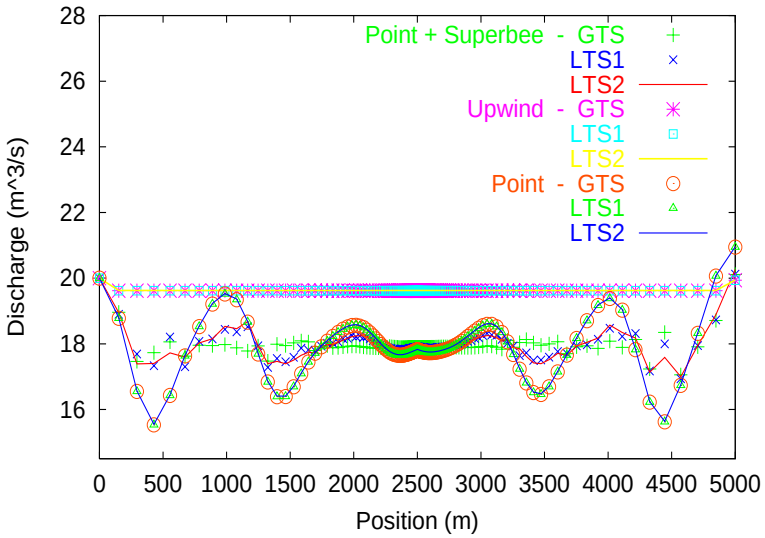

Figure 6.33: Discharge profiles for S6 on 128 grid.

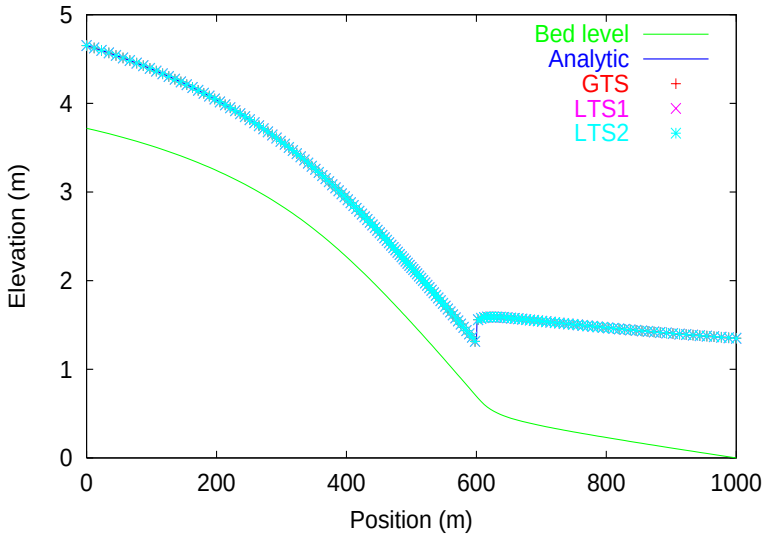

Figure 6.34: Elevation profile for S7 on 4 grid with upwind source terms.

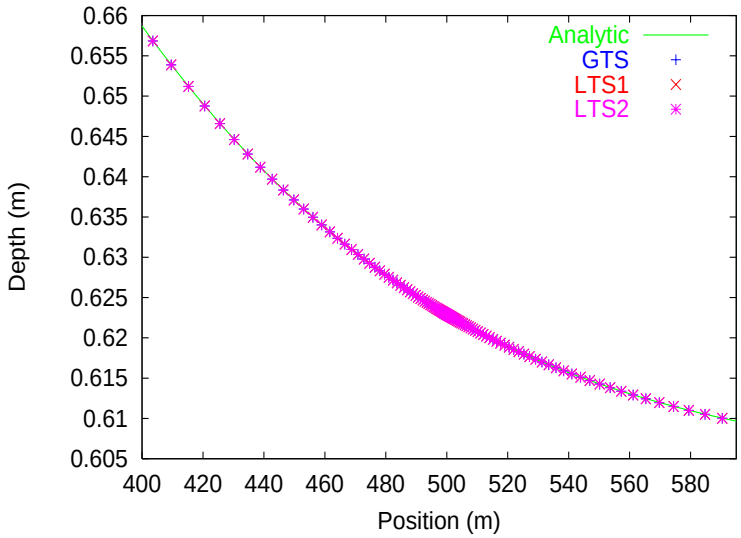

Figure 6.35: Depth profile for S7 on 128 grid with upwind source terms.

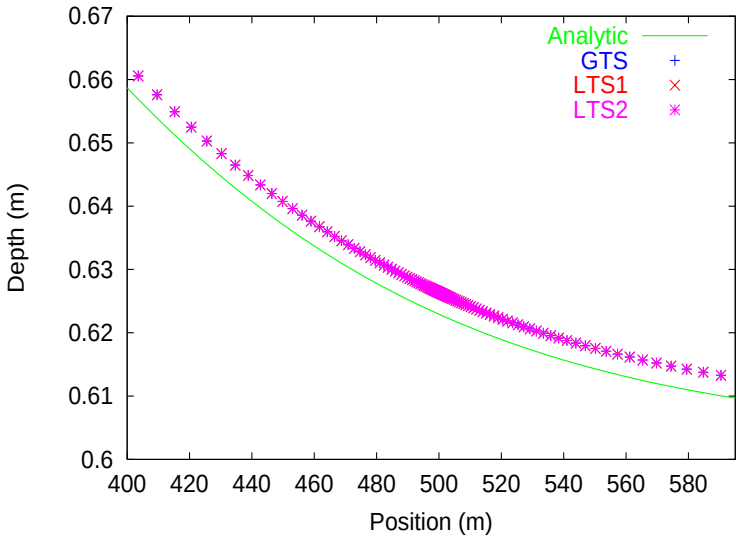

Figure 6.36: Depth profile for S7 on 128 grid with pointwise source terms.

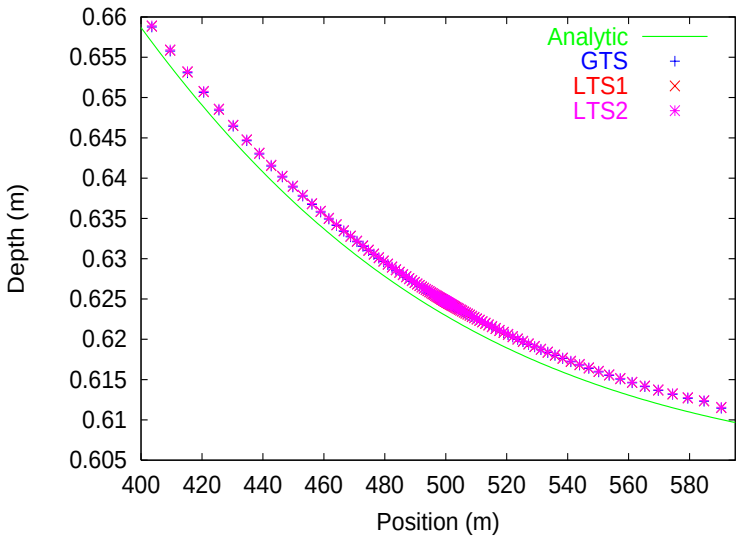

Figure 6.37: Depth profile for S7 on 128 grid with pointwise source terms and Superbee.

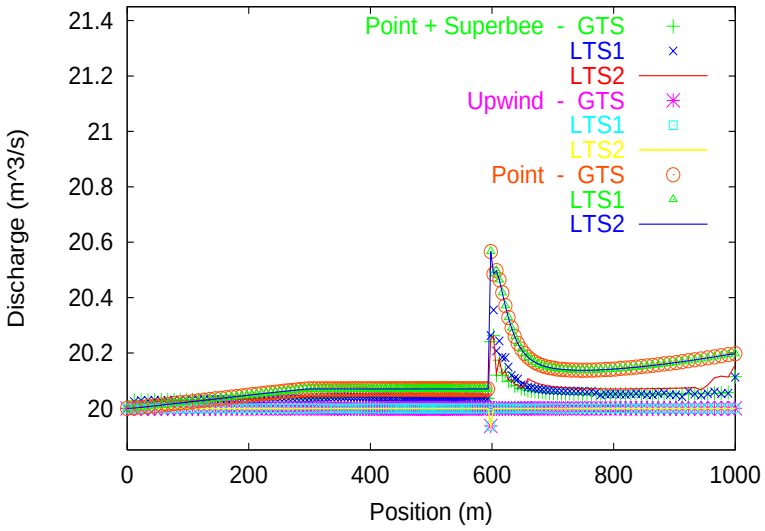

Figure 6.38: Discharge profiles for S7 on 4 grid.

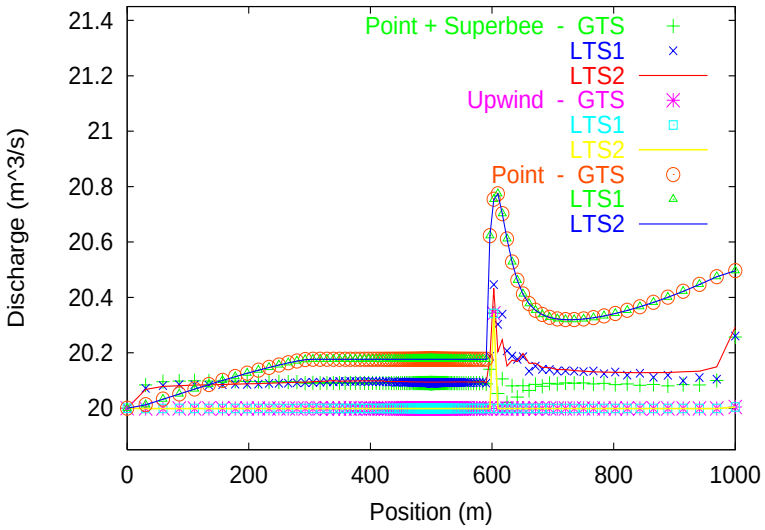

Figure 6.39: Discharge profiles for S7 on 128 grid.

6.3.2 Transient/Unsteady results

The first transient test case to be considered is the dam-break problem (**U1**). As there are no source terms involved in the calculations, the results using the first and second order versions of Roe's scheme with the various time stepping strategies can be compared. Figures 6.40 and 6.41 show the depth profiles obtained using the first order methods. It can be seen that there is some distinction between the results, particularly in the region of the bore and the beginning of the depression. Figures 6.42 and 6.43 show the first $200m$ of the channel on a larger scale. On the 4 grid, it can be seen that both the LTS approaches come slightly closer to predicting the correct depth value in the region where the depression meets the uniform state. Further on, there is a section where the GTS and LTS2 results almost agree, whilst the LTS1 values show more deviation from the analytic value. Towards the end of the region highlighted, the differences between the results becomes less noticeable. On the 128 grid, there is a marked improvement on the GTS results when the LTS1 algorithm is applied, with the LTS2 approach forming an intermediate solution. Figures 6.44 and 6.45 focus on the bore region, where in the previous chapter, the solution was seen to be improved by the use of local time stepping. On the 4 grid, the LTS1 and LTS2 results are comparable, with the LTS1 appearing slightly better due to a more uniform value in the constant region. There is a slight improvement in the resolution of the bore visible in the LTS results. The 128 grid profiles show the GTS and LTS2 results to be very similar, whilst the LTS1 solution captures the discontinuity much more sharply.

Figures 6.46 and 6.47 show the complete solution when the Superbee flux limiter is used. These figures suggest that the differences apparent before are now less noticeable. Figures 6.48 and 6.49 show the region at the beginning of the depression. In general a much closer agreement to the analytical solution is seen than with the first order results. On the 4 grid, the LTS2 results represent the best solution, with the GTS method producing only slightly different values. However the LTS1 results show a significant amount of diffusion and are only a slight improvement on the first order values. On the 128 grid, the GTS and LTS2 results are almost identical, and the LTS1 results are again quite diffusive. The solution profiles in the bore region are given in Figures 6.50 and 6.51. The distinction between the GTS and LTS results is less marked than with the first order solutions, and little improvement in the quality of the solution is seen in this case by using either of the LTS strategies. In fact both LTS solutions on the 4 grid show less agreement with the analytical solution than the GTS results. On the 128 grid the LTS1

results are overall slightly better.

The run time and flux count measurements are given in Table 6.2. The increase in computational cost of applying the flux limiter is immediately apparent from the higher run time values. For the regular grid (and the 2 grid for LTS1) , it can be seen that the run times for the LTS strategies exceed the GTS values, though there is a reduction in the number of flux calculations performed. As was apparent with the steady state measurements, the efficiency improvement observed increases with the largest to smallest cell grid ratio. For the LTS1 approach, the run time efficiency gains for the second order results, are generally higher than for the first order values. However the flux count efficiencies are much more comparable. The LTS2 values (both run time and flux count) are generally similar for the first and second order schemes on the same grid. As noted before, the run time efficiency gains of the LTS2 approach are significantly higher than for the LTS1 strategy. However the flux count efficiencies are slightly higher for LTS1. In this example, the range of efficiencies seen for the LTS2 results, are quite similar to the steady state values. The same is true for the second order LTS1 measurements, but the first order run time efficiencies are generally lower than those seen before.

The complete solutions for **U2** are shown in Figures 6.52 to 6.55. As no analytic solution is available for this problem, a reference solution produced on a fine regular grid is included in the plots. The behaviour for the first section of the channel is quite similar to that seen for the dam-break problem. The region of most interest in this case is focussed on in Figures 6.56 to 6.59. The first order LTS results on the 4 grid are slightly better than those produced using global time stepping. On the 128 grid, the LTS1 results show the closest match to the reference solution, with the GTS and LTS2 values appearing quite similar. The downstream discontinuity is captured more sharply than the upstream one by the LTS1 method. The second order results show much better resolution of the discontinuities and closer agreement to the reference solution. The GTS and LTS2 results appear much smoother than those produced by the LTS1 strategy and overall the GTS results are marginally the best. The trends evident in the run time and flux count data are the same as for the previous example, though the maximum efficiency gains for LTS2 are slightly less, as only a maximum of four temporal levels (m =2) are permitted.

Figures 6.60 to 6.63 show the solution profiles over the entire range for **U3**. Again a reference solution is included in the plots for comparison. The upstream and

downstream discontinuities are shown in greater detail in Figures 6.64 to 6.71. The first order results in the region of the first discontinuity on the 4 grid appear very similar, whilst there is a greater distinction between the values on the 128 grid, where the LTS1 depth predictions generally lie closest to the reference values. On the 4 grid, applying the Superbee flux limiter improves the quality of all of the solutions, which are again very similar. However on the 128 grid both LTS algorithms experience difficulty in producing a smooth profile in the region to the right of the discontinuity. Looking at the downstream discontinuity, on the 4 grid the LTS1 results show the best shock resolution, with the LTS2 algorithm producing a slightly sharper profile than global time stepping. The GTS and LTS2 results on the 128 grid are very similar, and again the LTS1 approach is seen to resolve the discontinuity in fewer cells. The results in Figure 6.70 in which the flux limiter is used on the 4 grid, are all very similar, with the LTS1 values appearing to be not quite constant in the region upstream of the shock. The effect is more apparent on the 128 grid, and does not appear to afflict the LTS2 solution. The efficiency measurements show the same trends as the previous two examples, with the additional feature of a drop in all of the efficiency values between the 1 and 2 grids (see Table 6.3). This was observed for the run time efficiencies for the steady state problems, but not for the flux count values. However it should be noted that the flux count efficiencies all remain positive.

Example **U4** has a non-uniform bed and so includes the effects of source terms. Figures 6.72 to 6.75 show the complete profiles using the upwind and pointwise plus Superbee treatments on the 4 and 128 grids. For this problem the upwind and pointwise results are indistinguishable. The bore region is shown in more detail in Figures 6.76 to 6.79. The first order upwind LTS1 results on both the 4 and 128 grids capture the shock more sharply than the other methods, with the LTS2 values being slightly better than the GTS results. However when the flux limiter is used in conjunction with the pointwise source terms (note the source terms are zero in this section of the channel), the LTS1 results show some anomalous behaviour. On the 128 grid this can also be observed in the central region of the channel in Figure 6.75. In terms of shock resolution, the results from the different time stepping approaches are all comparable. The measured data again shows the drop in efficiencies between the 1 and 2 grid, together with the other trends previously observed. The efficiency gains are quite similar to those recorded with the steady state examples, and maximum level utilised by the LTS2 algorithm is 5, which is more in line with the steady results than with the unsteady problems that do not contain source terms.

The complete solutions obtained for problem **U5** using the various techniques are shown in Figures 6.80 to 6.85. The reference solution on each plot corresponds to the results produced using the same source term treatment as the results illustrated, together with global time stepping on a fine regular grid. These figures show a contrast in the reference solutions, with only the upwind solutions appearing similar to the profile presented by Savic and Holly [54]. This example represents an extreme test case in the sense of the sudden channel contraction which is implemented over one cell at $55km$, corresponding to where the pointwise and pointwise plus Superbee results experience difficulty. By extending the region over which the contraction takes place, more sensible solution profiles are produced, and the geometry becomes more in line with the Saint Venant hypothesis. However it is interesting to see how the upwind source term treatment is able to cope with these conditions, with the solutions generated from the the differing time stepping methods appearing quite similar. In producing these results it became apparent that the LTS1 algorithm needed some modification in order to obtain stable solutions, and this resulted in the need to limit the number of local time steps which could be performed over a global time step. The limits applied are noted in the recorded data in Table 6.4 and generally increase with the grid ratio. This approach was found to be the most successful and extending the interface region was found not to eliminate the problem. Looking at the upwind results, drops in the limit and maximum levels (and subsequently reduced efficiencies) can be seen for both LTS algorithms, though the gains do remain positive.

In example **U6**, the channel contraction is replaced by an expansion, with the result that all of the source term methods produce viable solutions. Over the complete range the profiles appear similar, and the upwind results on the two grids are shown in Figures 6.86 and 6.87. The region affected by the contraction is highlighted in Figures 6.88 to 6.93 and again the reference solution tallies with the methods used to generate the results illustrated. In comparing the solutions, it can be seen the pointwise results show a greater deviation from the reference solution than do the upwind values. Introducing the flux limiter brings the pointwise values closer to the reference line, as well as sharpening the profile. In this example the application of the LTS procedures does not appear to increase the accuracy of the solution, though this is difficult to judge in the absence of an analytical solution. For some cells in the 65 to 70 km region, the LTS results differ slightly from the GTS values. The LTS1 method again requires a limit to be placed on the number of local time steps per global cycle, with the limit tending to be higher for the

upwind results. The decrease in the limit and level apparent in the previous example for the higher ratio grids, is not present in this case. The general trends evident so far in the tabulated data for in all of the problems are again visible in this example.

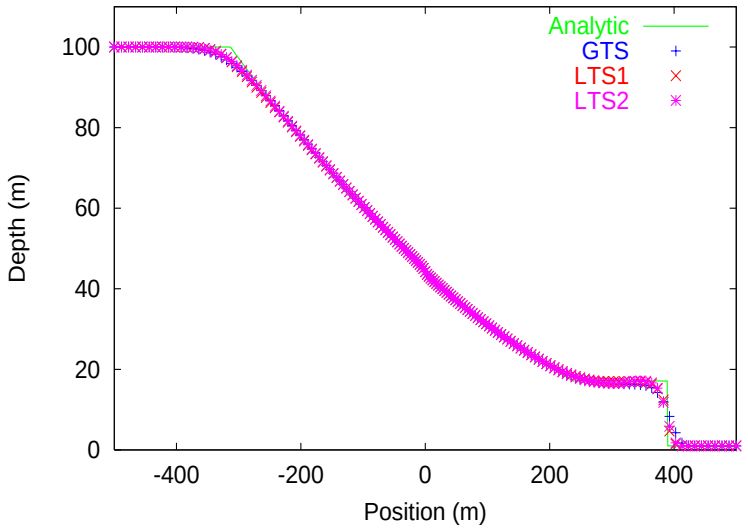

Figure 6.40: Depth profile for U1 on 4 grid using the 1st order schemes.

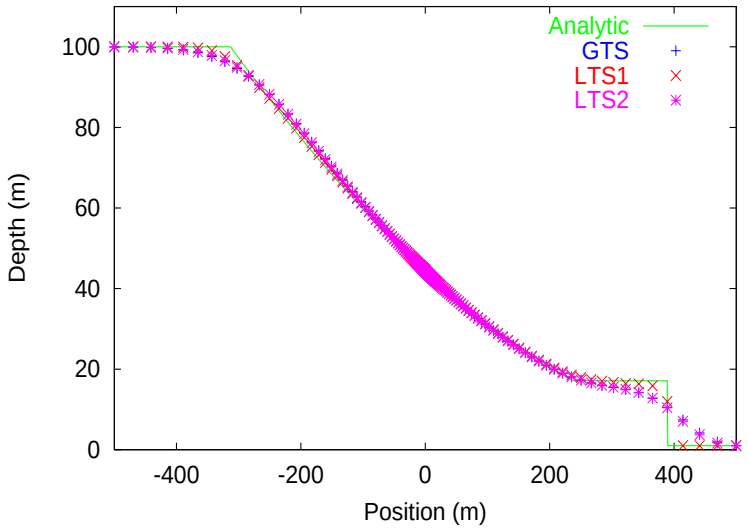

Figure 6.41: Depth profile for U1 on 128 grid using the 1st order schemes.

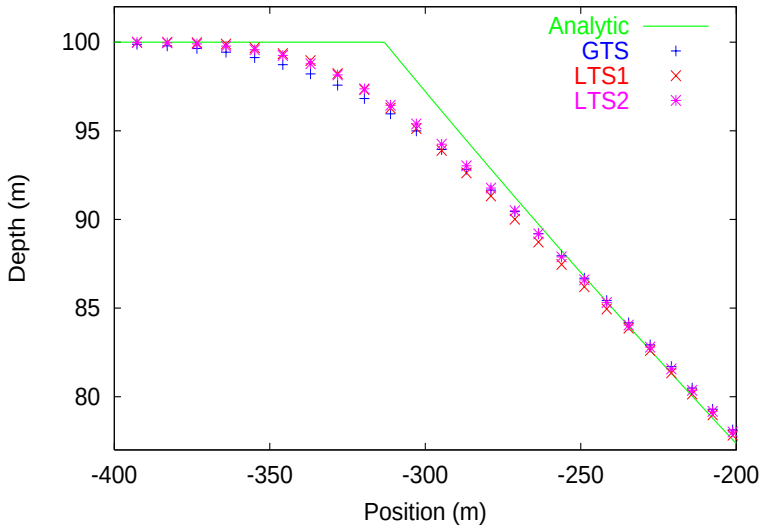

Figure 6.42: Depth profile for U1 on 4 grid using the 1st order schemes.

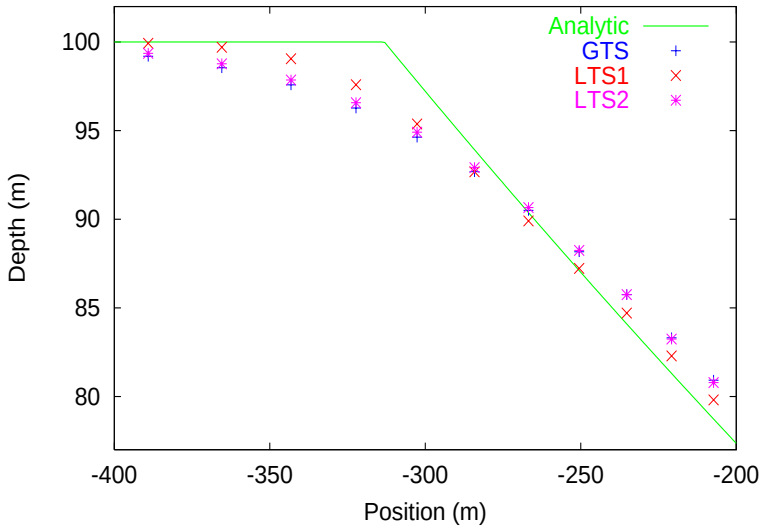

Figure 6.43: Depth profile for U1 on 128 grid using the 1st order schemes.

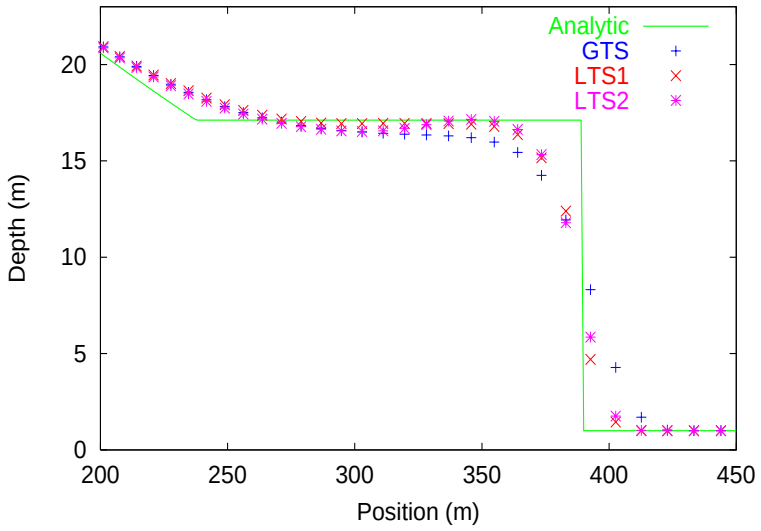

Figure 6.44: Depth profile for U1 on 4 grid using the 1st order schemes.

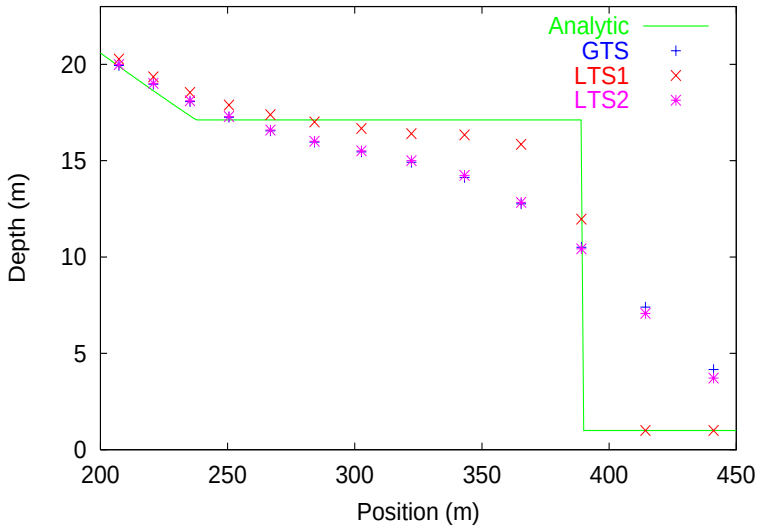

Figure 6.45: Depth profile for U1 on 128 grid using the 1st order schemes

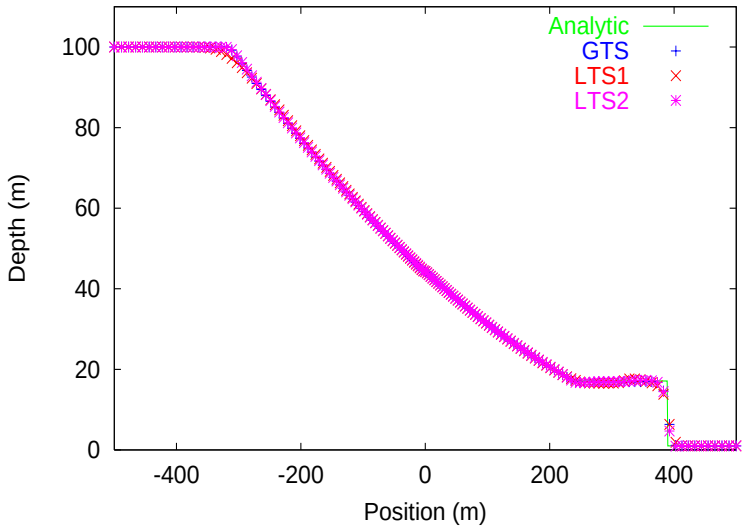

Figure 6.46: Depth profile for U1 on 4 grid using the 2nd order schemes.

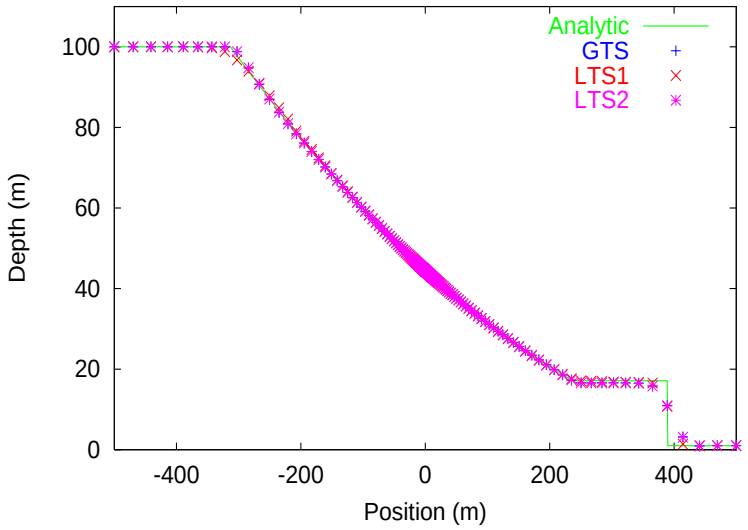

Figure 6.47: Depth profile for U1 on 128 grid using the 2nd order schemes.

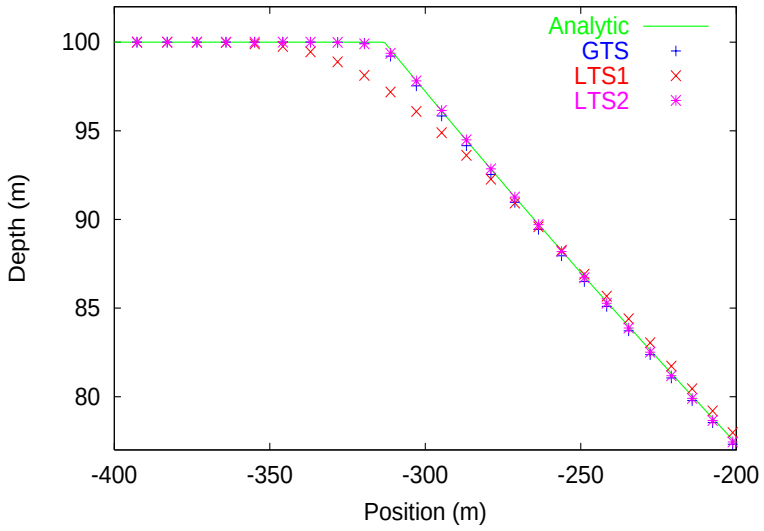

Figure 6.48: Depth profile for U1 on 4 grid using the 2nd order schemes.

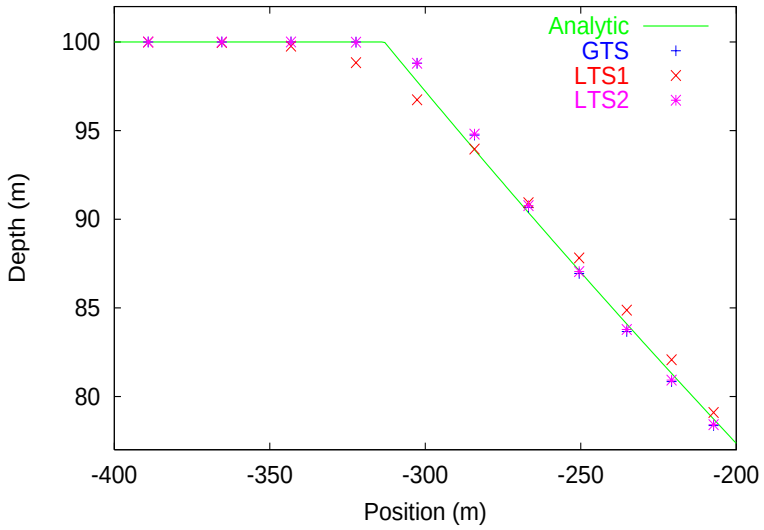

Figure 6.49: Depth profile for U1 on 128 grid using the 2nd order schemes.

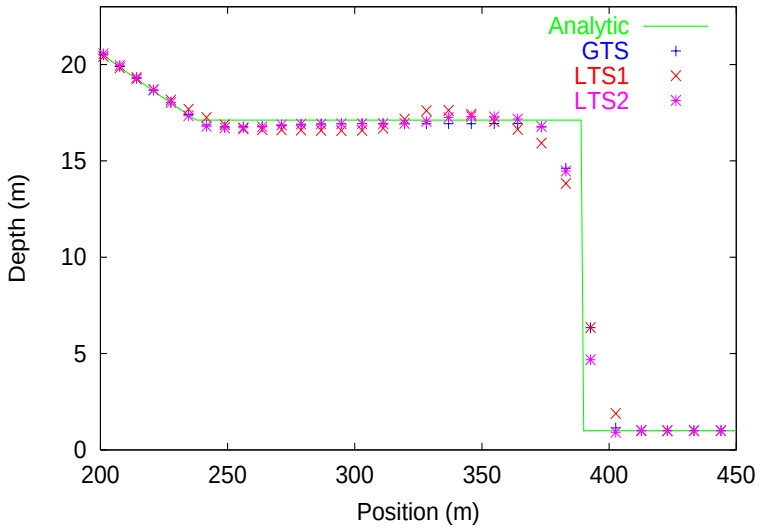

Figure 6.50: Depth profile for U1 on 4 grid using the 2nd order schemes.

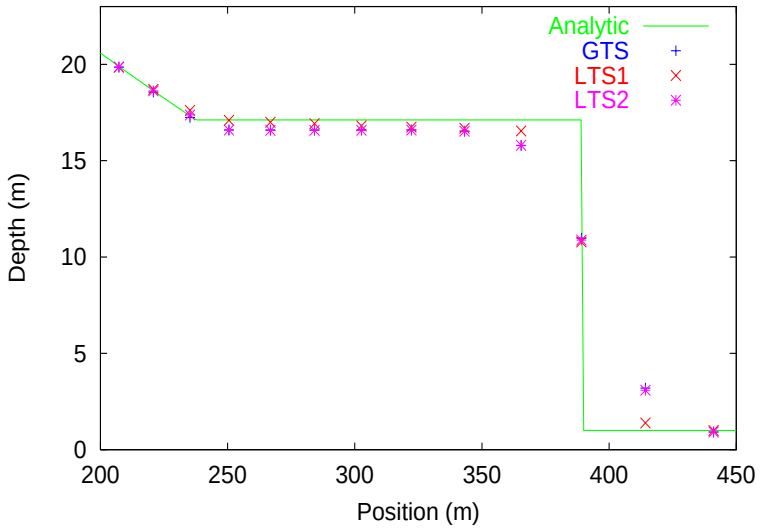

Figure 6.51: Depth profile for U1 on 128 grid using the 2nd order schemes.

Problem	Scheme	Grid	GTS		LTS1				LTS2				
			Time (s)	Count	Time (s)	Gain	Count	Gain	Level	Time (s)	Gain	Count	Gain
U1	1st order	1	0.02141	13120	0.02274	-6.21	9666	26.33	2	0.02164	-1.07	10390	20.81
		2	0.02653	16480	0.02729	-2.86	10949	33.56	2	0.02563	3.39	12158	26.23
		4	0.03874	24640	0.03829	1.16	14734	40.20	2	0.03456	10.79	16390	33.48
		8	0.05838	37760	0.05533	5.22	19679	47.88	3	0.04521	22.56	21750	42.40
		16	0.09333	61120	0.08486	9.08	27714	54.66	2	0.07086	24.08	32770	46.38
		32	0.1529	100960	0.1342	12.23	40537	59.85	2	0.1096	28.32	50127	50.35
		64	0.2580	171200	0.2204	14.57	61809	63.90	3	0.1518	41.16	70354	58.91
		128	0.4450	296160	0.3694	16.99	95521	67.75	3	0.2459	44.74	112606	61.98
	2nd order	1	0.03479	13776	0.03687	-5.98	9998	27.42	2	0.03604	-3.59	10926	20.69
		2	0.04320	17220	0.04372	-1.20	11615	32.55	2	0.04136	4.26	12437	27.78
		4	0.06264	25256	0.06024	3.83	15632	38.11	2	0.05562	11.21	16720	33.80
		8	0.09561	38868	0.08661	9.41	21522	44.63	2	0.07701	19.45	23059	40.67
		16	0.1533	62648	0.1284	16.24	29982	52.14	2	0.1126	26.55	33531	46.48
		32	0.2527	103648	0.1986	21.41	44144	57.41	2	0.1731	31.50	51360	50.45
		64	0.4276	175644	0.3181	25.61	67228	61.72	2	0.2774	35.13	82019	53.30
		128	0.7401	304226	0.5232	29.31	105180	65.43	3	0.3975	46.29	115557	62.02

Table 6.2: Results table for U1.

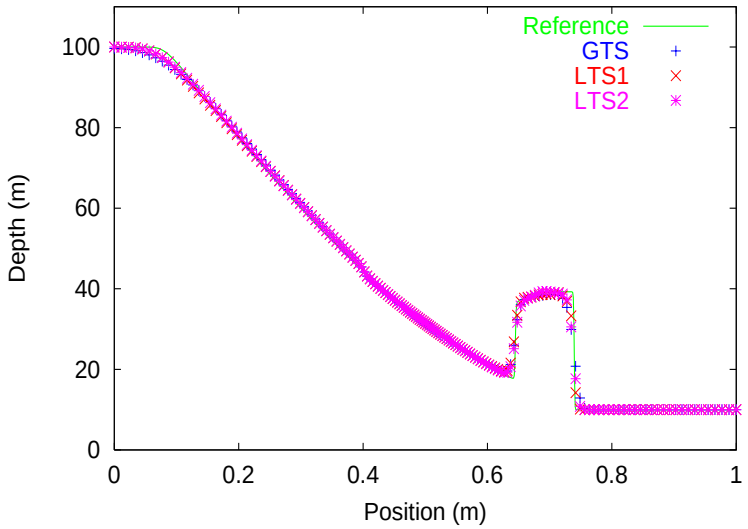

Figure 6.52: Depth profile for U2 on 4 grid using the 1st order schemes.

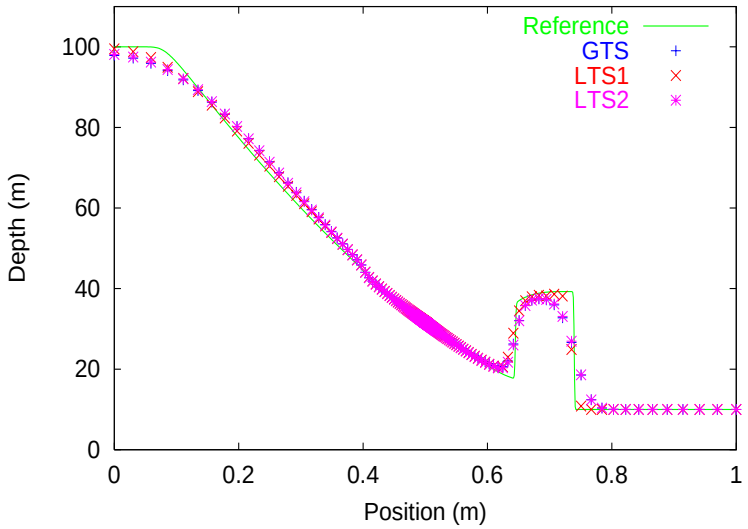

Figure 6.53: Depth profile for U2 on 128 grid using the 1st order schemes.

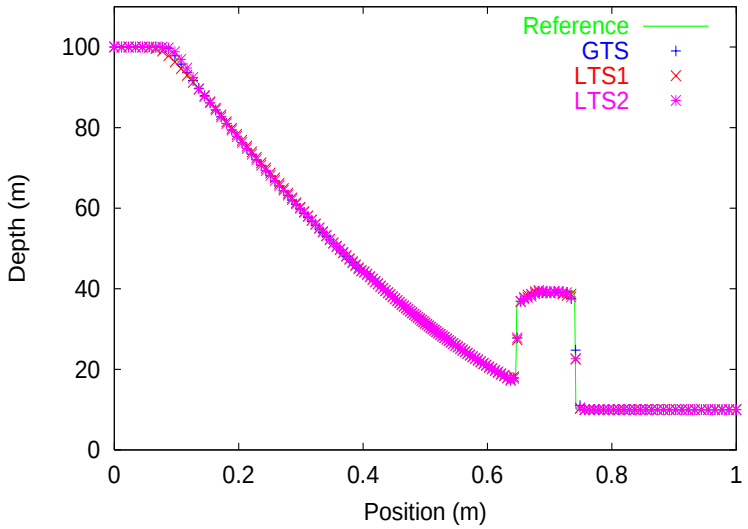

Figure 6.54: Depth profile for U2 on 4 grid using the 2nd order schemes.

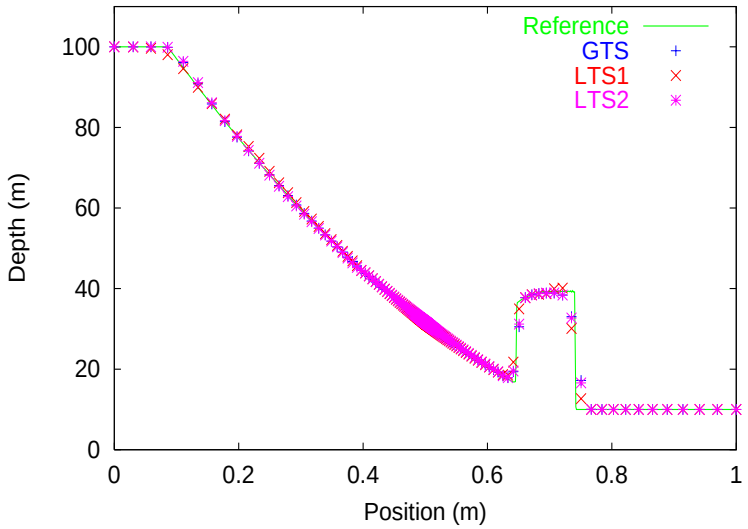

Figure 6.55: Depth profile for U2 on 128 grid using the 2nd order schemes.

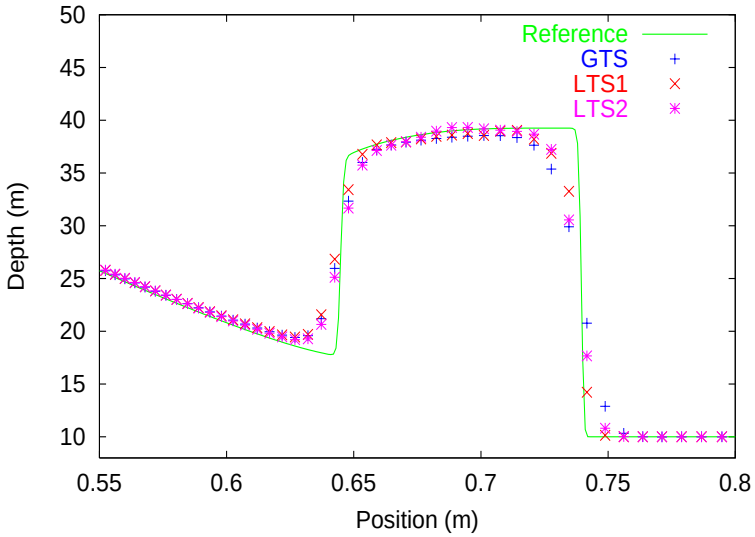

Figure 6.56: Depth profile for U2 on 4 grid using the 1st order schemes.

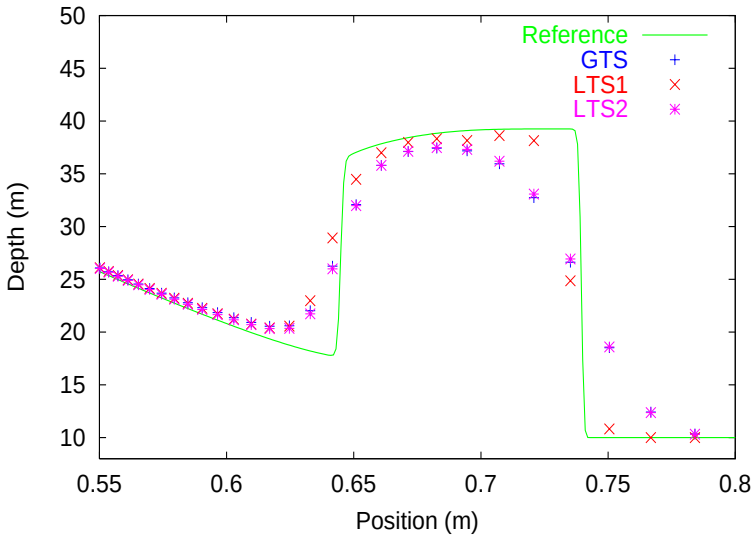

Figure 6.57: Depth profile for U2 on 128 grid using the 1st order schemes.

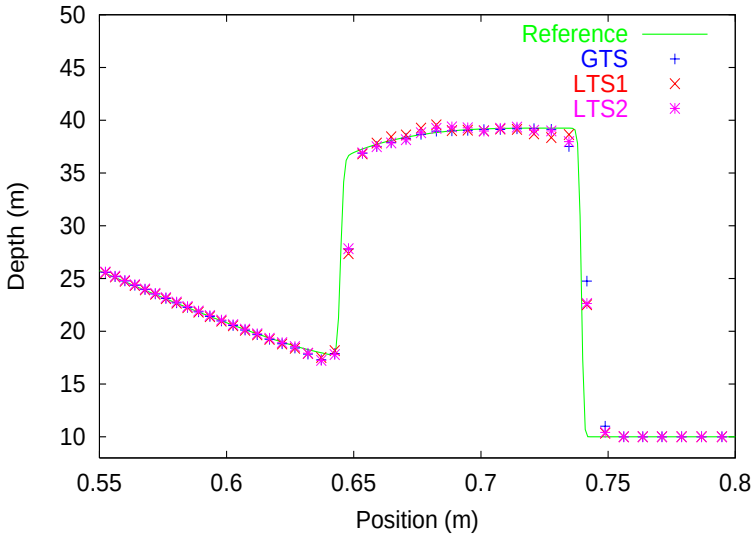

Figure 6.58: Depth profile for U2 on 4 grid using the 2nd order schemes.

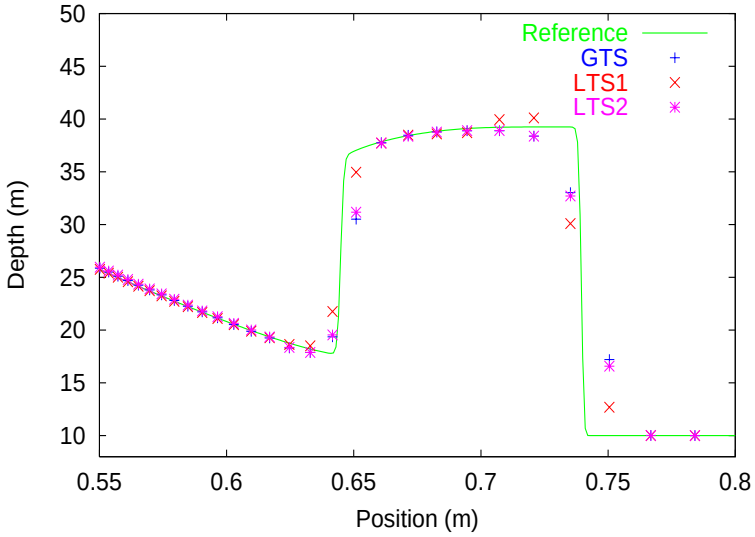

Figure 6.59: Depth profile for U2 on 128 grid using the 2nd order schemes.

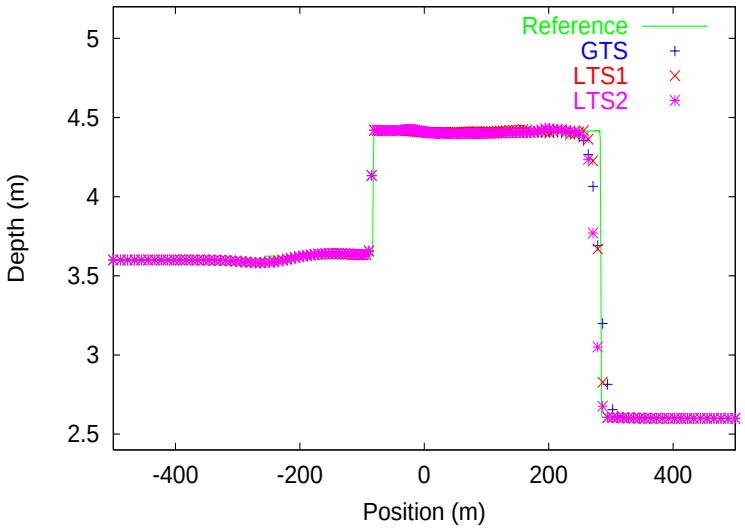

Figure 6.60: Depth profile for U3 on 4 grid using the 1st order schemes.

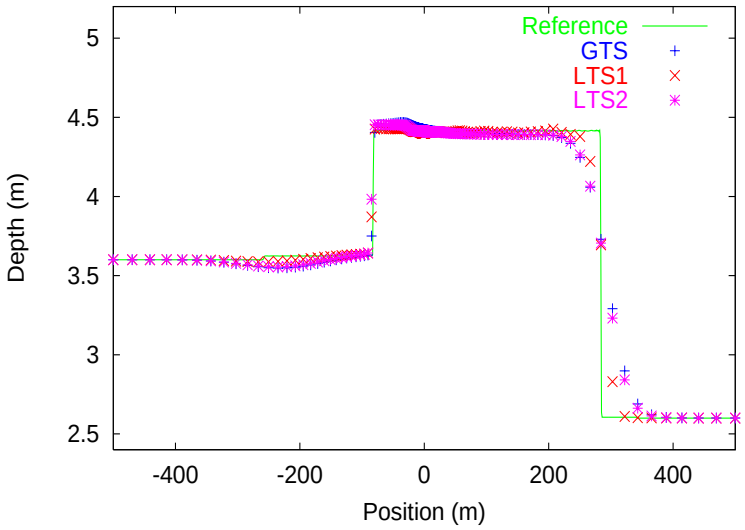

Figure 6.61: Depth profile for U3 on 128 grid using the 1st order schemes.

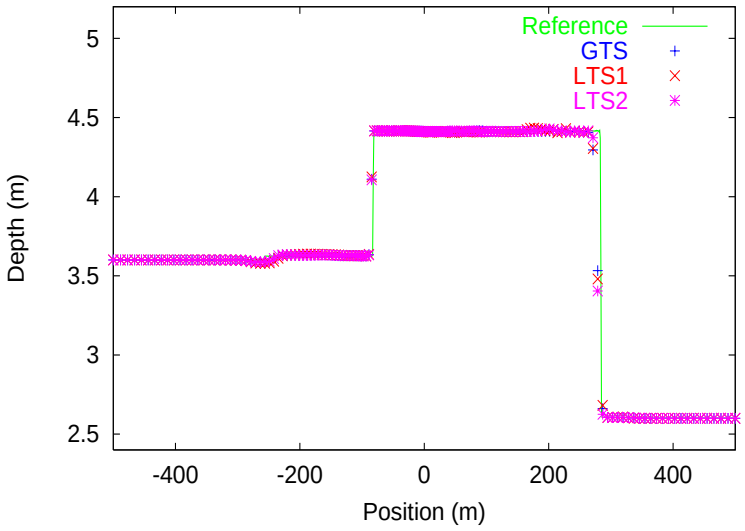

Figure 6.62: Depth profile for U3 on 4 grid using the 2nd order schemes.

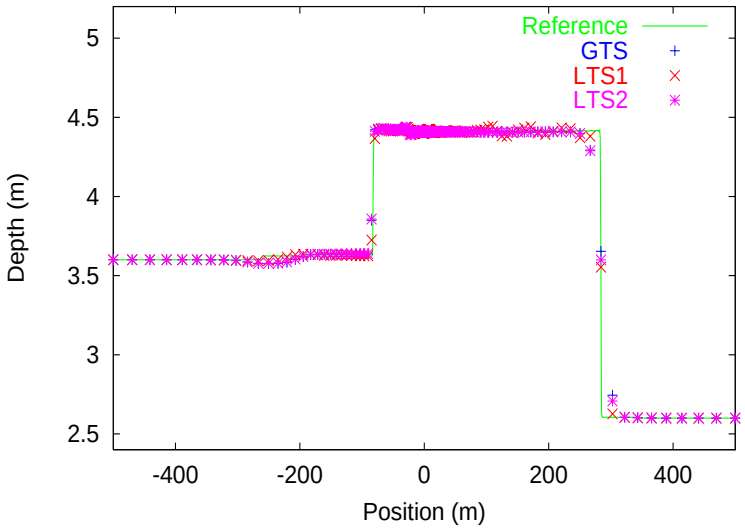

Figure 6.63: Depth profile for U3 on 128 grid using the 2nd order schemes.

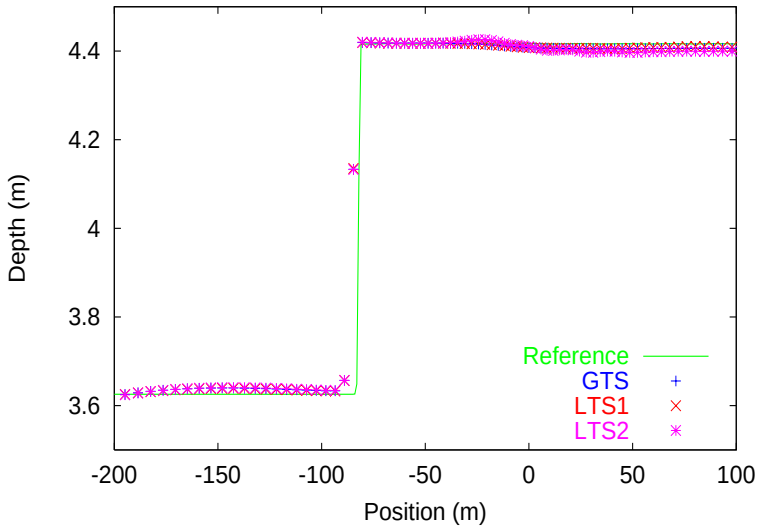

Figure 6.64: Depth profile for U3 on 4 grid using the 1st order schemes.

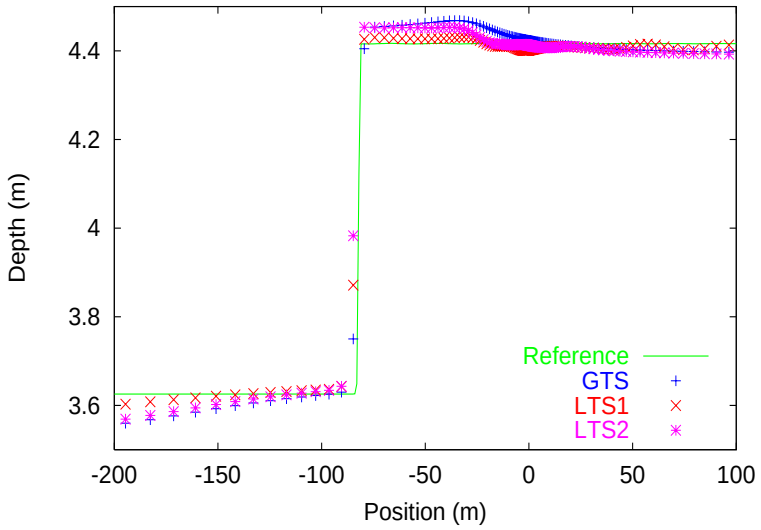

Figure 6.65: Depth profile for U3 on 128 grid using the 1st order schemes.

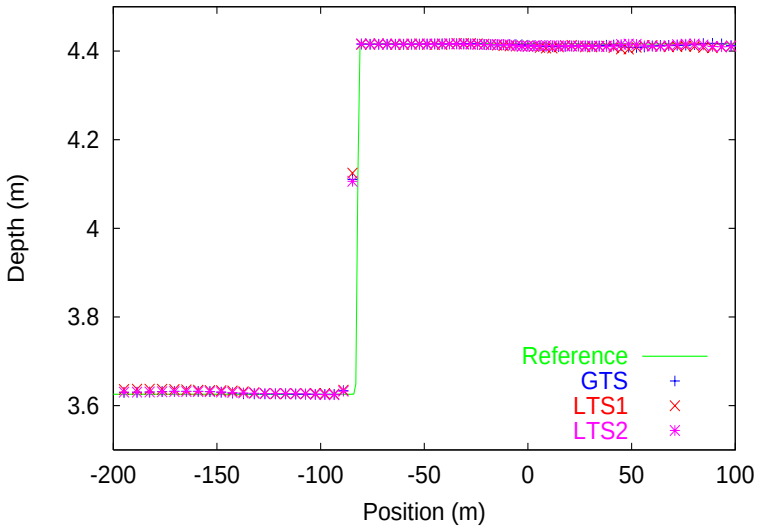

Figure 6.66: Depth profile for U3 on 4 grid using the 2nd order schemes.

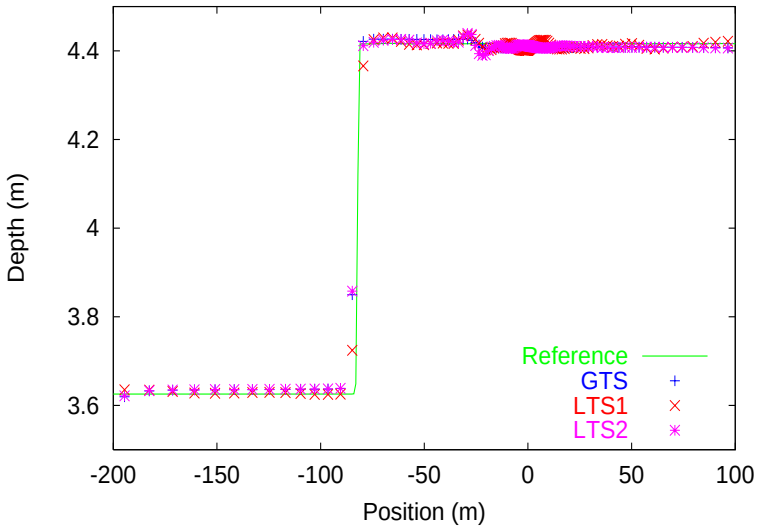

Figure 6.67: Depth profile for U3 on 128 grid using the 2nd order schemes.

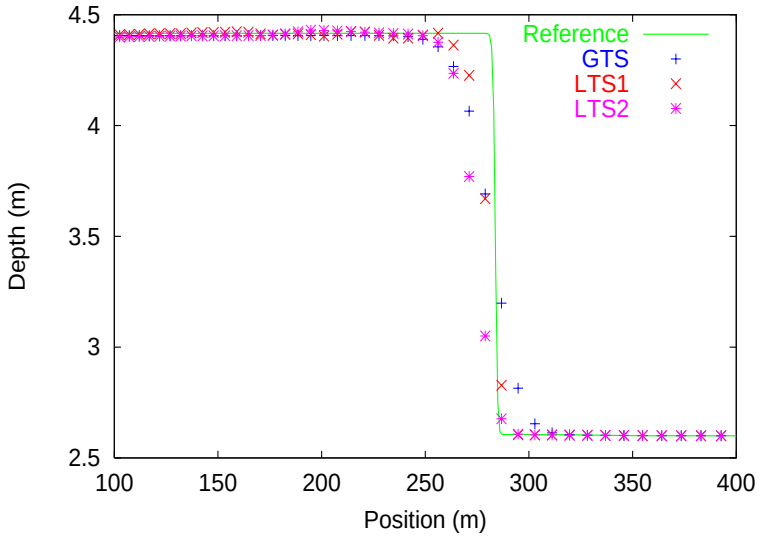

Figure 6.68: Depth profile for U3 on 4 grid using the 1st order schemes.

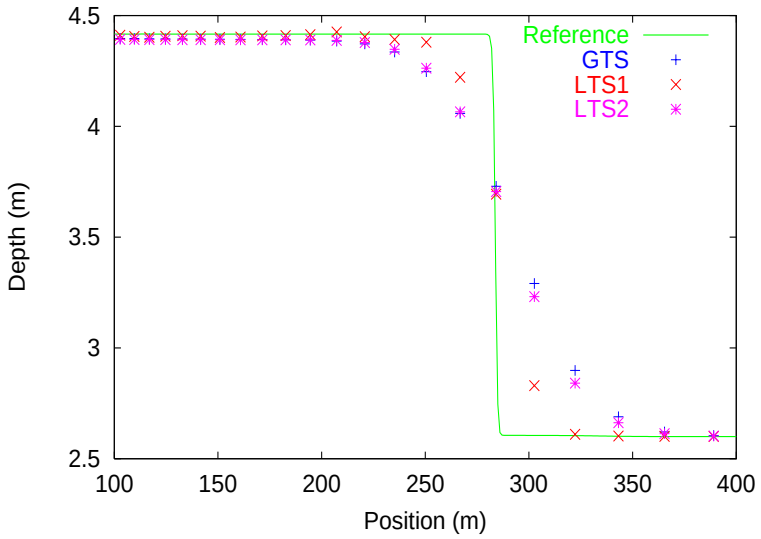

Figure 6.69: Depth profile for U3 on 128 grid using the 1st order schemes.

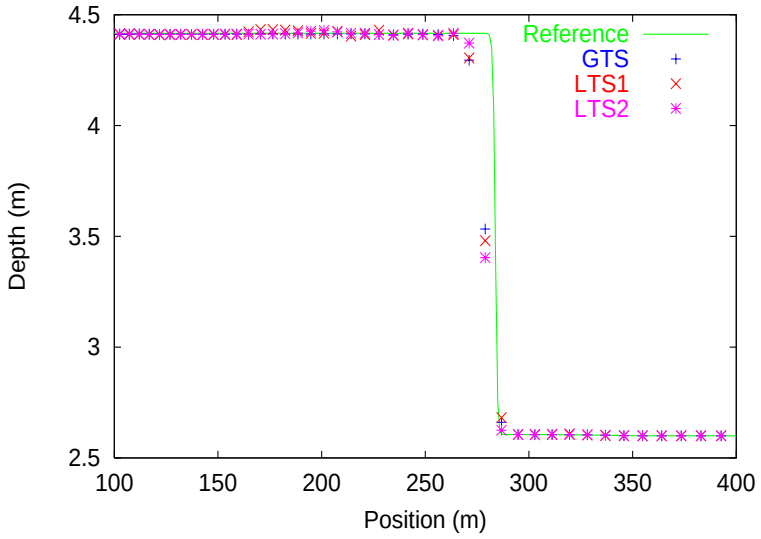

Figure 6.70: Depth profile for U3 on 4 grid using the 2nd order schemes.

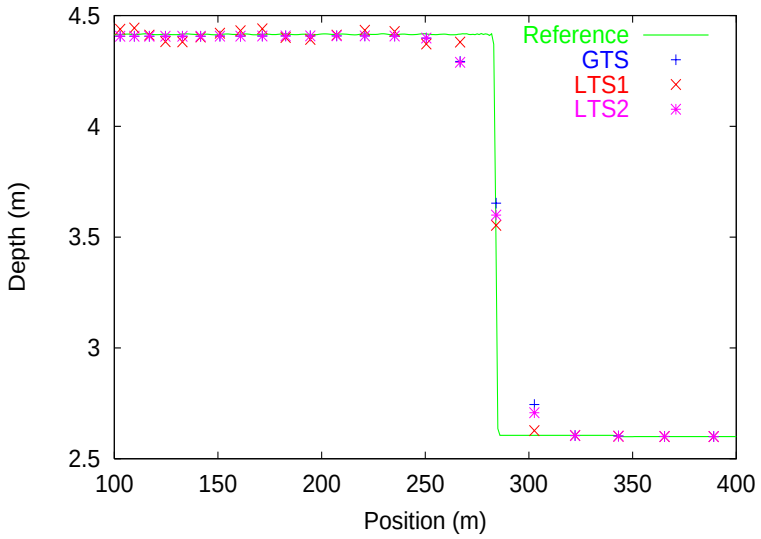

Figure 6.71: Depth profile for U3 on 128 grid using the 2nd order schemes.

Problem	Scheme	Grid	GTS		LTS1				LTS2				
			Time (s)	Count	Time (s)	Gain	Count	Gain	Level	Time (s)	Gain	Count	Gain
U3	1st order	1	0.04141	25760	0.04012	3.12	19014	26.19	1	0.04351	-5.07	19203	25.45
		2	0.04620	28819	0.04738	-2.55	23371	18.90	2	0.04920	-6.49	22958	20.34
		4	0.05884	37030	0.06050	-2.82	27896	24.67	3	0.05768	1.97	27227	26.47
		8	0.08364	53130	0.08229	1.61	34156	35.71	3	0.07223	13.64	33514	36.92
		16	0.1305	83559	0.1219	6.59	43973	47.37	3	0.09811	24.82	44782	46.41
		32	0.2123	136689	0.1903	10.36	61626	54.92	3	0.1420	33.11	63700	53.40
		64	0.3551	229425	0.3059	13.86	87931	61.67	3	0.2163	39.09	95553	58.35
		128	0.6239	403949	0.5191	16.80	133882	66.86	3	0.3517	43.63	153161	62.08
	2nd order	1	0.06612	26240	0.06139	7.15	19219	26.76	1	0.06534	1.18	19564	25.44
		2	0.07444	29520	0.07549	-1.41	24566	16.78	2	0.07854	-5.51	23451	20.56
		4	0.09527	37884	0.09723	-2.06	28432	24.95	2	0.09471	0.59	28148	25.70
		8	0.1360	54284	0.1297	4.63	35667	34.30	3	0.1184	12.94	34560	36.33
		16	0.2128	85280	0.1873	11.98	46057	45.99	3	0.1588	25.38	45868	46.21
		32	0.3470	139400	0.2840	18.16	66367	52.39	3	0.2289	34.03	65831	52.78
		64	0.5802	233372	0.4417	23.87	96259	58.75	3	0.3437	40.76	98275	57.89
		128	1.017	409508	0.7304	28.18	149326	63.54	3	0.5557	45.36	158217	61.36

Table 6.3: Results table for U3.

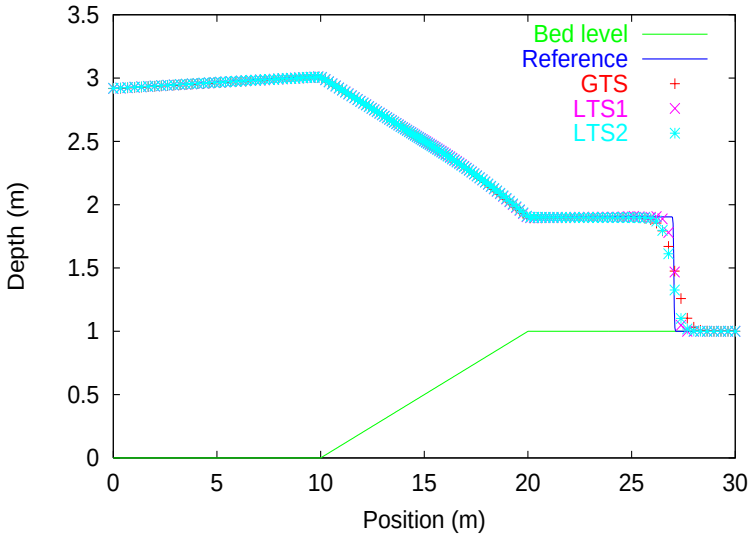

Figure 6.72: Depth profile for U4 on 4 grid with upwind source terms.

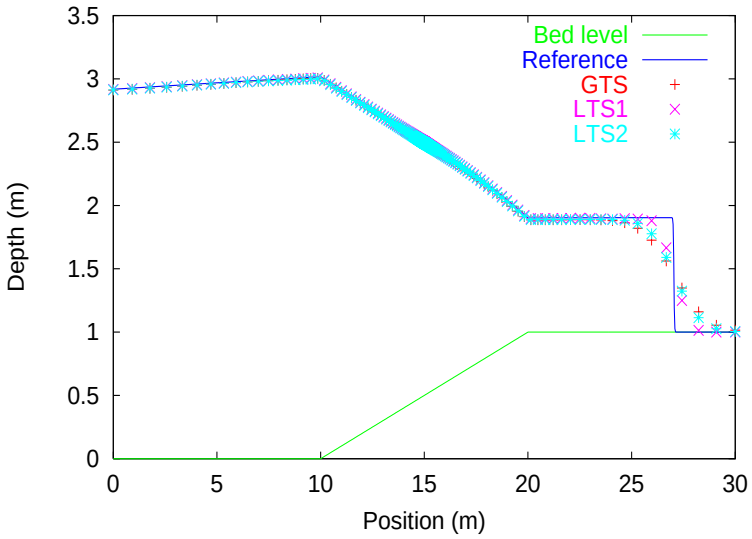

Figure 6.73: Depth profile for U4 on 128 grid with upwind source terms.

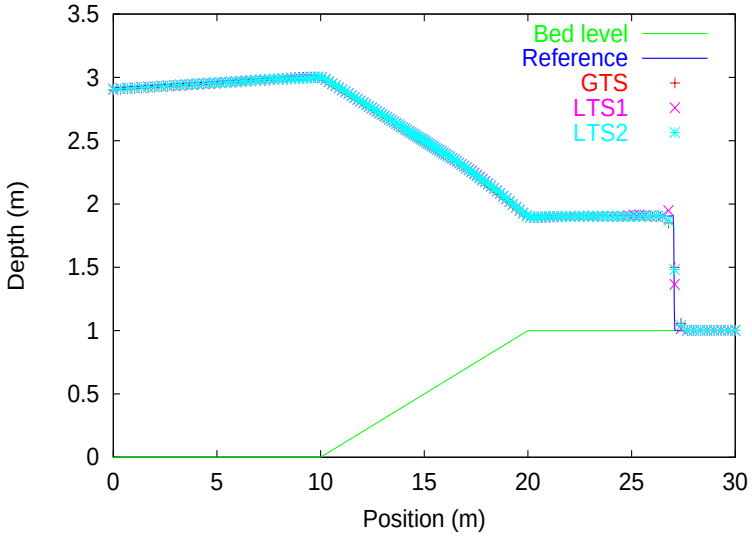

Figure 6.74: Depth profile for U4 on 4 grid with pointwise source terms and Superbee.

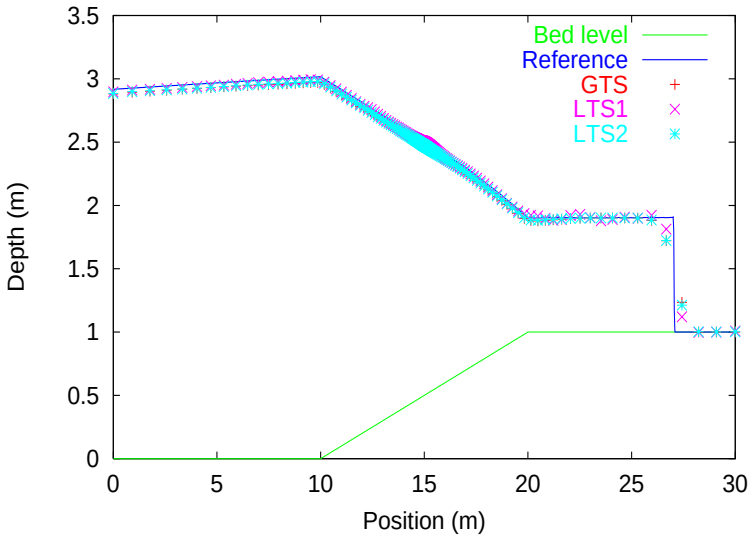

Figure 6.75: Depth profile for U4 on 128 grid with pointwise source terms and Superbee.

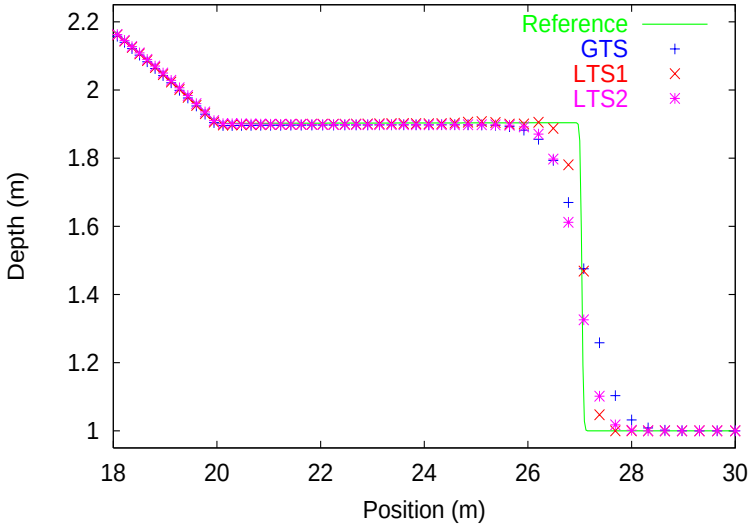

Figure 6.76: Depth profile for U4 on 4 grid with upwind source terms.

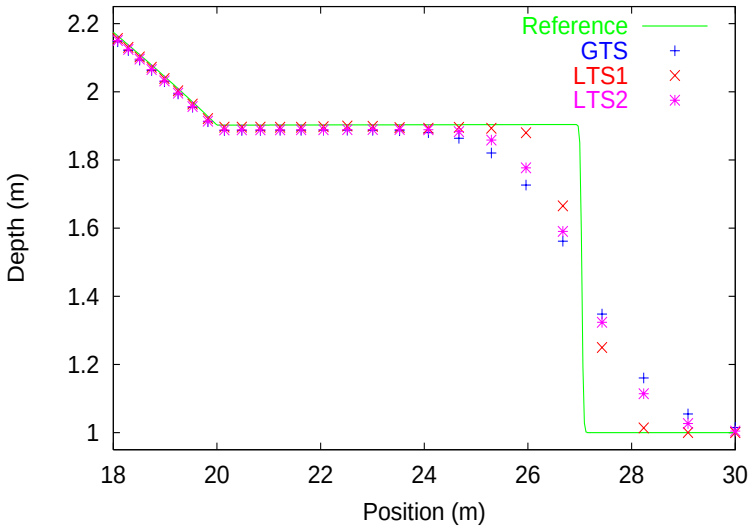

Figure 6.77: Depth profile for U4 on 128 grid with upwind source terms.

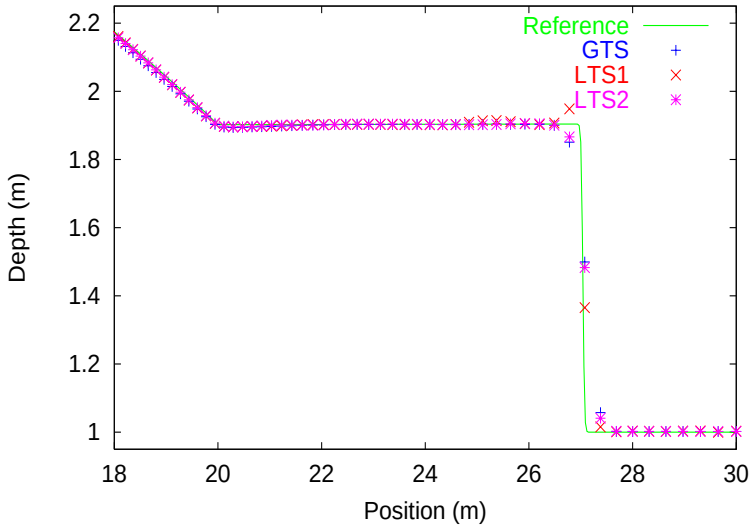

Figure 6.78: Depth profile for U4 on 4 grid with pointwise source terms and Superbee.

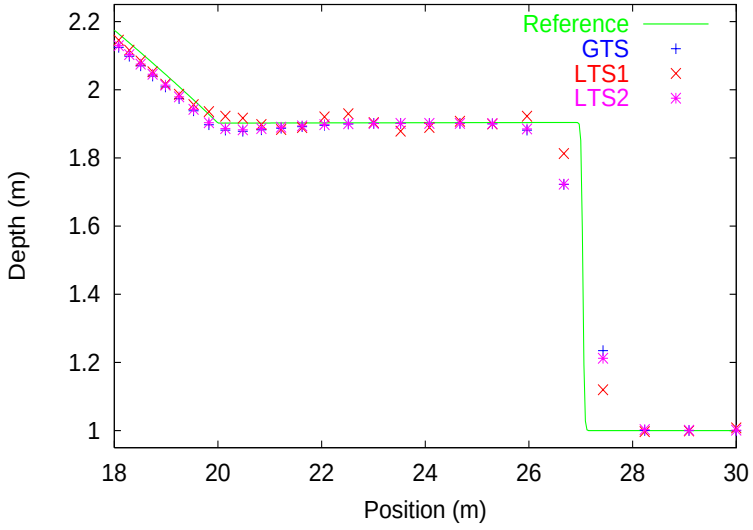

Figure 6.79: Depth profile for U4 on 128 grid with pointwise source terms and Superbee.

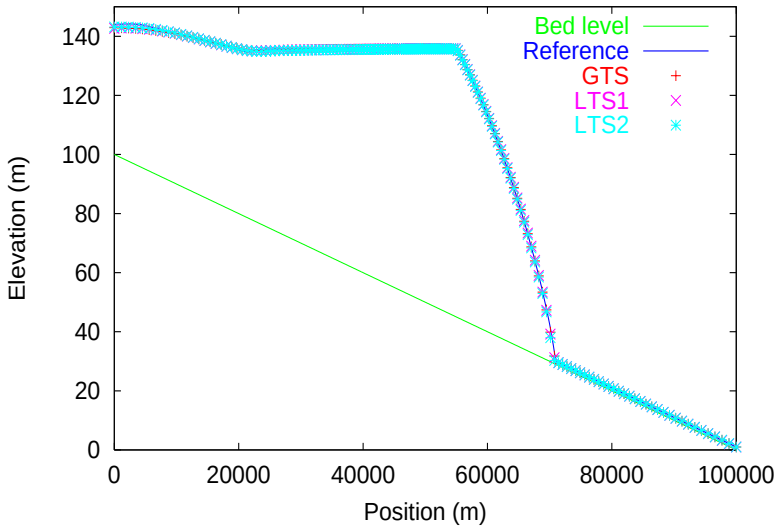

Figure 6.80: Elevation for U5 on 4 grid with upwind source terms.

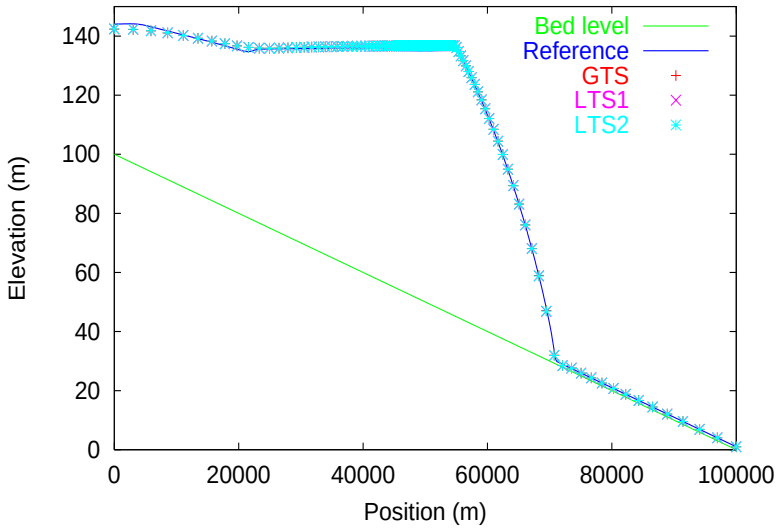

Figure 6.81: Elevation for U5 on 128 grid with upwind source terms.

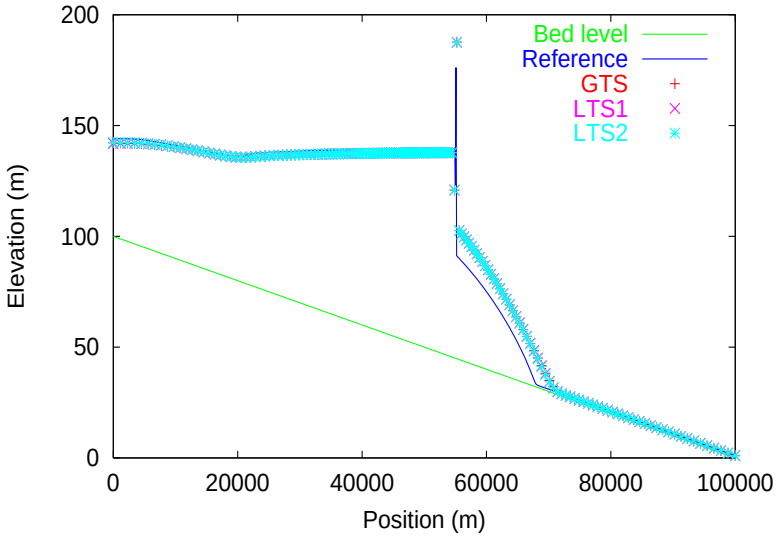

Figure 6.82: Elevation for U5 on 4 grid with pointwise source terms.

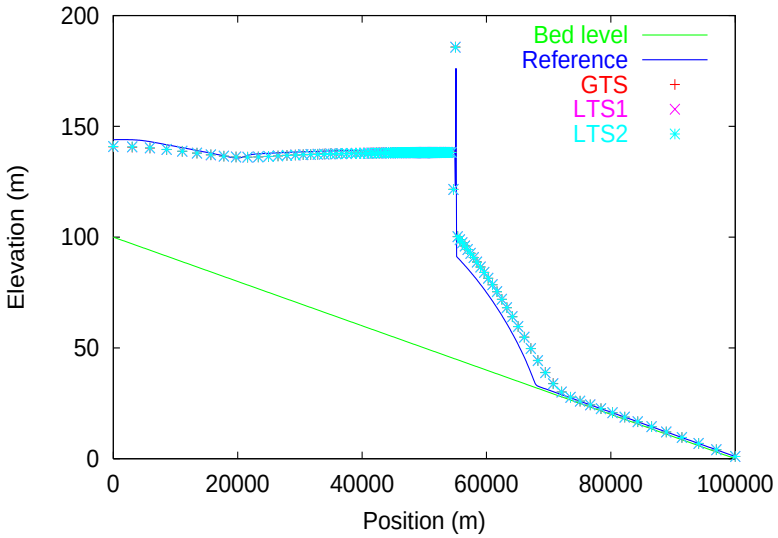

Figure 6.83: Elevation for U5 on 128 grid with pointwise source terms.

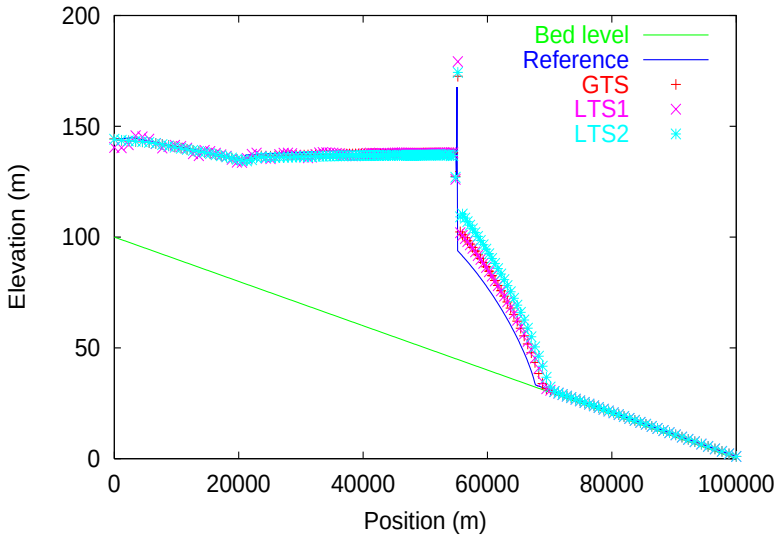

Figure 6.84: Elevation for U5 on 4 grid with pointwise source terms and Superbee.

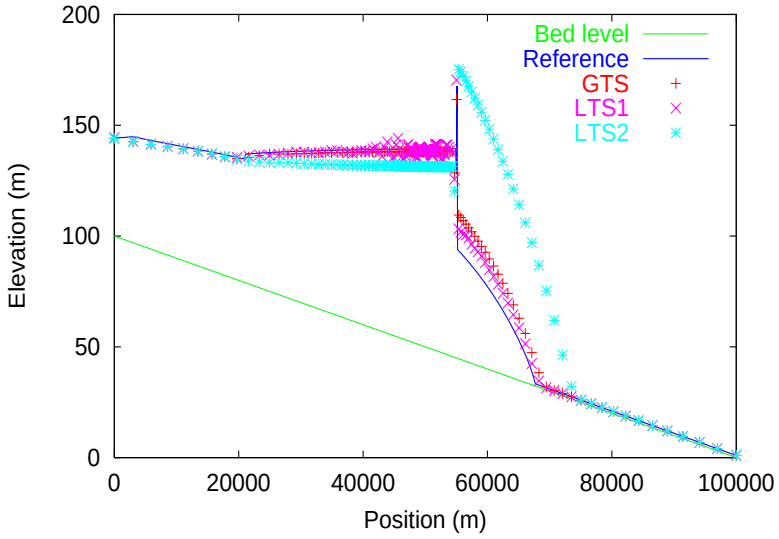

Figure 6.85: Elevation for U5 on 128 grid with pointwise source terms and Superbee.

Problem	Source term	Grid	GTS		LTS1				LTS2				
			Time (s)	Count	Limit	Time (s)	Gain	Count	Gain	Level	Time (s)	Gain	Count	Gain
U5	Upwind	1	0.04160	19040	7	0.04026	3.22	13600	28.57	2	0.03868	7.02	14489	23.90
		2	0.05540	25600	10	0.05138	7.26	16384	36.00	2	0.04898	11.59	18359	28.29
		4	0.07950	37120	11	0.07031	11.56	21368	42.44	3	0.06108	23.17	23048	37.91
		8	0.1227	57760	17	0.1037	15.48	29528	48.88	3	0.08689	29.19	32664	43.45
		16	0.1960	92800	20	0.1572	19.80	41831	54.92	3	0.1247	36.38	46254	50.16
		32	0.3231	153600	25	0.2480	23.24	61414	60.02	1	0.2741	15.17	97345	36.62
		64	0.5447	260960	22	0.4047	25.70	94693	63.71	1	0.4568	16.14	161296	38.19
		128	0.9480	452320	6	0.7047	25.66	186468	58.78	2	0.5670	40.19	200587	55.65
	Point	1	0.05271	29760	7	0.04637	12.03	15234	48.81	1	0.04781	9.30	19212	35.44
		2	0.07004	39840	9	0.05985	14.55	18403	53.81	2	0.05212	25.59	21472	46.10
		4	0.09031	51680	9	0.07715	14.57	23969	53.62	2	0.06572	27.23	27407	46.97
		8	0.1141	65600	9	0.09847	13.70	31369	52.18	3	0.07742	32.15	33750	48.55
		16	0.1596	92160	10	0.1370	14.16	43293	53.02	2	0.1193	25.25	51159	44.49
		32	0.2631	152640	10	0.2176	17.29	64554	57.71	2	0.1811	31.17	76095	50.15
		64	0.4458	259360	10	0.3573	19.85	99988	61.45	3	0.2571	42.33	109394	57.82
		128	0.7709	449280	10	0.6037	21.69	160858	64.20	3	0.4121	46.54	172666	61.57
	Point + Superbee	1	0.07675	28864	6	0.06860	10.62	17808	38.30	1	0.07160	6.71	20665	28.41
		2	0.1021	38540	7	0.08206	19.63	19863	48.46	2	0.07834	23.27	22101	42.65
		4	0.1320	50020	7	0.1052	20.30	25541	48.94	2	0.09931	24.77	28231	43.56
		8	0.1689	64124	7	0.1361	19.42	33554	47.67	2	0.1275	24.51	36578	42.96
		16	0.2486	94628	8	0.1980	20.35	48366	48.89	2	0.1824	26.63	52625	44.39
		32	0.4106	156620	8	0.3076	25.09	72408	53.77	2	0.2739	33.29	78360	49.97
		64	0.6971	266172	10	0.4950	28.99	109782	58.76	2	0.4426	36.51	126012	52.66
		128	1.208	461332	11	0.8278	31.47	176768	61.68	3	0.6319	47.69	178151	61.38

Table 6.4: Results table for U5.

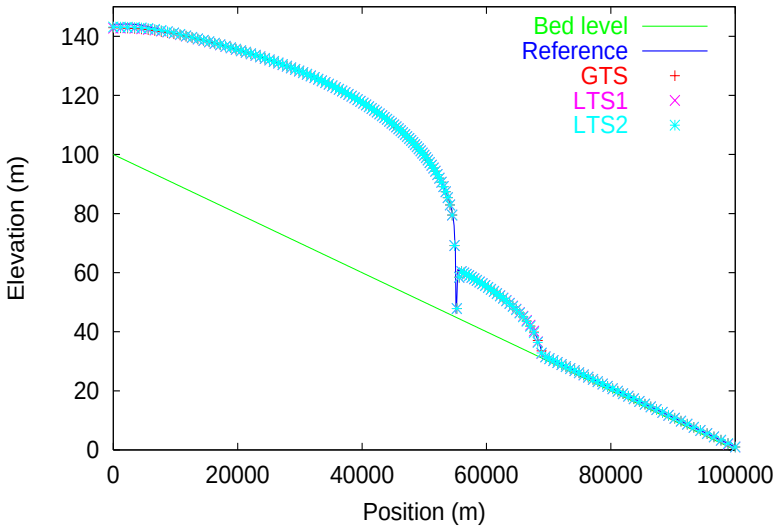

Figure 6.86: Elevation for U6 on 4 grid with upwind source terms.

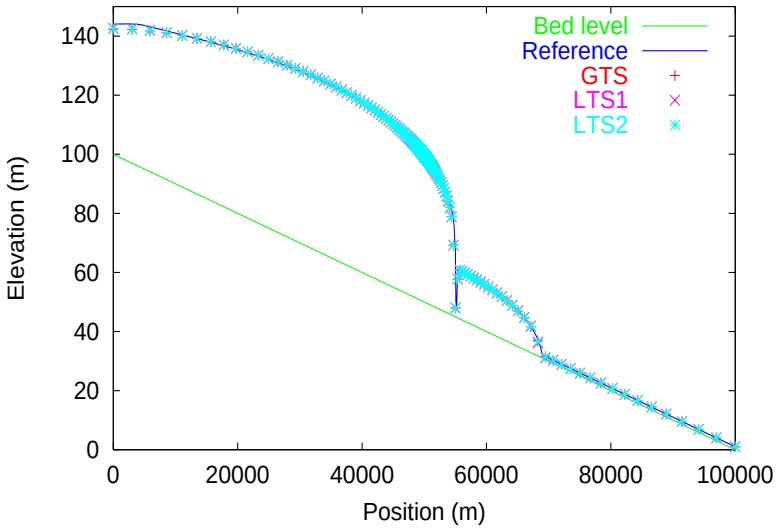

Figure 6.87: Elevation for U6 on 128 grid with upwind source terms.

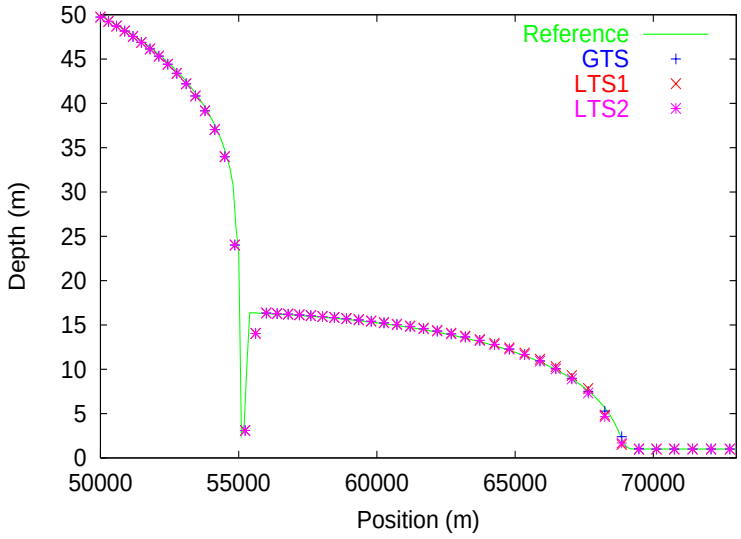

Figure 6.88: Depth profile for U6 on 4 grid with upwind source terms.

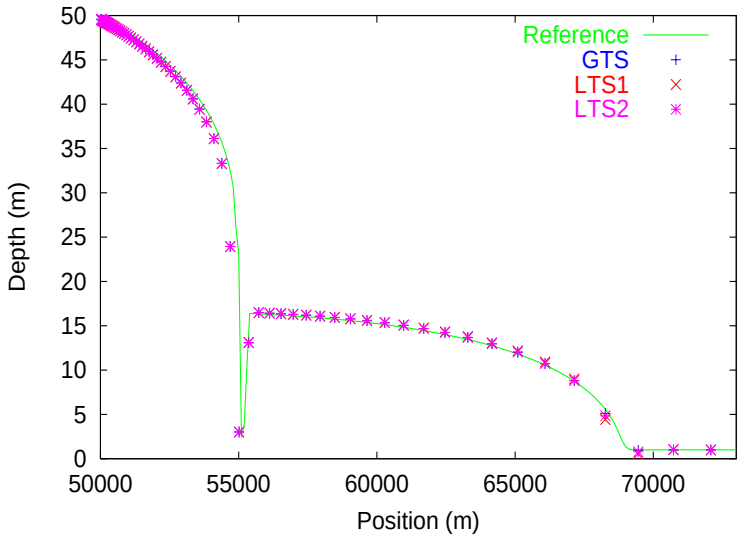

Figure 6.89: Depth profile for U6 on 128 grid with upwind source terms.

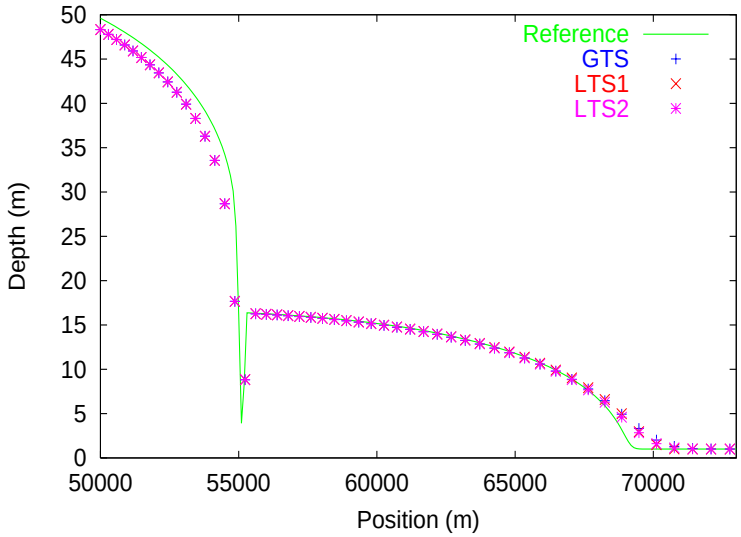

Figure 6.90: Depth profile for U6 on 4 grid with pointwise source terms.

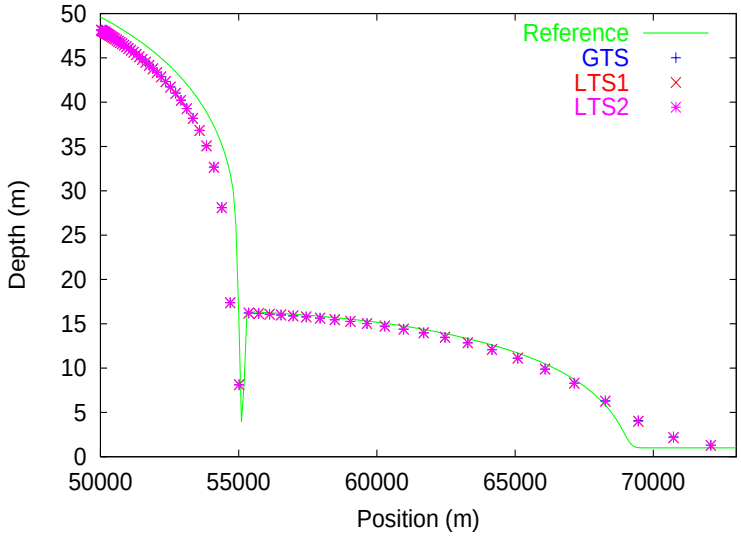

Figure 6.91: Depth profile for U6 on 128 grid with pointwise source terms.

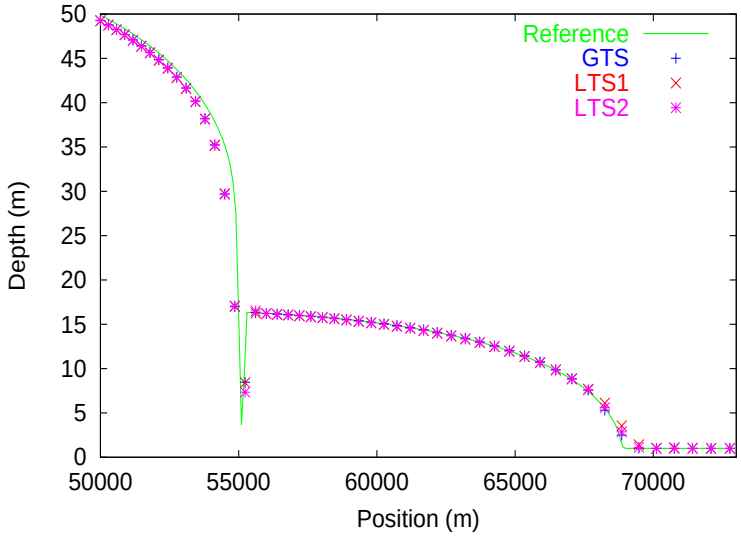

Figure 6.92: Depth profile for U6 on 4 grid with pointwise source terms and Superbee.

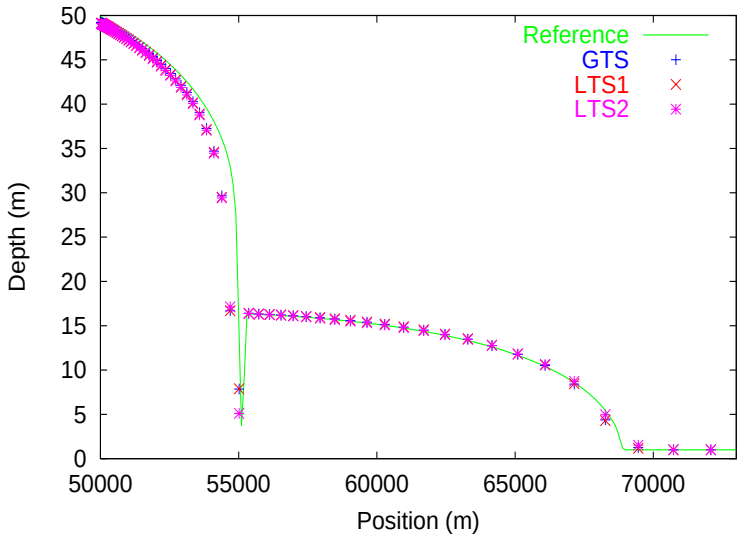

Figure 6.93: Depth profile for U6 on 128 grid with pointwise source terms and Superbee.

6.4 Summary of results

The test cases considered have highlighted a number of trends. In terms of the source term treatment, in the examples where the source terms play a more dominant role, the benefits of using an upwind based treatment over a pointwise approach are apparent. For the steady state problems, only the upwind approach generated the constant discharge throughout the channel, with the appearance of a spike at the location of hydraulic jumps. The pointwise source term results showed the greatest deviation from the exact value, and the application of a flux limiter reduced the discrepancy. For both the upwind and pointwise results, the GTS and LTS discharge values were the same. However, when the flux limiter was used in conjunction with the pointwise treatment, the GTS and LTS results differed, with the GTS results appearing slightly better. In terms of the depth profiles, then in the regions where there was a high degree of curvature in the solution, the upwind results showed the closest agreement to the analytical solution. Using a flux limiter was again seen to improve the pointwise values, though they were still not as good as the upwind results. For the transient problems, the source terms had the most significant effect in example **U5**, where only the upwind treatment produced a reasonable solution. The other test case in which the source terms were dominant was example **U6**. Here the difference between the reference and various time stepping solutions was greatest for the pointwise results, particularly in the region of the wave advancing downstream. The run times were also affected by the source term treatments, as the upwind calculations were more computationally expensive than the pointwise approach. The upwind run times were however less than the pointwise and Superbee values.

The benefits of using local time stepping have also been seen. For the steady state problems considered, applying the LTS techniques did not result in a change of accuracy of the solution, as the GTS and LTS depth results were virtually identical for nearly all of the problems. However, a reduction in both the run time and the number of flux calculations performed was seen, with the improvement generally increasing with the grid ratio n. In contrasting the two LTS strategies, the run time efficiencies for the LTS1 procedure were generally lower than for the LTS2 approach, though the flux count gains tended to be quite similar. This reflected the fact that the LTS1 algorithm updates all of the cells at every local time step using the frozen flux. In this manner, the need to have a series of temporal levels (as with the LTS2 algorithm) is eliminated. Typically, the LTS2 procedure led

to the fastest run times when the maximum level became either 2 or 3, resulting in either 4 or 8 temporal levels per global time step. For the first order results, the LTS1 and LTS2 procedures tended to produce similar results on the 4 grid, which in examples **U1** to **U4** generally led to sharper solution profiles. On the 128 grid, the LTS1 results tended to show the best shock resolution, with the GTS and LTS2 profiles appearing quite similar. Overall the improvements observed in using local time stepping increased with the grid ratio.

The benefits of using local time stepping in conjunction with a flux limiter were less apparent, as generally the solution profiles were quite similar. However the run times and number of flux calculations were reduced. In some instances, using local stepping within the second order scheme deteriorated the results (most noticeably for the LTS1 procedure) though this tended to affect only isolated points. If the number of local time steps per global cycle is restricted (as in examples **U5** and **U6**), this problem can sometimes be reduced. However this can also lead to the solution deteriorating in other parts of the channel. A number of other problems were also experienced, such as the temporal stiffness effect with the LTS2 procedure (which restricted the maximum value of m that could be used on stability grounds), and the need to specify a limit on the number of local time steps for LTS1 in examples **U5** and **U6**. This problem was overcome by enforcing a maximum number of local time steps per global cycle as suggested by Pervaiz and Baron [48], though the origins of the difficulties experienced were different. In addition, the run time measurements showed that it was not always beneficial to use local time stepping, particularly for the lower grid ratios as the run times tended to exceed the GTS values.

Chapter 7

Conclusions

7.1 Discussion

The objective of this thesis was to investigate ways in which the software currently available to hydraulic engineers might be improved. More specifically, the intention was to focus on techniques which could lead to reduced run times and improved solution accuracy. Recent trends within the field of computational hydraulics research have tended towards finite volume techniques and the use of Riemann based solvers. For this reason, the Roe Riemann solver was chosen as a focal point for the investigation. As much of the pioneering development for the methods used within the hydraulics environment was conducted within the field of aeronautics, attention was drawn towards any ideas which as yet remained unexploited by the hydraulics community. To this end the application of time accurate local time stepping to open channel flow has been considered.

The use of local time stepping in steady state problems in CFD is a widely accepted practise. However its application to transient problems has received much less attention due to the additional complexity of ensuring a time accurate solution. The strategies presented by Zhang *et al* ([70], [71]) and Kleb and Batina [40] were particularly appealing for this project, as both were constructed within the finite volume framework, and developed for the Euler equations. The availability of suitable test cases and the need to develop the techniques presented for open channel flows, suggested that the investigation should be conducted on the 1-d Saint Venant equations, with the view that ideas could be extended to higher order systems, where there is a greater need to develop faster algorithms. The

effects of incorporating the source terms within the LTS framework were also investigated, together with a comparison between the results obtained by using a pointwise approach and an upwind implementation proposed by García-Navarro and Vázquez-Cendón [26], specifically constructed for the first order Roe scheme.

In applying the LTS procedures, strategies were developed for the construction of the interface regions within the respective algorithms, and the second order Roe scheme (via the Superbee flux limiter) was incorporated into the LTS framework. Following the work of García-Navarro and Vázquez-Cendón, the upwind source term treatment was extended to trapezoidal channels, and the application to irregular grids was considered. From the test cases identified from the literature, results were shown for a number of problems, which represented a range of conditions and included the effects of varying beds, friction and changes in channel cross section.

In the cases considered, a number of general trends were observed which can be used to assess the relative merits of utilising local time stepping and an upwind source term treatment. For the steady state problems, applying LTS did little to affect the quality of the solutions, and the depth and discharge profiles were generally more dependent upon the source term treatment and the order of the scheme used. It was observed that only the upwind source term results were able to consistently reproduce a uniform value for the steady state discharge. In addition, improvements in the depth profiles were seen for some of the test cases. This was most noticeable in regions of curvature in the depth profile. Differences between the GTS and LTS results for the time dependent problems were apparent. For the first order results, the LTS solutions tended to improve the resolution of the discontinuities. On the 4 grid, the two LTS procedures were comparable, whereas on the 128 grid, the LTS1 procedure tended to give the best solutions, with the GTS and LTS2 results appearing similar. One explanation for why the LTS2 procedure tended to give more favourable results on the 4 grid could lie in the temporal stiffness effect which restricted the maximum number of temporal levels that could be used. As consequence of this, the number of local time steps that can be applied is limited which may also restrict the solution improvement attainable. With the exception of examples **U5** and **U6**, this was not a problem experienced with the LTS1 algorithm, which showed the most significant solution improvements at the higher grid ratios in the coarser regions. The second order results generally showed no solution improvement when local time stepping was used, and in some instances caused the solution to deteriorate, particularly for the

LTS1 results. It is suspected that this is connected to the value of Δt used in the limited second order component of Roe's scheme. The original testing suggested that selecting the minimum value of the corresponding left and right cells gave the best performance. However in light of these results, further testing is necessary. The run time and flux count measurements typically showed the LTS algorithms to be more efficient than global time stepping and illustrated a correlation between the grid ratio, and the benefits of using local time stepping. In essence, it became more desirable to use local time stepping, as this ratio increased. This data also highlighted that the LTS1 suffered from the need to update every cell at every time step, reducing the run time efficiency gain, even though the flux count values were similar to the LTS2 procedure. However the LTS2 run times were generally higher than the LTS1 values when only two time levels were permitted, though this also tended to coincide with the grids for which both procedures were slower than using global time stepping.

A number points must be made to put the work conducted within the thesis into perspective. Firstly, the local time stepping procedures presented were applied to the 1-d Saint Venant equations, and generally the computational cost involved in solving this system is not regarded as excessive. The problems considered were not representative of the sort of situations which engineers encounter, and did not reflect the irregular geometries typical of most rivers. In terms of the increased solution accuracy reported, it can be argued that the improvements seen would not be of significant consequence in a more realistic situation, particularly given the uncertainties which are normally involved in any simulation process.

It must also be pointed out that within the research community the use of second order schemes is now considered the norm, and it would be seen as unusual to implement a first order method on an irregular grid. With this in mind, there is an obvious need to investigate the LTS strategies further, as the solutions obtained when the algorithms were applied to the second order Roe scheme showed a number of anomalies. There is also the issue of the limiting strategy needed for the LTS1 procedure in examples **U5** and **U6** and the necessity of specifying a maximum level for the LTS2 algorithm.

In terms of what the thesis set out to achieve, the main conclusion to be drawn from this work is that time accurate local time stepping can successfully be applied to both steady and transient open channel flow problems. Moreover, local time stepping can lead to reduced computer run times and increased solution accuracy,

most noticeably in the vicinity of discontinuities. In addition, the source term calculations can be included within the LTS structure, and the benefits of using an upwind biased treatment have been observed. One possibility which may go some way to alleviate the temporal stiffness problem is to consider implementing local time stepping within an implicit framework, as the limits needed for both LTS procedures were related to the onset of numerical instability. It could be said that combing an LTS approach with an implicit method would seem pointless, as implicit schemes permit the use of arbitrarily large time steps. However, solution accuracy must also be considered when selecting the time steps and so this tends to restrict the CFL numbers used. In addition, implicit methods tend to suffer from numerical diffusion in the region of discontinuities. As the use of LTS has been seen to improve this situation in an explicit method, it could also be beneficial to apply the technique to implicit schemes.

To render the application of local time stepping to be a consideration for commercial software, a number of issues would need to receive further consideration. It would be necessary to develop a strategy which enabled the restrictive limits on the LTS algorithms to be predetermined, as mentioned previously. In addition, further validation of the interface procedures would also be required, as it is likely that a more complex strategy would be necessary for more realistic situations, especially for the LTS1 method. The overheads entailed in implementing the LTS routines must also be considered, as it is apparent that local time stepping will not always be beneficial. As with all techniques, there may be ways of reducing these costs, making the concept of LTS more attractive.

One final point to be made is that throughout this thesis, the application of local time stepping has been considered on a fixed irregular grid. Any further development should consider the issue of spatial adaptivity, and investigate the relative merits of combining temporal and spatial grid adaptation.

Although a number of areas have been identified for further investigation, the issues which need to be addressed are not insurmountable. It is hoped that this thesis conveys the potential gains of employing local time stepping, which could be extended beyond the scope of this project and be of benefit to the hydraulic community.

7.2 Possibilities for further work

With the points mentioned in mind, a number of possibilities for extending the application of local time stepping can be identified. In expanding the work conducted as part of this thesis, further work could include

- Application of the ideas developed to higher order systems, such as the 2-d shallow water equations
- An investigation into the benefits of employing LTS within implicit numerical schemes
- Extension of the project to include irregular geometries
- Implementation of local time stepping in conjunction with spatial grid adaptivity
- Further investigation of the interface procedures and development of strategies for predicting the maximum number of local time steps per global cycle.

Another possibility which could be investigated is to consider applying LTS to non-TVD schemes such as McCormack's scheme. Although this would not render such methods as TVD, it might go some way to minimizing the oscillations which occur in regions of strong gradients, due to the ability of the approach to utilise time steps close to the stability limit throughout the channel.

Bibliography

[1] Abbott M and Minns A : Computational Hydraulics (second edition), Ashgate Publishing Ltd, 1998.

[2] Alcrudo F, García-Navarro P and Savirón J : Flux difference splitting for 1-d open channel flow equations. Int. J. Numer. Methods Fluids, **14**, 1009–1018, 1992.

[3] Alcrudo F, García-Navarro P : High resolution Godunov-type scheme in finite volumes for the 2-d shallow water equations. Int. J. Numer. Methods Fluids, **16**, 489–505, 1993.

[4] Ambrosi D : Approximation of the shallow water equations by Roe's Riemann solver. Int. J. Numer. Methods Fluids, **20**, 157–168, 1995.

[5] Ames W : Numerical Methods for Partial Differential Equations, Academic Press, 1992.

[6] Anastasiou K and Chan C : Solution of the 2d shallow water equations using the finite volume method on unstructured triangular meshes. Int. J. Numer. Methods Fluids, **24**, 1225–1245, 1997.

[7] Baines M : Initial value problems, Lecture notes, Dept. of Mathematics, University of Reading, 1993.

algorithm fo

[8] Bermúdez A and Vázquez M E : Upwind methods for hyperbolic conservation laws with source terms. Computers and Fluids, **23**, 8, 1049–1071, 1994.

[9] Bermúdez A *et al* : Upwind schemes for the two-dimensional shallow water equations with variable depth using unstructured meshes. Computer Methods in Applied Mechanics and Engineering, **155**, 49–72, 1998.

[10] Bellos C, Soulis J and Sakka J : Experimental investigation of 2-dimensional dam-break induced flows. J. Hydraul. Res., **30**, 1, 47–63, 1992.

[11] Chow V : Open Channel Hydraulics, McGraw Hill, 1959.

[12] Cunge J, Holly F and Verwey A : Practical aspects of computational river hydraulics, Pitman Publishing Ltd, 1980.

[13] Delis A and Skeels C : TVD schemes for open channel flow. Int. J. Numer. Methods Fluids, **26**, 791–809, 1998.

[14] Engquist B and Osher S : One-sided difference approximations for non-linear conservation laws. Math. Comput., **36**, 321–352, 1981.

[15] Fennema R and Chaudhry M : Explicit numerical schemes for unsteady free-surface flows with shocks. Water Resources Research, **22**, 13, 1923–1930, 1986.

[16] Fennema R and Chaudhry M : Simulation of one-dimensional dam-break flows. J. Hydraul. Res., **25** 41–51, 1987.

[17] Fennema R and Chaudhry M : Implicit methods for two-dimensional free-surface flows. J. Hydraul. Res., **27**, 321–332, 1989.

[18] Fennema R and Chaudhry M : Explicit methods for 2-d transient free-surface flows. J. Hydraul. Eng., **116**, 1013–1034, 1990.

[19] Fletcher C : Computational Techniques for Fluid Dynamics, Volume 1, Springer-Verlag, 1991.

[20] Fraccarollo L and Toro E : Experimental and numerical assessment of the shallow water model for two-dimensional dam-break type problems. J. Hydraul. Res., **33**, 843–864, 1995.

[21] García-Navarro P and Savirón J : McCormack's method for the numerical simulation of one-dimensional discontinuous unsteady open channel flow. J. Hydraul. Res., **30**, 95–105, 1992.

[22] García-Navarro P, Alcrudo F and Savirón J : 1-d open channel flow simulation using TVD-McCormack scheme. J. Hydraul. Eng., **118**, 1359–1372, 1992.

[23] García-Navarro P and Alcrudo F : A high resolution Godunov-type scheme in finite volumes for 2D shallow-water equations, Int. J. Numer. Methods Fluids, **16**, 489–505, 1993.

[24] García-Navarro P, Priestley A and Alcrudo F : An implicit method for water flow modeling and channels and pipes, J. Hydraul. Res., **32**, 721–742, 1994.

[25] García-Navarro P, Hubbard M and Priestley A : Genuinely multidimensional upwinding for the 2d Shallow Water equations. J. Comput. Phys., **121**, 79–93, 1995.

[26] García-Navarro P and Vázquez-Cendón M E, Roe's scheme for 1-d irregular geometries, Proceedings of Hydroinformatics 98, 1998.

[27] Glaister P : Approximate Riemann solutions of the shallow water equations. J. Hydraul. Res., **26**, 293–306, 1988.

[28] Glaister P : Approximate Riemann solvers of the two-dimensional shallow-water equations. J. Eng. Mathematics, **24**, 45–53, 1990.

[29] Glaister P : Difference schemes for the shallow water equations, University of Reading Numerical Analysis Report, 9/97, 1987.

[30] Harten A and Hyman J : Self adjusting grid methods for one-dimensional hyperbolic conservation laws. J. Comput. Phys., **50**, 235–269, 1983.

[31] Harten A, Lax P D and van Leer B : On upstream differencing and Godonuv-type schemes for hyperbolic conservation laws. SIAM Rev., **25**, 35–61, 1983.

[32] Henderson F : Open Channel Flow, Maxmillian, 1966.

[33] Hirsch C : Numerical Computation of Internal and External Flows, Vol. 1, Wiley, 1988.

[34] Hirsch C : Numerical Computation of Internal and External Flows, Vol. 2, Wiley, 1990.

[35] Hicks F, Steffler P and Yasmin N : One-dimensional dam-break solutions for variable width channels. J. Hydraul. Eng., **123**, 5, 464–468, 1997.

[36] Jha A, Akiyama J and Ura M : Modelling unsteady open-channel flows—modification to Beam and Warming scheme. J. Hydraul. Eng., **120**, 4, 120, 1994.

[37] Jha A, Akiyama J and Ura M : First- and second-order flux difference splitting schemes for dam-break problem. J. Hydraul. Eng., **121**, 12, 877–884, 1995.

[38] Jha A, Akiyama J and Ura M : A fully conservative Beam and Warming scheme for transient open channel flows. J. Hydraul. Res., **34**, 5, 605–621, 1996.

[39] Jin M and Fread D : Dynamic flood routing with explicit and implicit numerical solution schemes. J. Hydraul. Eng., **123**, 3, 166–173, 1997.

[40] Kleb W L, Batina J T and Williams M H : Temporal adaptive Euler/Navier-Stokes algorithm involving unstructured dynamic meshes, AIAA Journal, **30**, 8, 1980–1985, 1992.

[41] LeVeque R : Numerical methods for conservation laws, Birkhäuse, 1992.

[42] MacDonald I, Baines M, Nichols N and Samuels P : Analytic benchmark solutions for open-channel flows. J. Hydraul. Eng., **123**, 11, 1041–1045, 1997.

[43] Meselhe E, Sotiropoulos F and Holly F : Numerical simulation of transcritical flow in open channels. J. Hydraul. Eng., **123**, 9, 774–783, 1997.

[44] Mingham C and Causon D : High-resolution finite volume method for shallow water flows. J. Hydraul. Eng., **124**, 6, 605–614, 1998.

[45] Molls T and Molls F : Space-Time conservation method applied to Saint Venant Equations, J. Hydraul. Eng., **124**, 5, 501–508, 1998.

[46] Nujić M : Efficient implementation of non-oscillatory schemes for the computation of free surface flows. J. Hydraul. Res., **33**, 101–111, 1995.

[47] Osher S and Solomon F : Upwind difference schemes for hyperbolic systems of conservation laws. Math. Comput., **38**, 339–374, 1983.

[48] Pervaiz M and Baron J : Temporal and spatial adaptive algorithm for reacting flows, Comm. Appl. Numer. Methods, **4**, 97–111, 1988.

[49] Peyret R : Computational Fluid Mechanics, Academic Press, 1996.

[50] Press W *et al* : Numerical Recipes, Cambridge University Press, 1986.

[51] Roe P : Approximate Riemann solvers, parameter vectors and difference schemes, J. Comput. Phys., **43**, 357–372, 1981.

[52] Roe P and Pike J : Efficient construction and utilisation of approximate Riemann solutions, Computing Methods in Applied Sciences and Engineering, **6**, 499–518, 1984.

[53] Roe P : Upwind differencing schemes for hyperbolic conservation laws with source terms, Lecture Notes in Mathematics, **1270**, 41–51, 1987.

[54] Savic L and Holly F : Dam-break flood waves computed by the modified Godunov method. J. Hydraul. Res., **31**, 187–204, 1993.

[55] Sleigh P : private communication, 1995.

[56] Sleigh P, Gaskell P, Berzins M and Wright N : An unstructured finite-volume algorithm for predicting flow in rivers and estuaries. Computers and Fluids, **127**, 4, 479–508, 1998.

[57] Smith G : Numerical Solution of Partial Differential Equations : Finite Difference Methods, Oxford, 1985.

[58] Stoker J : Water Waves, Interscience Publishers, 1957.

[59] Sweby P : High resolution schemes using flux limiters for hyperbolic conservation laws. SIAM J. Numer. Analysis, **21**, 9995–1011, 1984.

[60] Sweby P : Computing techniques and modelling, Lecture notes, Dept. of Mathematics, University of Reading, 1993.

[61] Sweby P : Theory of differential equations, Lecture notes, Dept. of Mathematics, University of Reading, 1993.

[62] Toro E : Riemann problems and the WAF method for solving the two-dimensional shallow water equations, Phil. Trans. R. Soc. Lond. A, **338**, 43–68, 1992.

[63] Toro E : Riemann solvers and numerical methods for fluid dynamics — a practical introduction. Springer, 1997.

[64] Vázquez-Cendón M E: Improved treatment source terms in upwind schemes for the shallow water equations in channels with irregular geometry, J Comput. Phys., **148**, 497–526, 1999.

[65] Versteeg H and Malalasekera W : An introduction to computational fluid dynamics the finite volume method, Longman, 1995.

[66] Weiyan T : Shallow water hydrodynamics, Elsevier Science Publishers, 1992.

[67] Yang J, Hsu C and Chang S : Computations of free surface flows - Part 1 : One-dimensional dam-break flow. J. Hydraul. Res, **31**, 19–34, 1993.

[68] Yang J and Hsu C : Computations of free surface flows - Part 2 : Two-dimensional unsteady bore diffraction. J. Hydraul. Res., **31**, 403–414, 1993.

[69] Yee H : Construction of explicit and implicit symmetric TVD schemes and their applications. J. Comput. Phys., **68**, 151–179, 1987.

[70] Zhang X D, Trépanier J-Y, Reggio M and Camarero R : A new local time stepping approach for the unsteady Euler equations, AIAA Paper 94–0525, 1994.

[71] Zhang X D, Trépanier J-Y, Reggio M and Camarero R : Time-accurate local time stepping method based on flux updating, AIAA Journal, **32**, 9, 1926–1929, 1994.

[72] Zhao D, Shen H, Lai J and Tabios III G : Approximate Riemann solvers for 2d hydraulic shock wave modelling. J. Hydraul. Eng., **122**, 12, 692–702, 1996.

Appendix A

Analytic solutions of steady problems

Analytic solutions for steady state Saint Venant problems which contain no energy losses, i.e. no friction terms, can be found by using the Bernoulli equation. The Bernoulli equation is based upon conservation of energy (or head) and for open channel flow is written as

$$h + \frac{u^2}{2g} + z = H$$

where H is the total head. If the total head is known at a particular point along the channel, then providing that the steady state discharge is known, the depth profile throughout the channel can be determined via the solution of a cubic equation, assuming that no energy losses occur. For a rectangular channel where $h = A/b$, the resulting cubic expression is

$$h^3 + h^2(z - H) + \frac{Q^2}{2b^2g} = 0.$$

This can be solved at each point by using the formula for finding solutions to cubic equations [50]. For a general cubic polynomial of the form

$$x^3 + a_1x^2 + a_2x + a_3 = 0,$$

the values R and S are defined by

$$S = \frac{a_1^2 - 3a_2}{9}$$

and

$$R = \frac{2a_1^3 - 9a_1a_2 + 27a_3}{54}.$$

The number of real roots to the equation is dependent upon the value of $S^3 - R^2$. If this value is greater than or equal to zero, then there are three real roots to the equation. If this value is less than zero, there is only one real root.

In relation to Bernoulli's equation, then the value of h found from the general formula should be real. In the case of there being three real roots, the appropriate value must be chosen. In this instance there will be one non-physically acceptable negative root, and two positive roots. The correct choice of positive root depends upon the local flow conditions. If the flow is subcritical, then the maximum of the two values is the appropriate one, else it is the minimum of the two. Assuming that the flow is subcritical at the upstream boundary, then it will remain so along the channel unless the width becomes less than or equal to the critical width. When the Froude number is unity, the critical depth is given by

$$h_c = \left(\frac{Q}{b_c \sqrt{g}} \right)^{2/3}$$

and substituting this into Bernoulli's theorem then gives the critical width as

$$b_c = \frac{Q}{\sqrt{g}} \left[\frac{2}{3} (H - z) \right]^{-3/2}.$$

Should the flow reach supercritical conditions, then it will remain supercritical unless a subcritical downstream boundary condition is specified. This will necessitate the formation of a hydraulic jump, across which there will be an energy loss and the Bernoulli equation can no longer be applied. However, the head downstream of the jump will also be constant and so Bernoulli's equation can be applied locally to both the sections upstream and downstream of the jump, providing that the two head values are known.

To connect the two regions, the Conjugate Depths or Belanger equation is used. This relates the flow conditions immediately before and after the jump via the equation

$$h_2 = \frac{h_1}{2} \left(\sqrt{1 + 8F_{r_1}^2} - 1 \right) \tag{A.1}$$

where 1 denotes the conditions upstream of the jump and 2 is for the downstream section. By applying Bernoulli's equation throughout the channel using both the upstream and downstream heads, Equation (A.1) can then be used to determine the position of the jump. Given the depths calculated upstream, together with the conjugate depth values, the point at which the conjugate depth matches the downstream depth value corresponds to the location of the hydraulic jump.

This process enables analytical solutions to be found to a range of idealised problems where no friction terms are present. However it does require a knowledge of the total head value throughout the channel, which in the case of flows containing hydraulic jumps, means that either the head, or both the discharge and depth must be known at two points either side of the jump.

Appendix B

Exact solution to the dam-break problem

The analytic solution detailed in this appendix was presented by Glaister [29].

The problem is specified by the upstream depth, h_1, and the downstream depth h_0, where it is assumed that $h_1 > h_0$. A third region exists over which the variables are constant, and this lies behind the bore where the depth and velocity are h_2 and u_2 respectively.

The first stage of the procedure is to determine the speed of propagation, S, of the bore as it travels downstream. This is found from the positive root of the equation

$$u_2 + 2\sqrt{\phi_2} - 2\sqrt{\phi_1} = 0 \tag{B.1}$$

where $\phi = gh$ (as the bed is flat) and

$$\phi_2 = \frac{1}{2}\left(\sqrt{1 + \frac{8S^2}{\phi_0}} - 1\right)\phi_0$$

$$u_2 = S + \frac{\phi_0}{4S}\left(1 + \sqrt{1 + \frac{8S^2}{\phi_0}}\right).$$

Substituting the expressions for ϕ_2 and u_2 into (B.1) then gives a formula for S, which may be written as

$$S - \frac{\phi_0}{4S}\left(1 + \sqrt{1 + \frac{8S^2}{\phi_0}}\right) + \left(2\sqrt{1 + \frac{8S^2}{\phi_0}} - 2\right)^{1/2}\sqrt{\phi_0} - 2\sqrt{\phi_1} = 0. \tag{B.2}$$

Once S has been calculated the exact solution is given by

$$\left.\begin{array}{c}\phi = \phi_1 \\ u = 0\end{array}\right\} \qquad x \le -\sqrt{\phi_0}\, t_0$$

$$\left.\begin{array}{c}\phi = \dfrac{1}{9}\left(2\sqrt{\phi_1} - \dfrac{x}{t_0}\right)^2 \\ u = \dfrac{2}{3}\left(\sqrt{\phi_1} + \dfrac{x}{t_0}\right)\end{array}\right\} \qquad -\sqrt{\phi_1} t_0 < x \le (u_2 - \sqrt{\phi_2}) t_0$$

$$\left.\begin{array}{c}\phi = \phi_2 \\ u = u_2\end{array}\right\} \qquad (u_2 - \sqrt{\phi_2}) t_0 < x \le S t_0$$

$$\left.\begin{array}{c}\phi = \phi_0 \\ u = 0\end{array}\right\} \qquad S t_0 < x$$

where t_0 is the evaluation time.

One possible way to obtain a value of S from Equation (B.2) is to use an iterative procedure such as the Newton-Raphson method, whereby subsequent iterations are given by

$$S^{k+1} = S^k - \frac{F(S^k)}{F'(S^k)},$$

where the function $F(S)$ is define as

$$F(S) = S - \frac{\phi_0}{4S}(1+d) + (2\phi_0 d - 2)^{1/2} - 2\sqrt{\phi_1} = 0$$

if $d = \sqrt{1 + \dfrac{8S^2}{\phi_0}}$, and the derivative is

$$F'(s) = 1 + \frac{\phi_0}{4S^2}(1+d) - \frac{2}{d} + \frac{8S}{d}\frac{1}{(2\phi_0(d-1))^{1/2}}.$$

The procedure is repeated until two successive iterations produce the same value of S to within some tolerance.

Appendix C

Irregular grid generation

Consider an irregular grid of the form shown in Figure C.1 , whereby for a particular cell i, the cell centre is denoted by x_i and the corresponding interfaces are $x_{i-1/2}$ and $x_{i+1/2}$.

The position of the interface between cells $i-1$ and i, is then defined by

$$x_{i-1/2} = \frac{1}{2}\left(x_{i-1} + x_i\right),$$

and the corresponding right hand interface for cell i is

$$x_{i+1/2} = \frac{1}{2}\left(x_i + x_{i+1}\right).$$

If the cell length is defined as the distance between the cell interfaces, then

$$\Delta x_i = x_{i+1/2} - x_{i-1/2} = \frac{1}{2}\left(x_{i+1} - x_{i-1}\right).$$

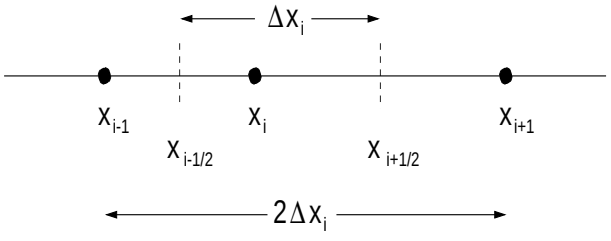

Figure C.1: An irregular grid.

C.1 Construction of irregular grid A

Consider the situation of an irregular grid which is symmetric about the centre of the reach being modelled. Considering only the first half of the grid, then let the innermost cells be of a fixed length d, and those at the outer region (upstream boundary) be of length nd, where n is an integer. These two regions are then connected through a series of cells whose length varies uniformly by a factor f. Let there be a cells of length nd, b cells of varying length and c cells of length d (not including the central cell). The grid is constructed such that it is symmetric about the centre most cell which is of length d. It is assumed that the total number of cells (numcell) is odd, and that the cell centres of the first and last cells correspond to the up and downstream boundary positions.

Following this approach it is possible to build an irregular grid by calculating the positions of the cell centres. The interface coordinates $x_{3/2}, x_{5/2}, ..., x_{\text{numcell}-1/2}$ are then found from the cell centre positions and the corresponding cell lengths can be calculated.

From the position of the first cell centre (the upstream boundary), the position of the next cell centre is given by

$$x_2 = x_1 + nd.$$

The next centre will then be given by

$$x_3 = x_2 + nd$$

and so

$$x_m = x_{m-1} + nd. \tag{C.1}$$

In total this relationship is applied a times, such that the final position to be found from the formula is x_{a+1}. The distance between adjacent cells centres then begins to contract by the factor f. The position of cell centre x_{a+2} is given by

$$x_{a+2} = x_{a+1} + f^{b-1}d,$$

followed by

$$x_{a+3} = x_{a+2} + f^{b-2}d,$$

such that

$$x_{a+m} = x_{a+m-1} + f^{b-m-1}. \tag{C.2}$$

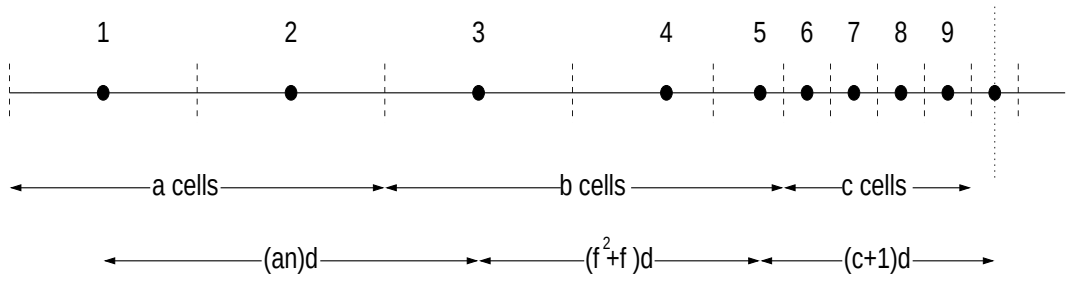

Figure C.2: Irregular grid A.

This series progresses up until the $(a+b)th$ cell for which

$$x_{a+b} = x_{a+b-1} + fd.$$

The following positions, i.e. x_{a+b+1} up to x_{a+b+c}, are then all a distance d apart, and the $(a+b+c+1)th$ cell is then the central cell of the reach. These positions are calculated from

$$x_{i+1} = x_i + d. \tag{C.3}$$

This mirror image of this process is then applied to define the cells from the central region to the downstream boundary.

This procedure is illustrated in Figure C.2 which shows the upstream portion of the grid, in the case where $a = 2$, $b = 3$ and $c = 4$. The total number of grid cells is numcell=$2(a+b+c)+1$=19 and the factor f has a value of 2.

In terms of calculating the various parameters, within the algorithm, the relationship (C.1) is applied a times, (C.2) is used $b-1 = b'$ times, and (C.3) is applied c times. From this, the cell lengths and the reach length are related by

$$\frac{\text{length}}{2} = d\left(na + \sum_{k=1}^{b'} f^k + c'\right), \tag{C.4}$$

where $c' = c+1$. The summation is fact a geometric series for which

$$\sum_{k=1}^{b'} f^k = \frac{f(1-f^{b'})}{1-f}$$

and f, n and b are connected through the relationship

$$f^{b'} = n$$

such that given n and b, then f maybe calculated from

$$f = n^{1/b'}.$$

If the grid is specified by the number of cells, numcell, and the factor n, then it remains to determine a, b, c and d from (C.4) and the relationship

$$a + b + c = \frac{\text{numcell} - 1}{2}.$$

As there are four unknowns, and two equations, two of the values must be specified. If b is chosen, and a and c are connected through

$$c = (n-1)a,$$

then the system is completely specified from which

$$a = \frac{1}{n}\left(\frac{\text{numcell} - 1}{2} - b\right), \tag{C.5}$$

$$c = (n-1)a,$$

$$d = \frac{\text{length}}{2\left(na' + \sum_{k=1}^{b'} f^k + c'\right)}.$$

Due to the fact that a, b and c are integer values, numcell and b must be chosen so that equation (C.5) is satisfied. This is ensured if numcell is odd and selected to be an integer multiple of n, and by defining b to also be a multiple of n, such as by a relationship like

$$b = \text{int}\frac{\text{numcell}}{\text{scaling factor}} \times n.$$

This information then enables the grid positions to be calculated.

This construction permits certain information to be obtained about the properties of the grid. For instance, it is possible to determine the number of cells whose length is greater that say twice the value of d. From Figure C.2, it can be seen that going from right to left, the length of the first stretched cell l_1 is given by

$$l_1 = \frac{1}{2}(f^0 d + f^1 d),$$

and for the second

$$l_2 = \frac{1}{2}(f^1 d + f^2 d) \text{ etc.}$$

such that

$$l_j = \frac{1}{2}(f^{j-1} d + f^j d).$$

From this it is then possible to determine the value of j which corresponds to a cell length greater than $2d$, from

$$l_j > 2d$$

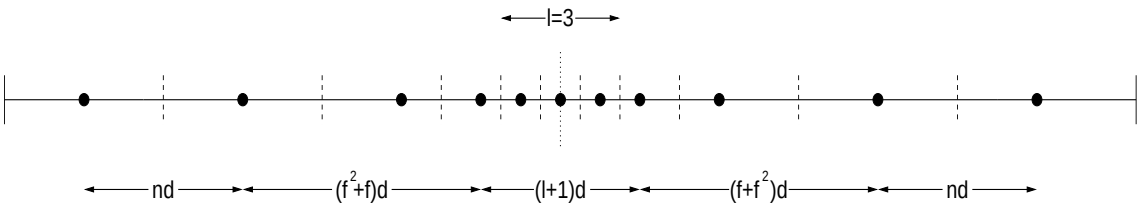

Figure C.3: Irregular grid B.

$$\text{i.e.} \quad \frac{1}{2}(f^{j-1} + f^j) > 2$$
$$f^{j-1} + f^j > 4$$
$$f^{j-1}(1+f) > 4$$
$$f^{j-1} > \frac{4}{1+f}.$$

Taking logs then gives

$$\log(f^{j-1}) > \log\left(\frac{4}{1+f}\right)$$
$$(j-1)\log(f) > \log\left(\frac{4}{1+f}\right)$$

and so

$$j > \frac{\log(4/(1+f))}{\log(f)} + 1. \tag{C.6}$$

The total number of cells on the grid which have a length greater than $2d$ is then $2(a + (b - (j-1))$.

C.2 Construction of irregular grid B

The strategy presented may be further simplified by removing the choice of the number of outer cells of width nd i.e. a, and the number of variable width cells, b. Following a similar procedure, consider an irregular symmetric grid which has numcell cells. Let there be l central cells of width d, and the outermost cells at the boundaries are of width nd. The intermediate cells vary by a continuous factor f in width. If both numcell and l are chosen to be odd values, then a grid will appear similar to Figure C.3.

From this construction, there will be a total number numcell $- l - 2$ of variable width cells. In terms of calculating the positions of the cell centres, this translates

to there being $2k$ cells whose centres are positioned at varying lengths, where

$$2k = \text{numcell} - l - 4$$

and

$$f^{k-1}d = nd.$$

In this case the total length is then

$$\text{length} = \left(2n + 2\sum_{i=1}^{k-1} f^i + l + 1\right) d$$

such that

$$d = \frac{\text{length}}{2\left(n + \frac{f(1-f^k)}{1-f} + \frac{l+1}{2}\right)}.$$

As before, it is possible to find the number of cells of length $2d$ or more by applying (C.6) which is found to be $\text{numcell} - l - 2(j-1)$.

Appendix D

Run time and flux count data

The following Appendix presents tables containing the measured run time and flux count data for the test cases considered in Chapter 6.

Problem	Source term	Grid	GTS		LTS1				LTS2				
			Time (s)	Count	Time (s)	Gain	Count	Gain	Level	Time (s)	Gain	Count	Gain
S1	Upwind	1	1.424	679360	1.442	-1.26	685123	-0.85	1	1.671	-17.35	677152	0.33
		2	1.477	704320	1.603	-8.53	702427	0.27	1	1.723	-16.66	700214	0.58
		4	2.190	1046240	2.171	0.87	857548	18.04	2	2.225	-1.60	864175	17.40
		8	3.391	1622560	3.084	9.05	1006994	37.94	3	2.765	18.46	1055743	34.93
		16	5.443	2607840	4.518	16.99	1309886	49.77	3	3.677	32.45	1399209	46.35
		32	9.005	4319680	7.009	22.17	1860207	56.94	3	5.347	40.62	1994032	53.84
		64	15.28	7337120	11.33	25.85	2769639	62.25	3	8.760	42.67	3037868	58.60
		128	26.47	12724480	18.78	29.05	4234467	66.72	3	13.37	49.49	4840618	61.96
	Point	1	1.165	678720	1.184	-1.63	684511	-0.85	1	1.412	-21.20	676570	0.32
		2	1.209	704320	1.345	-11.25	705639	-0.19	1	1.449	-19.85	700315	0.57
		4	1.792	1045600	1.822	-1.67	842636	19.41	2	1.881	-4.97	860935	17.66
		8	2.772	1620800	2.631	5.09	1030873	36.40	2	2.340	15.58	1052790	35.05
		16	4.446	2603840	3.910	12.06	1333548	48.79	3	3.108	30.09	1395140	46.42
		32	7.350	4310880	6.120	16.73	1874322	56.52	3	4.535	38.30	1986883	53.91
		64	12.46	7318720	9.953	20.12	2826385	61.38	4	6.647	46.65	2910229	60.24
		128	21.58	12686400	16.61	23.03	4180629	67.05	3	11.41	47.13	4826376	61.96
	Point + Superbee	1	1.833	697820	1.854	-1.15	691158	0.95	1	2.123	-15.82	695626	0.31
		2	1.898	722256	2.167	-14.17	711701	1.46	1	2.274	-19.81	714059	1.13
		4	2.817	1072724	2.861	-1.56	888688	17.16	1	2.908	-3.23	884429	17.55
		8	4.364	1663452	4.034	7.56	1045753	37.13	2	3.673	15.83	1076922	35.26
		16	7.012	2673200	5.862	16.40	1437722	46.22	3	4.945	29.48	1424475	46.71
		32	11.61	4427344	9.001	22.47	2081536	52.98	3	7.131	38.58	2029572	54.16
		64	19.68	7518252	14.19	27.90	3086498	58.95	3	10.99	44.16	3103275	58.72
		128	34.20	13035048	22.96	32.87	4712482	63.85	2	20.47	40.15	5787442	55.60

Table D.1: Results table for S1.

Problem	Source term	Grid	GTS		LTS1				LTS2				
			Time (s)	Count	Time (s)	Gain	Count	Gain	Level	Time (s)	Gain	Count	Gain
S2	Upwind	1	6.610	3231592	6.704	-1.42	3251663	-0.62	1	7.844	-18.67	3231592	0.00
		2	8.930	4389987	9.183	-2.83	4077700	7.11	1	9.900	-10.86	3970104	9.56
		4	13.43	6567673	12.65	5.81	4726208	37.91	2	12.56	6.48	4946217	24.69
		8	20.88	10211103	18.19	12.88	5978343	41.45	3	16.20	22.41	6303111	38.27
		16	33.60	16429084	27.62	17.80	8125196	50.54	4	22.10	34.23	8524573	48.11
		32	55.68	27224778	47.71	14.31	11446829	57.95	5	31.70	43.07	12104170	55.54
		64	94.58	46248538	69.23	26.80	16894541	63.47	5	48.01	49.24	18051001	60.97
		128	164.0	80200218	114.9	29.94	25916129	67.69	5	75.40	54.02	27926776	65.18
	Point	1	5.383	3231753	5.475	-1.71	3251825	-0.62	1	6.617	-22.92	3231753	0.00
		2	7.320	4395139	7.631	-4.25	4110095	6.49	1	8.353	-14.11	3974415	9.57
		4	10.95	6572825	10.65	2.74	4723538	28.14	2	10.57	3.47	4932490	24.96
		8	17.01	10216094	15.56	8.52	5926806	41.99	3	13.67	19.64	6306438	38.27
		16	27.36	16434075	23.83	12.90	8041678	51.07	4	18.64	31.87	8515534	48.18
		32	45.34	27229286	37.28	17.78	11641034	57.25	5	26.80	40.89	12106321	55.54
		64	77.01	46252402	60.84	21.00	16979938	63.29	5	40.70	47.15	18052532	60.97
		128	133.5	80202955	101.7	23.82	26165925	67.38	5	64.10	51.99	27927579	65.18
	Point + Superbee	1	8.482	3293776	8.574	-1.08	3273531	0.61	1	9.910	-16.84	3295908	-0.06
		2	11.56	4472608	12.13	-4.93	4052896	9.38	1	13.03	-12.72	4038675	9.70
		4	17.31	6690872	16.54	4.45	4871563	27.19	2	16.82	2.83	5018530	24.99
		8	26.91	10402356	23.75	11.74	6370402	38.76	3	21.96	18.39	6395023	38.52
		16	43.29	16735708	35.96	16.93	8848538	47.13	4	30.08	30.52	8649506	48.32
		32	71.67	27731744	55.11	23.11	12727692	54.10	3	44.17	38.37	12600541	54.56
		64	121.9	47108180	86.82	28.78	18975118	59.72	3	68.00	44.22	19428857	58.76
		128	211.3	81690204	140.5	33.51	29104890	64.37	3	110.4	47.75	31016872	62.03

Table D.2: Results table for S2.

Problem	Source term	Grid	GTS		LTS1				LTS2				
			Time (s)	Count	Time (s)	Gain	Count	Gain	Level	Time (s)	Gain	Count	Gain
S3	Upwind	1	2.262	1104299	2.293	-1.37	1111157	-0.62	1	2.684	-18.66	1104299	0.00
		2	3.229	1576673	3.504	-8.52	1545389	1.98	1	3.809	-17.96	1556987	1.25
		4	4.832	2359455	4.636	4.06	1773140	24.85	1	4.732	2.07	1822559	22.76
		8	7.515	3670317	6.678	11.14	2194336	40.21	2	5.999	20.17	2295846	37.45
		16	12.10	5908378	9.885	18.31	2901871	50.89	3	8.045	33.51	3062513	48.17
		32	20.05	9796045	15.49	22.74	4213391	56.99	4	11.56	42.34	4382877	55.26
		64	34.09	16651908	25.00	26.66	6085913	63.45	5	17.30	49.25	6503136	60.95
		128	59.17	28907228	41.56	29.76	9356573	67.63	5	27.10	54.20	10031472	65.30
	Point	1	1.843	1104299	1.873	-1.63	1111157	-0.62	1	2.264	-22.84	1104299	0.00
		2	2.630	1576673	2.893	-10.00	1547095	1.88	1	3.197	-21.56	1556870	1.26
		4	3.935	2359455	3.893	1.07	1767528	25.09	1	4.015	-2.03	1817422	22.97
		8	6.120	3670156	5.697	6.91	2194481	40.21	2	5.089	16.85	2295718	37.45
		16	9.851	5908217	8.543	13.28	2916077	50.64	3	6.818	30.79	3062809	48.16
		32	16.33	9795401	13.50	17.33	4192686	57.20	4	9.782	40.10	4379987	55.29
		64	27.76	16650942	21.96	20.89	6224055	62.62	5	14.66	47.19	6502773	60.95
		128	48.18	28905296	36.76	23.70	9503328	67.12	5	23.05	52.16	10031141	65.30
	Point + Superbee	1	2.914	1126024	2.944	-1.03	1118997	0.62	1	3.403	-16.78	1126024	0.00
		2	4.158	1606872	4.703	-13.11	1574382	2.02	1	5.040	-21.21	1581978	1.55
		4	6.221	2404896	6.093	2.06	1786935	25.70	1	6.141	1.29	1859707	22.67
		8	9.677	3741168	8.771	9.36	2307286	38.33	2	7.961	17.73	2347593	37.25
		16	15.58	6022408	12.92	17.07	3215800	46.60	3	10.83	30.49	3141478	47.84
		32	25.83	9985140	20.02	22.49	4613097	53.80	3	16.00	38.06	4609988	53.83
		64	43.89	16971868	31.59	28.02	6997136	58.77	5	23.57	46.30	6714712	60.44
		128	72.60	29463584	51.06	29.67	10559625	64.16	3	39.84	45.12	11316881	61.59

Table D.3: Results table for S3.

Problem	Source term	Grid	GTS		LTS1				LTS2				
			Time (s)	Count	Time (s)	Gain	Count	Gain	Level	Time (s)	Gain	Count	Gain
S4	Upwind	1	0.3904	189440	0.3952	-1.23	191806	-1.25	1	0.4632	-18.65	189440	0.00
		2	0.5220	253600	0.6083	-16.53	256113	-0.99	1	0.6183	-18.45	252790	0.32
		4	0.7805	379680	0.7319	6.23	288488	24.02	2	0.7704	1.29	296870	21.81
		8	1.214	590880	1.066	12.19	354860	39.94	3	0.9803	19.25	374795	36.57
		16	1.952	951200	1.607	17.67	470699	50.52	4	1.320	32.38	503004	47.12
		32	3.235	1576800	2.516	22.23	670265	57.49	4	1.881	41.85	712902	54.79
		64	5.496	2679520	4.051	26.29	988315	63.12	5	2.805	48.96	1053839	60.67
		128	9.531	4647680	6.711	29.59	1513623	67.43	5	4.390	53.94	1626728	65.00
	Point	1	0.3184	189440	0.3232	-1.51	207682	-9.63	1	0.3913	-22.90	189440	0.00
		2	0.4254	253440	0.5017	-17.94	256758	-1.31	1	0.5217	-22.64	252651	0.31
		4	0.6360	379520	0.6146	3.36	308158	18.80	2	0.6559	-3.13	297811	21.53
		8	0.9884	590560	0.9100	7.93	356475	39.64	3	0.8311	15.91	374592	36.57
		16	1.590	950560	1.385	12.89	473309	50.21	4	1.114	29.94	500609	47.34
		32	2.634	1575520	2.190	16.86	674697	57.18	4	1.592	39.56	712261	54.79
		64	4.473	2676960	3.555	20.52	996594	62.77	5	2.376	46.88	1052914	60.67
		128	7.756	4642560	5.931	23.53	1528499	67.08	5	3.733	51.87	1624899	65.00
	Point + Superbee	1	0.5037	194176	0.5085	-0.95	208968	-7.62	1	0.5881	-16.76	194176	0.00
		2	0.6738	259940	0.8184	-21.46	257696	0.86	1	0.7881	-16.96	258959	0.38
		4	1.008	389172	0.9470	6.05	295098	24.17	1	1.004	0.40	304171	21.84
		8	4.566	605324	1.390	69.56	381589	36.96	2	1.303	71.46	383892	36.58
		16	2.520	974324	2.085	17.26	532910	45.30	3	1.772	29.68	513984	47.25
		32	4.175	1614908	3.266	21.77	768869	52.39	4	2.552	38.87	733220	54.60
		64	7.092	2743720	5.120	27.81	1127130	58.92	5	3.818	46.16	1087421	60.37
		128	12.30	4758296	8.254	32.89	1721519	63.82	5	5.959	51.55	1684710	64.59

Table D.4: Results table for S4.

Problem	Source term	Grid	GTS		LTS1				LTS2				
			Time (s)	Count	Time (s)	Gain	Count	Gain	Level	Time (s)	Gain	Count	Gain
S5	Upwind	1	0.7197	353395	0.7305	-1.50	355450	-0.58	1	0.8545	-18.73	353275	0.03
		2	0.9732	478170	1.071	-10.05	478949	-0.16	1	1.158	-18.99	476076	0.44
		4	1.455	715484	1.413	2.89	552810	22.74	1	1.441	0.96	558117	21.99
		8	2.263	1113154	2.023	10.61	687996	38.19	2	1.830	19.13	701825	36.95
		16	3.641	1761930	2.977	18.24	892462	49.35	3	2.457	32.52	937507	46.79
		32	6.035	2970450	4.636	23.18	1271691	57.19	4	3.492	42.14	1323562	55.44
		64	10.25	5047350	7.483	27.00	1859702	63.15	5	5.249	48.79	1974137	60.89
		128	17.78	8754697	12.42	30.15	2841871	67.54	5	8.224	53.75	3046890	65.20
	Point	1	0.5857	353356	0.5965	-1.84	355613	-0.64	1	0.7206	-23.03	353442	-0.02
		2	0.7918	478331	0.8827	-11.48	473485	1.01	1	0.9712	-22.66	476205	0.44
		4	1.184	715645	1.185	-0.08	557384	22.11	1	1.224	-3.38	558289	21.99
		8	1.840	1113315	1.723	6.36	680719	38.86	2	1.552	15.65	702020	36.94
		16	2.961	1792252	2.569	13.24	916638	48.86	3	2.082	29.69	937758	47.68
		32	4.907	2971094	4.034	17.79	1292159	56.51	4	2.959	39.70	1323834	55.44
		64	8.337	5048799	6.567	21.23	1848888	63.38	5	4.450	46.62	1974709	60.89
		128	14.46	8757756	10.97	24.14	2853145	67.42	5	6.993	51.64	3048001	65.20
	Point + Superbee	1	0.9286	360144	0.9394	-1.16	357811	0.65	1	1.085	-16.84	360019	0.03
		2	1.256	487244	1.443	-14.89	482257	1.02	1	1.535	-22.21	482253	1.02
		4	1.878	729144	1.865	0.69	554119	24.00	1	1.873	0.27	567269	22.20
		8	2.920	1134060	2.661	8.87	698291	38.43	2	2.428	16.85	712469	37.18
		16	4.698	1825156	3.886	17.28	965930	47.08	3	3.303	29.69	951673	47.86
		32	7.785	3025308	5.989	23.07	1393474	53.94	4	4.728	39.27	1344798	55.55
		64	13.23	5140580	9.451	28.56	2065216	59.83	5	7.132	46.09	2008203	60.93
		128	22.94	8916024	15.22	33.65	3154242	64.62	5	11.13	51.48	3106055	65.16

Table D.5: Results table for S5.

Problem	Source term	Grid	GTS		LTS1				LTS2				
			Time (s)	Count	Time (s)	Gain	Count	Gain	Level	Time (s)	Gain	Count	Gain
S6	Upwind	1	0.3822	176800	0.3867	-1.18	179008	-1.25	1	0.4555	-19.18	176800	0.00
		2	0.5281	244640	0.5828	-10.36	246873	-0.91	1	0.6320	-19.67	244623	0.01
		4	0.7878	365440	0.7691	2.37	276682	24.29	1	0.7815	0.80	285710	21.82
		8	1.224	568160	1.108	9.48	351594	38.12	2	0.9941	18.78	360625	36.53
		16	1.967	913760	1.631	17.08	456638	50.03	3	1.334	32.18	480914	47.37
		32	3.255	1512960	2.548	21.72	638795	57.78	4	1.902	41.57	681729	54.94
		64	5.522	2567200	4.124	25.32	941868	63.31	5	2.846	48.46	1012718	60.55
		128	9.559	4444960	6.862	28.21	1445057	67.49	5	4.442	53.53	1558186	64.94
	Point	1	0.3124	175360	0.3169	-1.44	178360	-1.71	1	0.3852	-23.30	175360	0.00
		2	0.4272	240160	0.4850	-13.53	244869	-1.96	1	0.5266	-23.27	240004	0.06
		4	0.6365	358400	0.6131	3.68	276265	22.92	1	0.6580	-3.38	280637	21.70
		8	0.9871	556480	0.9137	7.44	352756	36.61	2	0.8323	15.68	352620	36.63
		16	1.585	894080	1.389	12.37	458347	48.74	3	1.117	29.53	470800	47.34
		32	2.621	1479520	2.199	16.10	641631	56.63	4	1.592	39.26	667181	54.91
		64	4.446	2510400	3.574	19.61	952172	62.07	5	2.384	46.38	990784	60.53
		128	7.701	4349600	5.992	22.19	1469130	66.22	5	3.733	51.53	1526175	64.91
	Point + Superbee	1	0.4849	180072	0.4893	-0.91	179791	0.16	1	0.5684	-17.22	180072	0.00
		2	0.6666	247804	0.7747	-16.22	247720	0.03	1	0.7824	-17.37	247764	0.02
		4	0.9942	369984	0.9353	5.92	297243	19.66	1	0.9947	-0.05	289752	21.69
		8	1.543	574492	1.377	10.76	379599	33.92	2	1.287	16.59	364427	36.57
		16	2.476	922500	2.067	16.52	512883	44.40	3	1.745	29.52	485935	47.32
		32	4.092	1525200	3.209	21.58	734553	51.84	4	2.505	38.78	689868	54.77
		64	6.912	2576768	5.055	26.87	1095166	57.50	5	3.752	45.72	1025233	60.21
		128	11.96	4458668	8.154	31.82	1663170	62.70	5	5.830	51.25	1581675	64.53

Table D.6: Results table for S6.

Problem	Source term	Grid	GTS		LTS1				LTS2				
			Time (s)	Count	Time (s)	Gain	Count	Gain	Level	Time (s)	Gain	Count	Gain
S7	Upwind	1	0.9062	420160	0.9181	-1.31	425410	-1.25	1	1.080	-19.18	420160	0.00
		2	1.286	596640	1.349	-4.90	570706	4.35	1	1.470	-14.31	563149	5.61
		4	1.925	893440	1.821	5.40	636386	28.77	2	1.793	6.86	664103	25.67
		8	2.993	1389920	2.632	12.06	805244	42.07	3	2.336	21.95	859911	38.13
		16	4.816	2237120	4.011	16.72	1089584	51.30	4	3.194	33.68	1162924	48.02
		32	7.981	3708000	6.253	21.65	1555873	58.04	4	4.623	42.07	1658962	55.26
		64	13.56	6300160	10.13	25.29	2308480	63.36	5	6.938	48.83	2468494	60.82
		128	23.51	10926400	16.89	28.16	3545447	67.55	5	10.88	53.72	3814586	65.09
	Point	1	0.7467	420320	0.759	-1.62	425734	-1.29	1	0.9211	-23.36	420320	0.00
		2	1.060	597120	1.129	-6.51	568138	4.85	1	1.249	-17.83	563432	5.64
		4	1.586	894240	1.550	2.27	640256	28.40	2	1.530	3.53	664965	25.64
		8	2.467	1391360	2.275	7.78	802010	42.36	3	1.992	19.25	860366	38.16
		16	3.970	2239840	3.498	11.89	1098863	50.94	4	2.728	31.28	1164501	48.01
		32	6.581	3713280	5.509	16.29	1566016	57.83	4	3.960	39.83	1661581	55.25
		64	11.18	6310400	9.005	19.45	2325609	63.15	5	5.948	46.80	2472750	60.81
		128	19.40	10946720	15.09	22.22	3578167	67.31	5	9.349	51.81	3821832	65.09
	Point + Superbee	1	1.159	430992	1.171	-1.04	428529	0.57	1	1.359	-17.26	430992	0.00
		2	1.645	611884	1.780	-8.21	568020	7.17	1	1.922	-16.84	574603	6.09
		4	2.462	916104	2.357	4.26	649325	29.12	2	2.374	3.57	678522	25.93
		8	3.830	1425160	3.339	12.82	870094	38.95	2	3.118	18.59	879731	38.27
		16	6.165	2293868	5.144	16.56	1218059	46.90	3	4.284	30.51	1187750	48.22
		32	10.22	3802176	7.989	21.83	1720541	54.75	4	6.188	39.45	1692330	55.49
		64	17.36	6460452	12.56	27.65	2558560	60.40	5	9.316	46.34	2517681	61.03
		128	30.11	11204972	20.38	32.31	3914549	65.06	5	14.55	51.68	3895084	65.24

Table D.7: Results table for S7.

Problem	Scheme	Grid	GTS		LTS1				LTS2				
			Time (s)	Count	Time (s)	Gain	Count	Gain	Level	Time (s)	Gain	Count	Gain
U1	1st order	1	0.02141	13120	0.02274	-6.21	9666	26.33	2	0.02164	-1.07	10390	20.81
		2	0.02653	16480	0.02729	-2.86	10949	33.56	2	0.02563	3.39	12158	26.23
		4	0.03874	24640	0.03829	1.16	14734	40.20	2	0.03456	10.79	16390	33.48
		8	0.05838	37760	0.05533	5.22	19679	47.88	3	0.04521	22.56	21750	42.40
		16	0.09333	61120	0.08486	9.08	27714	54.66	2	0.07086	24.08	32770	46.38
		32	0.1529	100960	0.1342	12.23	40537	59.85	2	0.1096	28.32	50127	50.35
		64	0.2580	171200	0.2204	14.57	61809	63.90	3	0.1518	41.16	70354	58.91
		128	0.4450	296160	0.3694	16.99	95521	67.75	3	0.2459	44.74	112606	61.98
	2nd order	1	0.03479	13776	0.03687	-5.98	9998	27.42	2	0.03604	-3.59	10926	20.69
		2	0.04320	17220	0.04372	-1.20	11615	32.55	2	0.04136	4.26	12437	27.78
		4	0.06264	25256	0.06024	3.83	15632	38.11	2	0.05562	11.21	16720	33.80
		8	0.09561	38868	0.08661	9.41	21522	44.63	2	0.07701	19.45	23059	40.67
		16	0.1533	62648	0.1284	16.24	29982	52.14	2	0.1126	26.55	33531	46.48
		32	0.2527	103648	0.1986	21.41	44144	57.41	2	0.1731	31.50	51360	50.45
		64	0.4276	175644	0.3181	25.61	67228	61.72	2	0.2774	35.13	82019	53.30
		128	0.7401	304226	0.5232	29.31	105180	65.43	3	0.3975	46.29	115557	62.02

Table D.8: Results table for U1.

Problem	Scheme	Grid	GTS		LTS1				LTS2				
			Time (s)	Count	Time (s)	Gain	Count	Gain	Level	Time (s)	Gain	Count	Gain
U2	1st order	1	0.02039	13122	0.02080	-2.01	9102	30.64	2	0.01988	2.50	9552	27.21
		2	0.02738	17982	0.02641	3.54	11006	38.79	2	0.02416	11.76	11313	37.09
		4	0.03889	26082	0.03636	6.51	13840	46.94	2	0.03225	17.07	15117	42.04
		8	0.05661	38556	0.05139	9.22	18392	52.30	2	0.04486	20.76	21096	45.28
		16	0.08562	58968	0.07556	11.75	24592	58.30	2	0.06467	24.47	30291	48.63
		32	0.1335	92664	0.1145	14.23	36381	60.74	2	0.09669	27.57	44966	51.47
		64	0.2180	152118	0.1821	16.47	52835	65.27	2	0.1518	30.37	70228	53.83
		128	0.3637	254664	0.2973	18.26	82375	67.65	2	0.2456	32.47	112775	55.72
	2nd order	1	0.03391	13776	0.03840	-13.24	9443	31.45	2	0.03287	3.07	9987	27.50
		2	0.04518	18532	0.04207	6.88	12087	34.78	2	0.03904	13.59	11694	36.90
		4	0.06491	26896	0.05761	11.25	15076	43.95	2	0.05223	19.53	15685	41.68
		8	0.09514	39688	0.08090	14.97	20475	48.41	2	0.07267	23.62	21853	44.94
		16	0.1452	60844	0.1170	19.42	28340	53.42	2	0.1045	28.03	31354	48.47
		32	0.2280	95776	0.1739	23.73	39223	59.05	2	0.1554	31.84	46501	51.45
		64	0.3753	157932	0.2736	27.10	59316	62.44	2	0.2447	34.80	73117	53.70
		128	0.6333	266664	0.4381	30.82	90575	66.03	2	0.3961	37.45	118108	55.71

Table D.9: Results table for U2.

Problem	Scheme	Grid	GTS		LTS1				LTS2				
			Time (s)	Count	Time (s)	Gain	Count	Gain	Level	Time (s)	Gain	Count	Gain
U3	1st order	1	0.04141	25760	0.04012	3.12	19014	26.19	1	0.04351	-5.07	19203	25.45
		2	0.04620	28819	0.04738	-2.55	23371	18.90	2	0.04920	-6.49	22958	20.34
		4	0.05884	37030	0.06050	-2.82	27896	24.67	3	0.05768	1.97	27227	26.47
		8	0.08364	53130	0.08229	1.61	34156	35.71	3	0.07223	13.64	33514	36.92
		16	0.1305	83559	0.1219	6.59	43973	47.37	3	0.09811	24.82	44782	46.41
		32	0.2123	136689	0.1903	10.36	61626	54.92	3	0.1420	33.11	63700	53.40
		64	0.3551	229425	0.3059	13.86	87931	61.67	3	0.2163	39.09	95553	58.35
		128	0.6239	403949	0.5191	16.80	133882	66.86	3	0.3517	43.63	153161	62.08
	2nd order	1	0.06612	26240	0.06139	7.15	19219	26.76	1	0.06534	1.18	19564	25.44
		2	0.07444	29520	0.07549	-1.41	24566	16.78	2	0.07854	-5.51	23451	20.56
		4	0.09527	37884	0.09723	-2.06	28432	24.95	2	0.09471	0.59	28148	25.70
		8	0.1360	54284	0.1297	4.63	35667	34.30	3	0.1184	12.94	34560	36.33
		16	0.2128	85280	0.1873	11.98	46057	45.99	3	0.1588	25.38	45868	46.21
		32	0.3470	139400	0.2840	18.16	66367	52.39	3	0.2289	34.03	65831	52.78
		64	0.5802	233372	0.4417	23.87	96259	58.75	3	0.3437	40.76	98275	57.89
		128	1.017	409508	0.7304	28.18	149326	63.54	3	0.5557	45.36	158217	61.36

Table D.10: Results table for U3.

Problem	Source term	Grid	GTS		LTS1				LTS2				
			Time (s)	Count	Time (s)	Gain	Count	Gain	Level	Time (s)	Gain	Count	Gain
U4	Upwind	1	0.05456	26244	0.05344	2.05	21864	16.69	1	0.05698	-4.44	21973	16.27
		2	0.06768	32724	0.06830	-0.92	28743	12.17	2	0.07128	-5.32	28094	14.15
		4	0.09342	45522	0.08993	3.74	34034	25.24	3	0.08586	8.09	33561	26.28
		8	0.1413	69336	0.1240	12.24	41179	40.61	4	0.1099	22.22	42419	38.82
		16	0.2228	109836	0.1824	18.13	55259	49.69	3	0.1520	31.78	57431	47.71
		32	0.3669	181440	0.2814	23.30	76907	57.61	4	0.2153	41.32	81073	55.32
		64	0.6244	309420	0.4534	27.39	112278	63.71	4	0.3266	47.69	121436	60.75
		128	1.082	536868	0.7510	30.59	171938	67.97	5	0.5018	53.62	185444	65.46
	Point	1	0.04459	26244	0.04471	-0.27	21864	16.69	1	0.04843	-8.61	21995	16.19
		2	0.05524	32724	0.05714	-3.44	28523	12.84	2	0.05986	-8.36	27967	14.54
		4	0.07613	45522	0.07596	0.22	33744	25.87	3	0.07242	4.87	33569	26.26
		8	0.1150	69336	0.1061	7.74	41967	39.47	4	0.09297	19.16	42408	38.84
		16	0.1813	109998	0.1574	13.18	54857	50.13	3	0.1288	28.96	57348	47.86
		32	0.2982	181602	0.2451	17.81	77016	57.59	4	0.1827	38.73	81134	55.32
		64	0.5073	309744	0.3978	21.58	114526	63.03	4	0.2777	45.26	121522	60.77
		128	0.8790	537516	0.6632	24.55	171986	68.00	5	0.4264	51.49	185419	65.50
	Point + Superbee	1	0.06932	26568	0.06933	-0.01	22130	16.70	1	0.07363	-6.22	22279	16.14
		2	0.08663	33292	0.09061	-4.59	29193	12.31	1	0.09469	-9.30	28872	13.28
		4	0.11980	46248	0.1203	-0.42	34556	25.28	2	0.1161	3.09	34443	25.53
		8	0.1813	70356	0.1650	8.99	43621	38.00	3	0.1494	17.60	43466	38.22
		16	0.2870	111684	0.2401	16.34	59213	46.98	3	0.2094	27.04	59021	47.15
		32	0.4709	183680	0.3648	22.53	85650	53.37	3	0.2968	36.97	85231	53.60
		64	0.7993	312420	0.5773	27.77	128760	58.79	3	0.4582	42.67	130912	58.10
		128	1.384	541200	0.9372	32.28	194551	64.05	4	0.6932	49.91	196096	63.77

Table D.11: Results table for U4.

Problem	Source term	Grid	GTS		LTS1				LTS2			
			Time (s)	Count	Limit	Time (s)	Gain	Count	Gain	Level	Time (s)	Gain	Count	Gain
U5	Upwind	1	0.04160	19040	7	0.04026	3.22	13600	28.57	2	0.03868	7.02	14489	23.90
		2	0.05540	25600	10	0.05138	7.26	16384	36.00	2	0.04898	11.59	18359	28.29
		4	0.07950	37120	11	0.07031	11.56	21368	42.44	3	0.06108	23.17	23048	37.91
		8	0.1227	57760	17	0.1037	15.48	29528	48.88	3	0.08689	29.19	32664	43.45
		16	0.1960	92800	20	0.1572	19.80	41831	54.92	3	0.1247	36.38	46254	50.16
		32	0.3231	153600	25	0.2480	23.24	61414	60.02	1	0.2741	15.17	97345	36.62
		64	0.5447	260960	22	0.4047	25.70	94693	63.71	1	0.4568	16.14	161296	38.19
		128	0.9480	452320	6	0.7047	25.66	186468	58.78	2	0.5670	40.19	200587	55.65
	Point	1	0.05271	29760	7	0.04637	12.03	15234	48.81	1	0.04781	9.30	19212	35.44
		2	0.07004	39840	9	0.05985	14.55	18403	53.81	2	0.05212	25.59	21472	46.10
		4	0.09031	51680	9	0.07715	14.57	23969	53.62	2	0.06572	27.23	27407	46.97
		8	0.1141	65600	9	0.09847	13.70	31369	52.18	3	0.07742	32.15	33750	48.55
		16	0.1596	92160	10	0.1370	14.16	43293	53.02	2	0.1193	25.25	51159	44.49
		32	0.2631	152640	10	0.2176	17.29	64554	57.71	2	0.1811	31.17	76095	50.15
		64	0.4458	259360	10	0.3573	19.85	99988	61.45	3	0.2571	42.33	109394	57.82
		128	0.7709	449280	10	0.6037	21.69	160858	64.20	3	0.4121	46.54	172666	61.57
	Point + Superbee	1	0.07675	28864	6	0.06860	10.62	17808	38.30	1	0.07160	6.71	20665	28.41
		2	0.1021	38540	7	0.08206	19.63	19863	48.46	2	0.07834	23.27	22101	42.65
		4	0.1320	50020	7	0.1052	20.30	25541	48.94	2	0.09931	24.77	28231	43.56
		8	0.1689	64124	7	0.1361	19.42	33554	47.67	2	0.1275	24.51	36578	42.96
		16	0.2486	94628	8	0.1980	20.35	48366	48.89	2	0.1824	26.63	52625	44.39
		32	0.4106	156620	8	0.3076	25.09	72408	53.77	2	0.2739	33.29	78360	49.97
		64	0.6971	266172	10	0.4950	28.99	109782	58.76	2	0.4426	36.51	126012	52.66
		128	1.208	461332	11	0.8278	31.47	176768	61.68	3	0.6319	47.69	178151	61.38

Table D.12: Results table for U5.

Problem	Source term	Grid	GTS		LTS1				LTS2			
			Time (s)	Count	Limit	Time (s)	Gain	Count	Gain	Level	Time (s)	Gain	Count	Gain
U6	Upwind	1	0.04053	18560	8	0.03857	4.84	12695	31.60	2	0.03738	7.77	13926	24.97
		2	0.05498	25440	10	0.04959	9.80	15373	39.57	3	0.04353	20.83	16277	36.02
		4	0.08138	38080	14	0.06873	15.54	19581	48.58	3	0.05871	27.86	21819	42.70
		8	0.1255	59200	22	0.1023	18.49	27648	53.30	3	0.08378	33.24	31224	47.26
		16	0.2007	95200	26	0.1581	21.23	40673	57.28	3	0.1239	38.27	45860	51.83
		32	0.3313	157760	26	0.2514	24.12	61209	61.20	3	0.1943	41.35	71455	54.71
		64	0.5612	267840	26	0.4106	26.84	94111	64.86	3	0.3029	46.03	110084	58.90
		128	0.9722	464640	26	0.6896	29.07	149360	67.85	3	0.4902	49.58	176063	62.11
	Point	1	0.03649	20320	7	0.03592	1.56	13852	31.83	1	0.03790	-3.86	16194	20.31
		2	0.04886	27520	8	0.04559	6.69	16333	40.65	2	0.04174	14.57	17928	34.85
		4	0.06636	37760	10	0.05955	10.26	19946	47.18	2	0.05339	19.54	22856	39.47
		8	0.1027	59040	10	0.08921	13.14	28694	51.40	2	0.07752	24.52	33105	43.93
		16	0.1639	94880	14	0.1384	15.56	41568	56.19	2	0.1190	27.39	50737	46.53
		32	0.2705	157280	14	0.2210	18.30	62684	60.14	3	0.1666	38.41	72013	54.21
		64	0.4586	267360	14	0.3636	20.72	97183	63.65	3	0.2584	43.65	109804	58.93
		128	0.7940	463680	16	0.6159	22.43	155149	66.54	3	0.4193	47.19	175749	62.10
	Point + Superbee	1	0.05621	20992	6	0.05367	4.52	14509	30.88	1	0.05710	-1.58	16743	20.24
		2	0.07551	28372	8	0.06697	11.31	16974	40.17	2	0.06388	15.40	18325	35.41
		4	0.1029	38868	14	0.08633	16.10	20767	46.57	2	0.08157	20.73	23423	39.74
		8	0.1593	60516	14	0.1288	19.15	30348	49.85	2	0.1182	25.80	34007	43.80
		16	0.2551	97252	14	0.1994	21.83	46109	52.59	2	0.1850	27.48	53373	45.12
		32	0.4221	161212	14	0.3096	26.65	68480	57.52	2	0.2826	33.05	80890	49.82
		64	0.7164	273880	16	0.5023	29.89	106443	61.14	2	0.4525	36.84	129006	52.90
		128	1.242	475108	16	0.8348	32.79	170730	64.07	3	0.6461	47.98	182232	61.64

Table D.13: Results table for U6.